Università degli Studi di Padova

DIPARTIMENTO DI FISICA E ASTRONOMIA GALILEO GALILEI

CORSO DI DOTTORATO DI RICERCA IN ASTRONOMIA

Blue straggler stars in Galactic open clusters

A THESIS PRESENTED IN FULFILLMENT OF THE THESIS REQUIREMENT FOR THE DEGREE OF DOCTOR OF PHILOSOPHY IN ASTRONOMY

AUTHOR

MARÍA JOSÉ RAIN SEPÚLVEDA

COORDINATOR: DR. GIOVANNI CARRARO

SUPERVISOR: DR. GIOVANNI CARRARO

CO-SUPERVISOR: DR. JAVIER AHUMADA

MAY 30, 2022

PADOVA, ITALIA

Abstract

More than 60 years ago, in the optical color-magnitude diagram of the Galactic Globular Cluster M3 a new type of star was discovered: the blue straggler stars. Since then, these objects have been found in all types of stellar systems and environments, from the dense core of globular clusters to the low-density environment of the Galactic field. Understanding their formation has fascinated both observers and theorists, and today it is widely accepted that they have formed through the interaction with other stars. Among the multiple formation mechanisms proposed, two are the main scenarios: collision-induced stellar mergers and mass transfer in binary systems. Both scenarios, however, can be easily modified by the presence of a third (or more) star. What is still partially unclear is how much each mechanism contributes to the straggler population currently observed. With many authors proposing different pathways that dominate in different environments, it is not easy to identify the exact pathway without information about their BSS properties. To do so we require first having large and homogeneous compilations of these stars, suitable to find pathological cases on which these formation scenarios can be further tested.

This thesis presents an observational effort made to contribute to a better understanding of the properties of blue straggler stars in open clusters (OCs), improve membership-driven BS statistics, and shed light on which formation mechanism is the most predominant from a macro scale point of view. Two are the sides that define this thesis. From one side, this work presents the most comprehensive and homogeneous catalog of the BSS population in a sample of more than 400 OCs. After having compiled the catalog, we have revisited the most famous relations between the straggler numbers and the cluster environment (age, mass, integrated magnitude, binary fraction) ruling out previous claims and providing invaluable information about the BSS environments, which is crucial to building realistic models of their evolution.
Yellow straggler stars (YSS) are much less sampled and studied than BSS. Their importance, however, relies on the suggestion of these stars as possible evolved-BSS. As part of this thesis, we present the first and largest systematic search of YSS in OCs, where nearly 80 have been found in 45 OCs. This is the first time these systems are reported

as part of a catalog, their properties are important to have a complete picture of the formation and evolution of BSS stars.
After our internally consistent and accurate straggler selection, we have ranked the host clusters in terms of their internal dynamical evolution by using the so-called $\mathrm{A}_{\mathrm{r}}^{+}$ parameter, which measures the central concentration of BSS within the cluster. This thesis has extrapolated the calculation of $\mathrm{A}_{\mathrm{r}}^{+}$ from 10 Ocs (previously reported in the literature) to $\sim$ 40. Moreover, by estimating the parameter $\mathrm{N}_{\mathrm{relax}}$ (indicative of the dynamical state of the cluster) we showed the OCs distribution is completely different from that of the globular clusters.
From the other side and going more into detail, we tried to assess the binary nature of a few blue stragglers to investigate their origin. We managed to identify both, long and short-period binary stars, and we also obtained their rotational velocities. We showed most of them are fast-rotators stars with $V \sin\ i \geq 30$km s^{-1} and some of them up to 150 $km\ s^{-1}$. One unexpected finding is the large short-period binary fractions we found for a sample of 10 OCs. For all of them, we derived their periods between 5 hours and 3 days. Among them, we found more than $\sim$60 eclipsing-BSS binaries respectively, where nearly 90% are new discoveries. We also reported 7 short-period-YSS binaries which correspond to a $\sim$8% of the total population reported in out catalog, this is slightly larger than the recurrence among the BSS population, which is $\sim$7%.

Despite our contribution to describing the macro properties of BSS, further research is necessary to entirely understand their formation and evolution. From an observational point of view, it is important to carry out multi-wavelength on as many BSS and YSS as possible. Furthermore, very little is known about the companions of the BSS, and hence about their progenitors. Future high-resolution spectroscopy observations revealing the straggler companions are mandatory to investigate the initial conditions that lead to a straggler formation. But, also to study their (orbital)properties which can provide invaluable clues to understanding mass-transfer (MT) processes, including Roche Lobe Overflow and Common Envelope Evolution. To complete the picture, however, new theoretical models including observational constraints are important to understand the physics of MT in low- and intermediate-mass stars which are at the same time are essential to understand many other post-MT systems such as symbiotic stars, double white dwarfs, Type Ia supernovae, transients, X-ray binaries, among others.

Contents

Chapter 1

Blue straggler stars in stellar clusters: The current scenario and motivation

The cleaned color-magnitude diagrams (CMD)[1] that can now be achieved routinely with *Gaia* data [2], show very clearly that not all the cluster stars lie along the traditional single stellar population paths expected from theoretical models. In fact, the intense dynamical activity and the repeated interactions between stars in the environment provided by stellar systems allow the formation of numerous "exotic" objects[3], such as millisecond pulsars, cataclysmic variables (CVs), low mass X-ray binaries, subsubgiants (SSGB), but also blue, yellow straggler stars (BSS, YSS). The stragglers are

[1]Color-magnitude diagrams of open clusters are often contaminated by a variety of effects — photometric errors, unresolved binaries, evolutionary effects, field star contamination, stellar rotation and differential reddening— that make the true properties of cluster stars difficult to identify. For open clusters, the close proximity to field stars complicates the interpretation of the CMD's since many times the field stars and the cluster stars have roughly the same distance and consequently they are superimposed in the CMD. Therefore, on this thesis we refer to "clean CMD's to those on which bona-fide members have been properly identify, this means free of "field contamination".

[2]*Gaia* is a space observation of the European Space Agency (ESA) designed for astrometry: measuring the positions and distances of stars with unprecedented precision. The mission aims to construct the largest and the most precise 3D space catalog ever made, totaling approximately 1 billion astronomical objects, mainly stars, but also planets, comets, asteroids and quasars among others. Gaia is the successor to the Hipparcos mission and the the telescope is part of ESA's Horizon 2000+ long-term scientific program. More information regarding Gaia can be found in `https://www.esa.int/Science_Exploration/Space_Science/Gaia` and along this Phd thesis

[3]The quotes because what used to be considered "exotic" are now pretty much at the core of mainly research lines, like this Phd thesis for example.

objects defined roughly by their positions in the CMD of the stellar system they inhabit. These positions are not compatible at all with those predicted by the standard single star evolution theory—see Figure 1.1. In some open clusters (OCs), ≈25% of the evolved stars have been classified in alternative pathways of stellar evolution. Consequently, a quarter of the stars have not been accurately described by simple stellar evolutionary models. In this context, if we want to draw a more comprehensive picture of stellar evolution, we must include these exotic stars in our definition of standard stellar populations.

Furthermore, since many of the stars in our Galaxy are found to be in binary (or multiple systems) and with M-dwarfs (the most numerous stars in our Galaxy) having a binary fraction of ∼30% (Janson et al., 2012) and at least 50% of the sun-like stars having at least one companion , it is not surprising then, that all the previously above mentioned "exotic" stars can be (mostly) explained by binarity. Moreover, because of their sparse character, the wide range of properties they exhibit (found at all ages and almost all locations in the galactic disk) but also, because of their richness in binaries, proximity, and dynamical active structure (which allows both targeting observations and direct N-body simulations), they are useful to investigate stellar evolution and nucleosynthesis, stellar interactions, and dynamical processes, and star formation. . Historically, OCs have given us information about the role of binaries in cluster evolution; their study, however, also enables an in-depth analysis of the BSS characteristics such as frequency, orbital parameters, and masses, which are the most important diagnostic tools for determining their origin and nature, therefore helping to make the largest progress in improving our understanding of stellar evolution.

In the following sections we will briefly describe the current scenario of BSS in OCs, but also will give the motivations for this doctoral thesis.

1.1 Photometric properties

The presence of BSS poses a challenge for standard single-star evolution theory since main sequence stars with masses much higher than that of the cluster turnoff should

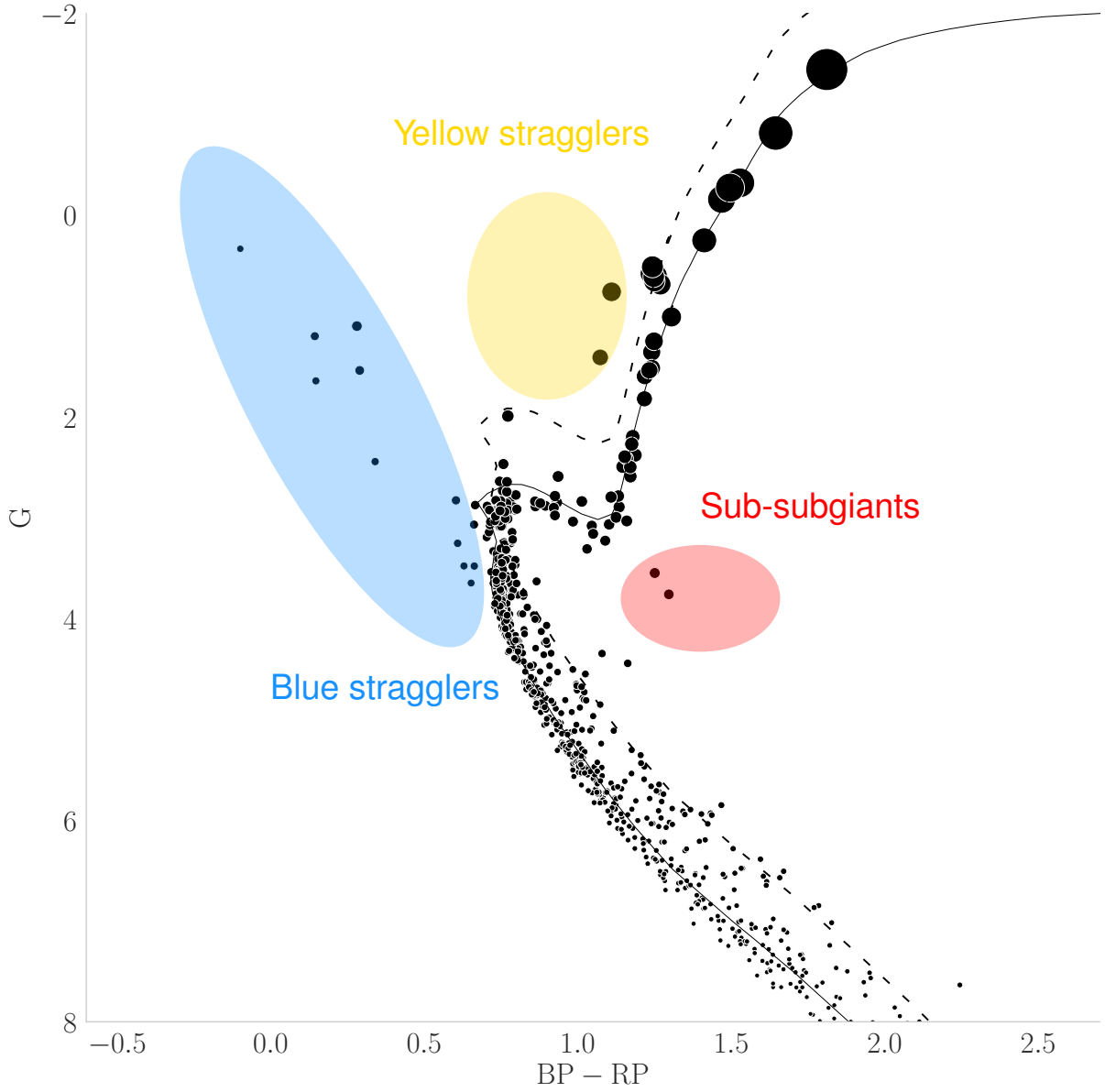

Figure 1.1 Optical color-magnitude diagram of the old open cluster NGC 2682 (M67). Astrometric members identified by Cantat-Gaudin et al. (2018) are in black circles. A 4-Gyr isochrone is shown in black with an equal-mass binary sequence shown as dashed black line (Bressan et al., 2012). Here stellar products that do not follow the single-star evolutionary theory, as indicated with the isochrones, are highlighted in blue for blue straggler stars, in yellow for yellow straggler stars, and in red for sub-subgiants stars.

have evolved into the white dwarf regime long ago. At present, these exotic stars have been identified in essentially all stellar systems: globular clusters (GCs, Piotto et al. 2004, Salinas et al. 2012), dwarf galaxies (Momany et al. 2007), open clusters (Ahumada and Lapasset 1995, 2007, hereafter AL95 and AL07), and the field population of the Milky Way (Preston and Sneden, 2000, Santucci et al., 2015). BSS were initially identified by Sandage (1953) in the color-magnitude diagram (CMD) of the globular cluster M3, appearing as an extension of the cluster main sequence, blueward, and above the cluster main sequence turnoff (TO). Though until today we still use this "definition" to identify the BSS, there are of course additional membership criteria such as the use of vector-point diagram, radial velocity measurements, and chemical abundances, which help to select bona fide BSS. In optical CMDs and in terms of magnitude, BSS typically spread from the TO to about two magnitudes brighter; in some clusters, however, the brightest BSS can be as much as 3 magnitudes above the TO. The low luminosity limit is not always clear. For example, in OCs, stars are bluer and fainter than the TO on the zero-age main sequence (ZAMS), so they appear younger and, therefore, they are BSS—for example, stars 1366 and 8104 in NGC 188 (Geller et al., 2008), or the BSS recently identified in several OCs by Leiner and Geller (2021) and Rain et al. (2021, hereafter R21b) using *Gaia* DR2.

In GCs, the brightest blue stragglers and the blue end of the horizontal branch tend to merge in optical CMDs. This suggested the possibility of not only studying the BSS properties in the optical range, but also in the UV where they clearly detach from the other populations (horizontal branch, turnoff stars) as shown by Ferraro et al. (2003). Additionally, stars located between the main sequence and the giant branch (Hertzprung gap) are also identified as BSS, or rather evolved blue stragglers—"yellow straggler stars" (YSS), see § 2.3.2 for more details regarding this population. Before *Gaia*, some isolated YSS were found and studied in a handful of GCs (Sills et al., 2009) and OCs (da Silveira et al., 2018, Leiner et al., 2016); today we see them even in the CMDs of relatively young OCs with ages greater than 200 Myr (R21b). Iben (1986) suggests that different formation mechanism for BSS could result in very different properties later in their evolution, and so observing evolved blue stragglers (or YSS) may help us constrain the details of their formation.

Today it is widely accepted that a straggler started as a normal, main sequence star that was "rejuvenated" by acquiring extra mass. The new, more massive star may reach an accordingly higher luminosity that can place it above the CMD TO. This increase in mass may be produced via several, non-exclusive mechanisms as described in § 1.2. It is logical then to think a BSS as an object more massive than the mean stellar mass of the host cluster. Their masses, however, are usually derived from evolutionary tracks for main sequence stars which, as the reader may know, do not include modifications to the standard theory of stellar evolution from either collisions or mass transfer. Particularly in OCs, the photometric masses of some BSS are very different from those derived directly from their binary orbits—e.g., Sandquist et al. (2003).

Even so, some low-mass BSS are hidden in the MS as demonstrated by Leiner et al. (2019); these "blue lurkers" have luminosities not high enough to appear above the turnoff in the cluster CMD as the classical BSS. The detection of these low-mass BSS is quite challenging and relies on the use of stellar spectra either by using stellar abundances measurements or rotation rates. Figure 1.2 shows the 11 low-mass and fast-rotation BSS found by Leiner et al. (2019) in the low-luminosity end of the blue straggler distribution. We expect to better understand these BSS as well as the classical ones with the upcoming astronomical facilities —Further information can be found in § 6.2 where we have reported part of our future plans and directions.

Finally, in a few globular clusters (M30, Ferraro et al. 2009; NGC 362, Dalessandro et al. 2013; NGC 1261, Simunovic et al. 2014), high-precision HST photometry has shown that the blue stragglers form two more-or-less parallel sequences in the CMD (see Figure 1.3). Both sequences are offset to the red of the ZAMS; the blue sequence is well fit by models of collision products, if all the collisions occurred 1–2 Gyr ago for M30, 2 Gyr in the particular case of NGC 1261 and 0.2 Gyr in the case of NGC 362. The red sequence starts about 0.75 mag above the ZAMS, and covers a region of the CMD which is populated by binaries that are currently undergoing mass transfer.

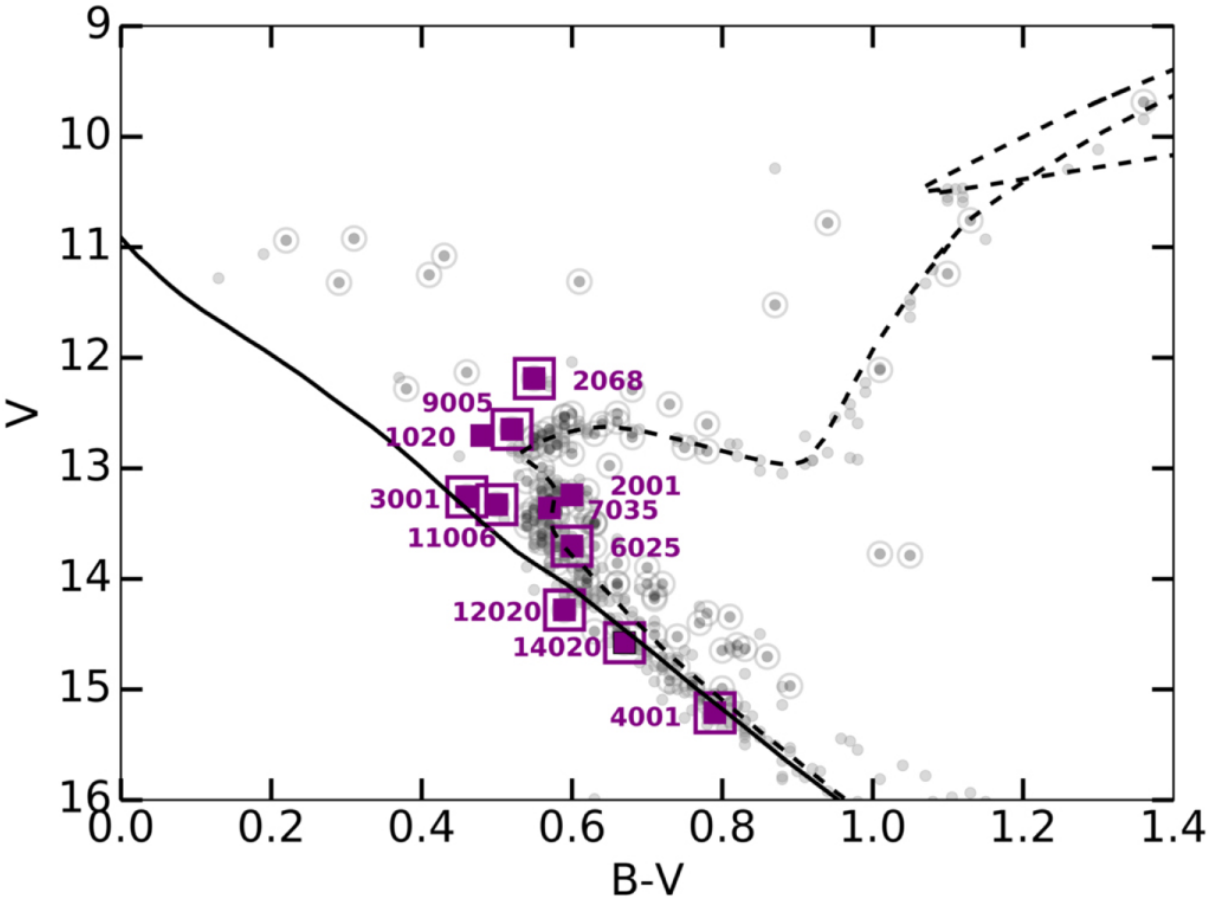

Figure 1.2 Color-magnitude diagram of M67, where binary members are boxed/circled (Geller et al., 2015). Purple points represent stars with rapid rotation rates, i.e., low-mass BSS which, according to the authors, are the products of recent stellar interactions. The black solid and dashed lines are the zero-age MS and a 4-Gyr PARSEC isochrone (Bressan et al., 2012), respectively. Figure taken from Leiner et al. (2019). Compare with Fig. 1.1.

1.2 Formation channels for BSS

Since the discovery of BSS almost 70 years ago in the globular cluster M3 (Sandage, 1953), their formation mechanisms have been extensively discussed. A lot of effort either theoretical or observational has been made in order to identify which one of these mechanisms is the dominant one, but also how much does each mechanism contribute to the observed straggler population. As seen extensively in the literature, the straggler population is composed of a wide variety of objects, from single stars

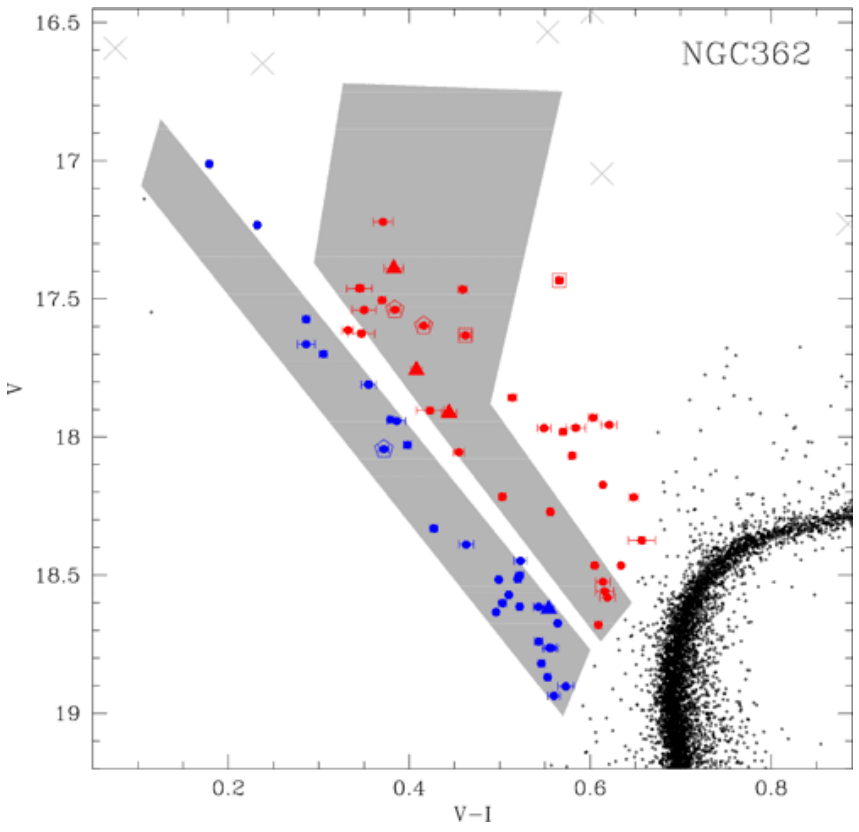

Figure 1.3 A partial view of the V vs. $(V - I)$ CMD of the globular cluster NGC 362, zoomed on the BSS region. BSS are highlighted as red and blue symbols, and the photometric errors are shown as error bars. The grey areas represent the fiducial loci of the red BSS and blue BSS of M30 (Ferraro et al., 2009). The red symbols are those BSS consistent with the binary scenario (see §1.2.1 and 1.2.6) while blue symbols arise from direct stellar collisions (see §1.2.2). According to the authors, both sequences arise from the collision rate, and the mass transfer activity in binary systems is enhanced as a consequence of the cluster "core collapse", a single short-lived event that might boost the formation of BSS. Figure taken from Dalessandro et al. (2013).

(e.g., chemically peculiar stars, X-ray emitters) to complex systems within binaries or triples systems. In Natalie Gosnell words, *The definition of a BSS is not physical, but empirical. Any star falling above the main sequence turnoff on a cluster CMD will be counted as a BSS, regardless of the mechanisms responsible for creating that object* (Gosnell, 2015).

So, in the following lines, we will briefly describe some of the main formation mechanisms proposed so far, with a special focus on stellar clusters, particularly in the OCs.

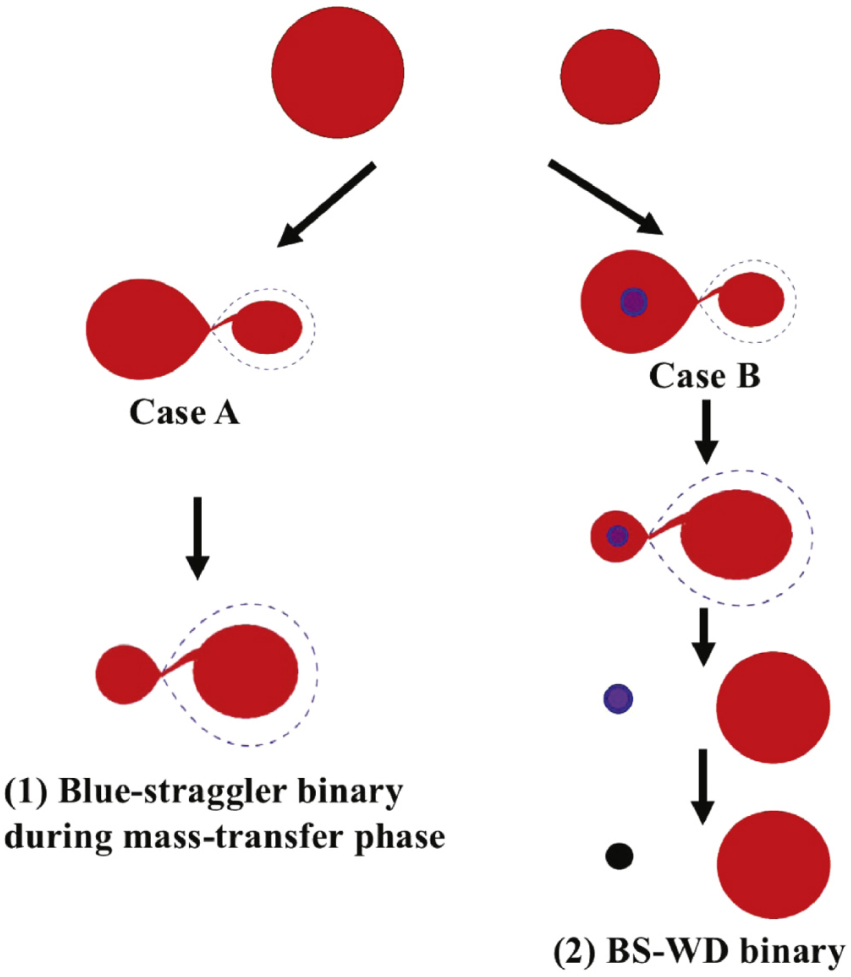

Figure 1.4 A schematic view of the evolutionary paths of binaries that may produce two kinds of blue straggler binaries. (1) Case A binary evolution may produce BS binaries that are experiencing mass transfer. (2) Case B binary evolution may result in BS binaries that have finished mass transfer and have a blue straggler orbiting a white dwarf (the BS-WD binaries). Figure taken from Jiang et al. (2017).

1.2.1 Blue stragglers via binary evolution

In this subsection we consider the formation of blue stragglers through the evolution of binary stars, with especial emphasis on mass transfer (MT) occurring from one (evolved) star to the other. This mechanism, originally proposed by McCrea (1964), can create a BSS in a cluster when the—originally—secondary star in a binary system (the accretor) receives enough mass from an evolved (or MS) star (the donor) via Roche lobe

overflow (RLOF), so that it exceeds the main sequence TO mass and its new luminosity places it in the BSS region—see § 1.1 and 2.3. Mass transfer is traditionally divided into three categories based on the evolutionary state of the donor: A, B and C. Since there is plenty of information in the literature regarding the MT-process and their implications, in the following lines we will focus on the outcomes of each category, as well as on the characteristics of the post-MT systems, i.e., periods, companions, masses of the components, etc.

- **Case A: The donor is a MS star, during hydrogen burning at its core.** When the MT starts via RLOF, the binary system can enter into contact and possibly merge. The binary separation must be small enough for the RLOF to ensue, at most of a few solar radii. It has been shown that only a few binaries in the Galaxy are close enough to undergo this formation channel (Raghavan et al., 2010). Case A MT can lead to either a single massive BSS (merged) or to a BSS with a short-period hydrogen-burning companion (unmerged) —see the schematic Figure 1.4. Star V1309 Sco is probably the best example of Case A MT with a single merger product (Tylenda et al., 2011). Some of these stars can be observed as W Ursae Majoris (W UMa)-type eclipsing binaries. However, in many cases contact binary merger products will not even exceed the TO mass in OCs, and therefore will not be classified as BSS.

- **Case B: The donor is RGB star before helium ignition.** Here, RLOF occurs in binaries with longer separations, of a few to some tens of solar radii. This formation channel will lead to a BSS with an intermediate period from a few to hundreds days and a helium WD companion of 0.45 $M_{\odot}$ —see the schematic Figure 1.4. The BSS could be quite massive, with 0.1–0.4 $\mathrm{M}_{\odot}$ of the final system residing in the WD. They are not expected to be observed as eclipsing binaries due to the small radius of the WD companion, as well as the expected wide separation.

- **Case C: The donor is an aysmptotic giant branch (AGB) star beyond helium ignition.** The separation between the donor and the accretor is quite large. Here, post-MT systems are expected to be composed by a BSS and a carbon-oxygen (CO) WD (the donor) with a typical mass of 0.6 $M_{\odot}$. Case C-MT scenario leads to long orbital periods with high eccentricity values. It is however highly inefficient

in transferring mass, and so the BSS can be up to $\Delta M = M_{BSS} - M_{TO} \approx 0.2\ M_{\odot}$ above the TO mass.

- **Case D (wind RLOF): A more efficient MT scenario:** If the separation (of the stars) is high enough (higher than 4 AU) the system will not evolve through RLOF because the primary will not fill its Roche lobe. In this particular case, MT will (still) occur via the accretion of slow wind material ejected from the donor (AGB in this case). The accretion efficiency of case D-MT can be as high as up 45% (and lower as 10%) according to Table 1 of Abate et al. (2013) —based on hydrodynamic simulations and for a binary system with a 1.0 $M_{\odot}$ AGB primary and a 0.6 $M_{\odot}$ MS companion. This method can form even more massive BSS with $\Delta M > 0.4\ M_{\odot}$, while the companion will still be a CO-WD. BSS formed via case D-MT could easily have wide orbit companions, with periods typically higher than the typical periods observed for BSS binaries in OCs.

What observational properties could be explained by the MT scenario? i) For some chemical peculiarities found in OCs, e.g., the low carbon-oxygen content of some BSS, case B may be invoked, and case C for the observed Barium-enhanced BSS found in the open cluster NGC 6819 (Milliman et al., 2014), since Barium is an element processed in the interior of AGB stars. More information regarding chemical peculiarities can be found in § 1.2.4. ii) The BS-WD systems (either CO or helium) detected using HST and UVIT—see § 1.2.6.1. iii) For long-period (LP) binaries, particularly cases B and C may be called into use. iv) Case A can explain some of the single blue stragglers with relatively initial low masses of primaries ($< 2\ M_{\odot}$), but also those that are still experiencing mass transfer; an example could be the semi-detached Algol system V228 in 47 Tuc (Kaluzny et al., 2007), since cases A and B MT are expected precursors of Algol systems. v) Finally, this scenario can explain the large number of W UMa contact binaries found among blue stragglers in GCs (Rucinski, 2000).

1.2.2 Dynamical encounters and stellar collisions

Almost parallel to the MT scenario, stellar collisions have been suggested as a channel for BSS formation (Hills and Day, 1976). Rather than for OCs, where the MT-scenario

probably contributes more to the straggler population, this channel could play a major role in BSS formation in GCs, especially in the dense cores. For collisions to contribute significantly to the observed blue straggler population in a stellar cluster —this scenario is irrelevant for the Field-BSS where physical collisions are rare!— a number of conditions must be satisfied: 1) collisions must occur at high rates within stellar clusters, where 60% to 70% of the collisions occurring whilst the star is on the MS. For evolved stars the percentage is lower ∼20% for giant stars, and less than 10% for HB and AGB stars.; 2) collisions must lead to the merger of stars and the very same must look like a moderately-massive main sequence star (i.e., consistent with observations) —collisions in GCs lead to mergers having little mass loss, typically 1-10% according to Benz and Hills (1992). Last but not least 3) the merger products must have a lifetime long enough to produce a sufficiently large population of blue stragglers —the merger must shed sufficient angular momentum to contract down to the MS (after the merger, the star does not appear immediately as an MS, as-is out of virial equilibrium and consequently expand).

In high density environments where dynamical encounters are more frequent than in GCs halos or in OCs, collisions between two single stars (s-s) can happen but not all of them lead to the formation of a blue straggler. Figure 1.5 shows some of the possible combinations (of stars on different phases of stellar evolution) that can be involved in collisions, but where only the interaction between two MS stars results in a straggler. On the other hand, if binaries are present instead, they will interact with other single star (s-b) or other binaries (b-b). During s-b and b-b encounters, physical collisions can occur between two or more MS stars taking part in the interactions. At present, however, there are no good diagnostics to observationally discriminate between collisional blue stragglers and binary mergers.

Some groups have modeled direct physical collisions between main sequence stars (Benz and Hills, 1987, Sandquist et al., 1997, Sills et al., 2001) and the subsequent evolution of the collision products (Sills et al., 1997) to investigate positions in the color–magnitude diagram, rotation rates and surface abundances. The equivalent work has not yet been done for binary mergers. With this approach, analytical studies of b-b and s-b encounters showed that the number of BSS in GCs cores can be recreated solely including collisions in b-b interactions. Here the resulting BSS is within a long period

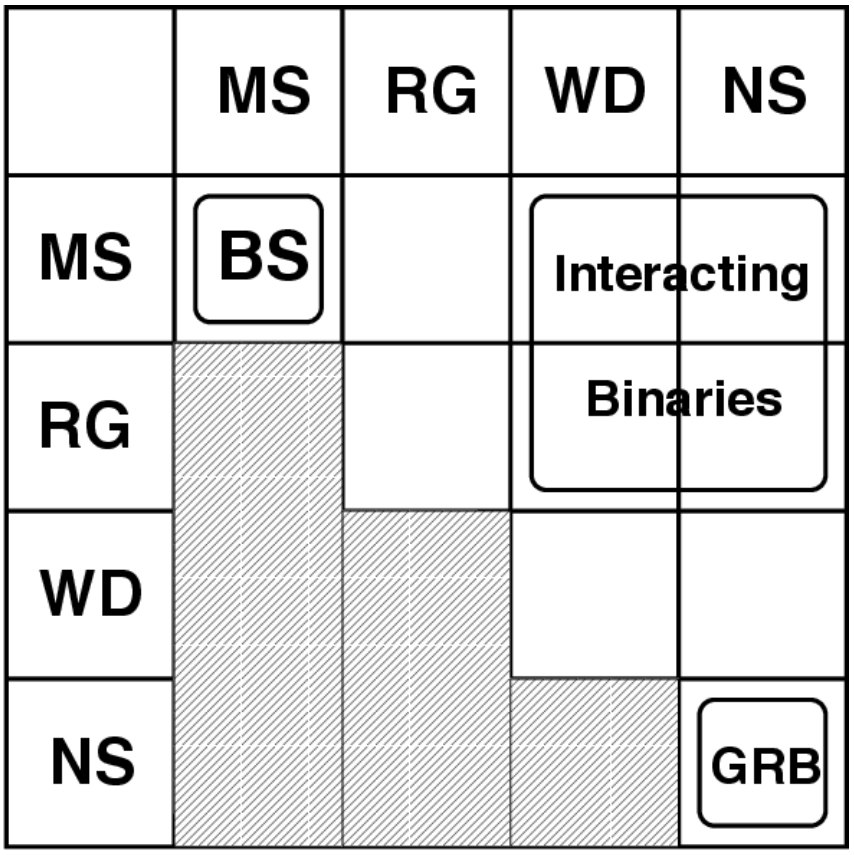

Figure 1.5 Results of possible collisions between various stellar species: main sequence stars (MS), red giants (RG), white dwarfs (WD) and neutron stars (NS). Collisions between two main sequence stars may produce at least some of the observed blue stragglers (BS). Collisions between either main sequence stars or red giants and white dwarfs or neutron stars may produce interacting binaries (cataclysmic variables and low-mass X-ray binaries). Encounters involving two neutron stars could potentially produce gamma-ray bursts (GRB). Figure taken from Davies et al. (2004).

binary system with a typical period of 10^3–10^4 days with an almost thermal eccentricity distribution. An example is shown in Figure 1.6 where the analytically calculated number of BSS almost perfectly match the observations only by assuming the BSS are created through binary star evolution with some contribution from collisions (Leigh et al., 2011). On the other hand, using Monte Carlo simulations, Chatterjee et al. (2013) found that for central densities of above $10^3\ M_\odot\ \mathrm{pc}^{-3}$, collisions in dynamical encounters is the dominant, if not the only, formation mechanism for BSS in globular cluster cores with a contribution up to 60% of the total BSS population. Here we would like to

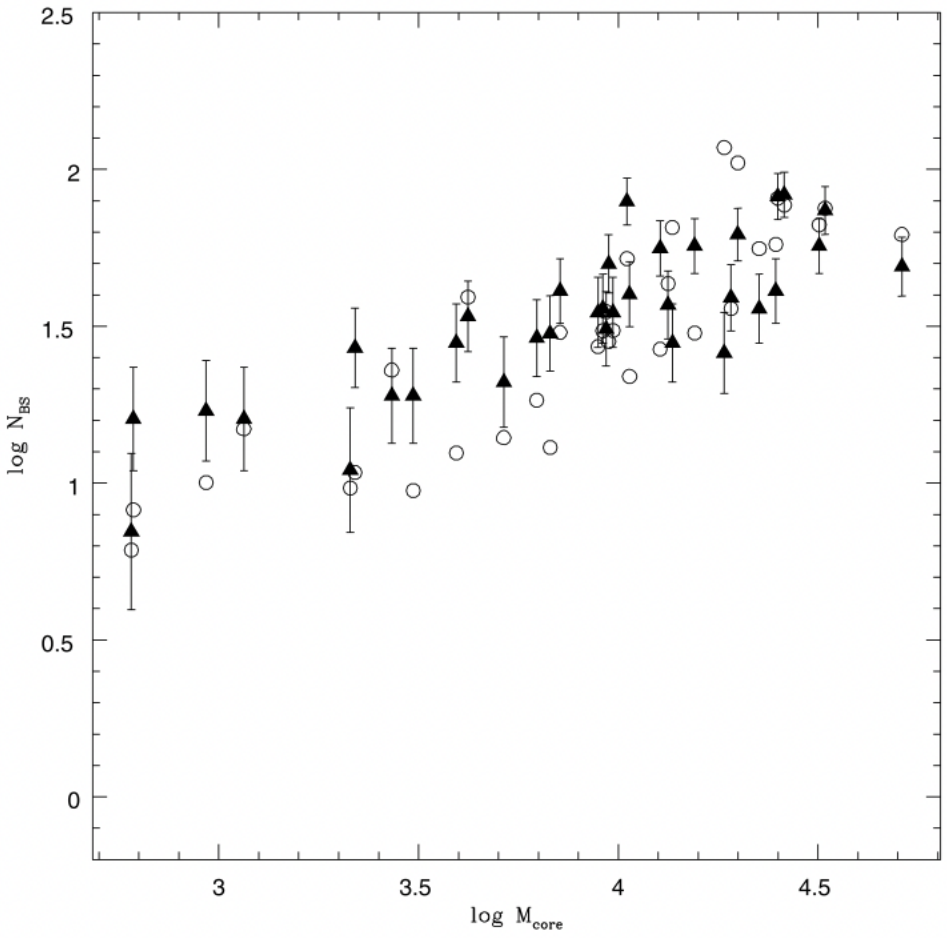

Figure 1.6 Comparison between the number of BSS in the core of GCs and the cluster core mass. Black triangles represent the observed numbers of BSS, while the analytically predicted ones are shown as open circles. Figure taken from Leigh et al. (2011).

point out that the majority of these collisions are binary-mediated, occurring during three-body and four-body interactions. Additionally, given the tight relation between the stellar collision rate (Γ_*) and the number density of stars, is it expected that there should be a strong correlation between Γ_* and the number of stragglers, especially in the cluster cores. However, only mild relations have been reported whose significance is not enough to safely assure that this correlation actually exists (Chatterjee et al., 2013, Piotto et al., 2004).

What observational properties can be explained by the collision scenario? i) The large

inferred masses from the CMDs. ii) The rapidly rotating blue stragglers with $v \sin\ i \geq 150$ km s^{-1} like, e.g., BSS-19 in 47 Tuc (Sills et al., 1997).

1.2.3 Kozai mechanism

Perets and Fabrycky (2009) suggested that triple stars could serve as natural progenitors for BSS, and in particular could explain the existence of eccentric and wide orbit BSS binaries observed in OCs (see § 1.2.6) as triples in which the inner binary has merged, leaving behind a BSS with a long period companion.

A hierarchical triple star system is a stable configuration of two stars orbiting each other (tight "inner binary"), in turn orbited by a third star at a much larger distance (wider "outer binary") with a common center of mass. If the inner binary initial inclination relative to the outer binary orbit is high enough, it is possible for the third star to introduce a combined effect of Kozai cycles and tidal friction in the inner binary which rapidly becomes a close or contact binary, which could then evolve through mass transfer or merger and produce a BSS. An example that clearly pictures this process is shown in Figure 1.7. Here, the initial system is an inner binary of two solar mass stars, at low eccentricity and $a = 2$ AU, orbited by a 0.5 $M_{\odot}$ star on a circular orbit at 50 AU. On short timescales, the eccentricity of the inner binary fluctuates (Kozai cycles, KC). On timescales of millions of years, tidal friction seals in a large eccentricity (KCTF), then damps the binary at constant orbital angular momentum (TF). Lastly, on a timescale of $\sim$1 Gyr, magnetic braking (MB) of the stellar spins drains the orbital angular momentum because the spins stay tidally locked, causing the binary to come into contact. After a contact evolutionary phase, the binary would merge to form a BSS accompanied by a main sequence star in a very wide orbit.

So, what observable BSS properties can be explained by this scenario? i) The binary frequency of BSS should be high, and most of them should be wide-orbit systems as found by Geller et al. (2015), Mathieu and Geller (2015). ii) The high inferred photometric masses of the BSS up to twice the TO mass in the case of a full merger of the inner binary that cannot be explained by MT cases B/C, where a significant mass is left on

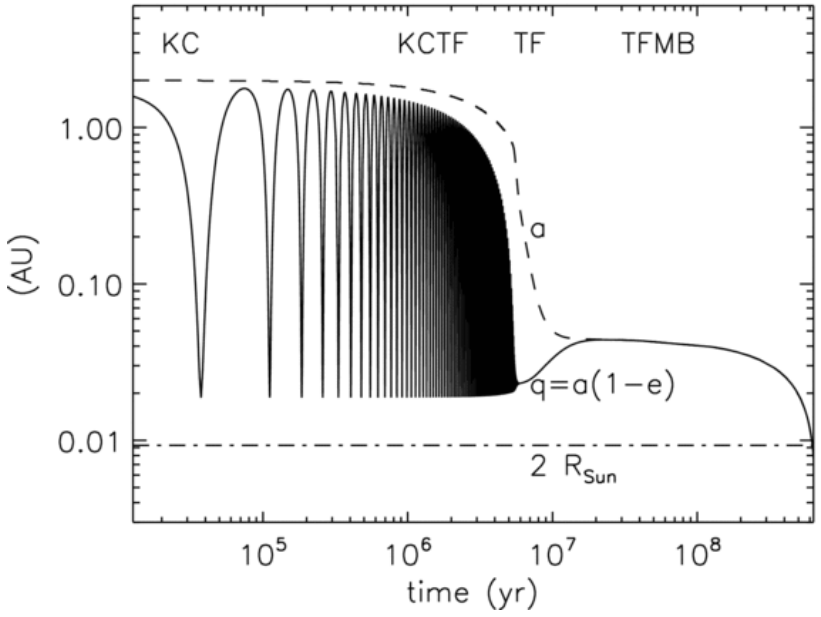

Figure 1.7 Merger of two stars of an inner binary (in a hierarchical triple system) over time, accomplished by a combination of Kozai cycles, tidal friction, and magnetic braking. Figure taken from Perets and Fabrycky (2009).

the WD companion and the MT efficiency is not expected to be high. iii) The period-eccentricity ($P - e$) diagram of BSS binaries should be similar to that of the outer binaries of triple systems (observed in the field) that have close inner binaries, which is difficult to reproduce by either the collisional or the binary mass transfer scenarios for BSS formation. Such comparisons can be found in Hurley et al. (2005) and Perets and Fabrycky (2009). iv) The presence of MS stars as companions of BSS within binary systems (e.g., WOCS 4004 in NGC 188, Milliman et al. 2014), in contrast with cases B/C MT whose outcome is a CO (0.5–0.6 $M_{\odot}$) or helium (0.15–0.45 $M_{\odot}$) WD—see § 1.2.1 for more details regarding the MT mechanism.

Current models of cluster populations that include the Kozai-Lidov mechanism show that it is unlikely that there is a dominant formation pathway for BSS. Monte Carlo models of GCs result in up to 10% of BSS forming through Kozai-Lidov cycles (Antonini et al., 2016), because of the complex interplay between triple evolution and other dynamical effects, specially in the dense cores. On the other hand, N-body models of OCs

yield 25% Kozai-Lidov BSS (Geller et al., 2013). These percentages are not far from observational studies that point to the same direction. Jadhav and Subramaniam (2021) have estimated, on a large sample of BSS in OCs (more than 800), that <10% formed via multiple interactions.

In conclusion, which mechanism is the dominant one? While case A MT can form a few BSS in a cluster, it cannot be a dominant formation scenario for BSS populations. Although case C MT scenario has instead been proposed to be the main mechanism for the BSS production in OCs (Geller et al., 2015, Gosnell et al., 2014, 2015), it is difficult to see how it can explain the majority of the OC BSS, especially because of the underestimated masses (i.e., too low luminosities), smaller than those inferred from the CMD locations. BSS formed through the case B of MT could easily have wide-orbit companions, and even their eccentricities need not to be much affected. However, the expected periods for this scenario are higher than the typical periods observed for BSS binaries in OCs. It is, however, highly probable MT is indeed the dominant scenario in low-density environments. On the other hand, evolution of primordial triples may help produce the observed binary BSS, not only naturally explaining the long orbital periods (this can also be explain with case C MT, e.g., in NGC 188) and high eccentricities (see Figure 1.11), but also explaining the very high binary fraction, and the high mass of the BSS inferred from the CMD. However, mergers in triple systems via Kozai-Lidov mechanism are not very common. In the collision scenario, the CMD location of full mergers is consistent with the observed BSS population, but then a third companion must be invoked to explain the binarity of the observed BSS populations; it can nevertheless be the responsible for forming the majority of BSS in dense stellar environments. In summary, independently of the formation channel, BSS are associated with binary or higher-order systems, but each channel is predicted to produce very different secondary companions and orbital parameters.

1.2.4 Chemical patterns

If BSS form through mass transfer, the material that is accreted last comes from more inner layers of the donor, where, e.g., the CNO cycle was active. We thus expect the

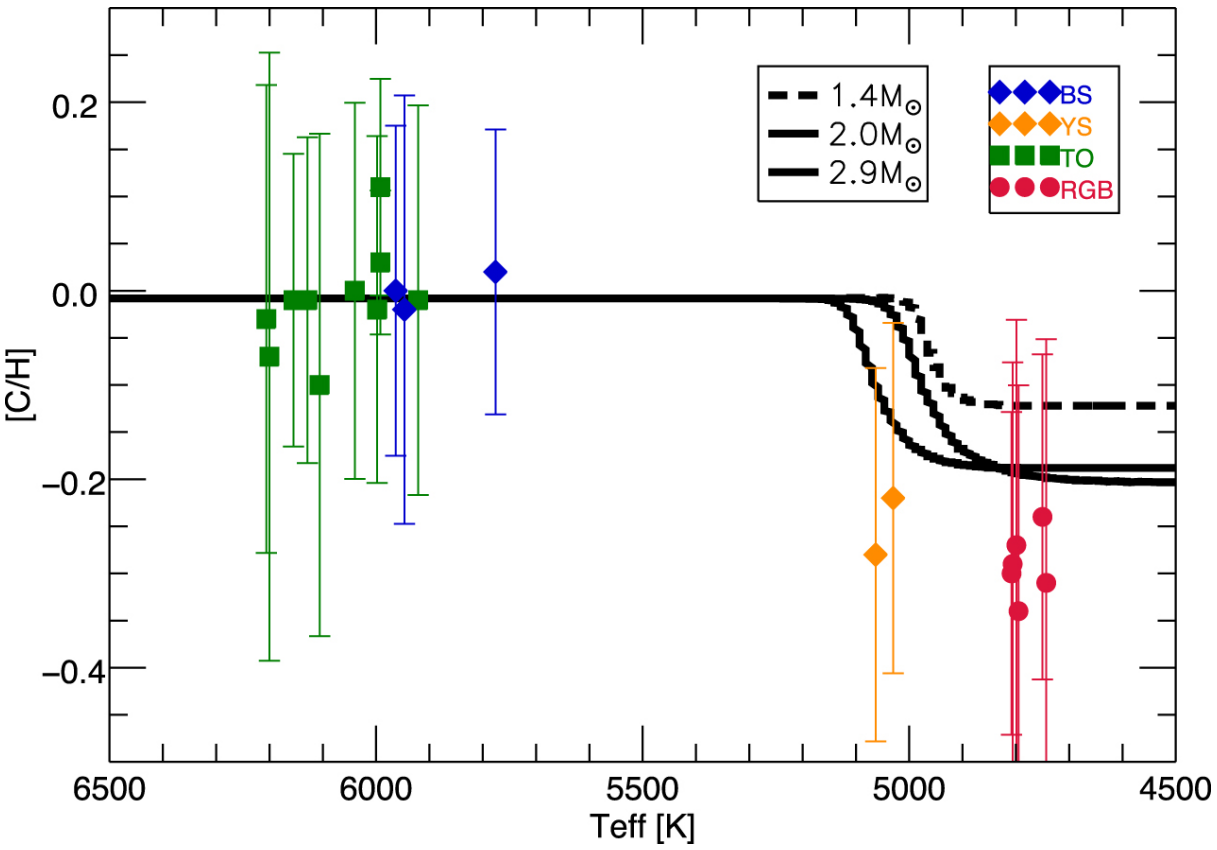

Figure 1.8 Carbon abundances obtained by Bertelli Motta et al. (2018) from their analysis for the BSS (blue diamonds), YSS (orange diamonds), and the control samples: RGB (red dots) and TO (green squares) stars, in the open cluster M67. Overplotted are the models of stellar evolution calculated for [Fe/H] = 0.00 dex and mass 1.4 $M_{\odot}$ (dashed line), 2.0 $M_{\odot}$ (solid line), and 2.9 $M_{\odot}$ (dotted line). Figure taken from the above reference.

BSS surface abundances of elements such as C, N, and O to be different from those of the parental cloud and, consequently, from the unevolved cluster members (Sarna and De Greve, 1996). If, instead, BSS form through a merger following the dynamical collision of two stars, simulations predict only a small amount of mixing between the stellar interior and the outer layers. For this reason, surface abundances in collisional BSS are expected to be the same as in MS or TO stars (Lombardi et al., 1995). Thus, the investigation of the surface chemical composition of BSS can provide hints of the circumstances under which they formed.

In this context, the Bologna group under the long-term Cosmic-Lab project[4] has contributed to make large strides in our understanding of the chemical compositions and characteristics of this exotic population. For some years they have been performing an extensive study of representative samples of BSS in several Galactic GCs, using the multi-object spectrograph FLAMES at the Very Large Telescope in Cerro Paranal, with the aim of obtaining abundance patterns and rotational velocities for these stars. In Ferraro et al. (2006) and Lovisi et al. (2013) a sub-population of carbon-oxygen-depleted BSS was found in 47 Tuc, M30 and ω Centauri. As mentioned above, this feature indicates that this material has been CNO-processed and then accreted by the blue straggler. On the other hand, in the GCs NGC 6397 and M4, but also in most on the stragglers of M30 and ω Centauri, no hints of CO depletion were found by Lovisi et al. (2013), suggesting that either the majority of BSS have a collisional origin (meaning no internal mixing), or that the CO depletion is a transient phenomenon. The same group reported for the first time evidence of radiative levitation[5] in BSS hotter than 8200 K and large spreads in iron content —up to more than 2 dex in NGC 6297 and up to ∼1 dex in NGC 6752. The stragglers suffering from this effect, cannot be used for the interpretation of C and O abundances in terms of BSS formation mechanisms. Another diffusion process generally ocurring simultaneously with radiative acceleration is the gravitational settling of Helium (He) — the same authors reported (in NGC 6397) an He content of Y=0.001, a value much lower than the normal He mass fraction of Y=0.25 .

In contrast to GCs, few spectroscopic analysis have been carried out on individual OCs. In NGC 6819, Milliman et al. (2013) found that five blue stragglers out of 12 have enhanced barium (Ba) abundances of up to 1.5 dex higher than cluster normal stars. The normal explanation for this chemical pattern is that the stars have accreted material from an AGB companion (case C of MT, § 1.2.1); however, none of these systems have binary properties consistent with those of an AGB donor. A similar attempt was carried out by Bertelli Motta et al. (2018) in M67 —see Figure 1.8. Here the analysis was performed only on three BSS (out of the 22 found by Geller et al. 2015) and on two YSS; the BSS candidates showed surface abundances similar to main sequence TO stars. The YSS were found to be instead consistent with the abundances of the red clump stars,

[4] http://www.cosmic-lab.eu/Cosmic-Lab/Home.html

[5] The main effect of Radiative levitation is that many chemical elements are pushed toward the stellar surfance, thus altering the initial chemical composition

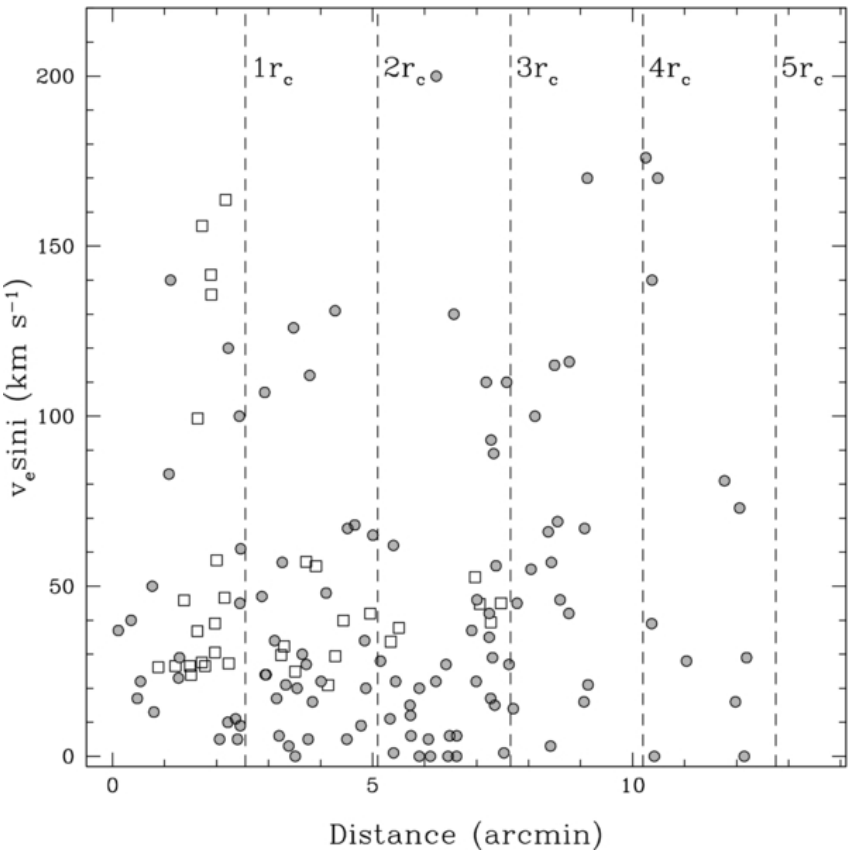

Figure 1.9 This figure taken from Mucciarelli et al. (2014) shows the rotational velocities for their BSS sample in ω Centauri, as a function of the distance from the cluster center. FLAMES targets are gray circles and BSS from Simunovic et al. (2014) are included (empty squares) for comparison. The vertical dashed lines mark the distance from the cluster center in units of the core radius.

by ∼0.25 dex carbon-depleted, which can be either interpreted as the signature of mass transfer or as the product of stellar evolutionary processes. Similarly, Andrievsky et al. (2000) found BSS showing the same chemical peculiarities as ordinary cluster and galactic field stars of the same spectral type, with only two BSS displaying a lower lithium content. In all the investigated stars for which the carbon abundance could be measured, they found moderate to strong deficiency of this element, as compared with which is observed in the GCs.

1.2.5 Rotational velocities

Accurate high-resolution spectroscopic studies not only revealed the presence of the chemical anomalies discussed above, but also showed that different stellar populations in GCs and OCs can behave differently also in terms of their kinematical properties, and in particular rotation. While TO and subgiant branch stars in GCs ($\sim$ 12 Gyr) always show low rotational velocities (a few km s^{-1}, Lucatello and Gratton 2003), a bimodal rotational velocity distribution has been observed in HB stars (whose analogous in OCs are the red clump stars): the cooler HB stars ($T_{\rm eff} < 11\ 000$ K) have rotations between 10 and 40 km s^{-1} (much faster than old MS stars), while hotter HB stars rotate at less than 10 km s^{-1} (Peterson et al., 1995, Recio-Blanco et al., 2002, 2004). On the other hand, rotational velocities of A and F —typical spectral types of BSS— stars in OCs are generally lower than 100–150 km s^{-1} and do not manifest obvious trends with stellar temperature or chemical abundance (Gebran et al., 2010).

Concerning BSS, a rapid rotation is expected in the MT scenario because of the angular momentum transfer (Sarna and De Greve, 1996). High rotational velocities are also expected for collisional produced BSS (Benz and Hills, 1987), but some magnetic braking or disk locking mechanism might intervene to significantly decrease the rotation (Leonard, 1996). Unfortunately, the efficiencies and time-scales of these mechanisms are still unknown, thus preventing a clear prediction of the expected rotational velocities. From an observational point of view, the GCs M4 (Lovisi et al., 2010) and ω Centauri (Mucciarelli et al., 2014) host the largest fraction of BSS with rotational velocities $\mathrm{V \sin\ i} > 50$ km s^{-1}, namely, $\sim$40% and $\sim$30%, respectively. Some hints of radial behavior of the fast rotating BSS in ω Centauri, showing a mild peak within one core radius and a possible rise in the external regions beyond four core radii has been suggested (Mucciarelli et al. 2014, Figure 1.9). These trends would imply that there might have been recent formation episodes of MT BSS that occurred preferentially at the outskirts of the cluster, or that braking mechanisms able to slow down these stars are less efficient in low-density environments. Furthermore, in other clusters the percentages of fast-rotator BSS are: 6% in NGC 6397 and 7% in M30 (Lovisi et al., 2013).

Observations of BSS in open clusters instead show that at least some of those in, e.g.,

NGC 188 (7 Gyr) and NGC 6819 (2.5 Gyr), are rotating more rapidly than normal main-sequence stars at the same effective temperature and at the corresponding age, with $V \sin\ i \leq 50$ km s^{-1} (Geller and Mathieu, 2011). Interestingly, the rotation rates decrease with decreasing surface temperature, as the MS stars do in the same temperature range. On the other hand, a detailed analysis on Kurucz's atmosphere models revealed that BSS in the open clusters NGC 3496, NGC 6475, NGC 6633 and IC 2602 (Andrievsky et al., 2000) have significantly smaller projected rotational velocities. Some extremely fast rotators BSS ($V \sin\ i \leq 100$ km s^{-1}) where found by Rain et al. (2020), hereafter R20, and Rain et al. (2021), hereafter R21, in Trumpler 5; however, also several BSS with $V \sin\ i \leq 30$ km s^{-1} in Collinder 261, Trumpler 20 and NGC 2477. No considerable rotation was detected in the only YSS they observed.

1.2.6 Binarity and mass distribution

Contrary to GCs, where BSS located in the crowded center are not suitable for spectroscopic studies, the much less dense OCs allow a deep dive into the blue straggler characteristics, particularly their binary nature. Thanks to long-term spectroscopic monitoring, we have an excellent understanding of the binary properties of blue stragglers in a few old open clusters: M67, NGC 188, NGC 6819 and NGC 7790.

Thanks to the tremendous effort carried out by the CIERA/Northwestern University group, using data of the WIYN Open Cluster Study (WOCS project, Mathieu 2000), there is now strong evidence that many BSS formed through MT from an evolved star onto a MS star. The BSS in NGC 188 and M67 (Geller et al., 2015, Mathieu and Geller, 2015) have a binary frequency of 80% for orbital periods less than 10^4 days, when in normal MS stars this percentage is around 25%. These LP binaries show a companion-mass distribution that is narrow and peaked around 0.5–0.6 $M_\odot$ (Figure 1.10). This distribution shows strong statistical evidence consistent with the fact that CO-white dwarfs are left behind after a case C of MT. On the same Figure is plotted, for comparison, the distribution of solar-type main sequence binaries.

In both NGC 188 and M67 a small fraction ($\sim 10\%$) of short-period binaries was also identified. Among them, some double-lined systems are present, in which we can

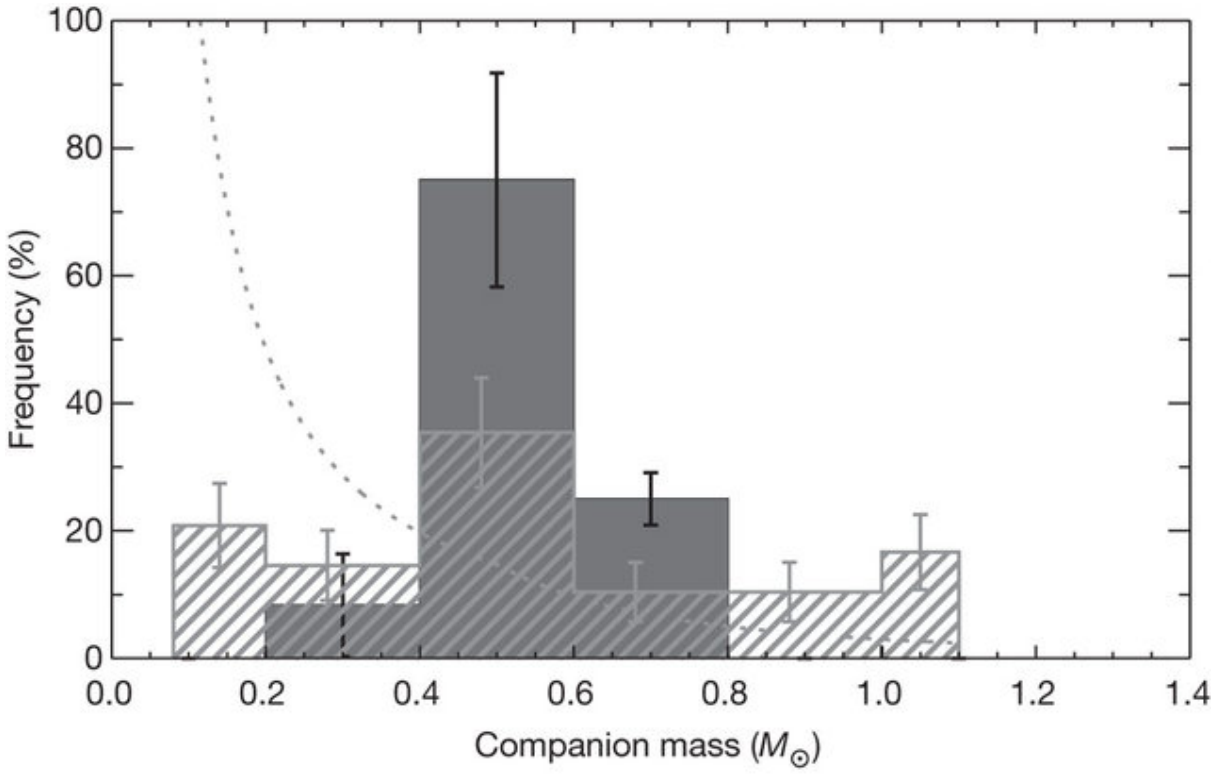

Figure 1.10 Secondary-star mass distribution for the 14 blue straggler binaries in the old open cluster NGC 188 with periods of about 1000 days (Mathieu and Geller, 2015). For the sake of comparison, it is also plotted with dashed line an initial mass function for single stars with masses between 0.08 $M_\odot$ and 1.1 $M_\odot$. This distribution is similar to that of the secondary masses of the NGC 188 main-sequence binaries. The grey hatched histogram shows the field tertiary mass distribution, evolved to 7 Gyr in isolation, not discussed in this thesis. The reader can find more information in the given reference.

directly detect a companion and infer a mass for each star. NGC 188 hosts an intriguing close system, WOCS ID 7782, that could have formed through dynamical channels. It is a double-lined binary whose circular orbit has a period of ~ 5 days, with a mass ratio of $q = 1.005$ and effective temperatures $T_{\rm eff} > 6300$ K for both primary and secondary (higher than the MSTO) makes this object unique since it contains two blue stragglers. None of the formation mechanisms proposed can explain the conditions to form two blue stragglers simultaneously in a 5-day-period binary, so this star is a clear evidence of one or more dynamical encounters. On the other hand, WOCS 5379 is a 120-day-period binary with a 0.4 $M_\odot$ helium WD companion, and is probably the most clear example of MT formation from a RGB, i.e., of case B MT (Gosnell et al., 2019), with a

mass transfer efficiency calculated to be 22% (Sun et al., 2021) that explains the star's redder position on the CMD, compared with other stragglers in the same cluster. The double eclipsing blue straggler S1082 in M67 is a star that displays a partial eclipse with a photometric period of 1.07 days, but with an almost negligible velocity variability, and no signs of a period consistent with the photometric one; this contradiction was resolved when it was shown that the system consists indeed of four stars comprising a short-period eclipsing binary and a more luminous blue straggler in a LP binary (Sandquist et al. 2003, van den Berg et al. 2001).
In NGC 6819, instead, only four out of 12 BSS display velocity variability, which is $\sim 30\%$ (Hole et al., 2009) as opposed to the large frequency of binaries in NGC 188. One of these variable stars has been found to be composed by a Barium-enhanced primary star and a luminous secondary that could be either a BSS or a MS star (not a white dwarf!). WOCS 4004, with a period of 297 days and $q = 0.73$, has a complicated history involving mass transfer from an evolved donor followed by a dynamical encounter (Milliman et al., 2014). Finally, in NGC 7789, as in the previous case, only a 33% of the BSS were detected as velocity-variable stars; four of them, with complete orbital solutions (WOCS 5011, 10011, 20009 and 36011), are single-line binaries. WOCS 5011 and WOCS 20009 are LP binaries and are consistent with mass transfer from AGB stars. WOCS 35011 has a shorter period of ~ 200 days and is likely the result of mass transfer from an RGB star, similar to WOCS 5379 in NGC 188. Many other interesting cases can be found in Boffin et al. (2014).

The period distribution of the BSS-binaries is different to that of the MS-binaries. An example (NGC 188) is shown in Figure 1.11. As mentioned above, most of the BSS-binaries have orbital periods of ∼1000 days (blue filled circles with errors), whereas the MS-binaries (green filled circles) populate all periods from very long (like in the case of the stragglers) down to only a few days. Moreover, the eccentricity distribution of the LP-BSS also differs from the solar-type binaries. For the particular case of NGC 188, the mean eccentricity of the LP-BSS (0.27±0.05) is higher than the one of MS-binaries (0.42±0.04) as reported by Geller et al. (2009). The fact the position on the $\mathrm{P} - \mathrm{e}$ diagram of BSS is strikingly similar to that of the post-AGB system, just confirms the hypothesis these stars have formed via MT. Furthermore, Gao et al. (2022) recently found RLOF from a tertiary in a hierarchical triple system can potentially lead to surface

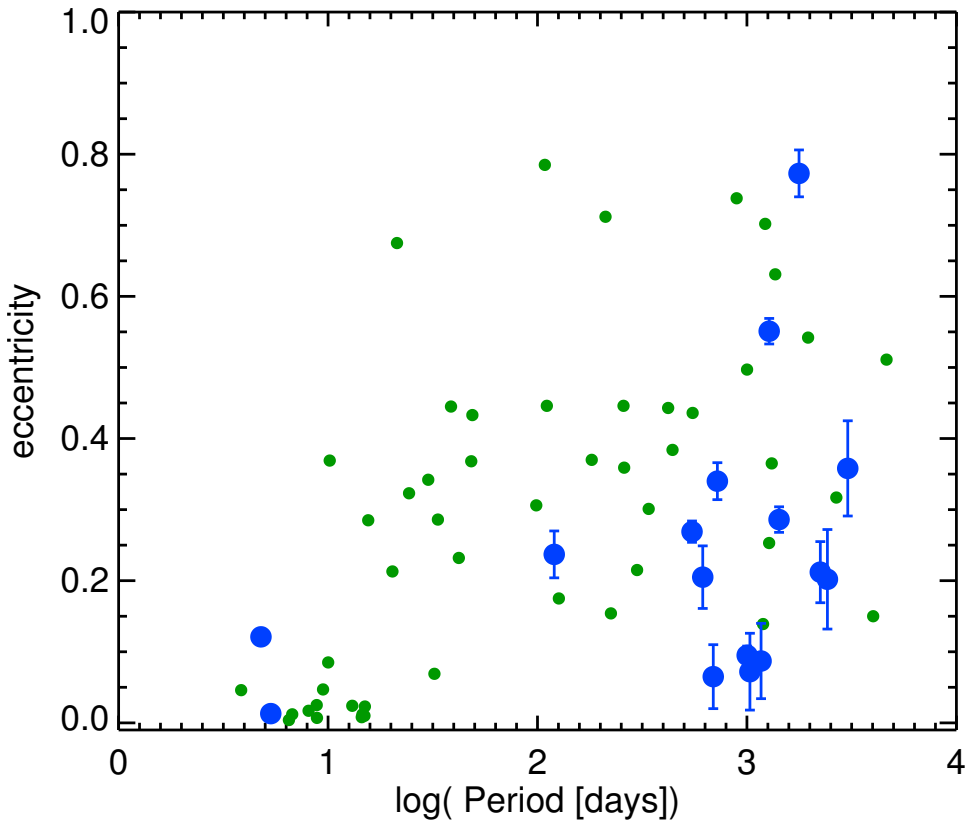

Figure 1.11 Eccentricity-Period diagram (e vs. log(P)) for the blue straggler binaries in the old open cluster NGC 188 with periods of about 1000 days (Mathieu and Geller, 2009). In green the solar-type main-sequence binary stars. In blue the Blue straggler binary stars. Errors in eccentricity are 1σ; errors in period are smaller than the data points.

barium enrichment within the inner binary, while at the same time causing the inner binary to merge, thereby producing a barium star and/or double BSS like that observed in NGC 188 (WOCS ID 7782) and by Milliman et al. (2014).

In any long-term spectroscopic follow-up study, there is always the risk of finding, beyond the detection threshold, non-radial velocity variable BSS that might still be binaries with long orbital periods. It is important therefore to explore different techniques to fully characterize the binary nature of BSS, which is not exclusive of the MT scenario since, as discussed above, it can be influenced by dynamical encounters and the presence of a third or more stars.

We know less about the binary properties of BSS in GCs. Although binaries in globular clusters are often identified by their offset to the red of the main sequence isochrone, defining a "second main-sequence" almost parallel to the real one —that we obviously called the "binary sequence"— we cannot clearly identify blue stragglers binaries by their position in the CMD alone, since there are no evolutionary tracks that can describe them as in the case of the binaries. Although different types of photometric short-period variables (eclipsing binaries, Algols, SX Phe stars and W UMa contact binaries) have been known among the blue straggler populations of globular clusters for many years (Mateo et al., 1990), spectroscopic monitoring is needed to be undertaken to fully characterize the binary nature of blue stragglers in globular clusters.

1.2.6.1 White Dwarf companions

As mentioned previously, white dwarf (WD) stars have been suggested to be the companions of BSS formed through Case B or Case C mass transfer (MT). If the mass transfer ended within the past 400 Myr, the WD companion should be hot enough to be detected as a far-ultraviolet (FUV) photometric excess above the emission expected for the BSS alone, as shown in Figure 1.12. Here, synthetic photometric models are compared together with the NGC 188 straggler population. The emission from BSS without a WD companion is faint and red (gray contours) but increasing temperature results in bright, blue emission (rainbow-colored tracks), the three blue stragglers FUV excess; WOCS 5379, WOCS 4540 and WOCS 4348 are overplotted in black dots together with their errors.

Using HST data Gosnell et al. (2014, 2015) found that around 30% of the stragglers of NGC 188 have young WD companions; seven out of the 14 LP BSS formed from recent MT, this is before 400 Myr and, among them, there are four “hot” stars ($T_{\rm eff} > 12000$ K), and three “cool” stars ($11000 < T_{\rm eff} < 12000$ K). Just because for the remaining seven stars no WD companions were detected, their formation through MT cannot be ruled out. Similar analyses were carried out in the straggler populations of the GC NGC 5466, and the OCs NGC 7789 and M67, using Ultra-Violet Imagining Telescope (UVIT) data. In M67, a FUV excess was detected in the brightest 11 out of the 14 BSS identified as members by Geller et al. (2015); WOCS 1025, WOCS 5005, WOCS 1006, WOCS 1007, WOCS 2011, WOCS

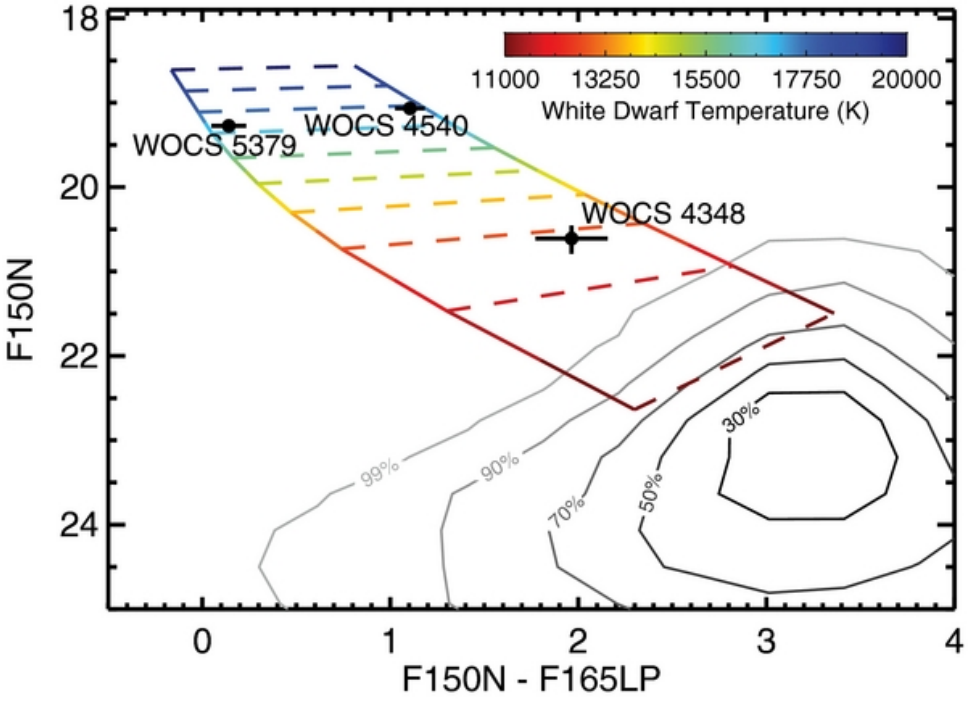

Figure 1.12 Far-UV color–magnitude diagram showing the positions of WOCS 4540, 5379, and 4348, with the respective 2σ error bars (Gosnell et al., 2014). The gray contours show the expected density distribution of single BSS with temperature and luminosity distributions matching the BSS population in NGC 188. The colored lines track synthetic BSS–WD pairs with increasing WD temperature as indicated by the color bar. The lower and upper solid lines follow binaries with BSS temperatures of 6000 K and 6500 K, respectively. The dashed lines track constant WD temperature from 11,000 K to 20,000 K in increments of 1000 K.

2009, WOCS 2013, WOCS 3005, WOCS 3013 and WOCS 4006 have WD companions within a mass range 0.20–0.35 $M_{\odot}$, $11000 < T_{\rm eff} < 24000$ K and ages between 25 and 300 Myr (Jadhav et al., 2019, Pandey et al., 2021). Since some of the detections are extremely low-mass (ELM) WDs (∼38%; 5/14 of the BSS), it is suggested that case B of MT has been the prevalent one in M67. In the case of NGC 7789, five hot companions to BSS were recently detected: WOCS 20009, WOCS 25008, WOCS 25010, WOCS 10011 and WOCS 15015, which corresponds to a ∼33% (5 out of 15 BSS candidates), with $11750 < T_{\rm eff} < 15500$ K and, as in the previous cluster, these stars are most likely ELM WDs with masses smaller than $0.18\ M_{\odot}$ (Vaidya et al., 2022). Finally, in NGC 5466 only one BSS (NH84), located at the outskirts of the cluster, revealed the presence of a hot companion with $T_{\rm eff} = 8000$ K and 32000 K for the BSS and WD, respectively (Sahu et al., 2019).

1.3 How BSS correlate with the cluster environment?

It is not a surprise that BSS have been identified in globular clusters, open clusters, the galactic bulge, disk, halo and even in external dwarf galaxies. Searching relations between the straggler number and cluster parameters such as mass, integrated magnitude, binary fraction, age, and the collision rate is something that has been done extensively in the literature. It is, however, in GCs where all of these relations have been studied, so most of the information that we at present manage today comes from these systems. The normalization of the number of stragglers to some global cluster parameter is common practice. The ratio ($F_{\rm ref}^{\rm BSS}$) is known as the "specific frequency" of blue stragglers, which plays a very important role when trying to perform meaningful comparisons between different clusters; *ref* is usually the number of a reference population that follows the cluster light, e.g., MS, TO, RGB, HB, etc. In the literature many definitions of $F_{\rm ref}^{\rm BSS}$ have been proposed (de Marchi et al., 2006, Ferraro et al., 2012, Momany et al., 2007, Sollima et al., 2008, and references therein). We present some of the most commonly used $F_{\rm ref}^{\rm BSS}$ in Appendix C. Some unavoidable sources of errors, however, could affect the blue straggler frequency, namely, photometric incompleteness, field contamination, confusion between BSS and normal MSTO stars, just to mention some of them.

The current information we manage is the following. The specific frequency of blue stragglers is basically the same—high—in the low-density environments of dwarf galaxies (Momany et al., 2007), the Milky Way halo and open clusters (de Marchi et al., 2006), and even in the lowest density globular clusters (Piotto et al., 2004). However, at a sufficiently high density, the specific frequency of blue stragglers begins to drop, and continues to decrease as the density increases. The last one trend appears contrary to expectations if blue stragglers are produced through stellar collisions, but may in fact be telling us that they are primarily made through binary processes. As the stellar density increases, the collision rate increases and destroys the binaries which would have made blue stragglers if they had been left undisturbed. This is supported by several findings where Milky Way GCs provide additional evidence that binaries are more important than collisions in producing BSS. For example, Piotto et al. (2004) found no statistically significant trends between the $F_{\rm HB}^{\rm BSS}$ and the expected collision rate in

the cluster core, but instead the straggler number ($N_{\rm BSS}$) correlates best with the core mass ($M_{\rm core}$), and hence the number of core binaries (Knigge et al., 2009, Leigh et al., 2013), even in the highest density clusters. This is shown in Figure 1.13, taken from Knigge et al. (2009); these authors found a power-law dependence $N_{\rm BSS} \propto M_{\rm core}^{0.38\pm0.04}$ and strong correlation values across the full sample (high-density and low-density GCs) given by the Spearman rank test[6]. There is also a correlation between the core binary fraction $f_{\rm bin}$ and $F_{\rm MS}^{\rm BSS}$ in low-density clusters (Sollima et al., 2008)[7] that becomes even stronger by including the central velocity dispersion of the cluster σ_v. Surprisingly enough, the binary fraction is not the strongest predictor of blue straggler population size, but $M_{\rm core}$ as reported by Leigh et al. (2013).

Only very recently (Jadhav and Subramaniam, 2021) the dependence of $N_{\rm BSS}$ and the total mass $M_{\rm tot}$ has been examined for OCs. The authors found a dependence of $N_{\rm BSS} \propto M_{\rm tot}^{0.37\pm0.10}$ for clusters with at least 10 BSS candidates; they also reported a maximum of $N_{\rm BSS} \propto M_{\rm tot}^{0.6}$ for all clusters. They also found that $N_{\rm BSS}$ is not dependent on the density, radius, distance, Galactocentric distance, or number of stars near the TO; finally, they also concluded that $F_{\rm TO}^{\rm BSS}$ has no correlation with age, but has positive correlation with respect to the cluster relaxation. This could be partly due to evaporation of lower mass stars in relaxed clusters, or more likely due to the inverse relation between cluster mass and relaxation. On the other hand, in R21b and Leiner and Geller (2021) a clear positive increment of the BS frequency with the cluster age (either in logarithm scale and linear) was observed for clusters of ages between 1 and 6 Gyr, with a plateau at $F_{\rm RGB}^{\rm BSS} \approx 0.35$.

[6]The Spearman correlation function provides both a correlation coefficient (r_s) and the significance level at which the null hypothesis of zero correlation is disproved (p-value), which basically represents the probability that any random sample of uncorrelated data-points would yield a correlation.

[7]In this study the authors chose to use the Pearson correlation test instead of Spearman's, like Knigge et al. (2009). They found a Pearson correlation coefficient $r = 0.820$ and a confidence level $p = 0.9998$ when comparing $f_{\rm bin}$ and $F_{\rm MS}^{\rm BSS}$.

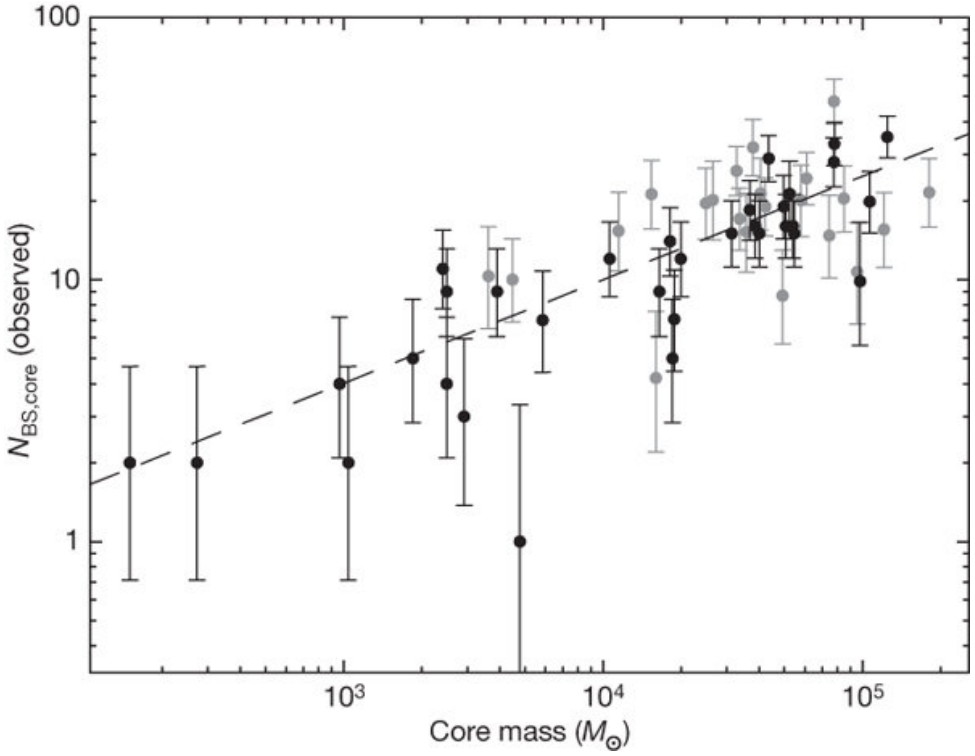

Figure 1.13 Relation between core mass ($M_{\rm core}$) and the straggler numbers ($N_{\rm BSS}$), according to Knigge et al. (2009). Black points correspond to high-density clusters ($\rho > 10^4$ pc^{-3}), and grey points to low-density clusters ($\rho < 10^4$ pc^{-3}). The error bars shown are approximately 68% Poisson confidence intervals. $N_{\rm BSS}$ and core masses are strongly correlated ($r_S = 0.71$, p-value $= 4 \times 10^{-10}$, $N = 56$), as expected if blue stragglers are descended from binary systems. The correlation with core mass also holds for the subset of dense clusters ($r_S = 0.84$, p-value $= 3 \times 10^{-10}$, $N = 34$), and in both cases is stronger than that with collision rates. The dashed line is a power-law fit to the full set of clusters, obtained by a method appropriate for this type of data set.

1.4 Blue straggler stars radial distribution and segregation

Estimating the formation epoch of a cluster (or chronological age of its stars) is relatively simple from the measure of the luminosity of the MSTO level, while measuring its "dynamical age" (corresponding to the level of dynamical evolution it reached since formation) is much more challenging. Irrespective of their formation mechanism (see § 1.2), BSS (because of their masses) can be used as powerful gravitational probes to

investigate key physical processes (such as mass segregation and dynamical friction[8]) characterizing the dynamical evolution of star clusters.

Figure 1.14 shows the specific frequency—calculated with Eq(1) of Appendix A—as a function of the radial distribution of several GCs. The distribution shows generally a large peak (per unit luminosity or per unit of "normal stellar population") at the center, a lack of blue stragglers a little further out (reaching a minimum at a radius $r_{\rm min}$ and then the frequency of blue stragglers rises again to a constant value in the outskirts of the cluster. Ferraro et al. 2012, (hereafter F12) found that the $r_{\rm min}$ value is related with the dynamical age of the cluster, and grouped the clusters in three different families. Although this fact had been previously suggested by some authors on a handful of individual clusters studies (Beccari et al., 2011, Dalessandro et al., 2008, Ferraro et al., 1993, 2006), the biggest compilation is that presented by F12. This grouping corresponds well to an effective ranking of the dynamical stage reached by stellar systems, thereby permitting a direct measure of the cluster dynamical age purely from observed properties, so they called it the *Dynamical Clock*. Clusters of *Family I*, or dynamically young GCs, show a flat distribution; in these systems the dynamical friction has not yet caused visible effects, even in the innermost regions. In *Family II* GCs, the dynamical friction has become more efficient and the mass segregation has started, which has led to the presence of a peak at the center, and a minimum at small radii of the blue straggler distribution. The outskirts of Family II clusters have still not been affected by the dynamical friction, i.e., it has not reached the most remote BSs, and therefore there is a rise of the BS density in these outer regions. Finally, when the system is highly evolved, the external maximum disappears, and the only noticeable peak in the distribution is the central one; GCs showing this profile are grouped in the *Family III*. A more refined *Dynamical Clock* was proposed by Alessandrini and Cosmic-Lab Team (2016), whose parameter A^{+} measures the area confined between the cumulative radial distribution of the BSS and a reference population—for a better understanding we

[8] *Dynamical Friction* effect explains why the most massive stars of stellar clusters tend to be found/-concentrated near the center of star cluster (mass-segregation!). This friction results when a heavy particle (in this case the BSS) moving through a "sea" (of normal stars of the cluster) of much lighter star particles experiences a retarding force due to the exchange of energy and momentum. The efficiency this effect decreases for increasing radial distance as a function of the velocity dispersion and mass density. Further, explaining dynamical friction effect on his totality is far from the scope of this thesis

added one example in Figure 1.15, so clusters with large A^+ values are more dynamically evolved. The great advantage of using A^+ instead of r_{min} is the binning of the data required to see the r_{min} in the distribution. So, as a cluster evolves, BSS start to segregate in the cluster center more rapidly than any reference population, leading to increasing separation between the two cumulative radial distributions. Lanzoni et al. (2016) performed the first observational estimation of A^+ in 25 GCs and found that this parameter nicely correlates with the position of the minimum of the BSS normalized radial distribution and with the cluster central relaxation time.

Many theories have been proposed to explain this bimodality as to be the signature of two formation mechanisms acting simultaneously in the same cluster: the external BSS would be generated from MT activity in primordial binaries, while the central BSS would be generated by stellar collisions leading to mergers (Ferraro et al., 1997), or that all the BSS were formed in the core by direct collisions and then were ejected to the outer regions by the recoil of the interactions (Sigurdsson et al., 1994). The BSS kicked out to a few core radii would rapidly drift back to the center of the cluster due to mass segregation, thus leading to the central BSS concentration and a paucity of BSS in the intermediate regions. More energetic recoils would kick the BSS to larger distances and, since these stars require much more time to drift back toward the core, they may account for the overabundace of BSS in the cluster outskirts. Nevertheless, models of BSS dynamical evolution in a number of specific clusters (Mapelli et al., 2004, 2006) demonstrate that the observed BSS bimodal distribution cannot be explained within a pure collisional scenario in which all the BSS are generated in the core through stellar interactions. Some other authors have pointed out, however, that the presence of r_{min} and its evolution with the dynamical time might be caused by dynamical friction of the heavier blue straggler progenitors against the normal stars in the cluster, causing them to fall into the center with time. This is also confirmed by the dynamical simulations of Mapelli et al. (2006) and Lanzoni et al. (2007), showing that the radial position of the dip of the BSS radial distribution sensibly depends on the dynamical friction efficiency within the cluster, while flat BSS distributions indicate little or no dynamical evolution of the system.

A similar work in open clusters has been recently carried out by Vaidya et al. (2020).

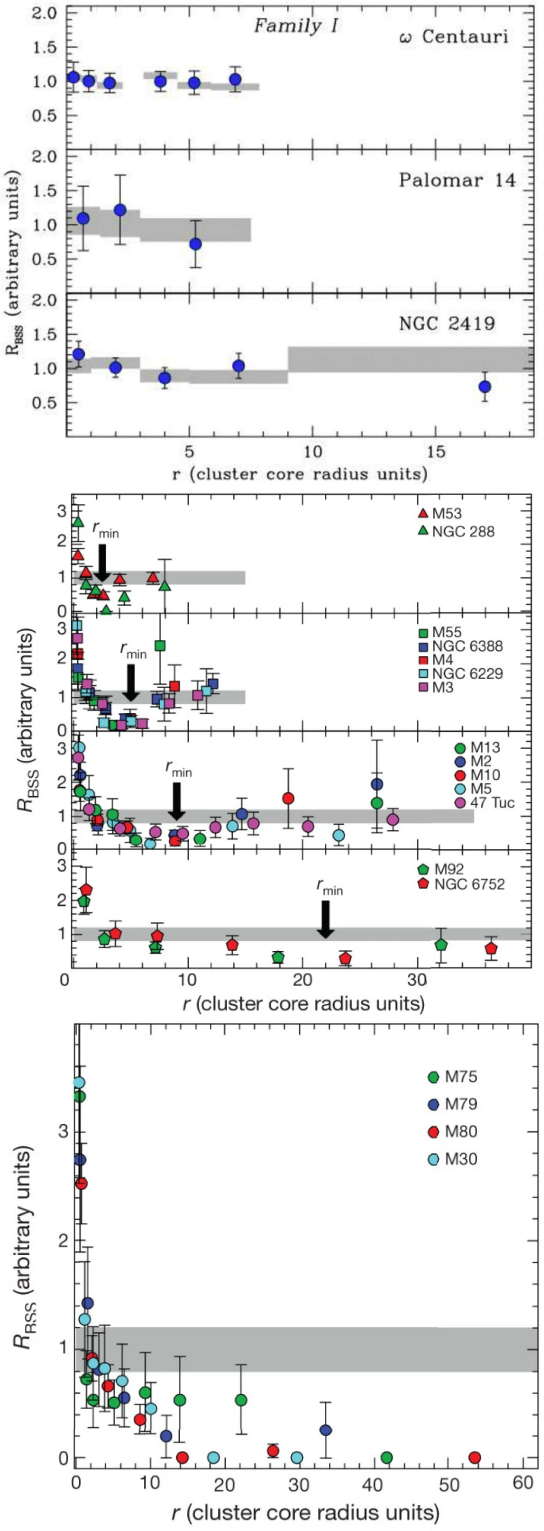

Figure 1.14 These plots taken from Ferraro et al. (2012) show the normalized radial distribution of BSS (colored symbols) compared to that of normal cluster stars taken as reference (gray strips) in the following families. Family I: dynamically young clusters (top panel); Family II: dynamically intermediate-age clusters (central panel); and Family III: dynamically old clusters (bottom panel).

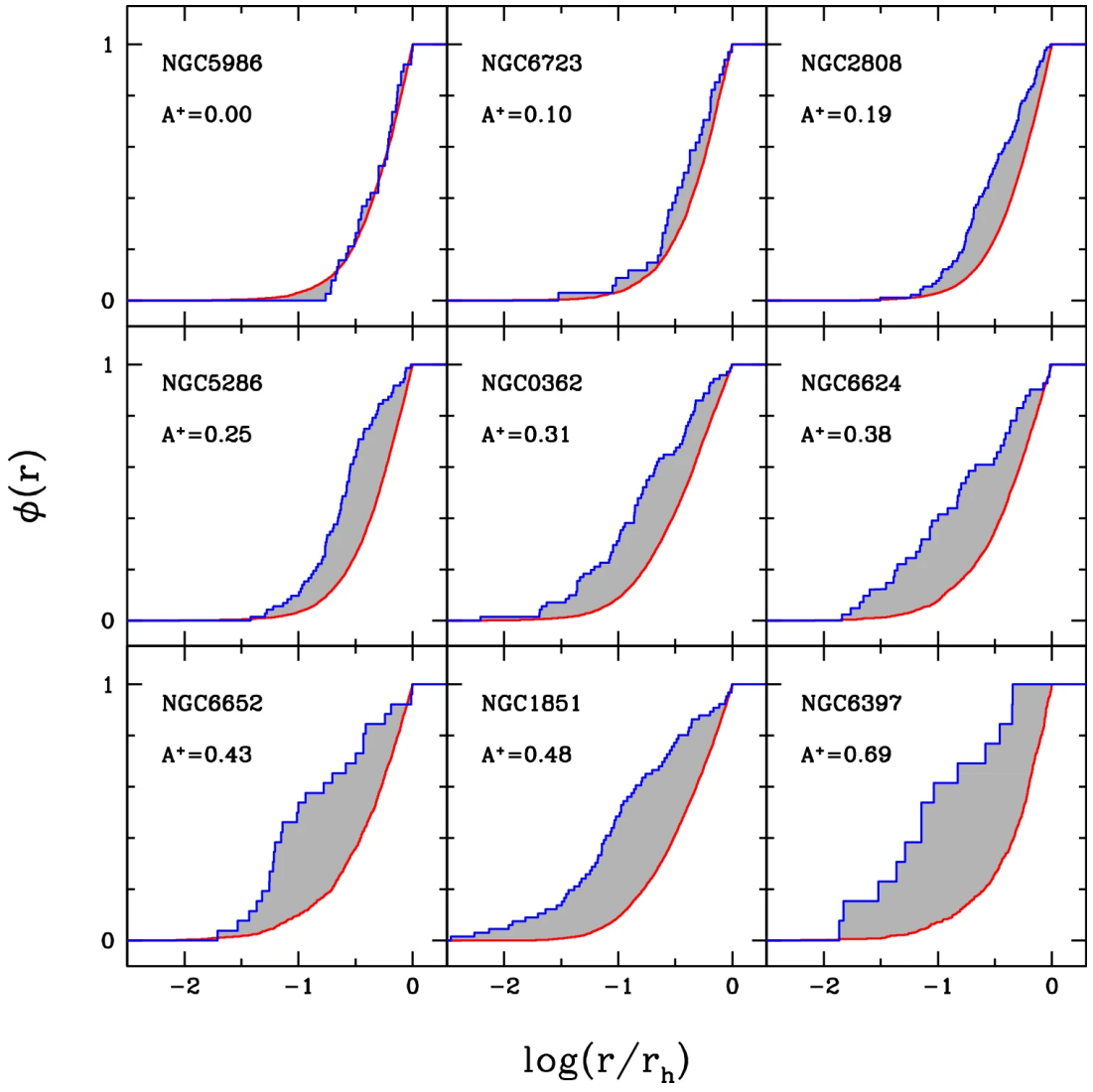

Figure 1.15 Cumulative radial distributions of BSS (blue lines) and the reference stars (red lines) in nine GCs (Lanzoni et al., 2016). The horizontal axis provides the logarithm of the cluster-centric distance, in units of the half-mass radius r_h. The size of the area between the two curves (shaded in gray) corresponds to the labeled value of A^+. Clusters are ranked in terms of increasing value of A^+.

The authors determined accurate stellar membership and studied the BS radial distribution in seven open clusters. Five of them (Melotte 66, NGC 2158, NGC 2506, NGC 188, and NGC 6791) were assigned to Family II. In the remaining two clusters (Berkeley 39 and NGC 6819) they found flat distributions. Recently, individual clusters have also

been analyzed in this context. Bhattacharya et al. (2019) studied the radial distribution of the very old cluster Berkeley 17 ($\sim$ 10 Gyr, Kaluzny 1994), and placed it into the Family II class of GCs; R20 showed that Collinder 261 ($\sim$ 9 Gyr, Dias et al. 2014) has a flat BSS distribution, like that of Family I clusters, and R21a found the same for Trumpler 5. The parameter A^{+} was also explored in 11 OCs by Rao et al. (2021), who found mild (or non-existent) relations between A^{+} and other markers of dynamical ages like $\mathrm{N}_{\mathrm{relax}}$ —defined as the number of central relaxation a cluster has experience since its formation— and the structural parameters of the clusters: core radius (r_c), effective radius (r_e), and concentration parameter (c). Additionally, Jadhav and Subramaniam (2021) defined a new parameter called *fractional mass excess* ($\mathcal{M}_e$), defined as $\mathcal{M}_e = (M_{\mathrm{BSS}} - M_{\mathrm{TO}})/M_{\mathrm{TO}}$, where M_{TO} is the mass of the TO of the cluster. They also found that BSS with $\mathcal{M}_e > 1.5$ (i.e., the more massive ones) are not segregated, leading to the speculation that these stars did not form from the already segregated stars, but from the non-segregated ones. It is possible that these are short-lived, and hence may evolve before getting radially segregated.

1.5 Motivation and goals

In the previous sections we have provided to the reader with a long list of reasons why blue straggler stars (and related) are important for stellar evolution. The presence of BSS in a cluster is far from insignificant, they posed challenges to standard stellar evolution theory in the sense that explaining their presence demands a complex interplay between stellar evolution and cluster dynamics.

The latest data releases of the *Gaia* mission allowed us to generate the largest homogeneous compilation of BSS in OCs using *Gaia* DR2. With two previous catalogs already available in the literature AL95 and AL07 our motivations rely on the basis of simple reasons; the burst of all-sky surveys that provide new, homogeneous data for an enormous amount of objects, allowing their study over larger sky areas, but also the need to identify straggler candidates more reliably and accurately, not merely based on their position in the CMD, but also on accurate astrometric memberships. The two previous compilations lack of both; homogeneous data and membership. This project aimed then, to provide to the astronomical community studying BSS with an homogeneous and internally consistent catalog. Such compilation can be further used to make photometric and spectroscopic observations of exotic BS population in the multi-wavelength regime, revealing and constraining the formation scenarios, and stellar parameters. It can also help to analyse the dependence of the straggler population on the cluster environments and occurrence in them, providing indirect information about their formation mechanism. While we made an attempt to accomplish the former providing information for few blue stragglers, the latter (spoiler alert!) has been fully achieved on this thesis, where we have revisited old relations, but also explored new ones that until now were limited only to GCs.

A better understanding of what type of cluster hosts BSS and the discovery of special cases on which formation theories can be tested have been the motivation of only a few studies in the past decades. With the latest *Gaia* data releases, however, this scenario has considerably changed and opened the opportunity to study BSS and their formation in a solid and precise way.

Chapter 2

A new, *Gaia*-based catalog of blue straggler stars in open clusters

This chapter is mainly based on:
A new, Gaia-based catalog of blue and yellow straggler stars in open clusters
Authors: M.J. Rain, J.A. Ahumada, G. Carraro
Astronomy & Astrophysics, 2021, 650, A67

and the work published on the booklet Hypatia Colloquium 2021.
Author: M.J. Rain ; Editors: H, M.J. Boffin, G. Beccari
Early Career Astronomer series at ESO, October 2021, 34

The complete catalog is online and available in
Vizier Online Data Catalog: J/A+A/650/A67

2.1 Short introduction

Defying the traditional single stellar evolution with its brighter and hotter location past the main sequence turnoff of a stellar population, BSS and recently YSS (possible evolved BSS) have equally fascinated theorists and observers for generations. While BSS were initially discovered in globular clusters (GCs), they are now known to exist in open clusters (OCs), dwarf galaxies, and in the field. In particular, the study of BSS in OCs is of great interest as, on the one hand, dynamical processes are less severe than in GCs, but we still deal with a single, well-defined (in terms of distance, age, metallicity, etc.) population of stars. The existence in the latter indicates that their formation in low stellar density regimes is principally due to binary evolution. In this context large compilations of these exotic population is OCs can be further used to make targeted observational of the straggler populations in the multi-wavelength regime, revealing and constraining the formation scenarios and stellar parameters.

In this chapter we present a new catalog of BSS in Galactic OCs. Its main aim is to provide a useful tool for further research on the topic. The catalog supersedes previous similar compilations because it takes into account the accurate astrometric information provided by the *Gaia* survey, therefore securing, for the first time, the cluster membership of the cataloged stars.

So far, the most extensive survey of BSS candidates in OCs has been performed by AL07, which took into account the bibliography up to 2005. This catalog was, in turn, a revision of the previous work by AL95, hereafter AL95, and it lists a total of 1887 blue straggler candidates in 427 OCs of all ages. AL07 found that: i) stragglers are present in clusters of all ages; ii) the BSS show a remarkable degree of central concentration, and iii) the fraction of BSS increases with the richness and age of the cluster. Drawbacks of AL07 are the lack of homogeneity of the open cluster data available at the time it was published, and that the straggler candidates are mostly of an uncertain membership. Thus, while useful, these compilations are not reliable enough to allow the derivation of statistical properties of BSS.

It should be clear that, to derive significant and meaningful statistical results for the straggler population in a cluster, it is first necessary to obtain reliable, accurate information on the stars' membership. Particularly in the case of OCs—given their mostly Galactic-plane locations—a main source of uncertainty is the high number of field stars lying in the straggler region in the CMDs (cf. Fig. 1.1), spuriously increasing the observed straggler population (Carraro et al., 2008). Today, however, a dramatic improvement in the selection of BSS has become possible thanks to the *Gaia* mission (Gaia Collaboration, Prusti, de Bruijne, Brown, Vallenari, Babusiaux, Bailer-Jones, Bastian, Biermann, Evans, and et al., Gaia Collaboration et al.). The availability of *Gaia* data has, not only in this field but in many others, brought about a revolution: by combining the parallax measurements, with the proper motions and the colors of the stars, it is now possible to establish membership with high accuracy and thereby, for the scope of this thesis, identify bona fide BSS. These are still candidates, however, and the definite proof of membership require radial velocity measurements. In particular, using *Gaia* second and third early data releases (*Gaia* DR2; Gaia Collaboration et al. 2018 and *Gaia* EDR3; Gaia Collaboration et al. 2021), we can determine accurate membership and, consequently, raise the study of BSS in OCs to much more solid statistical grounds for the first time.

This section presents a new catalog of blue straggler stars in a large sample of OCs. It is also, the first catalog of yellow straggler stars. It is based on the inspection of the CMDs of 408 clusters with a membership characterization provided by the *Gaia* DR2 astrometric solution. We describe the cluster sample and dataset in § 2.2 and our methodological improvements used to identify the BSS and YSS § 2.3. We discuss the completeness of the catalog in § 2.4 while in § 2.5 we give a detailed explanation of the contents of the catalog itself. In § 2.6 we provide some general statistics and comparisons with the previous studies and compilations of BSS in OCs. In § 2.7 and § 2.8 we identify interesting individual cases that can be use for further investigations and finally in § 2.9 we summarize and give the conclusions of this analysis.

2.2 Data

The catalog is based on the identification of blue straggler and yellow straggler candidates in color–magnitude diagrams of Galactic OCs of all ages.

For this new catalog we only made use of *Gaia* DR2 data—the last release at the moment of its compilation; some unavoidable problems with precisions—especially in the parallaxes ϖ, which have increased by 30 per cent in tha latest release *Gaia* EDR3—might be present. Data from *Gaia* EDR3 have indeed been used in the last section of this chapter, to study possible correlations with the cluster host properties, an analysis performed only in clusters with significant straggler populations.

2.2.1 Milky Way open clusters with *Gaia* DR2 and membership criteria

The survey *Gaia* DR2 provides a precise astrometric solution (RA, DEC, $\mu_{\alpha^*}(=\mu_\alpha \cos\delta)$, μ_δ, and ϖ) for ~ 1.7 billion objects. In addition, it contains photometric data in the G-band for all sources, while data in the $G_{\rm BP}$- and $G_{\rm RP}$-band are available for 80% of the sources (~ 1.4 billion objects). The limit for faint magnitudes is $G \approx 21$, while the bright limit for G is around 3. The calibration uncertainties reached on the individual observations are 2, 5, and 3 mmag for G, $G_{\rm BP}$, and $G_{\rm RP}$, respectively. The sources present a median uncertainty in parallax and position of about 0.04 mas for bright sources ($G < 14$ mag), 0.1 mas at $G = 17$ mag, and 0.7 mas at $G = 20$ mag. In the proper motion components, the corresponding uncertainties are 0.05, 0.2, and 1.2 mas yr^{-1}. The astrometric solution, the photometric contents and validation, and the properties and validation of radial velocities are described in Lindegren et al. (2018), Evans et al. (2018), and Katz et al. (2019). The homogeneity and quality of *Gaia* data allow us to reach an unprecedented level of detail in CMDs, particularly in the context of OCs, where accurate parallax information has often been lacking.

We took advantage of the selection of cluster members carried out by Cantat-Gaudin et al. (2018), hereafter CG18, and updated by Cantat-Gaudin and Anders (2020), hereafter CG20. The last version contains 1481 clusters and provides coordinates, proper motions, parallaxes, and distances for all of them. To assign membership probabilities

($P_{\rm memb}$), CG18 and CG20 applied the Unsupervised Photometric Membership Assignment in Stellar Clusters (UPMASK)[1] to the *Gaia* DR2 data in the field of each cluster. This field has a radius twice as large as the value $r_{\rm DAML02}$ reported by Dias et al. (2002), with proper motions within 2 mas yr^{-1}, and a parallax within 0.3 mas, of those of the cluster centroid (μ_{α^*}, μ_δ, ϖ). Since the uncertainties of G at ~ 21 mag reach 5 mas yr^{-1} for proper motions, and 2 mas for parallaxes, the Cantat-Gaudin catalog includes only stars with $G \leq 18$, which corresponds to typical uncertainties of 0.3 mas yr^{-1} and 0.15 mas in proper motions and parallax. See our discussion in § 2.4.1.

2.2.2 List of clusters

From the original list of AL07, we extracted 389 clusters, to which we added 19 recently discovered ones with the *Gaia* mission, for a grand total of 408; they all appear in CG18 — see Figure 2.1. This way, we dealt with a sample of clusters very similar to those in the previous catalogs. We note, however, that the list of clusters can be easily expanded.

Berkeley 42	Berkeley 64	Berkeley 66
Bochum 1	Bochum 2	Bochum 7
Bochum 10	Bochum 14	Collinder 96
Collinder 97	Collinder 121	Collinder 223
Collinder 228	Coma	Dolitze 25
Feinstein 1	Hogg 16	Hogg 22
Hyades	IC 2944	NGC 133
NGC 1252	NGC 1931	NGC 1976
NGC 2175	NGC 2384	NGC 2467
NGC 3247	NGC 6200	NGC 6514
NGC 6530	NGC 6604	Pismis 24
Ruprecht 46	Ruprecht 55	Ruprecht 120
Stock 13	Trumpler 24	Trumpler 27

Table 2.1 Open clusters with entries in AL07, but not included in this work.

[1]The classification scheme of UPMASK is unsupervised, and relies on no physical assumption about stellar clusters, apart from the fact that its member stars must share common properties, and be more tightly distributed on the sky than a random distribution. Although the original implementation of the method was created to stellar, photometric data, the approach was designed to be easily generalized to other quantities or sources. Few year ago, the method was successfully applied to the astrometric data of the *Gaia* Astrometric Solution and we refer the reader to Cantat-Gaudin et al. (2018) for more information regarding the complete procedure and the assignation of membership probability.

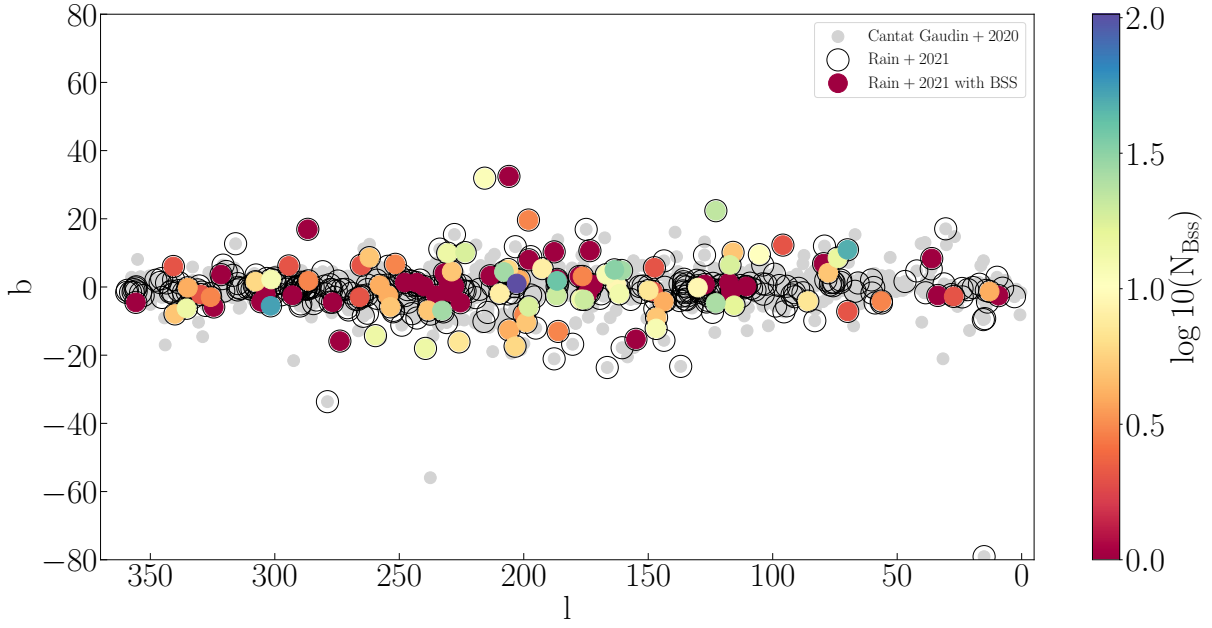

Figure 2.1 Galactic distribution of the 408 open clusters analyzed in this thesis. The plot presents the clusters in Galactic coordinates of CG20 in gray filled circles, in open black circles in all the clusters we analyzed in this work, while the colored filled circles are proportional to the number of blue straggler stars found on each cluster, in this sense reddest clusters have less blue straggler than the bluest ones.

Table 2.1 lists the clusters that are included in AL07 but not here; they are not considered to be bona fide clusters, mainly according to a non-compliance with two simple conditions using the *Gaia* DR2 astrometric solution: i) their proper-motion dispersions correspond to a physical velocity dispersion inferior to 5 km s^{-1}; and ii) their observed proper-motion dispersions are smaller than 1 mas yr^{-1} (three times the *Gaia* measurement errors; also see § 2.4.1). For more details, the reader is referred to CG20. Furthermore, our sample does not include two well known and close clusters, Hyades (Melotte 25) and Coma (Melotte 111), given their large extension on the sky and the more sophisticated membership determination technique required to identify their BSS properly. On the other hand, the clusters listed for the first time are in Table 2.2.

Table 2.2 Open clusters not included in previous versions of the catalog.

Gulliver 1	Gulliver 4	Gulliver 40
Gulliver 12	Gulliver 51	Gulliver 52
Gulliver 21	Gulliver 55	Coin 2
Gulliver 23	Coin 15	Coin 35
Gulliver 27	Trumpler 11	Trumpler 20
Gulliver 36	Waterloo 7	Pozzo 1
Gulliver 39		

2.3 Identification of the blue stragglers

Formally, a blue straggler is defined from its position in a CMD, that is, it is bluer and brighter than the TO, on or near the parent cluster ZAMS. Following AL95, AL07, and R20, we assumed a cluster star to be a blue straggler candidate if it appears on a specific area of the CMD (see Figure 2.2). This region is bounded on the blue side by the ZAMS and the red side by the TO color and the binary sequence. The lower limit corresponds to the magnitude at which the observed sequence of the cluster detaches from the ZAMS. In principle, we did not adopt a bright limit (but see § 2.3.1).

For more details, we refer the reader to the analogous definitions in AL95 and AL07, which are the models for the present one. To identify the BSS candidates, the procedure for each cluster was the following; we note that the reader may also find Section 2.2.1 of AL07 useful:

1. The photometric data for all CG18 members (§ 2.2.1) with probabilities of $P_{\rm memb} \geq 50\%$ were plotted in a G versus $(G_{\rm BP} - G_{\rm RP})$ diagram.

2. An approximate matching of a PARSEC theoretical isochrone (Bressan et al., 2012), with the *Gaia* DR2 passbands of Evans et al. (2018), was then performed on the main sequence and TO, and eventually on the red giant branch (RGB) and red clump if present. Cluster parameters, such as metallicity, extinction, and the age of DAML02, were first chosen. When the cluster was not listed in DAML02 or when the matching of the isochrone was unsatisfactory, parameters from Bossini et al. (2019) and Monteiro and Dias (2019) were used instead. However, the distance was always taken from CG18. Sometimes a refinement of the parameters was

necessary; in such cases, we kept the distance and extinction values fixed and varied the age—that is to say, we changed the isochrone, adopting the solar value when no metallicity was listed in the literature. Based on these parameter variations, we picked the appropriate PARSEC isochrone by eye, from a grid spaced 0.05 in $\log(\mathrm{age})$. These changes are reported in the catalog Notes (see § 2.5.4).

3. The equal-mass binary loci—obtained by displacing the isochrone by 0.75 mag upward—and the ZAMS were also plotted. The binary loci help constrain the region expected to be populated by binaries made of normal main sequence TO stars.

4. Finally, the straggler candidates were singled out in the corresponding region of the CMD. As an example, Figure 2.3 shows this selection in the CMD of IC 4651.

The aforementioned procedure was executed, taking the following considerations into account.

- Stars located slightly towards the blue of the ZAMS were also regarded as straggler candidates. The proximity to the ZAMS have always been a synonymous of youth. However, the reader must know when talking of BSS that this is not completely true, as shown by Gosnell et al. (2015)—stars 1366 and 8104 in NGC 188—and recently by Leiner and Geller (2021).

- Not all the stars fainter than the cluster TO and located between the ZAMS and the isochrone were included: Only objects significantly detached from the cluster isochrone, for instance ~ 0.03 mag as a minimum and down to 0.5–1.5 mag at most below the TO, were listed. This magnitude cut is consistent with our limit of $G \approx 18$ for the oldest and distant clusters in our sample (see § 2.4.1 and CG18).

- Although we took the TO color for the straggler region's red limit, an arbitrary cutoff in color was imposed for some clusters similarly as in AL07. Redder stars were considered as possible yellow stragglers (YSS, § 2.3.2).

- Finally, in this work, as in AL07, stars on the "blue hook" were not regarded as stragglers, given the dependence of this feature's extension and shape with the

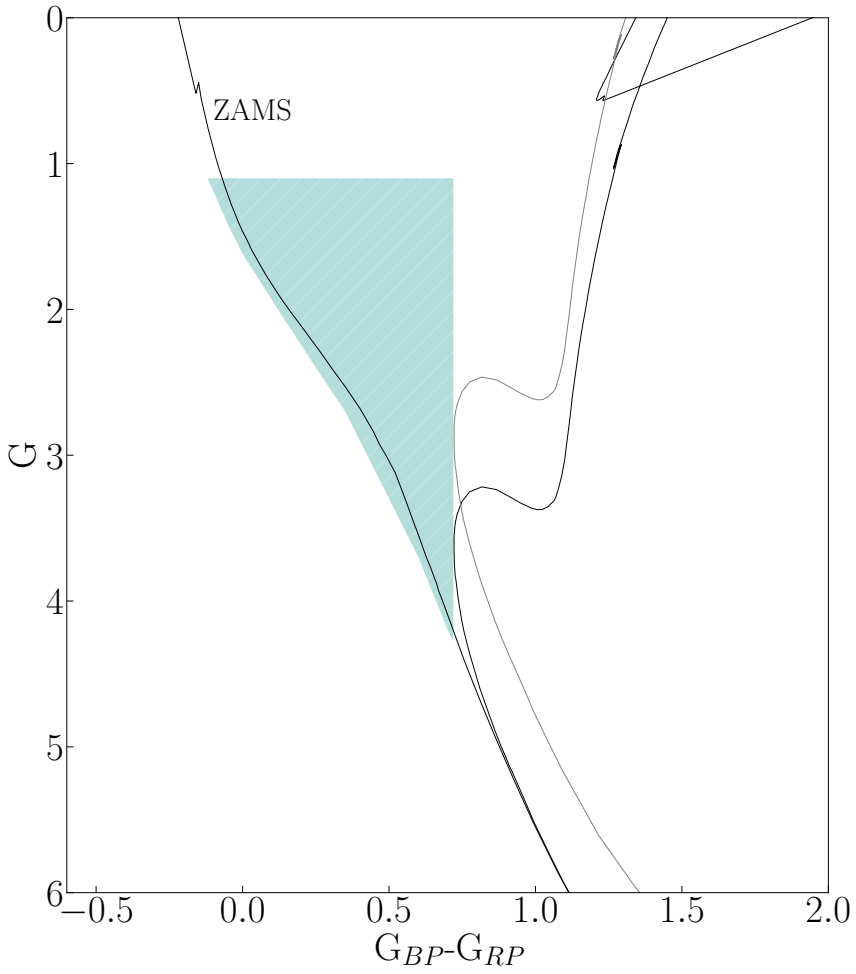

Figure 2.2 Schematic color–magnitude diagram for an old open cluster; the isochrone corresponds to $\log(\mathrm{age}) = 9.8$. The blue straggler area is shaded in blue. The grey line indicates the equal-mass binary loci.

stellar models adopted for the isochrone. In this sense, the adoption of the equal-mass binary sequence (see, e.g. Figure 2.3) was beneficial. This sequence wraps and helps to constrain the blue hook region of the cluster, when possible, since here normal photometric binaries may fall, increasing the straggler population spuriously.

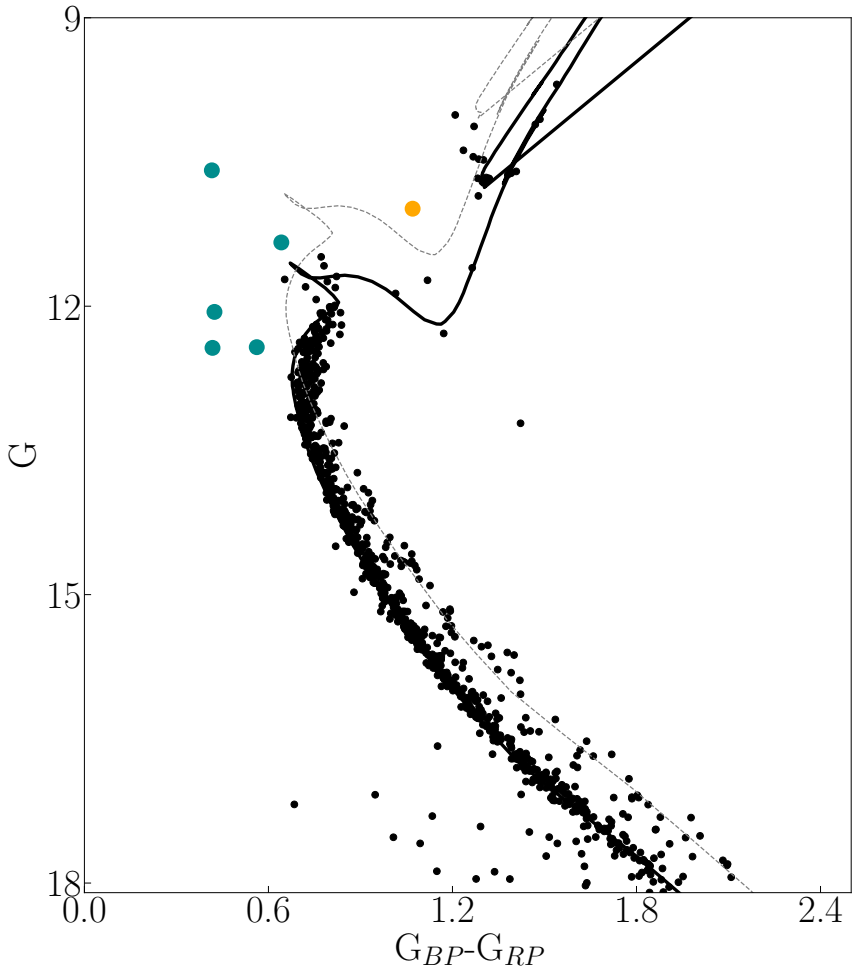

Figure 2.3 CMD of the open cluster IC 4651, built from *Gaia* DR2 photometry. Black filled circles are all the stars from CG18 with $P_{\rm memb} \geq 50\%$. Blue filled circles and yellow filled circles are the cataloged blue and YSS, respectively. The black solid line represents the PARSEC isochrone of solar metallicity and $\log(\text{age}) = 9.27$ (Bressan et al., 2012), set at $E(B-V) = 0.36$ and $(m-M)_0 = 9.82$. The second curve is the same isochrone displaced 0.75 mag, which helps to constrain the region of the binaries. See also Table 2.4.

2.3.1 Massive stragglers

Although we decided not to define a bright limit in the BS area (§ 5.2.5 and Fig. 2.2), there is actually a sort of frontier given by the theory of mass transfer in close binaries of 2.5 mag above the TO (Chen and Han, 2009, McCrea, 1964): This is the luminosity that would reach the complete merger of two identical (same mass) main sequence stars

at the TO. However, there is evidence of brighter, bona fide BSS similar to, for instance, star 677 in NGC 7789 (Breger and Wheeler, 1980). Stars similar to this could be the result, for example, of a three-body interaction and subsequent merger. We flagged these stars as "massive" to identify them as subjects of further, specific research. To locate them, we used isochrones whose TOs are 2.5 mag brighter than those of the isochrones employed to match the CMDs. In practice, this implied adopting an upper limit of about 1–1.5 mag above the 2.5 mag frontier.

2.3.2 Yellow stragglers

We name YSS the objects with colors between those of the TO and the RGB, and they are brighter than the subgiant branch (Clark et al., 2004).[2] They have been photometrically and spectroscopically identified in both open and globular clusters (da Silveira et al., 2018, Martinez et al., 2020, Rain et al., 2020, Sales Silva et al., 2014), and they are usually explained as evolved BSS—i.e., post-main sequence stars more massive than the TO—on their way to the RGB (Mathieu et al. 1990 and references therein). For example, four YSS have been identified in M67, one of them with a Helium white dwarf (WD) companion, indicating that it is an evolved straggler that formed from mass transfer, having an RGB star as a donor (Landsman and Simon, 1998, Landsman and Stecher, 1997). Leiner et al. (2016) reported the first asteroseismic mass and radius measurements of the yellow straggler S1237 in M67; they argue that it might be the result of a stellar collision or a binary merger. The methodology followed for finding YSS was similar to the one used for BSS (§ 5.2.5). Figure 2.4 shows the region where these stars were searched for. This region is limited to the left by the TO color or red limit depending on the cluster. Below and to the right by the grey equal-mass photometric binary sequence, which corresponds to the matched isochrone that moved 0.75 to brighter magnitudes and that represents the maximum brightness expected for an equal mass binary at the cluster TO. In OCs, however, the YSS regime can also contain the binaries'

[2] In the literature, there is a potential source of confusion regarding the naming of these stars since the "red straggler" term has also been systematically used for stars lying between the blue straggler area and the RGB (e.g., Albrow et al. 2001, Eggen 1983, Eggen and Iben 1988, Landsman and Simon 1998, Landsman and Stecher 1997). In this work, we chose to designate these objects as "yellow stragglers", and we encourage the community to adopt this nomenclature.

product of mass transfer or mergers (models of Tian et al. 2006 and Chen and Han 2008), and they can even be "contaminated" by binaries composed, e.g., by a red giant and a main sequence star, whose combined lights photometrically place the system within the Hertzsprung gap (Mermilliod et al., 2007).

Finally, although no upper limit was defined, and considering that the CMDs can be affected by differential extinction (which may distort the clump structure), those stars with magnitudes fainter than the clump and clearly differentiated from the cluster sequences were also labeled as possible YSS.

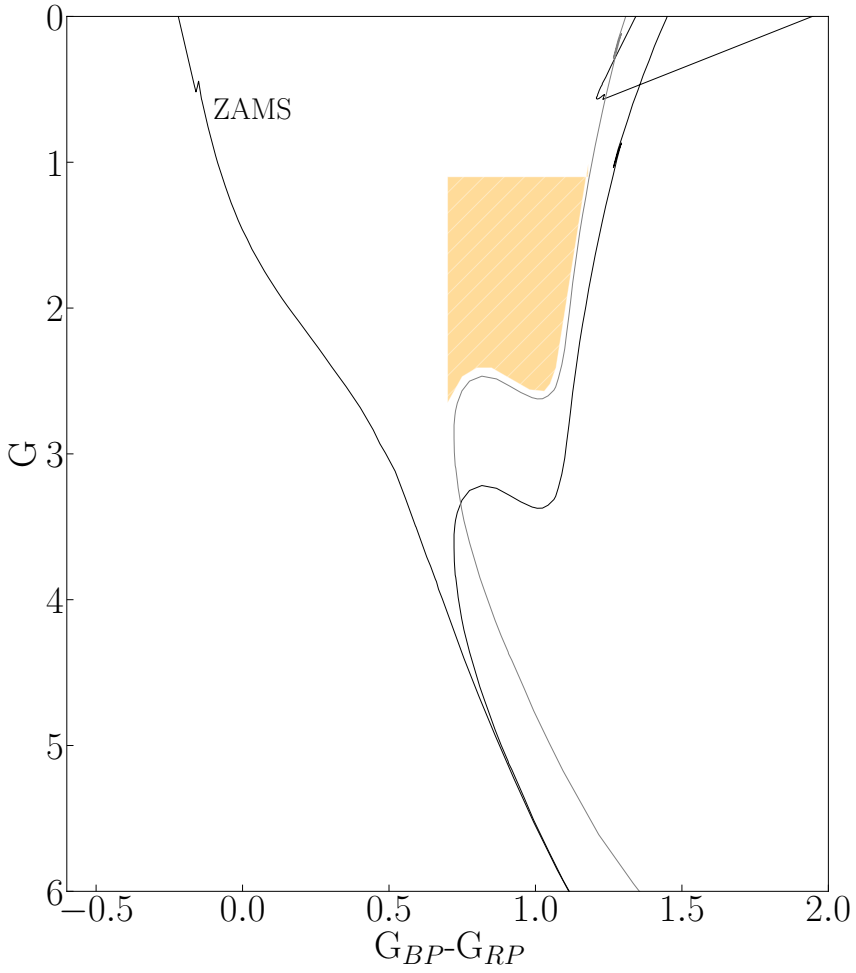

Figure 2.4 Yellow straggler area in a schematic color–magnitude diagram of an old open cluster ($\log(\text{age}) = 9.8$). The equal-mass binary loci is also plotted.

2.4 Completeness of the BSS selection

Gaia DR2 suffers from natural calibration problems and systematic errors, both for very bright and faint sources. Here, we briefly describe how these limitations can affect the completeness of our catalog.

2.4.1 Limitations of *Gaia* DR2 photometry

For faint sources ($G \geq$ 17–18 mag), problems in the background calibration and contamination from nearby sources have been reported (Evans et al. 2018; Arenou et al. 2018). For this reason, our catalog contains only sources brighter than $G \approx 18$, which is the limit adopted by Cantat-Gaudin et al. (2018). This cut in terms of distance corresponds to the de-reddened magnitude of a 3-Gyr star cluster's TO at 10 kpc. Hence, we did not include a few distant and old OCs with TOs fainter than $G \approx 18$ in the catalog because of the virtual impossibility of matching an isochrone to a CMD without a clear TO. An example is Berkeley 66, whose TO is at $G \approx 19$.

In *Gaia*, the sources described as "bronze" are photometrically non-calibrated objects, without color measurements, and for which only the G magnitude is provided. They tend to prevail in high-density stellar environments. These sources cannot be represented in a CMD, and therefore they will not be cataloged. An example is star 266 of NGC 2354, which is a β Lyrae eclipsing binary (V* QU CMa, Lapasset and Ahumada 1996).

On the other hand, the bright end ($G \leq 13$) is limited by photometric calibration errors. In clusters with a TO brighter than $G \approx 12$, where saturation and flux loss becomes important, and the instrument calibration is still very provisional and problematic, some BSS may be missing. For example, IC 2602 ($G_{\rm TO} \approx 4$) harbors the bright straggler θ Carinae (HD 93030, Nazé and Rauw 2008, Walborn 1979), which does not appear in *Gaia* and therefore has not been included in our list.

2.4.2 Field and "HB" stars contamination in the straggler region

Field stars located between us and a cluster contaminate its CMD. This is particularly true for OCs since most of them are located low onto the disk, and many are projected towards the Galaxy bulge. In fact, Carraro et al. (2008) showed that stars belonging to the young stellar population of the Milky Way disk tend to occupy the same region on the CMD as the BSS, artificially enhancing the clusters' BSS population. Cluster members, selected as in CG18 on an astrometric basis only, are expected to include a fraction of interlopers. Disk star contamination is then one of the main reasons we decided to retain only potential members with $P_{\rm memb} \geq 50\%$. This criterion should enhance the probability of picking up the most likely members (Banks et al., 2020, Carrera et al., 2019, Yontan et al., 2019) and providing more robust BSS statistics. We have however, studied the properties of stars with $P_{\rm memb} < 50\%$ (on every cluster) and make sure they present a uniform distribution in position space and have no obvious clumping structure in proper motion space. This is on line with Bai et al. (2022) who found the average contamination rate if 4% for bright sources and is around 5% towards G=18 mag when UPMASK (used on this thesis, see § 2.2) and Gaia data are used.

To estimate the field contamination rate (on clusters containing at least one BS and/or YSS) we performed the following;

- We counted the "field" stars in a "region" outside the tidal radius, defined as five times the reported r_{50} value of CG20. r_{50} is the radius from the centre of the cluster that encompasses 50 per cent of the members.
- We required the "region" of search to be equal to the area that contains the BSS candidates —see 2.3 for more information.
- Only stars with kinematics consistent with the cluster proper motions; this is within $\mu_\alpha \cos\delta \pm 3\sigma$, $\mu_\delta \pm 3\sigma$, and $\varpi \pm \sigma$ were selected.
- Finally, for the stars be counted as interlopers, they must be within the same color and magnitude limits of each sub-population (e.g BSS, YSS, RGB), which varies from cluster to cluster.

In general, and as expected we found most of the clusters are very low affected by field contamination, with a percentage between 0-5% in their BSS regions. Here, we classified the 114 clusters into three categories; those with high contamination >10% (or Group III), those with intermediate contamination rates 5-10% (Group II), and those with null or negligible contamination ≤5% (Group I). While >90% of the OCs lie in Group I classification, ∼3% of them fall on Group II and ∼5% on Group III.

On the other hand and under the possibility of the BSS region been contaminated by extreme field horizontal branch (EHB) stars as recently reported by Jadhav et al. (2021), Singh et al. (2020). We have estimated the number of "HB stars" in our clusters using the same technique of Jadhav and Subramaniam (2021). We basically assume the ratio of BSS and HB stars in OCs to be as follows:

$$\log\left(\frac{N_{\rm HB}}{N_{\rm BSS}}\right) \simeq 0.44\ \log\left(\frac{N_{\rm TO+1}}{1000}\right) + 0.36 \tag{2.1}$$

Equation (2.1) was obtained combining equations (3) and (4) of Leigh et al. (2009). Using the same control sample described in § 2.6.2 we found found there are ∼46(5%) HB among the ∼ 900 straggler candidates. If we considered, however, that only blue (or extreme) HB stars can contaminate the straggler region, there should be ∼12(1.2%) of blue HB among our sample.[3]

2.4.3 Differential reddening

It is well known that the patchy dust distribution in the field of view towards star clusters causes differential extinction (see, e.g., Platais et al. 2008); this manifests as a broadening of the stellar sequences in CMDs. For old OCs (age $\geq$ 1 Gyr), the effects of differential reddening are most noticeable in the TO and RGB morphologies. In particular, the *Gaia* photometric bands are broad enough to introduce large color differences caused by extinction as a function of the stellar SED. These spreads in color can introduce some dispersion in the CMD positions, affecting the selection, especially

[3]This only if we assume $\rm HB_{Blue}/HB \sim 0.25$ (Arimoto and Simoda, 1981).

near the TO. As shown by Leiner and Geller (2021), for clusters with low reddening values ($E(G_{\rm BP}-G_{\rm RP})<0.3$), it is sufficient to adopt reddenings from the literature and convert them to the *Gaia* passbands. On the other hand, for clusters with high reddenings, individual reddening corrections are recommended. Although a small number of clusters in our sample show high differential extinction across their field, we did not attempt to correct the photometry of the individual sources from interstellar extinction; in these cases, a warning was included in the Notes file (§ 2.5.4). Even though none of the cluster included in the catalog have reddening corrections, we explored in detail this effect in two OCs: Trumpler 5 and Trumpler 20; we refer the reader to § 5.2.1.1 for more information regarding the methodology used to quantify this effect in OCs using *Gaia* DR2 data, but also to § 3.2.1 where exactly the same procedure was performed in a sample of ∼26 OCs—those containing $N_{\rm BSS}\geq 10$—using *Gaia* EDR3.

2.4.4 Isochrone fitting in the *Gaia* era

As mentioned elsewhere along this thesis, with *Gaia* DR2 catalog, the astrometric membership determination has become much more precise than using ground-based data, leading to clearer CMDs and therefore enabling a more precise and reliable parameter's determination. In this conext, the high quality of *Gaia* photometry produces well-defined features, very clean main sequences, and a clear definition of the binary sequence in most of the cases —see for example Figure 2.3. While constructing this compilation we face minor problems with the isochrone fitting specially in young and poor clusters. Not only our decision of including age, metallicity, and absorption values to compute the isochrones and the lack of studies reporting these values but also the many unreliable determinations available on the literature have forced us to use grids of isochrones and/or refer to individual studies in the ADS with more precise parameters to find the best fit. Figure 2.5 show one example for the cluster NGC 3033. Here the dashed line correspond to the isochrone calculated with the parameters of DAML02 where the fit is far from being accurate. While astronomers got familiarized with *Gaia* DR2 new and large compilations came out. This is the case of Dias et al. (2021) on which the parameters were estimated using the cross-entropy (CE) method

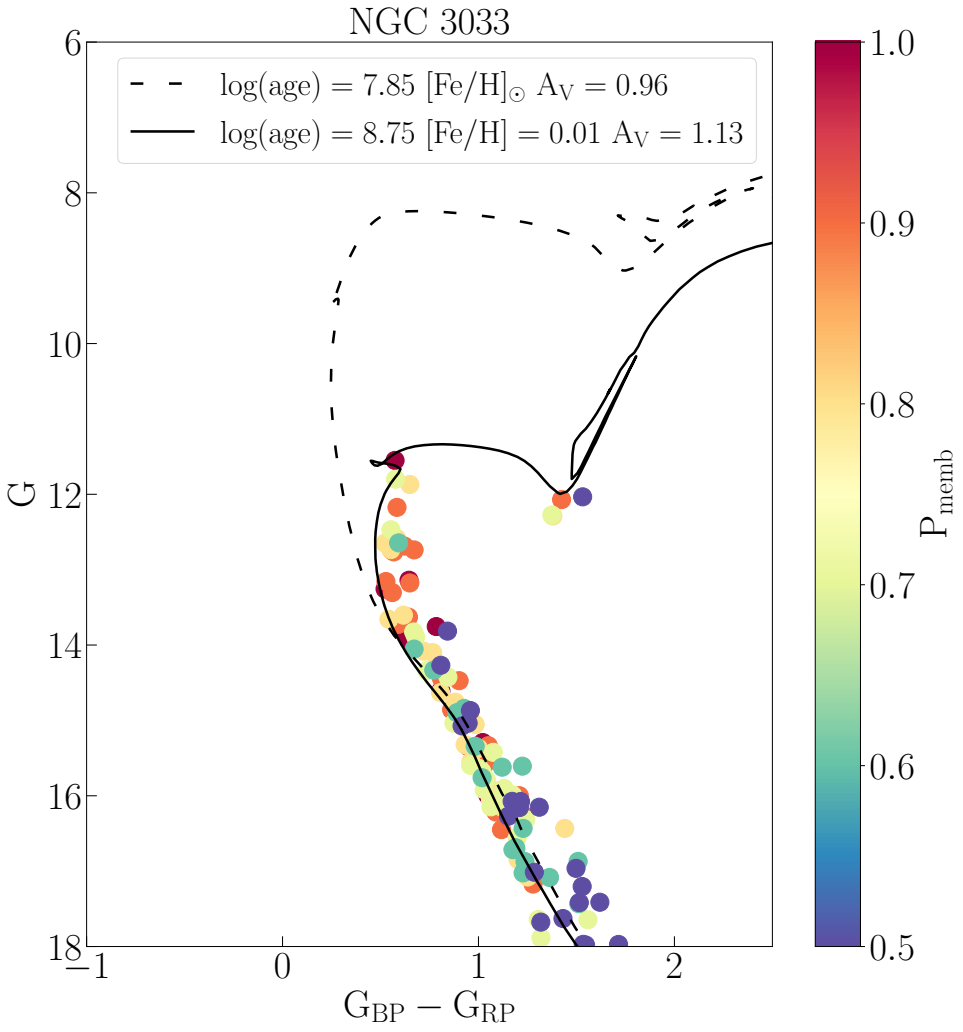

Figure 2.5 Comparison of the isochrones computed with different sets of stellar parameters. Straight line is the isochrone obtained using parameters from Dias et al. (2021) computed using *Gaia* DR2 data. Dashed line instead is the result of using the set of parameters of DAML02 based on UBVRI data. The colored circles are the members of the cluster NGC 3033 color-coded by the probability of membership given by CG20, CG18.

[4]. The resulting isochrone from the new set of parameters correspond to the straight line of Figure 2.5. NGC 3033 do not have sources lying in the blue straggler regime and that can be misclassify, in this case despite important the isochrone fitting was not crucial.

[4] `https://web.mit.edu/6.454/www/www_fall_2003/gew/CEtutorial.pdf`

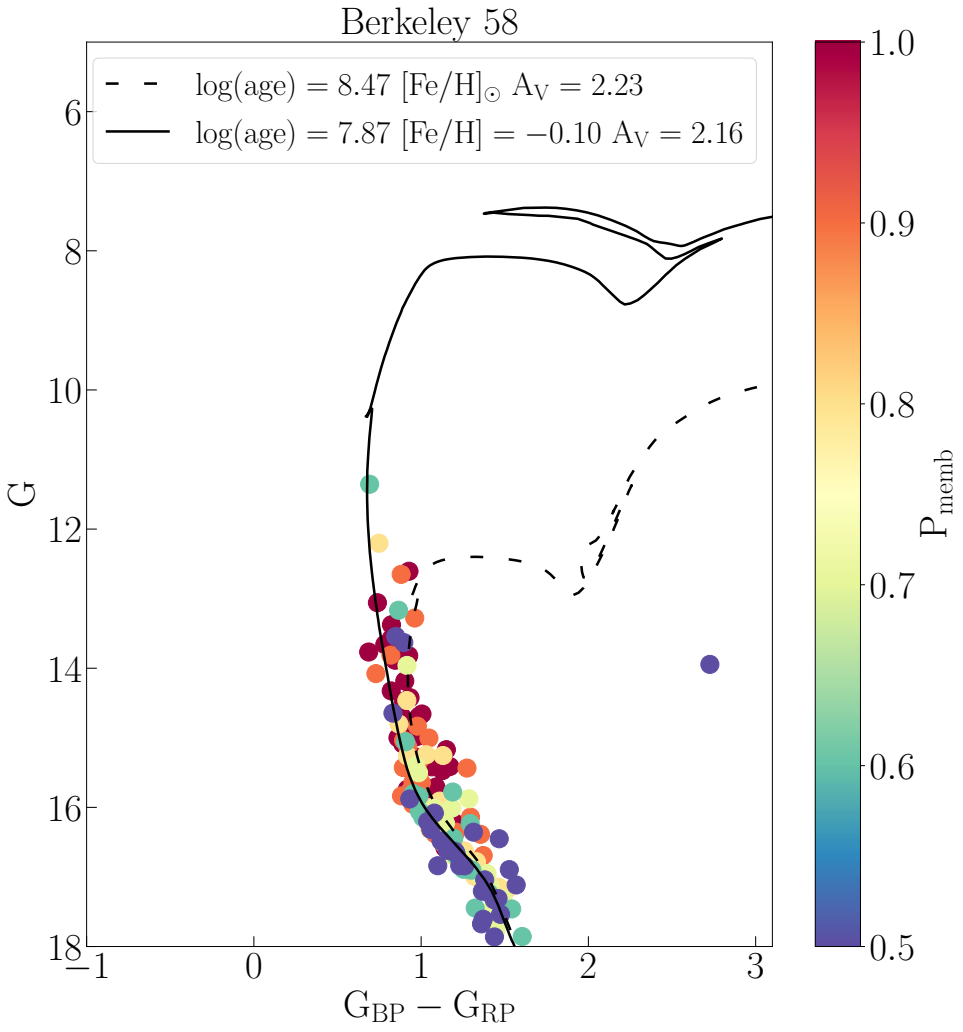

Figure 2.6 Same as 2.5 but for Berkeley 58.

Figure 2.6 shows instead the case of Berkeley 58. As for NGC 3033 the dashed line is the isochrone when using DAML02 and the straight line with Dias et al. (2021). The brightest star in the CMD —with a $P_{memb} = 0.6$— would be easily classified as a blue straggler candidate if we had only considered the values of DAML02. This is however not an isolated case, and for nearly 20% of the clusters in our sample, we faced similar problems —most of them relatively young and/or small clusters on which we didn't expect to find BSS. Further, for all the clusters on which a set of parameters different from that reported in the literature (see bullet N.2 of § 2.3) was used for the isochrone fitting a "Note" (§ 2.5.4) was added. Finally, since all the clusters have been analyzed

under the same conditions (see § 2.3) we do not expect bias in our selection.

2.5 The catalog

This new catalog of BSS in OCs contains the following files: one first table with open cluster data, a second table listing blue straggler data, a third table with the yellow straggler compilation, and, finally, a file with notes and comments. We also want to draw attention to an important difference that the reader will find between this work and AL07: The classification of straggler candidates in type 1 and type 2 defined by AL07 is not included in our catalog[5]. We instead give the coordinates, the astrometric solution, and the distance to the cluster center of each BSS and YSS.

2.5.1 First table: Open cluster data

The cluster parameters were mainly taken from DAML02, CG18, and Bossini et al. (2019). For clusters recently discovered, we used the data provided by Monteiro and Dias (2019). The parameters listed for each cluster are as follows: the equatorial coordinates (J2000.0), the logarithm of the age, the reddening, the mean proper motions, the parallaxes, the distance, the number of BSS and YSS candidates with $P_{\rm memb} \geq 50\%$, and eventual notes (cf. § 2.5.4). In total, the table comprises twelve columns. Table 2.3 is an extract of the full Table, which is only available in electronic form.

[5]Type 1 or category 1 includes stars with the following conditions: They have membership studies (proper motions, radial velocities, abundances analysis, etc), they appear in clusters with more than 100 stars in the upper MS, they are in a group greater than 10 BSS, they are located with respect to the cluster centre, at up to a relative radius of 0.3 and finally, they are clearly differentiated from the cluster sequences and not too bright. All the remaining stars falling outside this conditions were include in Type 2 or category 2 BSS. Since in our new catalog all the stars have membership information (from the astrometric solution), differentiation by categories was not necessary

Table 2.3 Excerpt of Table 1 of the catalog compiling general information of the open clusters. The full version of this table is only available with the electronic version of R21b

Cluster	RA [deg]	DEC [deg]	log(age)	$E(B-V)$	$\langle\mu_{\alpha^*}\rangle$ [mas yr^{-1}]	$\langle\mu_\delta\rangle$ [mas yr^{-1}]	$\langle\varpi\rangle$ [mas]	Distance [pc]	$N_{\rm BSS}$	$N_{\rm YSS}$	Notes
NGC_7788	359.179	61.395	7.26	0.52	−3.112	−1.762	0.300	3039.2	0	0	*
King_12	358.265	61.953	7.85	0.51	−3.416	−1.420	0.296	3080.6	0	0	
King_11	356.912	68.636	9.04	1.27	−3.358	−0.643	0.262	3433.2	18	0	*
King_20	353.305	58.469	8.30	0.65	−2.686	−2.585	0.496	1903.8	0	0	
NGC_7654	351.195	61.590	8.20	0.57	−1.938	−1.131	0.596	1600.1	0	0	
Berkeley_99	350.260	71.778	9.50	0.30	−3.139	−0.359	0.137	6029.4	5	1	*
Mrk_50	348.806	60.448	7.09	0.81	−3.465	−2.560	0.323	2837.6	0	0	
NGC_7510	347.767	60.579	7.35	0.90	−3.664	−2.193	0.286	3177.5	0	0	
King_19	347.053	60.523	8.55	0.54	−4.838	−2.651	0.343	2687.7	1	0	
King_10	343.748	59.170	7.44	1.13	−2.722	−2.088	0.259	3478.1	0	0	
NGC_7419	343.579	60.814	7.15	2.02	−2.759	−1.601	0.280	3235.9	0	0	
NGC_7380	341.817	58.125	7.07	0.60	−2.517	−2.144	0.333	2765.6	0	0	
Berkeley_96	337.478	55.408	7.60	0.17	−3.503	−2.994	0.252	3560.6	0	0	
NGC_7261	335.056	58.128	8.20	0.88	−3.932	−2.909	0.278	3261.9	0	0	
NGC_7243	333.788	49.830	8.00	0.18	+0.433	−2.857	1.116	873.3	0	0	
NGC_7235	333.083	57.271	7.00	0.81	−2.381	+2.935	0.152	5536.9	0	0	*
NGC_7209	331.224	46.508	8.53	0.17	+2.255	+0.283	0.820	1177.7	0	0	*
NGC_7160	328.448	62.589	7.27	0.37	−3.472	−1.378	1.050	926.7	0	0	
IC_5146	328.372	47.246	6.00	0.59	−2.910	−2.490	1.213	805.0	0	0	
NGC_7142	326.290	65.782	9.55	0.35	−2.747	−1.288	0.392	2376.4	10	1	*
⋮	⋮	⋮	⋮	⋮	⋮	⋮	⋮	⋮	⋮	⋮	⋮

Notes:
In the table, the clusters are sorted by right ascension.

2.5.2 Table 2: Blue stragglers in open clusters

In this table we list information on every identified straggler candidate. In total, the table contains eleven columns. The first column gives the cluster's common name, while the second column indicates the *Gaia* DR2 identification. Columns three to seven list the coordinates, the individual proper motions, and the parallaxes. Columns eight and nine provide the G magnitude and the $(G_{\rm BP}-G_{\rm RP})$ index. Column ten indicates the membership probability by CG18. Column eleven lists the distance from the cluster center. As an example, Table 2.4 shows the entries for the cluster IC 4651; the full Table is only available in electronic form.

Table 2.4 Blue straggler candidates in the open cluster IC 4651 (see also Figure 2.3). This is an extract of the full table, which is only available in electronic form.

Cluster	*Gaia* DR2 Source Id.	RA [deg]	DEC [deg]	μ_{α^*} [mas yr^{-1}]	μ_δ [mas yr^{-1}]	ϖ [mas]	G	$G_{\rm BP}-G_{\rm RP}$	$P_{\rm memb}$	r [arcmin]
IC_4651	5949561772753237248	260.920	−49.9	−2.29	−5.386	1.2379	11.23	0.64	0.6	11.61
IC_4651	5949565616715032064	261.128	−49.9	−3.36	−5.255	1.0841	11.95	0.42	0.6	3.21
IC_4651	5949553522087135616	261.231	−49.9	−2.10	−4.683	1.0457	12.33	0.41	0.7	2.86
IC_4651	5949553835654195968	261.273	−49.9	−2.26	−4.762	1.1896	10.48	0.41	1.0	2.93
IC_4651	5949584170973723520	261.507	−49.7	−2.02	−5.612	1.1522	12.32	0.56	0.6	17.13

2.5.3 Table 3: Yellow stragglers in open clusters

This table lists information on every identified yellow straggler candidate. It contains eleven columns in the same format as in Table 2.4 (see § 2.5.2 for more information).

2.5.4 Notes

This file gathers information that clarifies, complements, or simply adds content to the Tables previously mentioned.

2.6 Statistics

2.6.1 Comparison with AL95 and AL07

In total, 897 blue straggler candidates were identified in the 408 OCs investigated. The number of clusters with at least one blue straggler is 111 (27.20%). In comparison with AL95, where 959 BS candidates were found in 390 clusters, and where the number of clusters with any stragglers was 225 (57.7%), our percentage is $\sim 30\%$ less. The respective numbers for AL07 are as follows: 1887 stragglers, 427 clusters, and 199 clusters with stragglers (46.6%); here the difference is $\sim 20\%$. It can be safely assumed that a good part of this results from the greatly improved membership information available for the present work (i.e., *Gaia* data). Figure 2.1 shows the galactic distribution of all the

clusters analyzed on this thesis, where no relation of $\mathrm{N_{BSS}}$ with the Galactocentric distance is observed, and clusters hosting BSS are distributed randomly on the Galactic plane —in line with Jadhav and Subramaniam (2021)— the same behavior is observed for the YSS. Regarding the YSS, 77 candidates were identified in 43 clusters (10.53%), with most of them hosting only one yellow straggler. These clusters and their N_{YSS} are listed in Table 2.5. Figures 2.7 and 2.8 show the combined color-magnitude diagram for all our straggler candidates, corrected for distance (taken from Bailer-Jones et al. 2018) and extinction, and colored according to the cluster age (taken from DAML02). We see that the brightest BSS are in the young clusters, as expected, and they become progressively fainter in older clusters. Some general highlights from our work are i) no blue and yellow straggler candidates were found in clusters with $\log(\mathrm{age}) \leq 7.3$ and $\log(\mathrm{age}) \leq 8.2$, respectively. In AL95 and AL07, some stragglers—albeit a few—were identified in young clusters; this may reflect a bias towards bright magnitudes (see the case of IC 2602 in § 2.4.1), besides membership considerations. ii) The number of stragglers in clusters with ages below 1 Gyr is relatively low and around 70% (623) of them are in clusters older than $\log(\mathrm{age}) = 9.3$ (2 Gyr). And finally, iii) there are 2.19 BSS per cluster and 11 BSS per each YSS.

In Table 2.6 we list the clusters with $N_{\mathrm{BSS}} \geq 10$. In apparent contrast to our remarks in the preceding paragraph, it is interesting to note that some of the OCs show a greater number of BSS candidates in our catalog than in AL07. For example, we found that Trumpler 5 has the largest straggler population, but AL07 listed only 70 stars, of which just four were classified as of "type 1"—that is to say, bona fide stragglers given the then available membership information. The discrepancy may result from the different areas searched for BSS, a radius of $8'$ in AL07, and $30'$ in the present work. However, for most of the clusters, the opposite occurs, and the number of cataloged BSS decreases considerably. Most of the objects in Table 2.6 were also targeted by AL07 as the richest in BSS. As for the age of these clusters, all of them are old ($\log(\mathrm{age}) \geq 9.0$), just as AL95 and AL07 found. A comparison between our catalog and AL07 is possible only for those sources with RA and DEC information available. These were obtained from the OC database WEBDA[6] or any data linked to ADS. For the sources we matched, we found large inconsistencies between our catalog and AL07. First, for individual clusters,

[6] `https://webda.physics.muni.cz/`

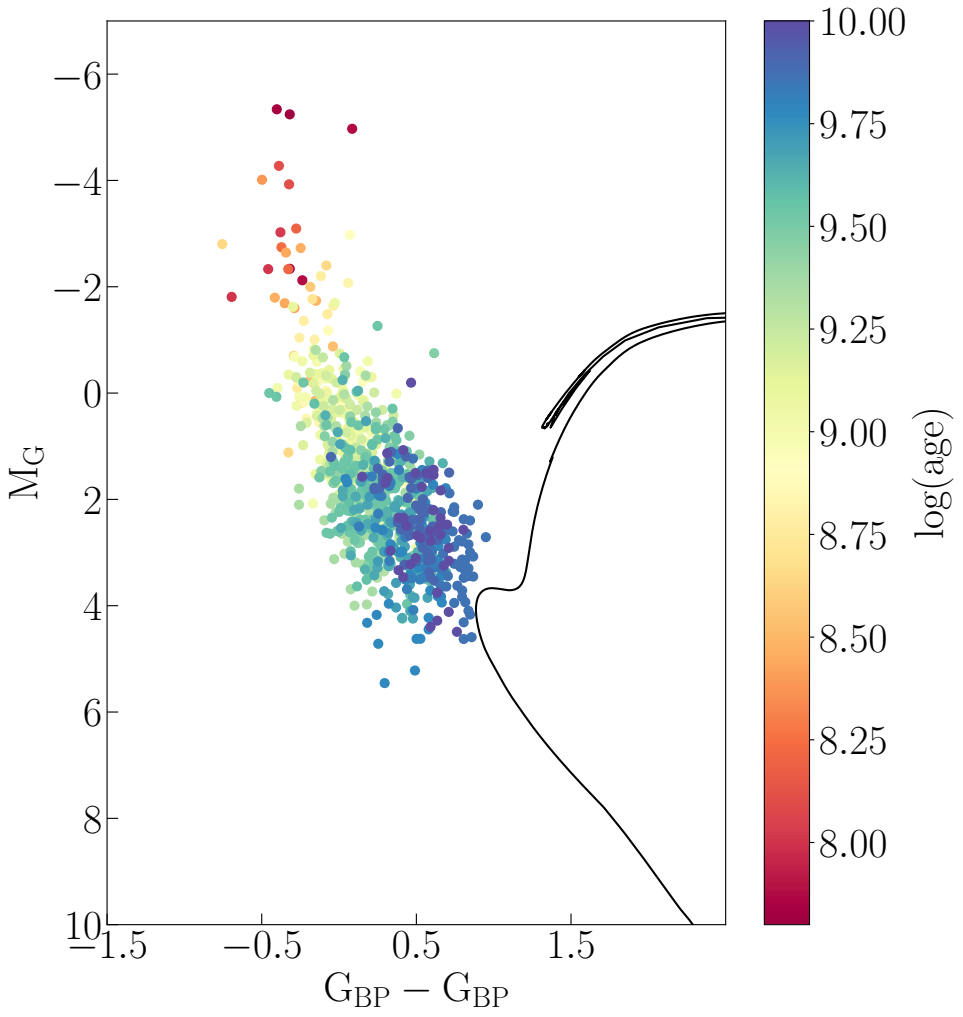

Figure 2.7 De-reddened color-magnitude diagram showing dereddened, corrected-by-distance BSS candidates. The BSS are colored according to the cluster age. For comparison is plotted and isochrone with $\log(\text{age}) = 10.00$ and solar metallicity from Dotter (2016).

the percentage of BSS found to be non-members according to our criteria (§ 2.2.1) is about 10–60% of the AL07 BSS. However, there are cases such as NGC 2477, whose AL07 BSS are all members, but that appear concentrated around the TO and sub-giant branch in the *Gaia* CMD. On the other hand, for close and very well studied clusters with spectroscopically confirmed BSS, it is possible to retrieve about 70% and, in some cases, up to 100%, as Vaidya et al. (2020) have demonstrated. Finally, we are aware that some bona fide BSS are lost, because of our stringent and conservative selection

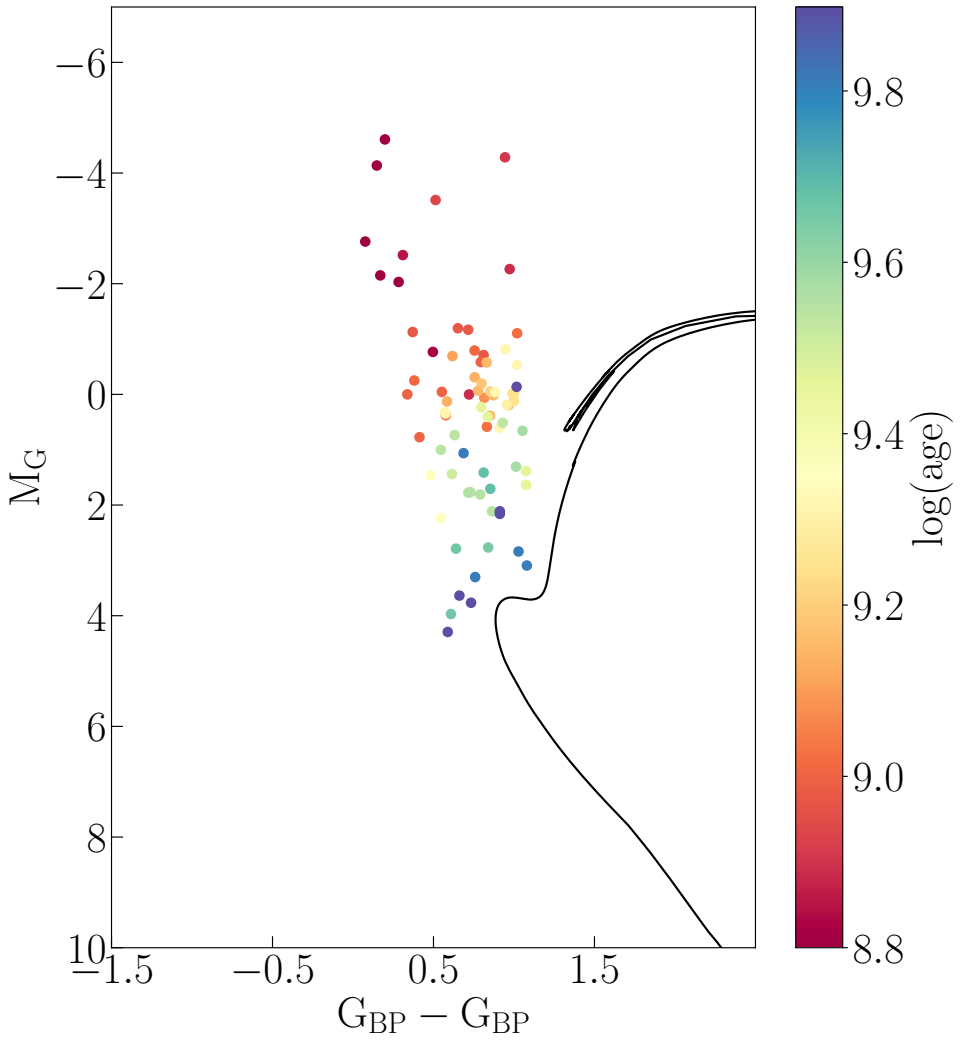

Figure 2.8 Same as Figure 2.7 but for 77 YSS.

criteria.

2.6.2 $N_{\rm BSS}/N_{\rm MSS}$ versus age

Figure 2.9 shows the ratio $N_{\rm BSS}/N_{\rm MSS}$ versus cluster age, in a logarithmic scale, for 107 OCs. The $N_{\rm MSS}$ is the number of cluster main sequence stars up to 1 magnitude below the TO, adopted as a proxy of the cluster richness. The clusters were chosen first by visually inspecting every CMD, built with stars of $P_{\rm memb} \geq 80\%$, and then by retaining

Table 2.5 Open clusters harboring YSS.

Cluster	log(age)	$N_{\rm YSS}$	Cluster	log(age)	$N_{\rm YSS}$
NGC 2477	8.80	4	Berkeley 69	8.95	1
Collinder 261	9.95	3	King 7	8.82	1
Berkeley 20	9.78	3	Trumpler 20	9.11	1
NGC 6253	9.70	3	Berkeley 70	9.67	1
NGC 2437	8.40	3	NGC 5823	8.90	1
Berkeley 19	9.40	3	Berkeley 29	9.02	1
NGC 2141	9.23	3	Pismis 3	9.02	1
Ruprecht 75	9.15	3	IC 1311	9.20	1
King 5	9.10	3	NGC 1245	9.00	1
NGC 2158	9.02	3	NGC 7142	9.55	1
Berkeley 23	8.90	3	Melotte 66	9.53	1
Trumpler 5	9.60	2	NGC 2243	9.03	1
Berkeley 39	9.90	2	NGC 3680	9.07	1
King 2	9.78	2	NGC 2192	9.15	1
Berkeley 32	9.70	2	NGC 6705	8.40	1
NGC 1193	9.70	2	NGC 752	9.16	1
NGC 2682	9.45	2	IC 4651	9.05	1
NGC 1798	9.25	2	NGC 2354	9.18	1
IC 166	9.09	2	Berkeley 99	9.50	1
NGC 2204	9.03	2	NGC 3114	8.09	1
Tombaugh 2	9.01	2	NGC 7654	8.20	1
Berkeley 81	9.00	2			

those that showed well-defined evolutionary phase signatures—main sequence, binary sequence, and red clump when it was possible—and those that were well matched to the corresponding isochrone. In the top x-axis of the Figure, the mass of the cluster TO for a given age is shown. Star counts are in Table 2.7.

The results can be summarized as follows. The ratio is approximately constant for young OCs until $\log(\text{age}) \sim 8.7$ (500 Myr, $M_{\rm TO} = 2.4\ M_{\odot}$), followed by a steep increase for older clusters. Previous works attempted to discern if this correlation between $N_{\rm BSS}/N_{\rm MSS}$ and the age is true and related with some intrinsic mechanism that would produce more stragglers in old clusters. We also observed signs of the plateau described by Leiner and Geller (2021) in the range $9.3 < \log(\text{age}) < 9.6$ (or 2 Gyr <age <4 Gyr) when using linear ages —see Figure 2.10. Surprisingly, our results are more similar to AL95 than AL07 (see Fig. 2.11) when the number of stragglers is normalized to main sequence stars. In AL07, the normalized number of stragglers grows with the

Table 2.6 Open clusters with the largest absolute population of blue stragglers ($N_{\rm BSS} \geq 10$) in comparison with AL07. Additionally, in parenthesis we have reported the rate of field contamination.

Cluster	log(age)	$N_{\rm BSS}$	$N_{\rm BSS}$(AL07)
Trumpler 5	9.60	103 (0.24)*	70
Collinder 261	9.95	53 (0.03)	54
NGC 6791	9.92	48 (0.02)	75
NGC 2158	9.02	39 (0.02)	40
Berkeley 18	9.63	32 (0.17)	126
Berkeley 32	9.70	27 (0.14)	37
NGC 1798	9.25	27 (0.02)	24
Tombaugh 2	9.25	27 (0.13)	...
King 2	9.78	26 (0.11)	30
NGC 188	9.88	22 (0.00)	24
Berkeley 17	10.0	20 (0.05)	31
Berkeley 21	9.34	20 (0.05)	51
NGC 2141	9.23	18 (0.10)	24
King 11	9.04	18 (0.05)	27
Berkeley 39	9.90	18 (0.00)	43
NGC 7789	9.52	16 (0.00)	22
NGC 6819	9.36	15 (0.00)	29
NGC 6253	9.70	14 (0.00)	27
Melotte 66	9.53	14 (0.00)	35
NGC 2243	9.03	14 (0.00)	09
NGC 2506	9.00	14 (0.00)	15
Berkeley 12	9.60	13 (0.06)	15
Berkeley 19	9.40	13 (0.09)	01
NGC 1193	9.70	12 (0.00)	19
Berkeley 70	9.67	12 (0.15)	64
Trumpler 20	9.11	12 (0.07)*	...
NGC 2682	9.45	11 (0.00)	30
NGC 7142	9.55	11 (0.00)	37

* The case Trumpler 5 and Trumpler 20 will be discuss in more detail on § 5.2.6. Here the values of contamination rates might be different given the different methodologies used on both Sections.

Table 2.7 Clusters with the largest relative population of blue stragglers ($N_{\rm BSS}/N_{\rm MSS} \geq 0.01$). Only stars with $P_{\rm memb} \geq 80\%$ were considered. Additionally we reported the contamination rate for MS stars —see§ 2.4.2. The rate of field contamination among the BSS can be found in Table 2.6

Cluster	$\log(\text{age})$	$N_{\rm BSS}$	$N_{\rm MSS}$	$N_{\rm BSS}/N_{\rm MSS}$
NGC 6253	9.70	06	39 (0.05)	0.16
Trumpler 20	9.11	08	70 (0.21)	0.13
NGC 188	9.88	19	217 (0.00)	0.09
NGC 2354	9.18	05	60 (0.05)	0.09
NGC 2682	9.45	08	99 (0.00)	0.08
King 5	9.10	03	41 (0.02)	0.07
NGC 2243	9.03	13	189 (0.00)	0.07
NGC 2158	9.02	28	504 (0.00)	0.05
NGC 2204	9.03	07	149 (0.02)	0.05
Melotte 66	9.53	13	285 (0.00)	0.05
Collinder 110	9.15	06	148 (0.01)	0.04
Melotte 71	9.12	05	126 (0.01)	0.04
NGC 2627	9.15	03	77 (0.02)	0.04
NGC 6005	9.08	02	62 (0.10)	0.04
NGC 2420	9.30	03	88 (0.00)	0.03
NGC 2660	9.03	03	97 (0.00)	0.03
NGC 2506	9.00	14	539 (0.00)	0.03
NGC 6940	8.85	02	77 (0.06)	0.03
NGC 2112	9.25	04	158 (0.14)	0.03
NGC 7044	9.10	06	260 (0.00)	0.02
NGC 7789	9.52	15	698 (0.01)	0.02
NGC 6134	8.95	03	150 (0.00)	0.02
NGC 2477	8.80	05	279 (0.00)	0.02
NGC 6067	8.07	02	130 (0.01)	0.02
NGC 3960	9.10	01	66 (0.00)	0.02
NGC 6603	8.30	01	96 (0.05)	0.01
NGC 6939	9.30	02	161 (0.00)	0.01
NGC 6705	8.07	02	183 (0.00)	0.01
IC 4651	9.04	01	141 (0.03)	0.00

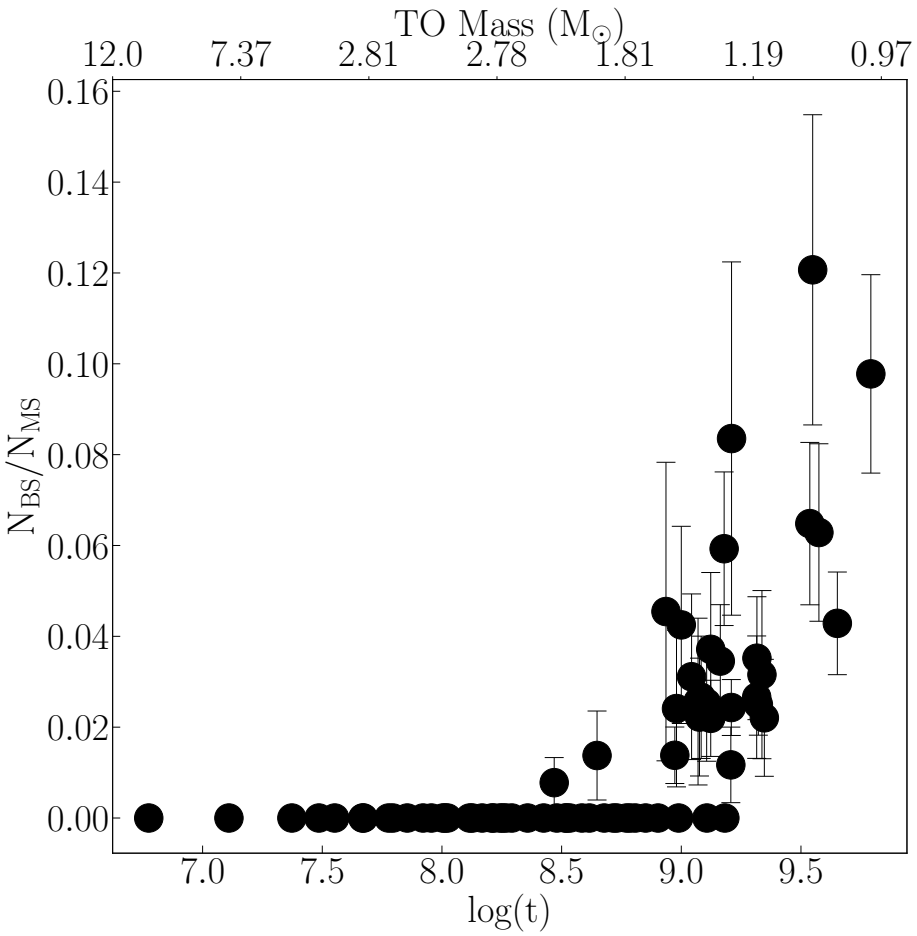

Figure 2.9 $N_{\rm BSS}$ $/N_{\rm MSS}$ as a function of cluster age. Only 107 clusters are included. Errors are Poisson. Cluster with and without BSS from all the ages (6.5 <log(age)<10) are plotted.

cluster age starting from $\log(\mathrm{age}) \sim 6.5$, while in AL95 the absolute number of stragglers shows two trends; One is approximately constant for young clusters and the second one grows with age. One scenario to explain the difference observed between both figures is related to the lack of BSS in young OCs and the confusion of defining an accurate TO in the CMD, which means that it is hard to distinguish MS stars from BSS, misclassifying them as stragglers. Concerning the sudden increase, it was proposed by AL07 that the number of stragglers observed in old OCs is a consequence of mechanisms such as mass transfer in close binaries. This remains an open issue that requires

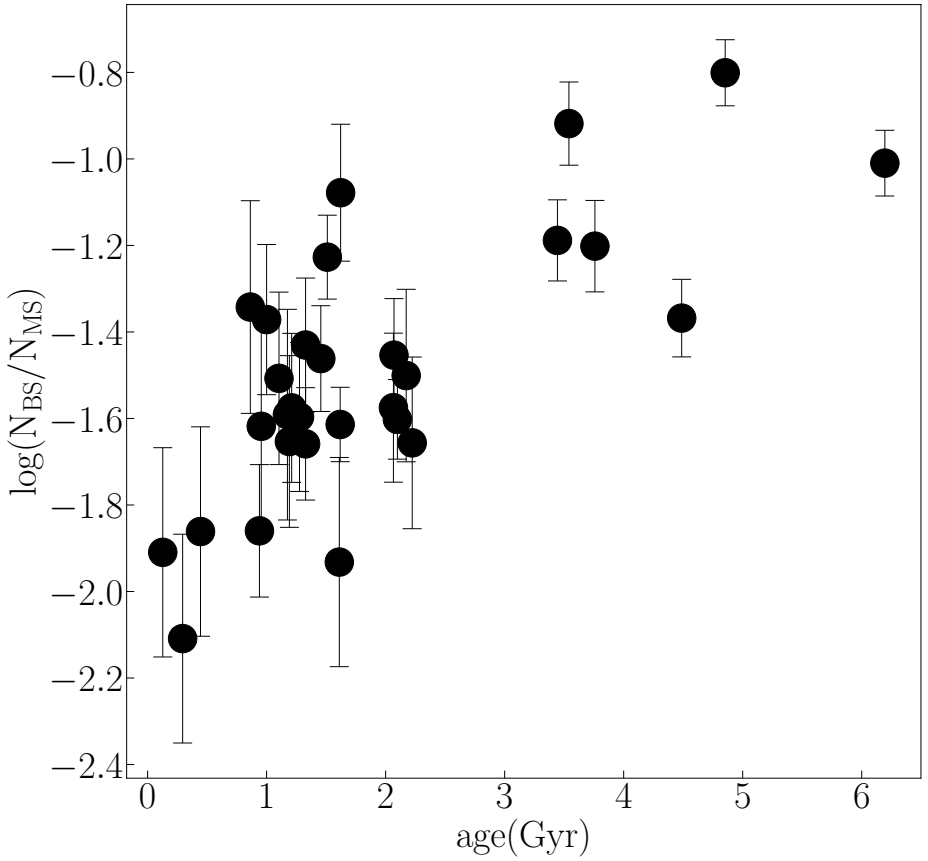

Figure 2.10 $N_{\rm BSS}$ $/N_{\rm MSS}$ (in logarithm scale) as a function of cluster age in Gyr. Only clusters with $N_{BSS} \geq 1$ and log(age)>8.5 are included. Errors are Poisson.

further investigation.

2.6.3 $N_{\rm BSS}/N_{\rm RC}$ versus M_V

It was reported by some authors the existence of a relation between the specific frequency $F_{\rm BSS}^{\rm HB} = \log(N_{\rm BSS}/N_{\rm HB})$ and the integrated magnitude M_V. Figure 2.12 is the only previously known Figure that gathers the data of different systems—in which BSS have been identified—in a single plot. The data comes mainly from several studies using

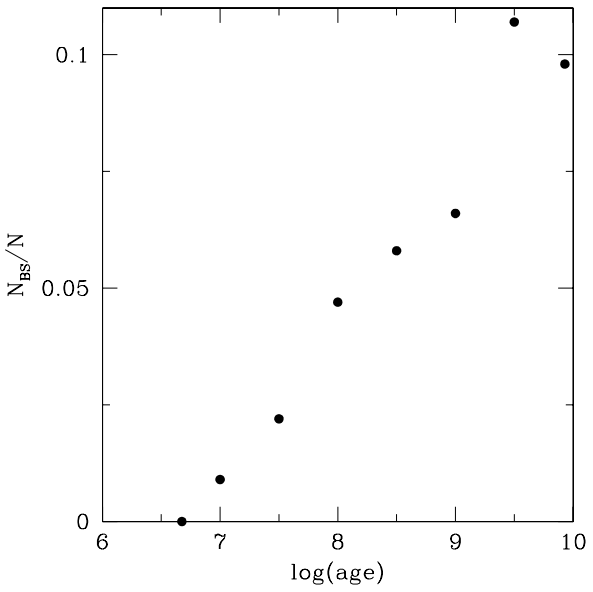

(a) AL95

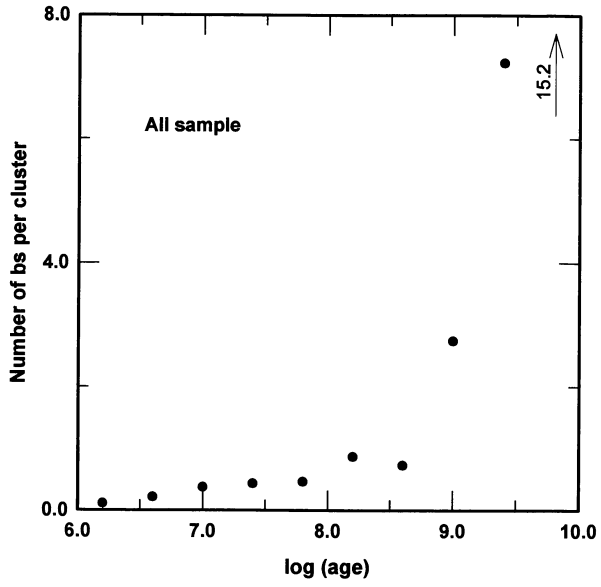

(b) AL95

Figure 2.11 Figures take from AL95 and AL07 corresponding to the only previous material available in the literature before our new catalog. Panel (a) indicates the average number of blue stragglers, per main-sequence star and cluster as a function of the age in logarithm scale. Panel (b) instead indicates the mean number of blue stragglers per open cluster and per logarithm of cluster age interval.

different samples and methodologies: GCs are from Piotto et al. (2004), OCs from de Marchi et al. (2006) and dwarf galaxies (dSphs) data from Momany et al. (2007). Figure 2.12 revealed the specific frequency of blue stragglers is basically the same (and high) in low density systems (low luminosity), while towards the high density (high luminosity) regime drops and continues to decrease as the density increase. Further, the main highlights derived from Figure 2.12 can be summarized as follow:

- $F_{\rm BSS}^{\rm HB}$ in all the systems is smaller than the relative frequency of field BSS.
- The BSS specific frequency of galactic OCs is "compatible" with that of dSphs with low luminosity values, which suggest a “saturation” at $F_{\rm BSS}^{\rm HB} \approx 0.3$–$0.4$ in the lower luminosity regime.
- dSphs with $M_V \leq -8.0$ possess a relatively higher BSS frequency with respect to GCs at any given M_V.

With this new compilation of BSS in OCs was almost unavoidable to see if the "compatibility" between dSphs and OCs holds, but also to see how looks this "universal" anti-correlation with the new data specially given the decrease of the $N_{\rm BSS}$ on almost every cluster studied. As mentioned before we made use of *Gaia* DR2 data which provides G, $G_{\rm BP}$ (blue wavelengths) and $G_{\rm RP}$ (red wavelengths). For a meaningful comparison we translated our G values into V to have our data in the same photometric band of those in Figure 2.12. For this purpose we used the color-relation recommended in the *Gaia* webpage[7]:

$$G - V = -0.01760 - 0.006860(G_{\rm BP} - G_{\rm RP}) - 0.1743(G_{\rm BP} - G_{\rm RP})^2 \qquad (2.2)$$

In order to avoid confusions of notations, on this sections when we talk of HB stars we refer to their analogous red clump (RC) stars in OCs, while for GCs and dSph the HB notation is the same as usual. The clump region in OCs is much less populated than the HB region in GCs, and before *Gaia* was less clearly defined. On this thesis however, only cluster with a relatively well populated RC have been selected (this is $\rm N_{RC} > 10$)

[7] `https://sci.esa.int/web/gaia`

and all our numbers have been corrected by field contamination — see § 2.4.2 for more details.

In Figures 2.13 and 2.14 are reported the new compilations after including our numbers. Two are the differences between both figures; i) In Figure 2.13 are included all the clusters with at least one BS, while in Figure 2.14 only those with $N_{\rm BSS} \geq 10$ and ii) In Figure 2.14 the cluster highly affected by field contamination are not plotted.

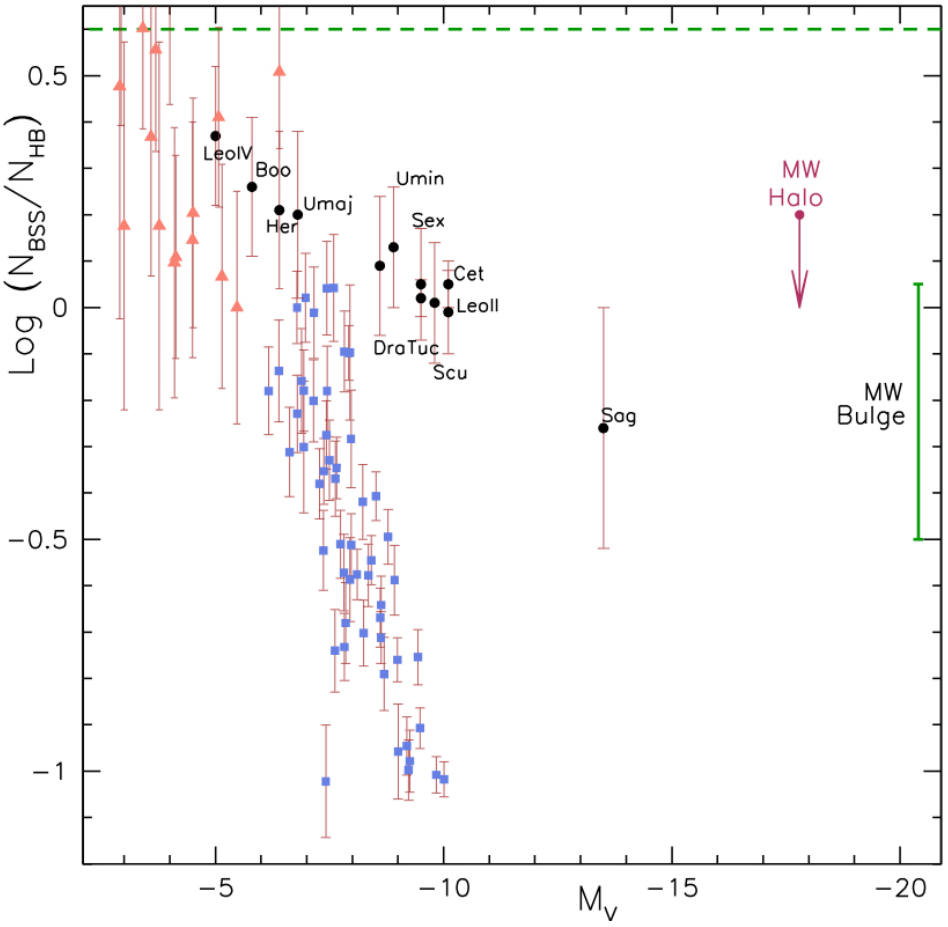

(a) Image taken from Momany et al. (2007)

Figure 2.12 $F_{\rm BSS}^{\rm HB}$ as a function of M_V from Momany et al. (2007). The figure corresponds to the only existing figure reported in the literature that gathers the information of GC's (Blue filled squares from Piotto et al. 2004), OC's (Orange filled triangles from de Marchi et al. 2006) and dSphs (Filled black circles from Momany et al. 2007) in one single plot. Green horizontal line shows the mean BSS frequency for Milky Way field stars Preston and Sneden (2000).

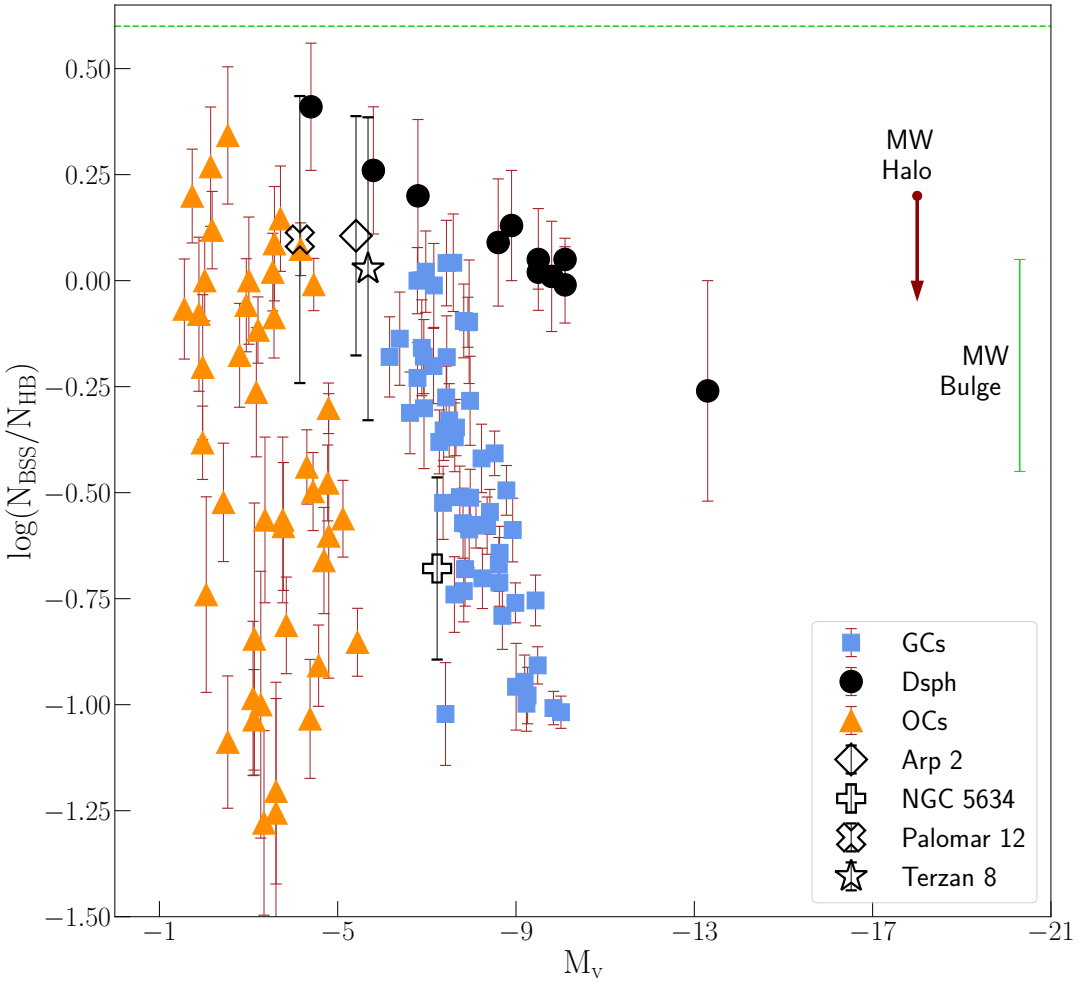

Figure 2.13 $F_{\rm BSS}^{\rm HB}$ as a function of M_V. Here all the clusters with at least one blue straggler are plotted in filled orange triangles. Data of GCs (blue filled squares), dSphs (black filled circles), Milky Way Halo , Bulge and the field is the same one used in Figure 2.12. Additionally, we have added the data of four GCs of the Sagittarius dwarf spheroidal galaxy in open black symbols. Errors are Poissonian.

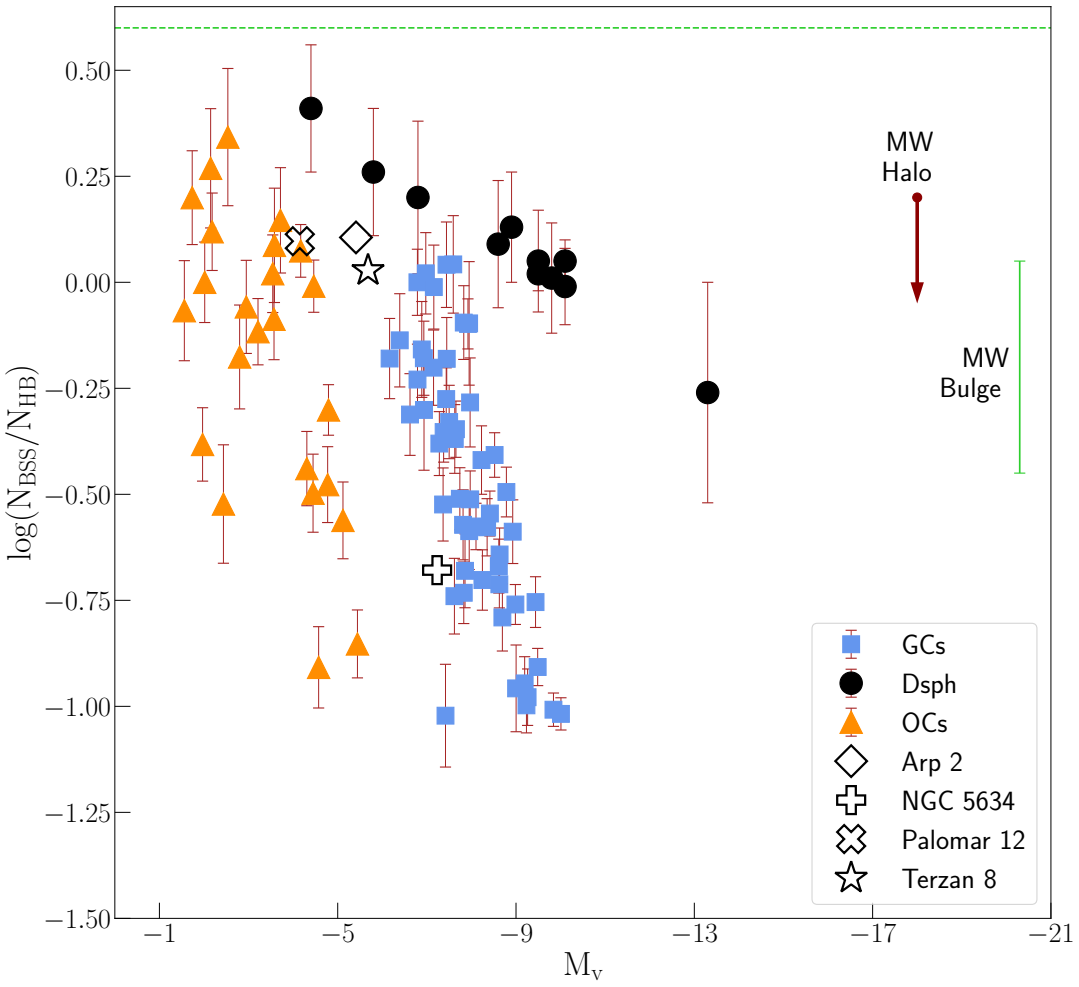

Figure 2.14 Same as 2.13 but for those clusters with $N_{\rm BSS} \geq 10$.

Our major findings can be summarized as follows:

- Although the anti-correlation between $F_{\rm BSS}^{\rm HB}$ and M_V still holds for OCs using our data, this follows however a different distribution than the one showed in de Marchi et al. (2006), Momany et al. (2007). The distribution of our data is more similar to the one described by the globular clusters (GCs), this is highly dispersed on the y-axis.

- As expected the OCs sample is shifted towards lower specific frequencies values ($F_{\rm BSS}^{\rm HB} < 0.2$) and fainter luminosities in comparison with what is shown in Figures

2.12 where de Marchi et al. (2006) OCs sample is used and the sample expands over $0.0 < F_{\rm BSS}^{\rm HB} < 0.6$.

- When considering OCs with $N_{\rm BSS} \geq 10$ (Panel b) the faintest clusters (Berkeley 12, Berkeley 17) have a specific frequency almost 30 times higher than the brightest ones (NGC 2506, NGC 7789). This is similar to what Piotto et al. (2004) found for GCs.

- By adding new data (not available when Figure 2.12 was compiled and published) of four GCs belonging to the Sagittarius dwarf spheroidal galaxy (Salinas et al., 2012) the gap between $-5 < M_V < -6$ "disappears". As reported previously by Momany et al. (2007) the gap it seems to be a selection effect, but also a consequence of using different populations (RGB, TO, MS, RC stars) to calculate the specific frequency.

Finally, we have explored the statistical significance of a correlation for our sample of OCs. By using the Spearman correlation function, we found $r_s = 0.32$ and $p = 0.021$ for Figure 2.13 and $r_s = 0.51$, $p = 0.004$ for Figure 2.14. Following Momany et al. (2007) we fit least-squares linear regression, we found the intercept and slope regression coefficients are $(a, b) = (0.14, 0.07)$ and $(a, b) = (0.37, 0.15)$ including and excluding the sample with $N_{\rm BSS} < 10$, respectively.

2.7 Radial distribution of the BSS

The dynamical clock described in § 1.4 has been fundamental in showing the importance of BSS and their radial distribution as tracers of GCs internal dynamics (Ferraro et al. 2009 and Beccari et al. 2013). In fact, due to their masses—significantly larger than the average—and their relatively high luminosities, BSS are the ideal objects to measure the effect of dynamical processes, like dynamical friction and mass segregation (Mapelli et al., 2006).
On this work and given the determination of $\rm r_{min}$ depends on the assumptions on the radial binning of the observational sample, which are somehow arbitrary, but also

because of the large errors present when using OCs we have decided to used the parameter A^{+} to measure the dynamical state of the clusters instead of the position of $\mathrm{r_{min}}$. Following Lanzoni et al. (2016) we calculate the parameter A^{+} as follows:

$$A_r^+(x) = \int_{x_{min}}^{x} \phi(x')_{BSS} - \phi(x')_{ref}\ dx' \tag{2.3}$$

where $\mathrm{x = r/r_{50}}$ and $\mathrm{x_{min}}$ are the outermost and innermost radii from the cluster centre. $\mathrm{r_{50}}$ is the radius containing half members —which is taken as a substitute for half-mass radius used in the case of GCs— and ϕ_{BSS} and ϕ_{ref} are the BSS and the reference population cumulative radial distributions, respectively. For this analysis we have decided to use the red giant branch (RGB) stars as the reference population. The parameter A^{+} is then defined as the are enclosed between ϕ_{BSS} and ϕ_{RGB}.
In total we have provided the A^{+} for all the clusters with $\mathrm{N_{BSS}} \geq 10$ listed in our new catalog — see Table 2.8. For the total sample composed of ≥25 clusters and on each of them we have taken a sub-sample of their straggler populations, where only BSS within $\mathrm{r_{50}}$ have been selected. The later allows a meaningful cluster-to-cluster comparison with A^{+} measured over equivalent radial portions on every system, but also on this way we avoid any completeness bias. The red giant branch stars where selected from the region defined within the range $\mathrm{G_{min} < G_{mag} < G_{max}}$, where $\mathrm{G_{min}}$ and $\mathrm{G_{max}}$ are the magnitude of the fainter and brighter blue straggler on each OC, as in the case of the BSS only RGB stars within $\mathrm{r_{50}}$ were selected. To quantify whether the radial distributions of BSS and RGB, are extracted from the same parent distribution, thus indicating an absence of segregation, we used the k-sample Anderson-Darling test (Scholz and Stephens, 1987, hereafter A-D test). The A-D test is similar to the more widespread Kolmogorov-Smirnov test, but has a greater sensitivity to the tails of the cumulative distribution. The A-D test indicates a difference of 86.9% - 99.9% between the distributions of BSS and RGB stars, for all the clusters.

Figure 2.15 shows the cumulative radial distribution for a representative sample of clusters (the remaining plots are in Appendix D) corrected by field contamination — see§ 5.2.6 for more details. The labeled values of $\mathrm{A_r^+}$ correspond to the size of the grey shaded areas. Formally we where expecting two behaviors: if the two populations are perfectly mixed, we expected a value of $\mathrm{A_r^+} \sim 0$. Instead, if the BSS are segregated

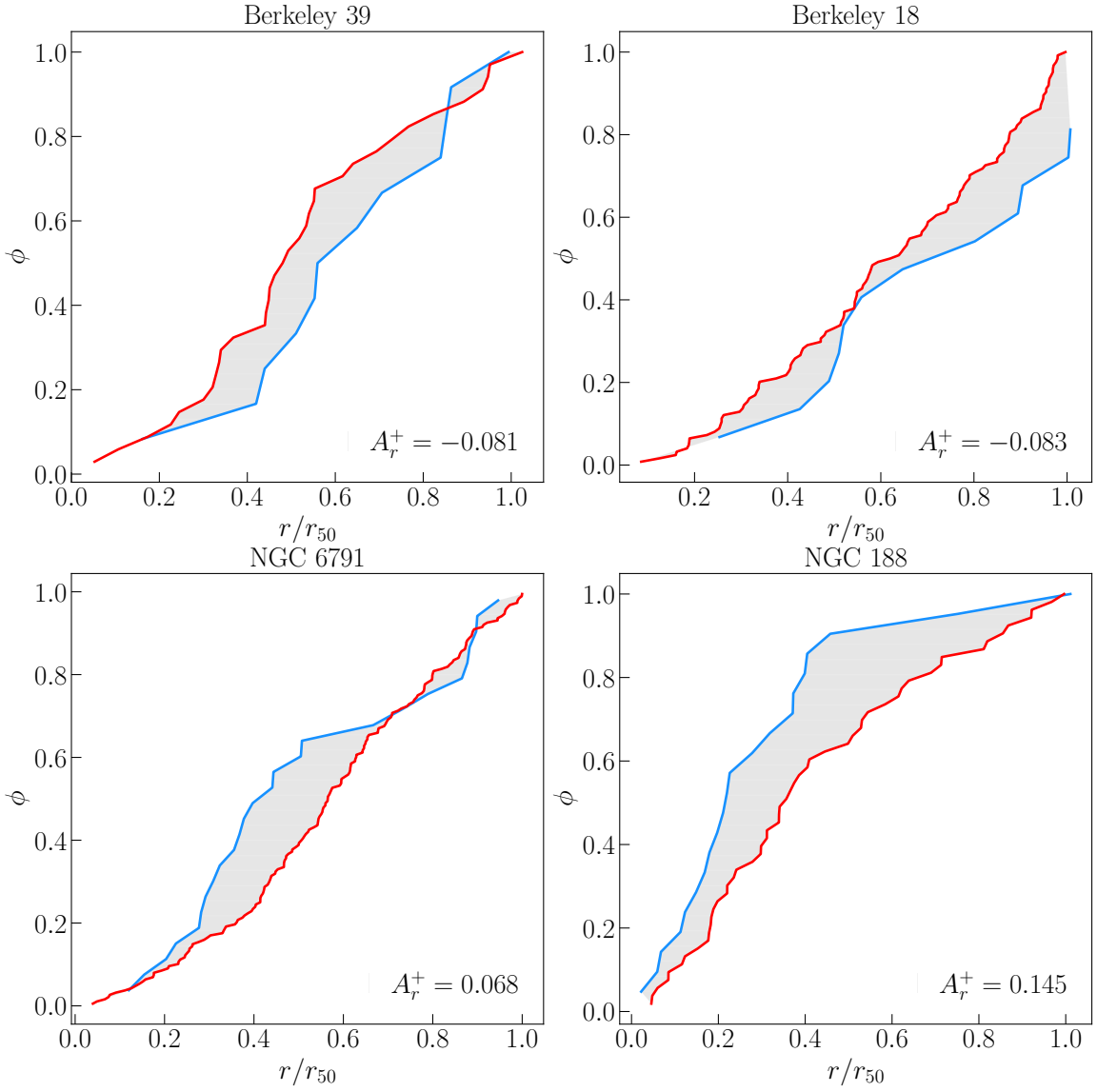

Figure 2.15 Cumulative radial distribution of BSS (blue line) and RGB (red line) observed within one r_{50} in four OCs. The size of the are between the two curves (shaded in gray) corresponds to the labeled valued of A_r^+.

Table 2.8 Cluster parameters; age in logarithmic scale, total number of stars in the cluster $\mathrm{N_{cluster}}$ with $\mathrm{P_{memb}} \geq 50\%$ and radius containing half of the cluster members r_{50}, and values of $\mathrm{A^{+}}$ and $\mathrm{N_{relax}}$

Cluster	$\log(\mathrm{age})$	N_{cluster}	r_{50}	$\mathrm{A^{+}}$	$\mathrm{N_{relax}}$
Berkeley 12	9.3	146	0.036	0.107	33.03
Berkeley 17	9.86	265	0.071	0.063	53.76
Berkeley 18	9.64	386	0.117	-0.083	6.26
Berkeley 21	9.33	78	0.031	-0.065	26.62
Berkeley 32	9.70	442	0.063	-0.021	43.32
Berkeley 39	9.55	552	0.055	-0.081	23.91
Berkeley 70	9.34	217	0.061	-0.244	11.95
Collinder 261	9.8	1866	0.108	0.166	16.94
King 2	9.61	140	0.051	0.157	20.47
King 11	9.65	273	0.062	0.082	45.15
Melotte 66	9.63	810	0.088	0.380	9.35
NGC 188	9.85	865	0.272	0.145	13.42
NGC 1193	9.71	218	0.027	0.115	94.01
NGC 1798	9.22	247	0.039	-0.048	16.23
NGC 2141	9.27	934	0.073	0.114	4.64
NGC 2158	9.00	1392	0.044	-0.170	6.16
NGC 2243	9.64	520	0.046	0.075	43.12
NGC 2506	9.22	1520	0.088	0.08	5.48
NGC 2682	9.63	755	0.166	0.039	46.68
NGC 6253	9.51	488	0.06	0.164	74.09
NGC 6791	9.80	1626	0.068	0.068	19.66
NGC 6819	9.36	1654	0.095	0.045	8.14
NGC 7142	9.49	417	0.102	0.097	19.08
NGC 7789	9.15	3901	0.211	0.056	1.68
Tombaugh 2	9.21	274	0.028	-0.108	10.34
Trumpler 5	9.50	2474	0.134	-0.057	5.02
Trumpler 20	9.00	1059	0.112	-0.163	2.37

towards the cluster center then we expected A_r^+ to increase. Surprisingly in some clusters, the BSS populations seems not be concentrated at all. This is the case of Berkeley 39 and Berkeley 18 with negative values of A_r^+ — top panels of Figure 2.15. In general however, we found for clusters with log(age)>9.0 (1 Gyr) BSS are indeed more centrally concentrated.

As in the case of GCs, we calculate N_{relax} (Ferraro et al., 2018, Lanzoni et al., 2016), a theoretical parameter commonly used as indicative of the dynamical age of the cluster. We used however the same method reported by Jadhav and Subramaniam (2021) to calculate this parameter N_{relax}. With this scope, we determine the central relaxation time using the following equation:

$$T_{relax} = \frac{8.9 \times 10^5 \ (N_{cluster} \ {r_{50}}^3)^{0.5}}{< m_* > \log(0.4 \ N_{cluster})} \tag{2.4}$$

and

$$N_{relax} = \frac{age}{T_{relax}} \tag{2.5}$$

where $< m_* >$ is the average mass of the stars in open clusters. We choose $< m_* > = 0.4 \ M_\odot$, which is the typical average mass in stellar clusters (Leigh et al., 2013). Finally, $N_{cluster}$ is the total number of stars in the cluster with $P_{memb} \geq 50\%$ to be consistent with the region on which the BSS where selected — see § 2.3.

Figure 2.16 shows the comparison between N_{relax} and A^+ for 27 clusters. For comparison, we also show both quantities for GCs from Lanzoni et al. (2016) and for OCs of Rao et al. (2021) on the same figure. We found the best-fit relation of OCs is:

$$\log(N_{relax}) = 2.07(\pm 1.25) \ A_r^+ + 1.18(\pm 0.12) \tag{2.6}$$

For equation 2.6 we used only those clusters with less than 5% of field contamination on their BSS population —see § 5.2.6.The best fitting correlation for OCs in Rao et al. (2021) (open black stars in Figure 2.16)

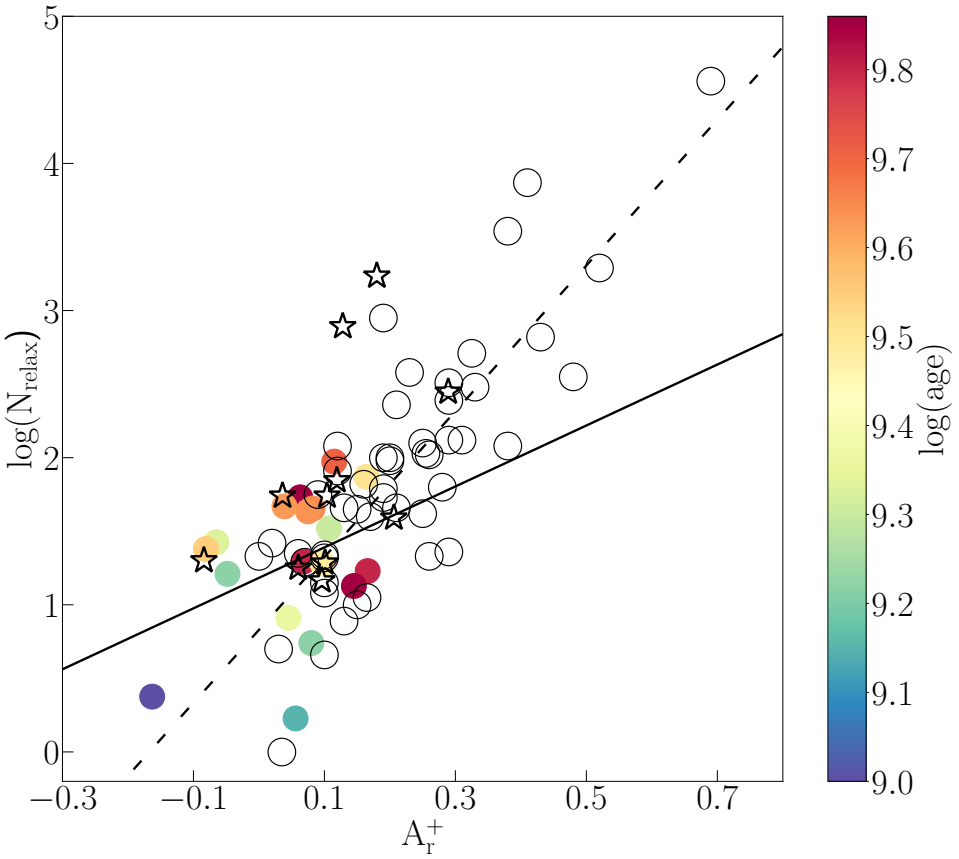

Figure 2.16 Relation between the new parameter A^+ and the logarithm of the parameter N_{relax} for all the clusters reported in Table 2.8. Open clusters in our sample (without Melotte 66) are color-coded by age, while GCs are in open black circles and OCs in black open stars from Rao et al. (2021). Solid and dashed line are the best-fit for our sample and GCs, respectively.

$$\log(N_{relax}) = 4.0(\pm 2.1)\ A_r^+ + 1.42(\pm 0.30) \tag{2.7}$$

and for GCs (open black circles in Figure 2.16) is

$$\log(N_{relax}) = 5.1(\pm 0.5)\ A_r^+ + 0.79(\pm 0.12) \tag{2.8}$$

Our sample exhibits a positive correlation (Eq.2.6) between A^+ and N_{relax} with a smaller slope than the correlation among the GCs (Ferraro et al., 2018, Lanzoni et al., 2016) and

OCs from Rao et al. (2021). Furthermore in Figure 2.16 our data looks as an extension towards lower regimes of A^{+} and $\mathrm{N}_{\mathrm{relax}}$, where nearly 30% of the clusters have negative values of A^{+}, implying they are less dynamically evolved than remaining 70% of the clusters that over-plotted with the distribution of less evolved GCs.

To probe the statistical significance of this correlation in our sample, we performed two correlation test; we found $\mathrm{r_s} = 0.39$ and $\mathrm{p_{value}} = 0.05$ and $\mathrm{r_p} = 0.43$ and $\mathrm{p_{value}} = 0.03$ for Spearman and Pearson tests, respectively. Both are significantly smaller than the values found by Rao et al. (2021) for OCs. Three are the biggest differences between our work and theirs: i) On their calculation of A^{+} they used the MSTO population as the reference one, ii) they used the stars within the half-light radius ($\mathrm{r_h}$) and iii) their sample is considerable smaller (∼10) than ours (∼30). Here we would like to recall we have used the same line-fitting procedure for both OCs samples (Rao et al. (2021) and our sample) and for GCs, in order to avoid differences on the slopes given the different minimization processes. they did (to compare their sample with that of GCs), we use COCOR[8] tool (Diedenhofen and Musch, 2015). This time however we compared their OCs sample with ours —because the COCOR tool only compares two correlations. The test implemented for two independent correlations are the Fisher test and the Zou test. By using $\alpha = 0.05$, $\mathrm{p_{value}} = 0.95$ we found:

- For the Spearman correlation we got a significance level (p-value) of the comparison done by the Fisher test of 0.4452 and from the Zou's test of -0.45507-+0.7052.
- For the Pearson correlation we got instead a significance level of the comparison done by the Fisher test of 0.7617 and from the Zou's test of -0.6298-+0.6023.

But what do these values imply? Since the p-values estimated by the Fisher test are both greater (for Spearman and Pearson) than the chosen α value means the the null hypothesis that two distributions are similar is not rejected. This is corroborated by the presence of Zero in the confidence intervals of the Zou's test. Hence, these tests suggest that the correlation coefficients estimated for the OCs of Rao et al. (2021) and our OCs are not different.

[8] `http://comparingcorrelations.org`

We did the same exercise but this time comparing our results with those of GCs. We found:

- For the Spearman correlation we got a significance level with the Fisher test of 0.032 and from the Zou's test of -0.8157-+0.1243.
- For the Pearson correlation we got instead a significance level of the comparison done by the Fisher test of 0.7617 and from the Zou's test of -0.7957 -+0.1342

On both tests (Fisher and Zou) the null hypothesisì) was rejected. Meaning both correlations are different, despite the visual effect of Figure 2.16.

2.8 Searching for binaries in the all-sky surveys

Living on the era of all-sky surveys a natural step on this thesis was the search of these exotica in short-long term variability surveys such us Transiting Exoplanet Survey Satellite (TESS[9]) and the Optical Gravitational Lensing Experiment (OGLE[10]) with the aim to search for variability among the straggler candidates.

The main goal of TESS (Ricker et al. 2015) is the monitoring of nearly 200,000 bright stars searching for exoplanets across the sky, with a 2-min short cadence, i.e., fixed aperture photometry is recorded every two minutes. However, TESS is also acquiring the Full Frame Images (FFIs) with a 30-min cadence. This survey has dramatically improved our ability to discover multiple star systems, and consequently properly identify the short period binaries present among the BSS. As TESS surveys the northern and southern ecliptic hemispheres, it monitors the members of many OCs and among them some of the clusters included in out catalog. There are several community-lead projects that focus on light-curves (LC's) extraction from TESS FFIs: the NASA Ames SPOC pipeline (Jenkins et al., 2010), the MIT Quick-Look-Pipeline (Huang et al., 2018), `ELEANOR` (Feinstein et al., 2019), the Oelkers and Stassun (2018) difference-imaging pipeline and

[9] `https://tess.mit.edu`
[10] `https://ogle.astrouw.edu.pl`

the TESS Asteroseismic Consortium (TASOC) pipeline (Lund et al., 2021, 2015). While most of them use aperture photometry, the PATHOS (PSF-based Approach to TESS High Quality Data of Stellar Clusters) project (Nardiello et al., 2021, PAPER I) uses the Point Spread Function (PSF) subtraction to mitigate crowding, allowing high-precision photometry for stars in the faint regime ($G > 13$). In (Nardiello et al., 2020, PAPER II) and using CG18 as the input catalog, more than 200,000 LC's of stars—available on the Mikulsi Archive for Space Telescopes[11]—in 645 open clusters located on the Southern ecliptic Hemisphere were extracted from the TESS FFIs. In summary the PATHOS pipeline, for each FFI the positions and magnitudes of the stars in the input catalog are transformed into the astrometric and photometric reference system of the single FFI. For each star and for each image, the routine considers all the neighbour stars within a radius of 20 TESS pixels in the *Gaia* DR2 catalog and transforms their calibrated magnitudes into instrumental fluxes. Then using the local PSF, the transformed fluxes and positions, the software constructs a model of the neighbour stars and subtracts them from the image. On the neighbor-subtracted images, the target flux of each star is then measured using aperture photometry with four aperture sizes of 1, 2, 3 and 4 pixel radius and PSF-fitting photometry.

To find the periodicity we used the classical Lomb-Scargle periodogram (named for Lomb 1976 and Scargle 1982), which is a classic method for finding periodicity in irregularly sampled data. The periodogram itself occupies a unique niche: it is motivated by Fourier analysis, but it can also be viewed as a least squares method. On this context, the `gatspy`[12] package (Vanderplas, 2015, VanderPlas and Ivezić, 2015) is a public, python-friendly algorithm which provides three different main implementations of the classic Lomb-Scargle periodogram; LombScargle, LombScargleFast and LombScargleAstroML. On this thesis we have used the LombScargleFast algorithm which implements an efficient pure-Python version of the Fast Fourier Transform-based algorithm from Press and Rybicki (1989) . The later is much faster than either of the remaining implementations of `gatspy`, especially as the number of data points and frequencies increases. It is limited however, to either a simple pre-centered model or a floating mean model, and the frequencies must be computed on a regular grid.

[11] `https://archive.stsci.edu`
[12] `http://www.astroml.org/gatspy/`

Since extreme outliers can often complicate the analysis of TESS LC's, after we downloaded the data we "cleaned" each LC following a similar procedure than the one reported by Nardiello et al. (2020); we excluded all the points whose: i) quality flag is higher than Zero `DQUALITY` > 0, those ii) with values above 2.5 $\sigma_{\rm flux}$ the median flux and iii) with values higher than 3.5 $\sigma_{\rm sky}$ the median value of the sky. Additionally, when considering the periodogram from the Fourier perspective, it is useful to normalize the periodogram such that in the special case of equal spaced data, it recovers the standard Fourier power spectrum. On this line, to define the continuum we binned our data in 10 bins of ∼2.5 days each and we estimated the highest points in each bin. Then, we interpolated these points with splines and divided each point of the LC's by this interpolation. An example is shown in Figure 2.17. Here, Panel (a) shows the normalized light curve of one BSS (Gaia DR2 2217989766712690432) in the cluster NGC 7142, while panels (b) and (c) of Figure 2.17 show the Lomb-Scargle periodogram and the corresponding phase of the star. The remaining short-period binaries for each cluster can be found in Appendix A.

To find the periodicity, we searched for objects having a period in the range 0.1 $\leq$ P (days) $\leq 0.5 \times \mathrm{T_{LC}}$ days, where $\mathrm{T_{LC}}$ is the maximum temporal baseline of the LC, usually for a single sector $\mathrm{T_{LC}}$ ∼27 days. Additionally, we downloaded the Target Pixel File (TPF) of each object to inspect possible contamination sources using `tpfplotter`[13] (Aller et al., 2020) tool. This check of the TPFs is especially important because of the faintness of our sample in comparison with most of the two-minute cadences targets observed by TESS. Figure 2.18 shows the TPF of star Gaia DR2 2217989766712690432 (the same of Figure 2.17), marked with a white cross. The red circles represent the Gaia sources from the DR2 catalogue Gaia Collaboration et al. (2018), scaled by magnitude contrast against the target source. We over-plotted all the sources with a magnitude contrast up to Δm = 2 (i.e. two magnitudes fainter than our target, which corresponds to ∼15% of contamination if entirely inside the aperture). `tpfplotter` gives an output list with the Gaia-ID and distances (in pixel and arcsec) of the nearest stars to our targets within the magnitude contrast selected. For our targets, if we found "fainter contaminants" inside 1-pixel radius (21 arcsec, pixel scale of TESS) we still use the LC. For these, ground-based photometry is probably necessary in order to discern the source

[13] `https://github.com/jlillo/tpfplotter`

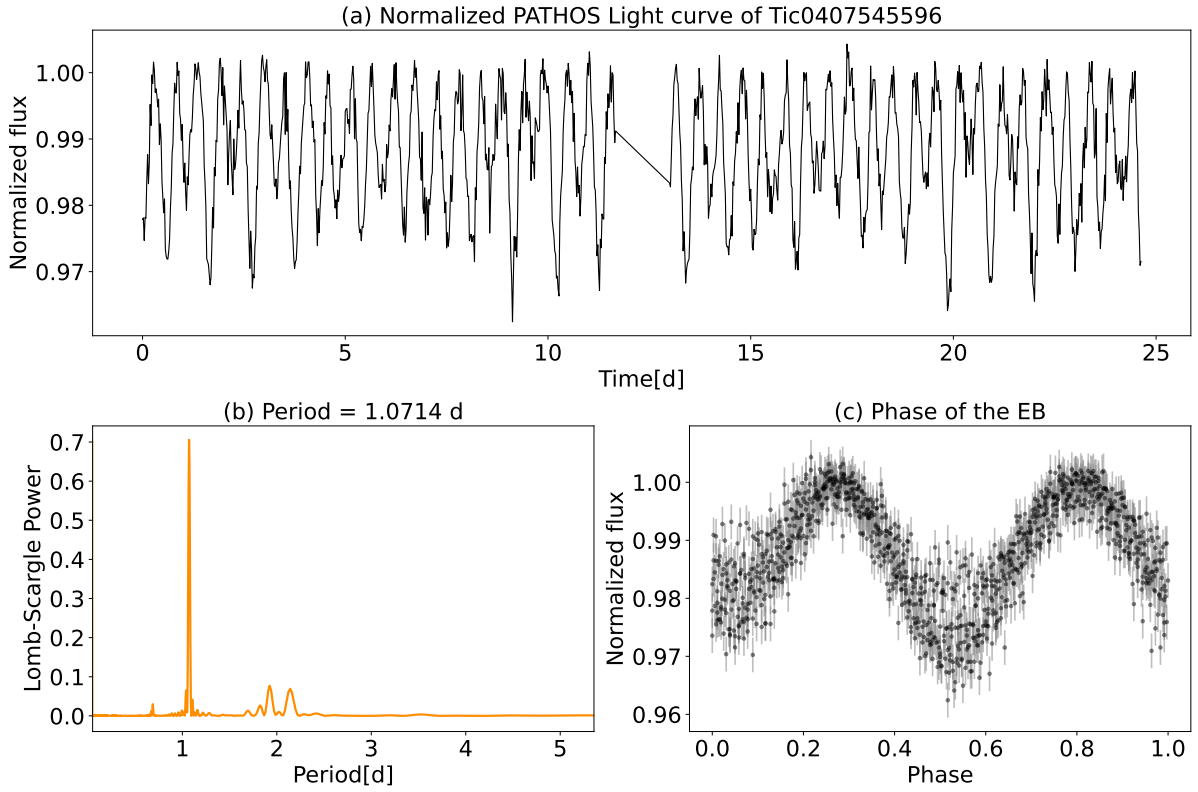

Figure 2.17 For both figures; panels (a) are the light curve of the BSS *Gaia* DR2 2217989766712690432 (or TIC 407545596); panel (b) shows the Lomb-Scargle periodogram from `gatspy`; and panel (c) is the phase transit of the eclipsing binaries. The BSS is a member of the cluster NGC 7142.

of the variability. Also, radial velocity follow-up is essential in all cases to constrain the orbital parameters of the binary candidates found in this work. If instead we found "brighter contaminants" inside 1-pixel radius we have discarded the LC completely.

In general, we found at least ∼7% of the nearly 900 blue stragglers are probably in short-period binary systems. Further, as mentioned in the Introduction of this thesis, it is well know that the fraction of short-period binaries found among BSS in the two most well studied Galactic open cluster; NGC 188 and M67 is about 10%. Surprisingly, with our analysis we found that eight open clusters in our catalog have large percentages of short-period binaries among their straggler populations —see Table 2.9— with orbital periods between 4.8 hours and 2.77 days. The percentages reported can be, however, considered as lower limits —in the case of Berkeley 32 influenced also by Field stars,

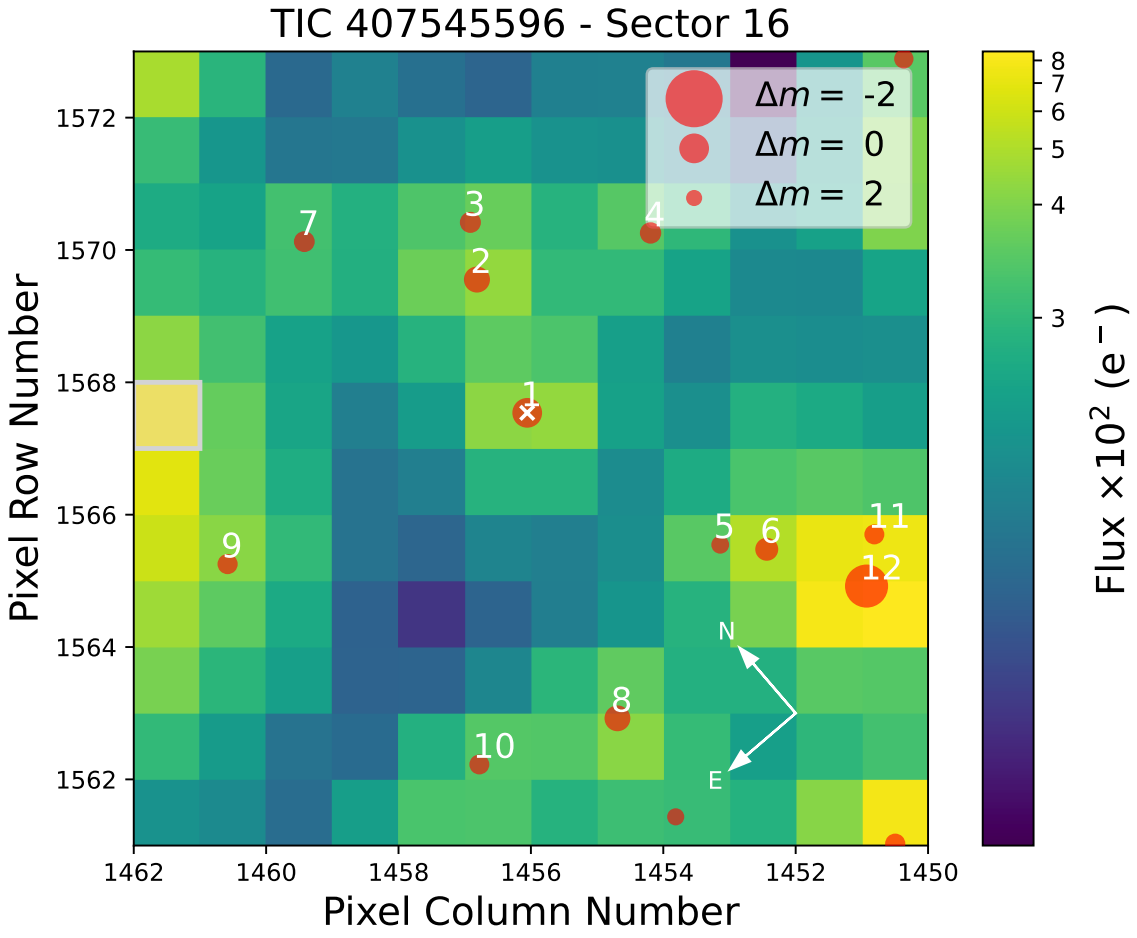

Figure 2.18 Target pixel file (TPF) of *Gaia* DR2 2217989766712690432 (or TIC 407545596, G_{mag}=13.96) for Sector 16. The red circles are the sources of the *Gaia* DR2 catalog in the field with scaled magnitudes (see legend). White cross indicate the location of the targets. Pixel scale is 21 arcsec pixel^{-1}. The closest stars 2 and 3 are at 2.15-pixel (45 arcsec) and 3-pixel (63 arcsec) of distance respectively.

see § 2.4.2. The latter because not all the BSS on each cluster where processed by the PATHOS project. Interesting enough, among these short-period systems we have apparently found not binaries, but multiple signal stars that can be either blended EBs or true hierarchical systems —see e.g NGC 2243, NGC 1193 and NGC 2141 LC's in Appendix A. These stars definitely need more attention in the future —see Prš a et al. (2022). Interesting enough are the cluster King 19 (600 Myr) and Melotte 105 (400 Myr) where both host only one BSS which at the same time is a short-period eclipsing binary.

Table 2.9 Open clusters having large number of close-binary systems among their straggler population. Column 1-4 are the Cluster name, age, metallicity, cluster mass and number of BSS candidates we found in our catalog. Column 5 indicates the percentage of short-period binaries we found on each. Clusters are sorted by age.

Cluster	log(age)	[Fe/H] dex	M_{TOT} $M_{\odot}$	N_{BSS}	%
Collinder_261	9.90	-0.003	35172	53	33–45%
Berkeley_32	9.68	-0.280	5136	27	11–23%
NGC_1193	9.66	-0.257	6522	12	25%
Melotte_66	9.65	-0.325	18163	14	14–29%
NGC_7142	9.55	+0.080	4717	10	20%
NGC_2243	9.53	-0.482	7576	14	21%
NGC_2141	9.46	+0.300	15302	32	13%

Regarding the yellow straggler sample. We found at least 8% of the total (6/77) are in close-binary systems with periods between 0.45 to 2.40 days. This is however just a lower limit as explained above. Something interesting we would like to pinpoint out, is how the names of the clusters having short-period YSS match with that of those having short-period BSS —Collinder 261, Berkeley 32, NGC 2141, King 2 and Melotte 66, see Table 2.9. The light curves of the YSS are reported in Appendix A.

Finally, few things are important to mention; i) the faintest magnitudes we reach in our cluster analysis is G_{mag} ∼16-17 and ii) we have not considered any other cause of variability such us starspots and oscillations in our analysis. It is however, in our future plans the analysis of their (O-C) diagrams, which carry much and valuable information — see Sterken (2005). Finally iii) the accuracy and precision of *Gaia* DR2 enable the discovery of astrometric binaries which are, however, significantly affected by the measurements and data processing. The *Gaia* single body 5-parameter astrometric solution is fitted to the binary, under the assumption that the binary moves like a single point mass which leads to considerable biases. In this sense, we are aware that CG18 astrometric selection of members likely leaves out some binaries. Long-period binaries will be affected by an excess of proper motions, and systems with periods around 1 year will have an effect on their parallax values (under- or over-estimation, Penoyre et al. 2020). On the other hand, in close-binary systems the proper motions will be affected by the orbital velocity.

The binaries we found and the BSS in general are still of course "candidates", and the definitive probe of membership is still needed, so RVs measurements for all the stragglers are mandatory. If confirmed, however, these fractions might give us important information about the parameter space (age, metallicity, cluster mass) on which short-period-BSS preferentially formed. Table 2.9 provides some hints that metal-poor and oldest clusters have the largest fractions of close-BSS binaries.

On the other hand, the OGLE collection of variable stars is probably the largest set of variable stars in the world. We searched the ∼900 BSS in OGLE searching for other type of variables stars (e.g long-period variables, delta Scuti stars, RR Lyrae, etc) different to the ones found in TESS. For the entire disk sample reported on the latest releases of OGLE (III+IV) we only found one δ Scuti in the open cluster Collinder 261 corresponding to the star Gaia DR2 5856527524085206656 (or OGLE-GD-DSCT-3748). Further, no YSS are reported as variable stars in OGLE.

Gaia also provided a "clean" list of confirmed all-sky RR Lyrae and Cepheid stars from contaminating objects and other types of variables falling into the same period domain. We employed the table access protocol (TAP) and the astronomical data query language (ADQL), together with the Tool for OPerations on Catalogues And Table (TOPCAT),[14] to access the *Gaia* data; specifically to the `vari_classifier_result` table of the Gaia archive. As in the previous case, however (with OGLE data) none of our stragglers have been classifying within these stars.

2.9 Summary and conclusions

In this chapter we have presented a new catalog of blue and yellow stragglers in OCs. The motivation for updating the previous versions is twofold. First, the burst of "all-sky and large surveys" over the whole range of the electromagnetic spectrum have provided new, homogeneous data for an enormous amount of objects, allowing their study over larger sky areas. Second, the need to identify straggler candidates more reliably and accurately, not merely based on their positions in the CMD, but also using

[14] `http://www.starlink.ac.uk/topcat/`

the more accurate astrometric membership provided by *Gaia* DR2. We thus defined homogeneous criteria for the selection of the BSS to derive proper-motion-cleaned BSS catalogs in all our OCs. In this edition, 897 stragglers were identified in 111 clusters of a total of 408 OCs, of which 19 are recently discovered objects that are not present in the catalog AL07; on the other hand, 39 clusters listed in AL07 are not present in this new version. Regarding yellow straggler counts, 77 YSS were identified in 43 OCs. The proper motion decontamination allowed an unambiguous selection of YSS in the CMD, which had not been possible in previous BSS studies in OCs, given the high field star contamination that the Galactic disk causes in the CMDs. We want to remark that this is the very first catalog containing this information.

We have reinvestigate two of the most explored relations between the straggler numbers and the cluster parameters; the age and the integrated magnitude. We confirmed that older cluster host larger populations of blue stragglers. We also found no evidence of BSS and YSS in clusters younger than log(age)=7.3 and log(age)=8.2, respectively. In contrast to previous claims we found the specific frequency of BSS in OCs follows a similar distribution than the one of the GCs, not been in agreement anymore with that of dSphs.

We also studied the radial distribution of the BSS in a sub-sample of 27 clusters. In open clusters older than 1 Gyr, blue stragglers are indeed more centrally concentrated, there are however some special cases in which no signs of central segregation were found. Using our data we have refined the relation to estimate the dynamical state of OCs.

We cross-correlated our catalog with the Transiting Exoplanet Survey Satellite (TESS) and we found several short-period binaries. Nearly ∼90% of them are new discoveries, for which we have provided the period and LC's. We found the percentage of short-period binaries in YSS (8%) is higher than in BSS (7%). Finally, among the southern clusters we found eight interesting cases having large fraction of close-binaries among their straggler populations; we hope be able to study them in the future.

Chapter 3

Blue straggler stars in *Gaia* EDR3

This chapter is mainly based on:

Statistical analysis of Blue straggler stars in Galactic star clusters

Authors: M.J. Rain, G. I, Perren, M.S Pera, G. Carraro, S. Villanova, J.A. Ahumada, R. A. Vazquez

in preparation

3.1 Short introduction

While finishing my PhD work, the *Gaia* Early Data Release 3 (*Gaia* EDR3) came out. With my collaborators we decided to not avoid the opportunity to explore how much our DR2 data had changed after the new release. *Gaia* EDR3 is based on the data collected during the first 34 months of the mission. This early part of the Third Release consists of an updated source list, astrometry, and broad-band photometry in the G, $G_{\rm BP}$, and $G_{\rm RP}$ bands, and represents a significant improvement in both the precision and accuracy of the astrometry and photometry in comparison with *Gaia* DR2—data used to construct our catalog. *Gaia* eDR3 should enable an improved census of the blue straggler population.

But also and as mentioned in the Introduction, both theoretical and observational efforts have been made to find the dominant formation scenario, and many authors have tried to explain the presence of the BSS either by pinpointing to one formation pathway or rather invoking multiple formation mechanisms simultaneously acting in the same cluster. The most natural assumption is to think that, whatever the mechanism that forms BSS is, it must be related with the cluster global properties.

Along this vein, this chapter aims to perform comparisons between *Gaia* DR2 and EDR3 data focused on the impact on the blue straggler population by either using one up above the other. The main scope however, is to search for correlations between the observed number of BSS ($\rm N_{BSS}$) with various physical parameters in fourteen open clusters. Some of these relations have been explored only in the older counterpart of OCs, the GCs, and while they are suspected to be present in OCs as well, no authors have reported them before.

The data use on this study namely the cluster and member selections are described in § 3.2. The description of the estimation of the fundamental parameters in § 3.3 while the comparison between *Gaia* DR2 and EDR3 is in § 3.4. Finally, we searched for possible correlations with the cluster mass, binary fraction and binaries in § 3.5. We summarize and conclude in § 3.6.

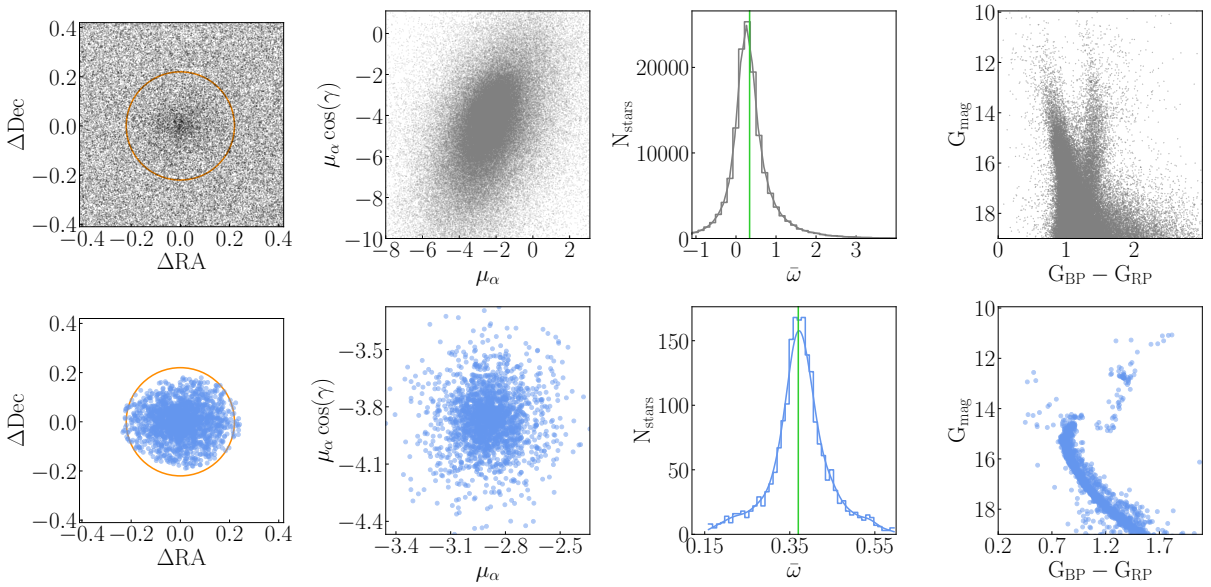

Figure 3.1 Output of the iterative process using pyUPMASK. From left to right the first row shows the right ascension RA and declination DEC plane, Proper motions distributions in RA and Dec (μ_α and $\mu_\alpha \cos(\gamma)$ respectively), parallaxes (ϖ values, and CMD of all the stars within the frame. Second row shows the same but for members only.

3.2 Members and cluster selection

The clusters were first selected on the basis of the number of blue stragglers. Only those with $N_{\rm BSS} \geq 8$ listed in our catalog were selected. The original list contained a total of 32 clusters with $\log(\text{age}) \geq 9.0 = 1$ Gyr (Dias et al., 2021), distances $d > 850$ pc (CG20), and masses $M_{\rm tot} > 1400$ $M_\odot$ (Jadhav and Subramaniam, 2021).

For the 32 clusters we performed a membership selection using Gaia astrometric solution. The clusters' members were estimated via a two-step process. First we downloaded the data of each cluster by using a simple script to query EDR3 data using the astroquery package[1]. This package generates two user-defined colors (not present in the raw Gaia data) with their associated uncertainties. The last will be useful for the process described in § 3.3. For each cluster, we then selected all the stars within 2 times the apparent radius reported in DAML02 and with magnitudes down to $G_{\rm mag} = 21$. Second, the most likely members for each cluster were identified with the pyUPMASK

[1] `https://github.com/Gabriel-p/GaiaQuery`

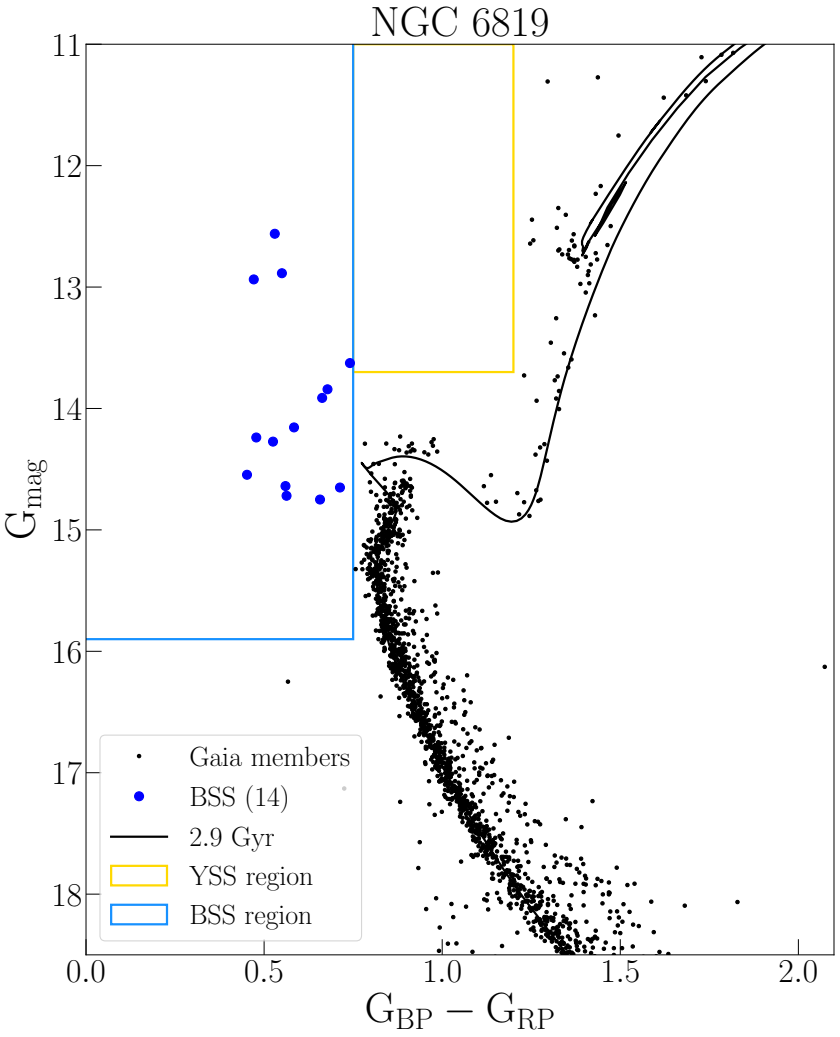

Figure 3.2 Color-magnitude diagram of the open cluster NGC 6819 shown to illustrate BSS and YSS selection. Light blue, yellow and red lines separate the different regions where these stars where searched for. The MIST isochrone is shown for comparison. The style of this figure has been inspired in the CMDs presented in Leiner and Geller (2021).

code (Pera et al., 2021). This tool assigns probability membership $\mathrm{P_{memb}}$ values to all the stars in an observed frame, based on input data selected by the user. In this case we employed parallax and proper motions data we downloaded from the Gaia EDR3 survey as the input data.

After assigning probabilities, the final members list is automatically generated by an

Table 3.1 Stars counts in the cluster sample used in this section. For comparison purposes the values given in R21b are also included.

Cluster	$N_{\rm BSS}$	$N_{\rm YSS}$	$N_{\rm BSS-R21b}$	$N_{\rm YSS-R21b}$	$N_{\rm MS}$
Berkeley 14	15	0	09	0	076
Berkeley 17	29	1	20	0	165
Berkeley 32	26	3	27	2	113
Berkeley 39	24	2	18	2	171
Collinder 261	46	4	53	3	331
Melotte 66	18	1	14	1	215
NGC 188	21	0	22	0	136
NGC 2141	41	1	18	3	206
NGC 2158	38	1	39	3	345
NGC 2243	10	0	14	1	113
NGC 2506	10	2	14	0	195
NGC 2682	09	0	11	0	098
NGC 6819	14	0	15	0	214
NGC 7789	15	0	16	0	251

Notes:
$N_{\rm BSS-R21}$ and $N_{\rm YSS-R21}$ are the number of blue straggler and yellow straggler selected as candidates in our catalog R21b.

iterative process. This process works by filtering out low probability stars at each step, and halts when the density of stars within the cluster region is consistent with the expected density (taking into account the field density value outside the adopted cluster region). An illustration of the process applied on the cluster NGC 6819 is shown in Figure 3.1 while the corresponding CMD and the blue and yellow straggler selection in Figure 3.2. On the later are shown the position on the sky, proper motions, parallax values and the CMD of all the stars within the frame and for the selected members. After this membership analysis, we removed six clusters from our list because of their sparse nature. With only a handful of sub-giant (SGB) and RGB stars, these clusters have large errors for the few observed stars and can lead to an over-estimation of the parameters (e.g, mass, age), and therefore we do not consider them reliable enough for the main aim of this work.

3.2.1 Reddening corrections

As described in § 2.4.3 given their proximity to the Galactic disk, OCs can be affected by extinction effects. We corrected this effect in the remaining 26 OCs using the technique described in 5.2.1.1 In some cases our correction for the differential extinction despite improving the data was not enough, particularly in those clusters with $d > 5.5$ kpc and $1.0 < A_V < 2.5$. Seven clusters, despite being rich enough, still show spread in color of their main sequence and giant branches, but most strikingly in the TO region, making difficult the isochrone fitting process and hence defining the BS region as described in § 2.3. As mentioned previously for the scope of this chapter, the proper identification of the bona fide blue stragglers is essential, so these clusters where left out from the sample.

3.3 Estimation of fundamental parameters with `ASteCa`

The fundamental parameters for all the clusters (age, binary fraction $\mathrm{f_{bin}}$, distance, metallicity, extinction, and cluster mass $\mathrm{M_{Tot}}$) were estimated with the **`ASteCA`** package (Perren et al., 2015). This package has been used to successfully analyze hundreds of clusters since its release (Perren et al., 2020, Perren et al., 2017). To simplify the Bayesian inference process that estimates the fundamental parameters, we assume a general solar metallicity and allow the rest of the parameters to vary within reasonable ranges. The estimation of the binary fraction depends on the chosen distribution of secondary to primary masses $q = m_2/m_1$ (mass ratio). Three mass ratios where employed to test the influence of this distribution on the results. These distributions are specified to be uniform in the $[q_{\min}, 1]$ range with the minimum mass ratio $q_{\min} = (0.5, 0.6, 0.7)$, this is:

$$q = \begin{cases} 0, & [0, q_{\min}) \\ 1, & [q_{\min}, 1] \end{cases} \tag{3.1}$$

The shape of these distributions approximates the empirical distributions found in works such as Fisher et al. (2005) and Raghavan et al. (2010), where the mass ratio is close to unity ($m_2 \approx m_1$) and drops rapidly for lower values ($m_2 \leq 0.5\ m_1$). For one cluster in our sample (King 11) the calculation of the parameters was particularly challenging given the large number of MS stars and the high levels of dispersion among them. When calculating $\mathrm{f_{bin}}$ for King 11, `ASteCa` takes into account both the large quantity of stars and the corresponding dispersion of the MS, and so estimates a large $\mathrm{f_{bin}}$ value, which is far from been real. The last shifts down the isochrone fitting (towards fainter magnitudes) and leads to a bad fitting of the sub-giant and red-giant branches. Similar problems were reported in Tosi et al. (2007) for the same cluster. For the above mentioned, we left out from our sample this cluster as well.

The results for the final list of clusters are reported in Table 3.2.

3.4 *Gaia* DR2 vs. *Gaia* EDR3

Among the fourteen clusters in the final list we found the following differences with our catalog (R21b) that are worth discussing:

- NGC 2141 shows a considerable increase ($\Delta \mathrm{N_{BSS}} = 23$)[2] in the number of straggler candidates in comparison with R21b. It is possible that our decision—in the present section—of not cutting by the same membership probability on every cluster ($P_{\mathrm{memb}} \geq 50\%$ in R21b), while instead using an iterative process that takes into account the density of stars within the cluster region and field, which helps, e.g., to remove those "members" with proper motions or parallaxes located far from the mean of the subgroup of stars with high membership probabilities. About the latter, we found that probability cut-off selection is particularly tricky for clusters with severe imbalance, i.e., there are many more points of one class (field) than another (cluster). Using a value of $P_{\mathrm{memb}} \geq 50\%$, although it sounds

[2] $\Delta \mathrm{N_x} = \mathrm{N_x} - \mathrm{N_{x(R21b)}}$ where x=BSS or YSS. For this quantity we decided not to used the absolute value because it can indicate a tendency between both data release.

Table 3.2 Parameters of open clusters in our sample adopted for this study.

Cluster	$Age_{0.5}$	$f_{bin_{0.5}}$	$Mass_{0.5}$	$dist_{0.5}$	$Age_{0.6}$	$f_{bin_{0.6}}$	$Mass_{0.6}$	$dist_{0.6}$	$Age_{0.7}$	$f_{bin_{0.7}}$	$Mass_{0.7}$	$dist_{0.7}$
Berkeley 14	9.58±0.01	0.48±0.07	8128±756	13.09±0.02	9.58±0.01	0.39±0.03	7514±877	13.03±0.01	9.59±0.01	0.42±0.03	9406±603	13.09±0.02
Berkeley 17	10.0±0.06	0.46±0.07	19731±2160	12.26±0.06	9.94±0.00	0.44±0.05	20223±1365	12.33±0.01	9.97± 0.01	0.38±0.03	17735±1222	12.31±0.02
Berkeley 32	9.82±0.04	0.42±0.07	15448±1544	12.51±0.01	9.79±0.01	0.30±0.06	414071±1120	12.50±0.01	9.84±0.00	0.29±0.01	16649±559	12.52±0.00
Berkeley 39	9.86±0.01	0.26±0.02	16051±9.04	13.00±0.00	9.86±0.01	0.26±0.02	16051±904	13.00±0.00	9.89±0.02	0.23±0.04	16716±967	12.98±0.02
Collinder 261	9.88±0.05	0.56±0.03	39675±2460	12.07±0.04	9.91±0.00	0.42±0.01	34644±1134	12.05±0.01	9.90±0.03	0.37±0.02	36941±2600	12.05±0.01
Melotte 66	9.72±0.00	0.37±0.02	25273±1068	13.35±0.00	9.72±0.00	0.37±0.02	25273±1068	13.35±0.00	9.67±0.00	0.34±0.02	20958±887	13.55±0.00
NGC 188	9.88±0.01	0.36±0.04	15018±782	11.20±0.00	9.88±0.01	0.36±0.04	15019±782	11.30±0.00	9.89±0.00	0.32±0.03	14860±607	11.20±0.00
NGC 2141	9.39±0.01	0.49±0.02	27337±1367	13.12±0.02	9.39±0.01	0.49±0.02	27338±1367	13.12±0.021	9.41±0.00	0.36±0.02	26251±1385	13.05±0.01
NGC 2158	9.35±0.00	0.38±0.01	39384±653	12.83±0.00	9.35±0.00	0.38±0.01	39384±653	12.83±0.00	9.48±0.12	0.36±0.05	38854±4453	12.77±0.06
NGC 2243	9.51±0.00	0.23±0.02	9448±295	13.05±0.00	9.51±0.00	0.23±0.02	9448±295	13.05±0.00	9.54±0.00	0.15±0.02	9279±888	13.05±0.00
NGC 2506	9.36±0.00	0.22±0.00	22250±213	12.49±0.00	9.36±0.00	0.22±0.00	22250±213	12.49±0.00	9.32±0.02	0.19±0.02	19934±1194	12.53±0.02
NGC 2682	9.65±0.02	0.38±0.03	8304±502	9.53±0.01	9.65±0.02	0.38±0.03	8304±502	9.53±0.01	9.71±0.02	0.23±0.04	7437±533	9.51±0.00
NGC 6819	9.43±0.04	0.30±0.16	28598±14357	11.91±0.04	9.43±0.04	0.30±0.16	28598±14357	11.91±0.04	9.66±0.06	0.17±0.02	28157±1326	11.64±0.03
NGC 7789	9.22±0.01	0.27±0.02	21676±857	11.39±0.01	9.22±0.01	0.27±0.02	21676±857	11.39±0.01	9.20±0.00	0.24±0.02	22150±778	11.40±0.00

Notes:
Columns 2–12 are the ages, binary fractions, masses, and distances we obtained for every running of **ASteCA**.
For more information related **ASteCA** we refer the reader to Perren et al. (2015)
The indexes indicate $q_{\min} = 0.5$, 0.6 and 0.7

reasonable, can still introduce outliers within the cluster members as mentioned in § 2.4. In particular, NGC 2141 is a cluster located in a very high field-star density region. To test a possible failure in our methodology we re-analysed the data of this cluster, but this time using Density-Based Spatial Clustering of Applications with noise (DBSCAN[3]) which is a well-known data clustering algorithm that is commonly used in data mining and machine learning. Based on a set of points, DBSCAN groups together points that are close to each other based on a distance measurement (usually Euclidean distance) and a minimum number of points. It also marks as outliers the points that are in low-density regions. After applying the algorithm and following the definition of a blue straggler (§ 2.3) we found ∼40 candidates. In agreement with our finding when using EDR3.

- For the YSS (evolved-BSS) instead and generally speaking the picture is more or less the same. NGC 2141, NGC 2158 and NGC 2506 show the largest variations, $\Delta N_{\rm YSS} = 2$. So far no authors have been able to quantify how many of these stars are expected in the yellow straggler region as function of the observed $N_{\rm BSS}$ of each OC. As mentioned in § 2.3.2 that region might be contaminated with field and normal binaries. Further, our selection of YSS (as in the case of the BSS) is highly dependent on the selection criteria for the cluster members.

- The mean difference for the remaining clusters are $< \Delta N_{\rm BSS} = 3.6 \pm 2.0 >$ and $< \Delta N_{\rm YSS} = 0.8 \pm 0.7 >$. As shown in Table 3.1, we systematically found less BSS and YSS when using EDR3 data.

- It is important to consider that the differences previously mentioned are also a consequence of the differences between *Gaia* DR2 and EDR3. In detail the situation is even more complex, a reflection of this is the case of Collinder 261. Using EDR3 we found 46 candidates while with DR2 we found 53! From those 53 only 39 are in common with the 46 recently found. The later means 7 out of the 46 are "new blue stragglers", not counted in our catalog (R21b). Further, in total there are approximately 14 stragglers missing (if we consider for Collinder 261 $\Delta N_{\rm BSS} = -7$) between our catalog using DR2 (§ 2.5) and our most recently study (this chapter) using EDR3.

[3] `https://cran.r-project.org/web/packages/dbscan/index.html`

3.5 Searching for correlations

As mentioned previously, different conventions are used in statistical studies of BSS. On this chapter however, we used two conventions; the first and simplest is the raw number of BSS, defined elsewhere as $\mathrm{N_{BSS}}$ and the a second is with the blue straggler population normalized by the MS, calculated as $\mathrm{F_{MS}^{BSS}}$ = $\log(\mathrm{N_{BSS}}/\mathrm{N_{MS}})$ —in the literature is however common to find normalizations using either TO, RGB or red clump stars as a cluster reference population within the same field of view; a discussion regarding this point is in Appendix A.

$\mathbf{N_{BSS}}$ vs. $\mathbf{f_{bin}}$. Open clusters are both less massive and younger than globular clusters. Their proximity and low density make the determination of the binary frequency particularly easy. Furthermore in open clusters the relation between this parameter and the $N_{\rm BSS}$ have never been explored in detail before. To test how strong the dependence between the $N_{\rm BSS}$ and the cluster age is, we determined the significance of our correlations via the Spearman rank test. Interestingly enough, Figure 3.3 shows a strong correlation between $N_{\rm BSS}$ and $f_{\rm bin}$. The strongest dependency is given with $q_{\rm min} = 0.7$ (panel c; $r_s = 0.66$), while the weakest is $q_{\rm min} = 0.5$ (panel a; $r_s = 0.59$). The correlation is continuous as in GCs (Milone et al., 2012) and extends to higher values of $f_{\rm bin}$. As expected $f_{\rm bin}$ decrease with increasing $q_{\rm min}$ in almost all the clusters.

In the case of Melotte 66 and NGC 2158, $f_{\rm bin}$ remains however almost constant. In the case of NGC 2141 and NGC 6819 the highest binary content is with $q_{\rm min} = 0.6$. As in the previous case when using $F_{\rm MS}^{\rm BSS}$ the strength of the relation increase for $q_{min} = 0.5$ (panel a; from $r_s = 0.59$ to $r_s = 0.72$), while in the remaining panels this dependency decreases (panel b; from $r_s = 0.63$ to $r_s = 0.60$ and panel c; from $r_s = 0.66$ to $r_s = 0.58$), these results are plotted in Figure C.1.

$\mathbf{N_{BSS}}$ vs. $\mathbf{N_{bin}}$: The cluster mass inside the core radius has been considered by different authors to be the best indicator of blue straggler population size in stellar clusters (e.g., Knigge et al. 2009, Leigh et al. 2011). In this work we found a dependence of $N_{\rm BSS} \propto M_{\rm tot}^{\delta}$, with $0.6 < \delta < 0.7$ — in Figure 3.4 is reported the relation between $N_{\rm BSS}$ and $M_{\rm tot}$. This values are considerably higher than the predicted value reported on Knigge et al. (2009) for GCs, $M_{\rm tot}^{\delta=0.4-0.5}$, but in agreement with the recently upper limit

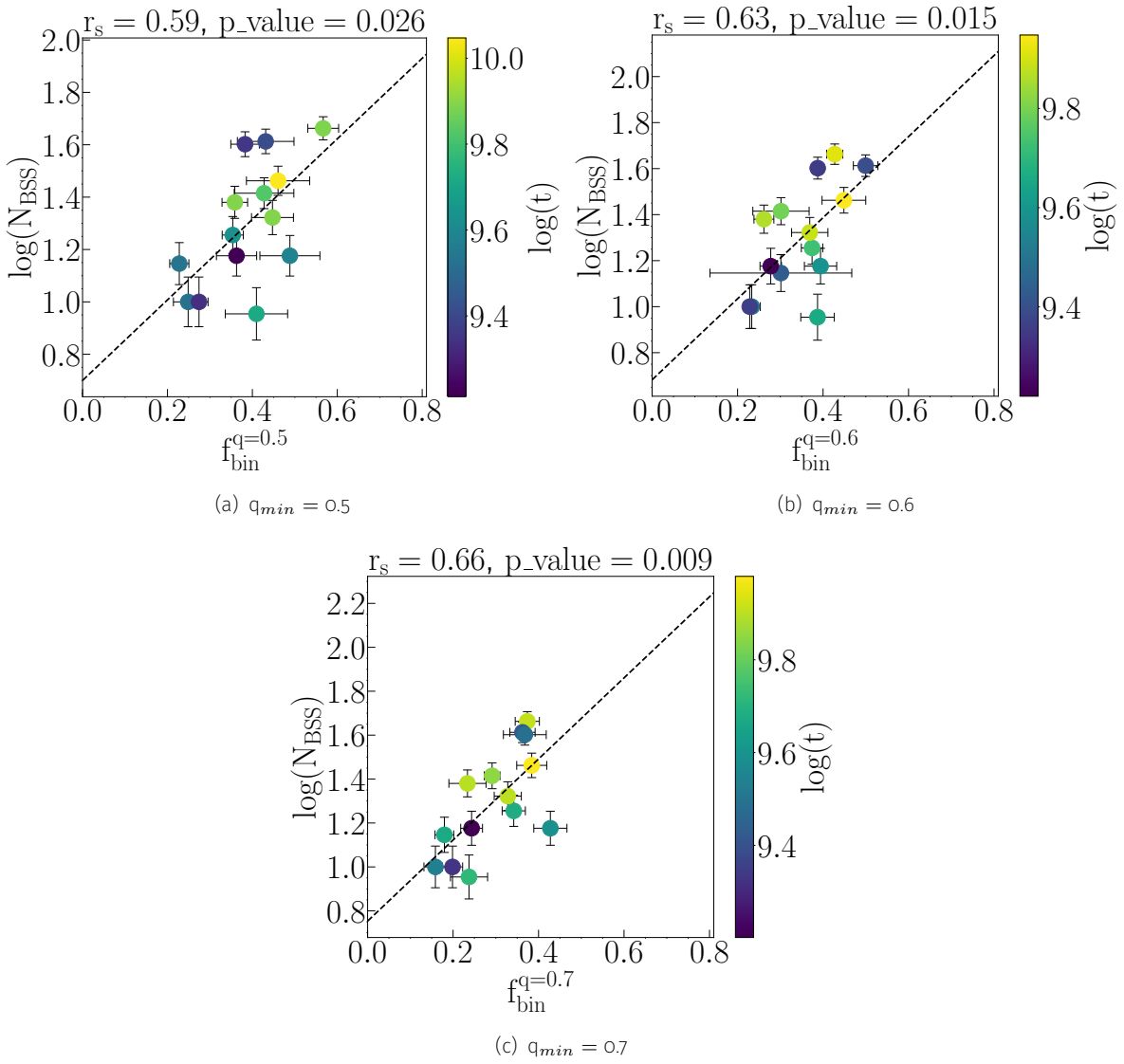

(a) $q_{min} = 0.5$

(b) $q_{min} = 0.6$

(c) $q_{min} = 0.7$

Figure 3.3 Logarithm of the observed number of blue straggler stars a function of binary fraction. The dashed black line indicates the best fit to the data —slope is reported in Table 3.3. Color bar indicates the age of each cluster. Errors are Poissonian. From left to right the different run of **ASteCA**, i.e., $q_{\rm min} = 0.5$, 0.6 and 0.7.

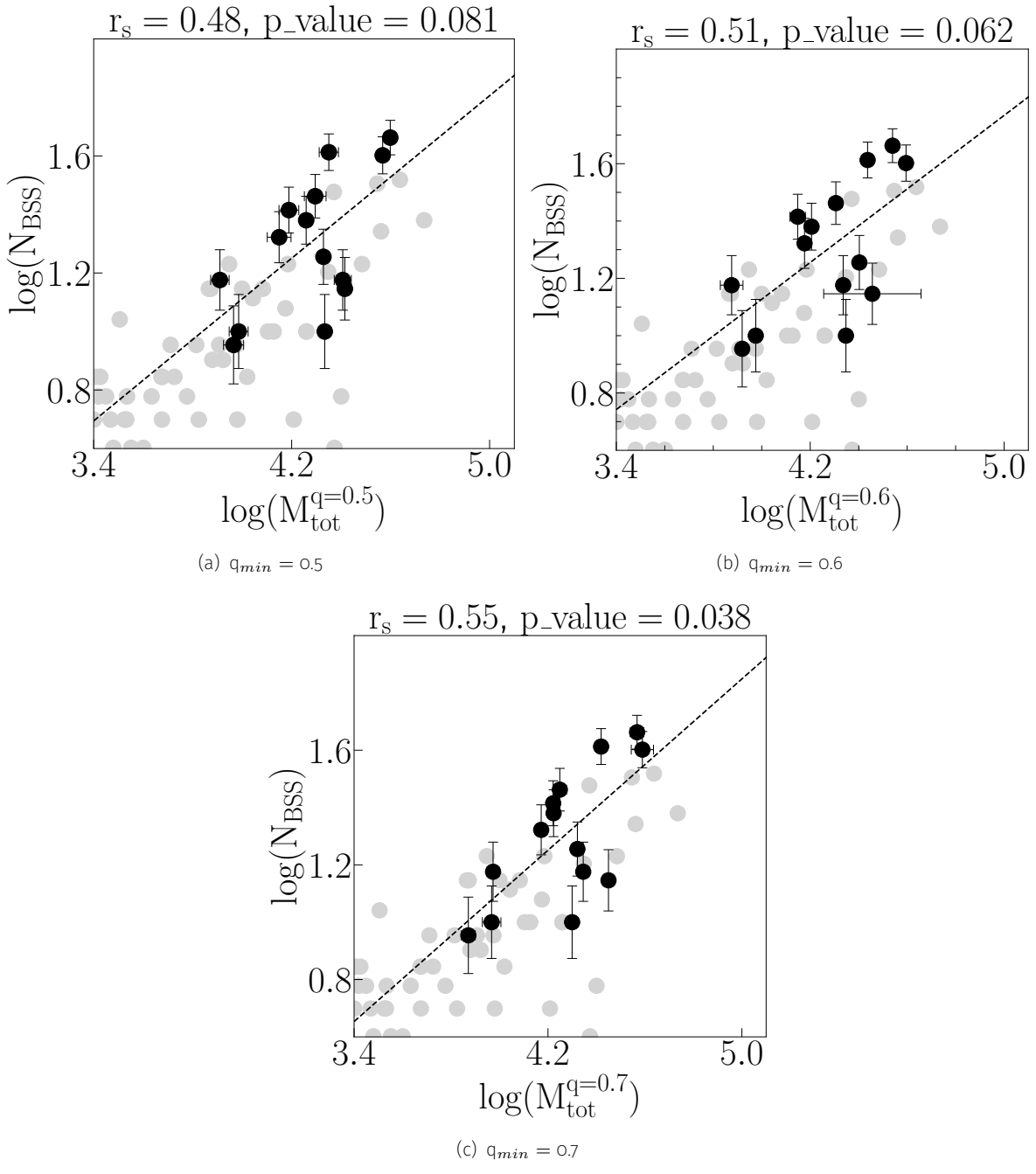

(a) $q_{min} = 0.5$ (b) $q_{min} = 0.6$

(c) $q_{min} = 0.7$

Figure 3.4 Logarithm of the observed number of BSS as a function of the cluster total mass. The dashed black line indicates the best fit to the data —slope is reported in Table 3.3. From left to right the different run of **ASteCA**, i.e., $q_{\rm min} = 0.5$, 0.6, and 0.7. Gray filled circles are the data from Jadhav and Subramaniam (2021).

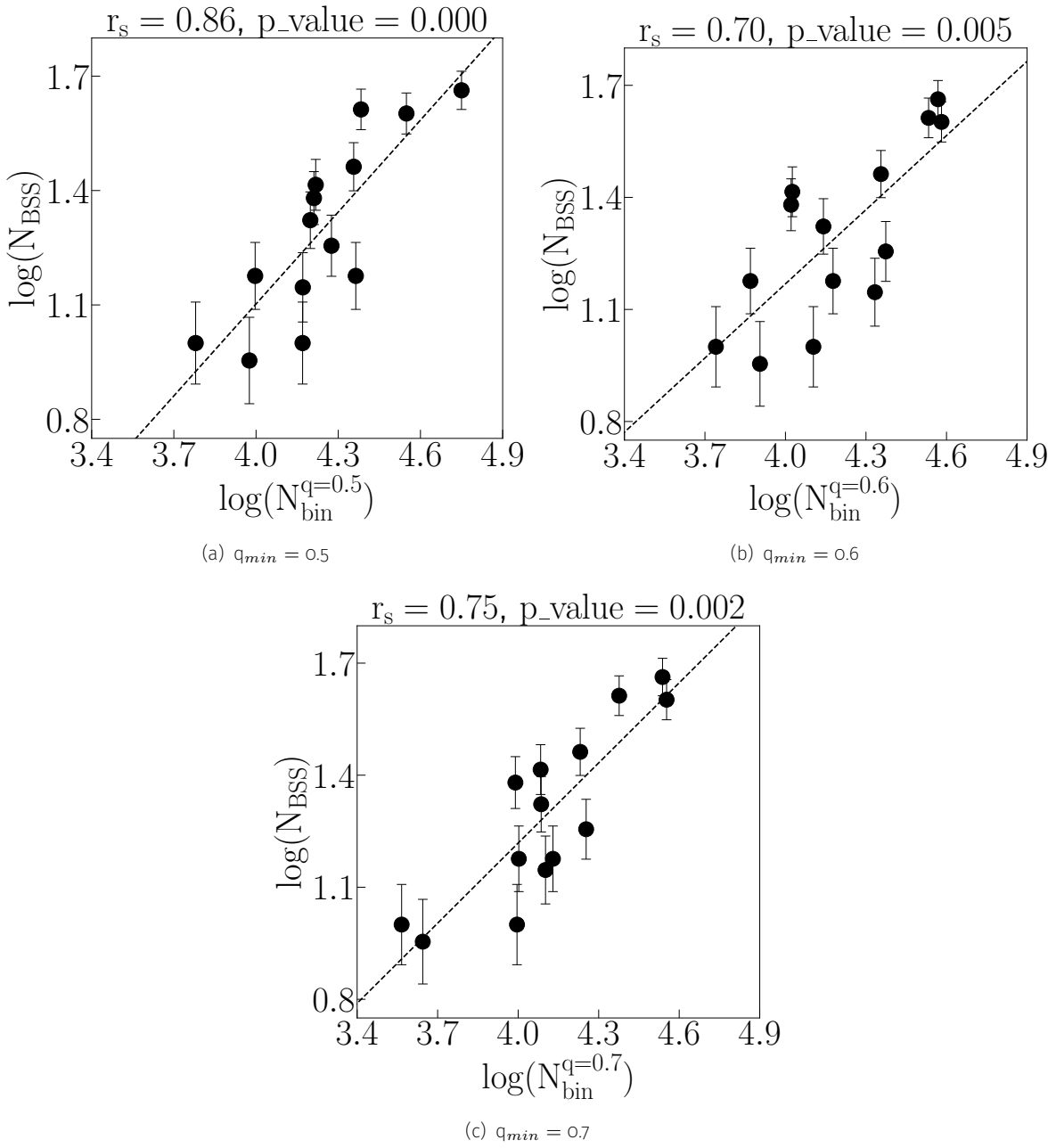

(a) $q_{min} = 0.5$

(b) $q_{min} = 0.6$

(c) $q_{min} = 0.7$

Figure 3.5 Logarithm of the observed number of BSS as a function of the number of binaries on each cluster. The dashed black line indicates the best fit to the data —slope is reported in Table 3.3. From left to right the different run of `ASteCA`, i.e., $q_{\rm min} = 0.5$, 0.6, and 0.7.

Table 3.3 Spearman coefficients r_s, their corresponding p-values, and the best-fit parameters for each panel of Figures 3.3, 3.4 and 3.5.

Relation	$r_{s_{0.5}}$	$p_{0.5}$	slope$_{0.5}$	$r_{s_{0.6}}$	$p_{0.6}$	slope$_{0.6}$	$r_{s_{0.7}}$	$p_{0.7}$	slope$_{0.7}$
$\log(N_{\rm BSS})$ vs. $f_{\rm bin}$	0.59	0.02	0.70±0.2	0.63	0.015	0.68±0.2	0.66	0.0	0.75±0.1
$\log(N_{\rm BSS})$ vs. $\log(M_{\rm tot})$	0.48	0.08	0.69±0.2	0.51	0.06	0.64±0.2	0.5	0.03	0.74±0.2
$\log(N_{\rm BSS})$ vs. $\log(N_{\rm bin})$	0.86	0.00	0.80±0.1	0.70	0.00	0.66±0.1	0.7	0.00	0.71±0.1

found for OCs, $M_{\rm tot}^{\delta=0.6}$, by Jadhav and Subramaniam (2021). According to Leigh et al. (2013) if most of the BSS are descended from binary evolution, there should exist a dependence of the form

$$N_{\rm BSS} \propto N_{\rm bin} \approx \frac{f_{\rm bin} M_{\rm tot}}{\overline{m}} \tag{3.2}$$

where $\overline{m}$ is the average stellar mass, for which the authors assume to be the same for every cluster. In this case we assumed a value of 0.4 $M_{\odot}$.

In comparison with the binary fraction the correlation with the $N_{\rm bin}$ is significantly higher. When using equation (3) the Spearman rank coefficient r_s increased considerably in two panels (b,c), but the best-fitting slope remains almost the same, with the exception of panel (a) where the differences of the slopes is $\sim$ 0.10. This means the correlation becomes stronger by adding $f_{\rm bin}$ —see Figure 3.5. This behavior was predicted by Knigge et al. (2009) and previously tested by Leigh et al. (2013) in GCs. Surprisingly, the latter found the strength of the correlation ($N_{\rm BSS}$ vs. $M_{\rm core}$) actually decreases if $f_{\rm bin}$ is included. Within our sample we found a dependence of the form $N_{\rm BSS} \propto N_{\rm bin}^{0.6-0.8}$. Finally, and on a difference of the previous cases no correlation at all was found between $F_{\rm MS}^{\rm BSS}$ and $M_{\rm core}$ or $N_{\rm bin}$; these results are plotted in Figures C.2 and C.3. The absence of a correlation between these parameters is however, not surprising, since according to Knigge et al. (2009), Equation 3.2 only holds for the $N_{\rm BSS}$ and not for the specific frequency.

The Spearman correlation coefficients and confidence levels for the considered parameter pairs are listed in Table 3.3.

3.6 Summary and conclusions

In this chapter we have studied the impact on the straggler population when EDR3 is used instead of *Gaia* DR2. Our main results are shown in Tables 3.2, 3.5 and 3.3 but also in Figure 3.3, 3.4 and 3.5. Complementary results are reported in Appendix C.

In the first part of this chapter, we have shown, that the systematic use of EDR3 over DR2 data will probably reflect a decrease in the population of stragglers (either blue or yellow stragglers) in our catalog, with a mean of three to four blue stragglers less per cluster. But also, despite obvious, that membership analysis is fairly sensitive to both data quality and analysis techniques.

Later we continued with the main scope of the section, and by taking advantage of the improvement in precision and accuracy of *Gaia* EDR3 with respect to *Gaia* DR2, we investigated the much less explored dependence of the straggler numbers with the binary fraction, mass and number of binaries. We confirm the number of BSS is dependent on the binary fraction, mass and number of binaries, while the specific frequency of BSS only correlates with the mass and the binary fraction. Contrary to GCs, we found the correlations between the stragglers and the binary fraction and the number of binaries improve the previously know sub-linear correlation between the straggler numbers and the mass of the clusters. We found relations of $\mathrm{N_{BSS}} \propto \mathrm{f_{bin}^{0.6-0.7}}$ and $\mathrm{N_{BSS}} \propto \mathrm{N_{bin}^{0.6-0.8}}$ respectively.

This is the first time that a relation between the binary content and the straggler numbers in OCs is presented. These studies were not feasible earlier as reliable membership information was lacking.

Chapter 4

The blue straggler population of Collinder 261

This chapter is mainly based on:
A study of the blue straggler population of the old open cluster Collinder 261
Authors: M.J. Rain, G. Carraro, J.A. Ahumada, S. Villanova, H. M.J. Boffin, L. Monaco, G. Beccari.
The astronomical Journal, 2020, 159, 59R

The very same study was chosen to be the highlighted research of the AAS nova magazine in the February/2020 edition.
AAS Novas, February 26, 2020

it is also based in our ongoing study:
Deep dive into the blue straggler population of Collinder 261
Authors: M.J. Rain, H. M.J. Boffin

4.1 Short introduction

The sparse nature and the proximity of the OCs enable an in-depth analysis of basic BSS characteristics such as frequency, orbital parameters, and masses. In this context, large and homogeneous catalogs like our recently published work (Rain et al., 2021) are needed to properly understand, identify, and characterize this population.

Particularly, the study of BSS provides invaluable clues to understanding MT processes, including Roche lobe overflow (RLOF) and Common Envelope Evolution (CE). Therefore, BSS provide significant constraints on the physics of MT in low- and intermediate-mass stars, which is essential to understand many other post-MT systems such as symbiotic stars, double white dwarfs, Type Ia supernovae, transients, X-ray binaries, etc. These kind of studies are still minimal, and we only know in detail the binary properties of the straggler population in two OCs: M67, NGC 188. In both clusters, the fraction of binaries among BSS (∼80%) is higher in comparison with the normal MS stars (25%) (Mathieu and Geller, 2009, 2015) and between those BSS being in binary system ∼75% of them have periods on the order of 1,000 days, and some are found to harbour white dwarf companions (Gosnell et al., 2014, 2015) – compatible with the outcome of stable RLOF MT, i.e., case B or Case C mass transfer (cf. § 1.2.1).

After a fast inspection on the ADS we found 12 dedicated refereed papers to the study of Collinder 261 (or Harvard 6, C1234−682), from metallicity and chemical abundances studies to the search of X-ray sources within the cluster and up to membership and distances measurements, but none on the blue straggler population. Further, given its age, this cluster moreover provides a useful link between younger open clusters such as NGC 6819, NGC 188, and M67, and globular clusters (typically 11 to 12.5 Gyr old), which are known to be very rich in BSS. Within this framework, we carried out the first spectroscopic study on the BSS of Collinder 261 and we search for clues about the origin of blue stragglers. We also complement this study with the Transiting Exoplanet Survey Satellite (TESS) data and search for binaries among the straggler sample.

The layout of the chapter is as follows. The cluster parameters values found in the literature are summarized in Table 4.1. The data use on this study either photometric

Table 4.1 Main parameters of Collinder 261.

RA hh mm ss	Dec [dd mm ss]	l^a [deg]	b^a [deg]	$R_c^{1,c}$ [arcmin]	$R_h^{2,c}$ [arcmin]	$R_a^{3,a}$ [arcmin]
12 37 57	−68 22 00	301.68	−0.53	2.6	6.4	9.0

Distance^{b,f,g} kpc	$E(B-V)^{a,f,g}$ [mag]	$\log(\text{age})^{a,e,g}$ [yr]	[Fe/H]^h [dex]	RV^d [km s^{-1}]
2.2–2.9	0.22–0.34	9.80–9.95	-0.03 to -0.01±0.11	-25.44 ± 0.93

Notes:
[1]Core radius, [2]Half-mass radius, [3]Apparent radius
[a] Dias et al. (2014), [b] Cantat-Gaudin et al. (2018), [c] Vats and van den Berg (2017), [d] Mishenina et al. (2015)
[e] Monteiro and Dias (2019), [f] Mazur et al. (1995), [g] Gozzoli et al. (1996), [h] Carretta et al. (2005)

and spectroscopic are described in § 4.2. The spectroscopic analysis, the RVs and rotational rates with their corresponding errors are describe in § 4.3, here we also defined our criteria of membership and evolutionary status using the radial velocity values, as well as the mass estimation of few of the straggler candidates. Finally, in § 4.4 we reported our results based on the photometric and spectroscopic analysis and in § 4.5 we reported the close-binary systems we found within the Transiting Exoplanet Survey TESS. We summarize and conclude in § 4.6

4.2 Datasets

4.2.1 Photometric data

The photometric data use in this chapter is exactly the same of our catalog (Chapter 2) as well the BSS and YSS selections. Briefly described we took advantage of the selection of cluster members already performed by CG18, the procedure is based on proper motions and parallax selection criteria. They considered as cluster members those stars located over a radius twice as large as the value of $r_{\rm DAML} = 9'$ reported by DAML02, with proper motions within 2 mas yr^{-1}, and with parallaxes within 0.5 mas from the cluster centroid. In this way, they selected about 2000 members of Collinder 261.

Cantat-Gaudin et al. (2018) report the mean values $\mu_\alpha \cos\delta = -6.35 \pm 0.16$ (0.004) mas yr^{-1}, $\mu_\alpha = -2.70 \pm 0.16$ (0.004) mas yr^{-1}, and $\varpi = 0.315 \pm 0.082$ (0.002) mas. Just to be cautious, we calculated our own mean proper motions (based on *Gaia* data) values following a similar procedure as that of Bhattacharya et al. (2019). As in § 2.8, we employed the table access protocol (TAP) and the astronomical data query language (ADQL), together with TOPCAT to access the *Gaia* data; for this, we identified the Gaia DR2 counterparts of confirmed Collinder 261 members, as follows. De Silva et al. (2007) measured RVs (RVs), metallicities, and chemical abundances (Mg, Si, Ca, Mn, Fe, Ni, Zr, and Ba) of 12 giant stars, and confirmed their membership; we cross-correlated the position on the sky of these stars and the *Gaia* DR2 catalog, looking for the nearest neighbors within 1″. Our mean proper motions and parallax values are: $\mu_\alpha \cos\delta = -6.35 \pm 0.13$ mas yr^{-1}, $\mu_\alpha = -2.73 \pm 0.14$ mas yr^{-1}, and $\varpi = 0.321 \pm 0.019$ mas, which are in complete agreement with those of CG18 and Gao (2018) ($\mu_\alpha \cos\delta = -6.340 \pm 0.006$ mas yr^{-1}, $\mu_\alpha = -2.710 \pm 0.004$ mas yr^{-1}, and $\varpi = 0.3569 \pm 0.0027$ mas). On the other hand, even considering the errors, our results are far from the values given by DAML02, namely, $\mu_\alpha \cos\delta = -0.65 \pm 4.94$ mas yr^{-1}, and $\mu_\alpha = -0.51 \pm 3.76$ mas yr^{-1}.

Arenou et al. (2018) report the differences between the average zero points of proper motions and parallaxes from DAML02 and *Gaia* catalogs. They found $\mu_{Gaia} - \mu_{\rm DAML02} = 0.0 \pm 0.19$ mas yr^{-1} and 0.41 ± 0.18 mas yr^{-1} for μ_α and $\mu_\alpha \cos\delta$ respectively, and $\varpi_{Gaia} - \varpi_{\rm DAML02} = -0.064 \pm 0.17$ mas for the parallaxes. Arenou et al. (2018) do not find evidence for the presence of significant systematic errors in the *Gaia* DR2 proper motions. Therefore, the differences between our results and the published values of DAML02 seem unlikely to be caused by systematic errors in the *Gaia* data. Since our values were calculated using giant stars of confirmed membership, we suggest that the DAML02 proper motions might suffer from the lack of reliable cluster membership, as well as from significant contamination by field stars; these may be the main reasons of the discrepancies noted above.

AL07 estimated a red limit of $(B-V) \simeq 0.86$ for the BS area of Collinder 261. To impose the same limit in the *Gaia* system, we used the relation of Jordi et al. (2010):

$$C_1 = 0.0981 + 1.4290\, C_2 - 0.0269\, C_2^2 + 0.0061\, C_2^3. \tag{4.1}$$

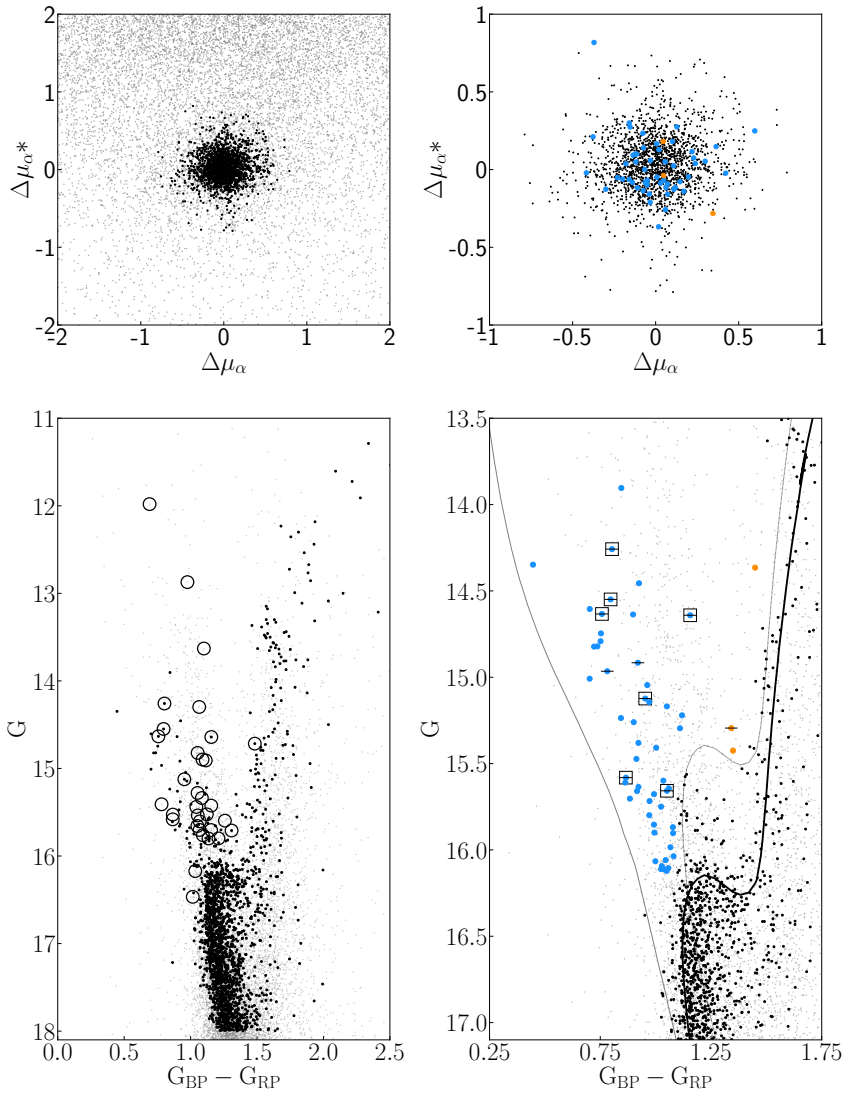

Figure 4.1 **Upper panels:** Proper motions plane of Collinder 261. In the left panel, gray dots represent all the sources listed by *Gaia* DR2 within 15′ around the cluster center. Black filled circles are cluster members selected by Cantat-Gaudin et al. (2018). In the right panel, we display a zoom of the center of the plane; here, Collinder 261 members are the same as in the plot of the left, filled blue circles are BS candidates, and filled orange circles are yellow straggler candidates. **Bottom panels:** Color-magnitude diagrams of Collinder 261. In the left panel, open black circles are BS candidates from Ahumada and Lapasset (2007). The right panel displays a zoom into the region of BSs; an isochrone from Bressan et al. (2012) with the adopted cluster age and metallicity, is shown in black solid line. The zero-age main sequence and the binary sequence are plotted in gray solid line. Black squares are BSs already identified by Ahumada and Lapasset (2007). Stars with spectroscopic data are crossed with a horizontal line.

With $C_2 = 0.86$, it results $C_1 = (G_{\rm BP} - G_{\rm RP}) = 1.30$. The coefficients are from Table 3 of Jordi et al. (2010) Stars redder than this limit can be considered as possible yellow stragglers.

In the top panel of Fig. 4.1 we plotted the distribution of proper motions for stars in the Collinder 261 area. Gray dots represent *Gaia* DR2 stars within $15'$ of the cluster center. Black filled circles are the cluster members of CG18. Light blue filled circles are the BS candidates, and orange filled circles are the yellow stragglers candidates. In the bottom panel of Fig. 4.1 we plotted the color-magnitude diagram of Collinder 261. The symbols are the same of the top panel. Open black circles are the BS candidates identified by AL07. Only 6 of 54 are classified as members according to *Gaia* data. The BS sample of AL07 follows the galactic field trend and is very different from the BS population found with *Gaia*.

From R21b we know Collinder 261 has 53 BS and three YS candidates. They are listed in Table B.1. When available, additional classification according to their binary nature, as reported in the astronomical database SIMBAD (Wenger et al., 2000), is also listed. The eclipsing, close binaries found among the BSs of Collinder 261 are of the following types: β Lyrae, Algol, and W Ursae Majoris (W UMa). Binaries classified as β Lyrae are semidetached systems, i.e., one of the components of the pair is filling its critical Roche lobe, the stars are close enough that they are gravitationally distorted, and the periods are usually longer than 1 day. Algol variables are also semidetached binaries, whose components have spherical or slightly ellipsoidal shapes. These stars have an extremely wide range of observed periods, from 0.2 to over 10,000 days. In the W UMa-type stars the components are in contact or almost in contact, and share a common envelope of material; the orbital period can be of just a few hours.

4.2.2 Spectroscopic data

Collinder 261 was observed with the fiber-fed spectrograph FLAMES[1] at the Very Large Telescope (VLT) of the European Southern Observatory (ESO, Paranal Observatory, Chile), using the combination of the mid-resolution spectrograph GIRAFFE and the fiber link

[1] `http://www.eso.org/sci/facilities/paranal/instruments/flames.html`

Table 4.2 Details of the spectroscopic observations carried out on February 24 and March 1–6, 2012, and February 3–4, 2018, with a S/N between 15 and 120.

Epoch	$\mathrm{MJD}^{a}_{\mathrm{start}}$ [days]	$\mathrm{MJD}^{a}_{\mathrm{end}}$ [days]	Exposure [sec]
1	55982.277794959	55982.3055727877	2400.0044
2	55988.222295996	55988.2500738154	2400.0036
3	55993.234082174	55993.2618600004	2400.0042
4	58153.314142684	58153.3419204942	2400.0028

Notes:
[a] Modified Julian date JD−24,00000.5

UVES. The data were collected in two periods: October 2011 to March 2012, and October 2017 to April 2018, under ESO programs 088.D-0045(A) and 0100.D-0052(A).

The UVES fibers were allocated to cluster's clump stars, whose membership is very solid, to set the zero point of the radial velocity. The reduction and analysis of the UVES data are described by Mishenina et al. (2015). GIRAFFE was used with the setup HR8, which covers the wavelength range 491.7–516.3 nm, with a spectral resolution $R \equiv \lambda/\Delta\lambda \equiv 20{,}000$. The integration time was $\sim$ 2,400 sec for all spectra. In total, Collinder 261 was observed in 4 epochs; some details of the observations are given in Table 4.2. For the GIRAFFE data we just performed the sky-subtraction and normalization using the IRAF[2] packages `sarith` and `continuum`, since the data were already reduced in Phase 3 —visit ESO webpage for more information regarding ESO phase 3 products[3].

4.3 Spectroscopic Analysis

This is the first high-resolution spectroscopic analysis of the BS population in Collinder 261. Unfortunately, not all the candidates were observed with FLAMES since, when we were allocated the observational time, we used the BS list of AL07 to select the targets, a list very different from that found in this work using *Gaia*. The spectroscopic

[2] IRAF is distributed by the National Optical Astronomy Observatory, which is operated by the Association of Universities for Research in Astronomy, Inc.., under cooperative agreement with the National Science Foundation.

[3] `https://www.eso.org/sci/observing/phase3.html`

analysis was carried out on nine out of the 53 BS in our list, and on one of the three YS candidates identified.

4.3.1 Radial Velocities and rotational rates

For each spectrum, RVs were determined with the IRAF `fxcor` cross correlation task (Tonry and Davis, 1979). Stellar spectra were cross-correlated with synthetic templates obtained with the SPECTRUM code[4] (Gray and Corbally, 1994). Each synthetic spectrum was computed adopting the atomic and molecular data file `stdatom.dat`, which includes solar atomic abundances from Grevesse and Sauval (1998), and the linelist `luke.lst`, suitable for mid-B- to K-type stars, which is perfect for our BSS. Model atmospheres were calculated with the code ATLAS9 (Castelli and Kurucz, 2003).

The selection of a proper template for each star was crucial mainly because the targets have different rotational velocities. In GCs little we know about rotation rates on BSS, where only a few clusters have been studied, and most stragglers are slow rotators, as one would expect for stars of these masses and ages. From OCs however, it is clear that a substantial fraction of BSS are rotating more rapidly (up to 50–120 km s^{-1}) than normal stars of the same temperature —some examples of intermediate-to fast rotating stars are shown in Figure 4.2. A possible explanation for this behavior can be connected with the formation pathway of each straggler; for example, the coalescence of two main-sequence stars is thought to lead to rapid rotation immediately after the merger, because the angular momentum of the orbit will have to be absorbed by the star. But the truth is that the current rotation rates of blue stragglers are still puzzles that have not been addressed in much detail —we refer the reader to Mucciarelli et al. 2014 for more information regarding the projected rotational velocities of BSS in GCs and to Mathieu and Geller (2015) for BSS in OCs .

We computed a set of templates with diffedent rotational velocities $v \sin(i)$ ranging from 10 to 100 km s^{-1}, adopting the following values: for the effective temperature, $T_{\rm eff} = 6000$ K, for the surface gravity, $\log g = 4.5$ cm s^{-2}, and for the micro-turbulence,

[4] `http://www.appstate.edu/~grayro/spectrum/spectrum.html`

$\xi = 0.0$ km s^{-1}. As shown previously and given their shallow convective (or fully radiative) envelopes, different assumptions for the ξ velocity have no impact on the determination of RVs and $v \sin(i)$. We carefully compared the spectrum of each star with the templates, and we visually estimated the rotation rate from the profiles of the spectral lines. However, if the template had too low a rotational velocity, the shape turned out to be very noisy because the profiles of the lines and the spectrum noise were mapped together. In these cases, we had to increase the rotational velocity of the template for the cross-correlation procedure. The derived rates are considered as upper limits. An example of this procedure is illustrated in Figure 4.3 and the RVs measurements for the blue and yellow stragglers are reported in Table 4.3. Finally the position of the stars observed with GIRAFFE are shown in Figure 4.1.

4.3.2 Errors

We consider the errors returned by `fxcor` as conservative estimates of the true uncertainties of the RV. For each star we have four RV measurements and `fxcor` error estimations. We computed the `fxcor` error for each star, and for each pair of measurements we calculated the RV difference divided by the root square of 2. We then built the distribution histogram and fitted a Gaussian. We take the standard dispersion σ of the Gaussian as the true RV error. We plotted the histograms together with the Gaussian fit and the true error in the upper panel of Figure 4.4. Additionally, we calculated the mean `fxcor` error for each rotational rate —estimated as we described above in § 4.3.1. Our results are plotted in the bottom panel of Figure 4.4. The typical uncertainties for the slow rotators stars ($v \sin(i) = 10$ km s^{-1}) is about 1 km s^{-1}. Stars rotating with velocities ranging approximately between 30 and 60 km s^{-1} have errors from 4 to 14 km s^{-1}. Similar uncertainties values were found by Mucciarelli et al. (2014) on their BS sample. Therefore, we decided to adopt the `fxcor` error as a conservative estimation for the RV uncertainty.

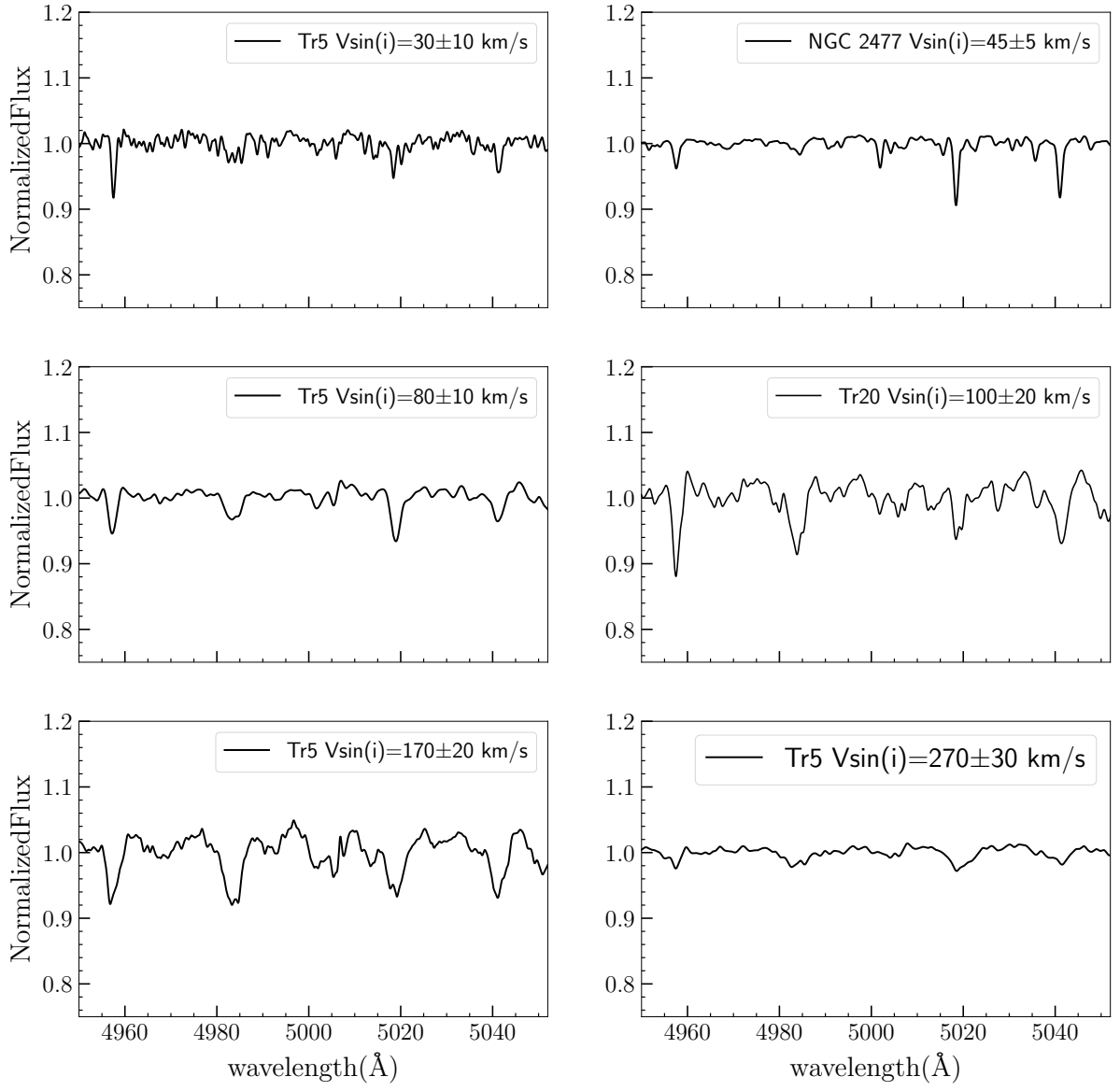

Figure 4.2 Examples of observed spectra for six BSs with different rotational velocities — members of different clusters— labeled on each panel, in the wavelength range between 4950 and 5050 Å.

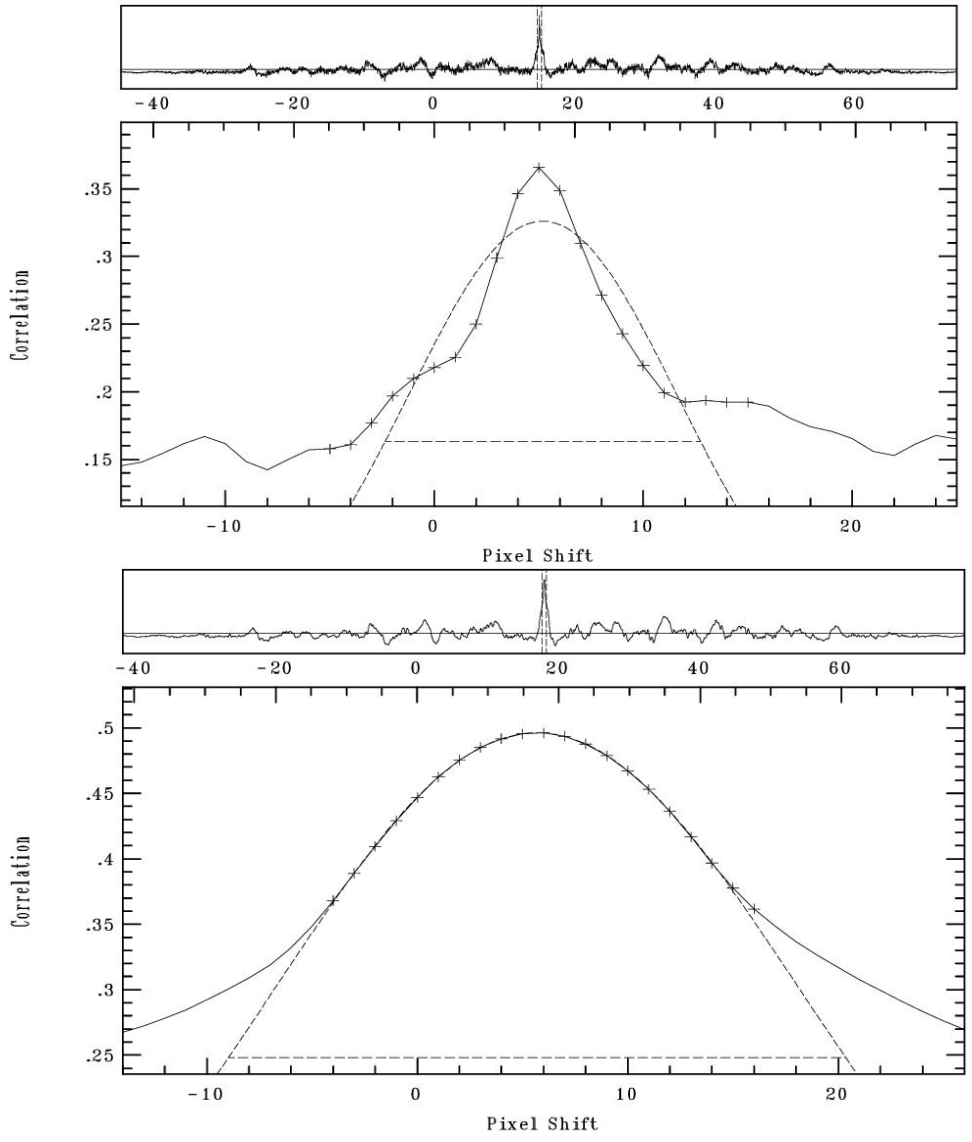

Figure 4.3 Cross-correlation peaks for star BS3, derived by the IRAF routine `fxcor`. The top panel shows one of the computed synthetic templates ($v \sin(i)$) equal to 10 km s^{-1}, cross-correlated with the spectrum of the star. Since the template is inadequate due to the low value of the rotational velocity, the cross-correlation curve is noisy. The bottom panel shows the same stellar spectrum cross-correlated with the correct template, with a rotational velocity of 30 km s^{-1}; in this case, the curve is smooth.

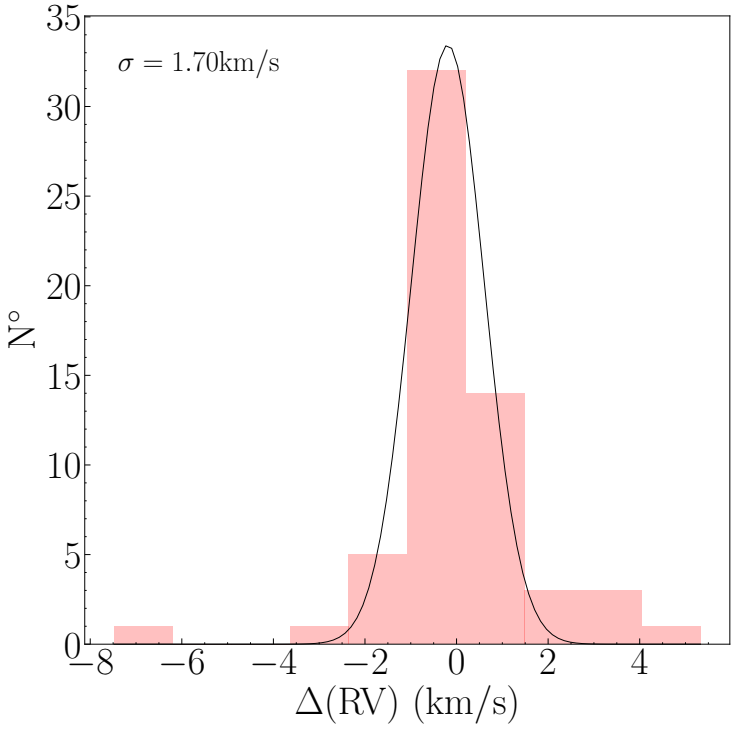

(a) Histogram

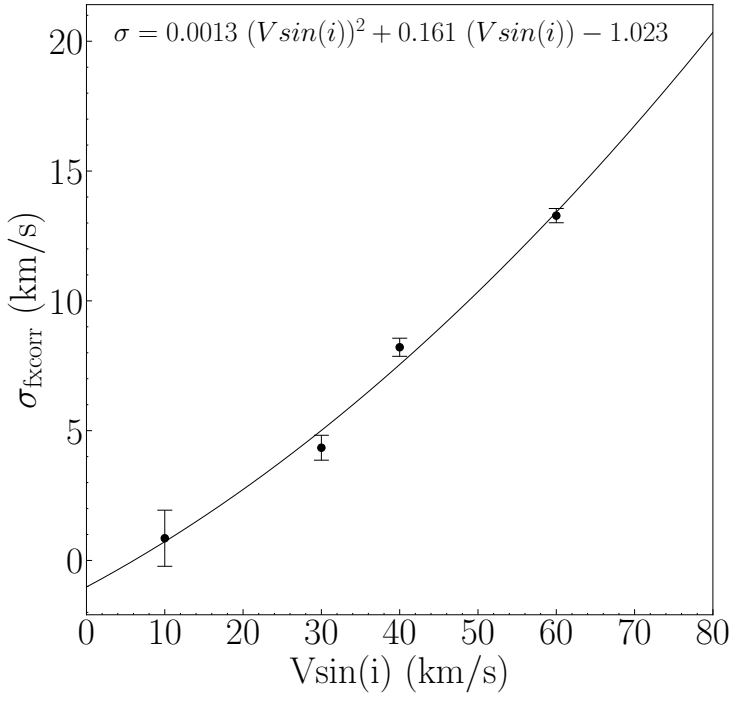

(b) fxcor mean errors

Figure 4.4 Panel (a) is the histogram of the differences—divided by the root square of 2—between pairs of RVs measurements for the same star. The best-fitting Gaussian to the distribution is plotted, and its standard deviation σ is indicated. Panel (b) gives `fxcor` mean errors as a function of the upper rotational rates estimated in this work for Collinder 261. See text for details.

4.3.3 Membership and evolutionary status

Comparing our RVs with the mean value derived by Mishenina et al. (2015) for clump stars, we can now try to determine the membership status of the objects in our sample. In what follows we will assume that BSS are the result of collisions, or that they are binary systems, with either relatively short periods (a few days or less), or rather long ones (about 1000 days). Tree epochs of observation are separated by a few days (∼6), and the fourth epoch is about 6 years later. To assess membership, the RVs of the stars can be compared to the mean RV of the cluster, taking into account the error bars—as derived in Section 4.3.1—and the possibility of binarity. The following classification however have been carried out assuming an oorbital plane that sits along the line-of-sight, without considering any effect of $\sin\ i$.

The TO mass of Collinder 261 is about 1.1 $M_{\odot}$ (Bragaglia and Tosi, 2006); if the companions are main-sequence stars, they have to be less massive since, by definition, they are the secondary components. If the systems are post-mass-transfer ones containing a white dwarf (e.g., Gosnell et al. 2014), then the mass of the companions are more likely peaked around 0.6 $M_{\odot}$, as found in NGC 188 (Geller and Mathieu, 2011). We can thus assume, for illustration purposes, that the binary would have a mass ratio of ∼ 0.5. For the system not to fill its Roche lobe —as this would imply a mass transferring system showing signs of accretion, which are not seen— the separation between the two stars should be larger than ∼ 3.5 $R_{\odot}$, with a minimal orbital period of the order of 0.5 days. In that case, the maximum orbital velocity would be 100 km s^{-1}. Thus, a star whose RV differs from that of the cluster by up to 100 km s^{-1} could still be a member, if it were a close binary; in this case, however, we would expect that its RV would change between two epochs[5]. If we now consider the typical, post-mass-transfer, long-period binaries, with periods around 1000 days like those found to constitute the bulk of the BSS in NGC 188, we would expect a maximum RV of 10–13 km s^{-1}. In this case, the difference in velocities between two epochs should be very small [6], i.e., below 1 km s^{-1}. Of course, it is possible to have a binary system in between these two cases. These

[5]Except of course, if mother Nature decided to play tricks with us and that the two epochs correspond exactly to the same orbital phase! This should be quite unlikely though and we therefore do not consider this here, as we are taking a conservative approach in assessing possible membership.

[6]This is particularly true because (Geller, 2010) showed that the eccentricities of most BS stars in NGC 188 are rather small, and so here, to be conservative, we assumed a mean eccentricity of 0.3.

considerations led us to define the following, rather conservative, approach to confirm membership of BS stars in Collinder 261:

- If the individual RVs are, given their error bars, compatible with the cluster mean V_R, and do not change significantly over the four epochs, it is considered a possible single-star member, the outcome of a collision or a merger. It could of course also be a binary with a long period —greater than ~ 1000 days. These stars are classified as members, **"M"**. If a star's velocity is compatible with the cluster mean V_R, but the velocity errors are too large (larger than 1/3 the RV value) to discriminate between long-period or close binaries, we indicate it as **"M?"**.

- On the other hand, if the individual RVs are, given their error bars, within 100 km s^{-1} with respect the cluster mean V_R, then:

    1. If the velocities differ more than 20 km s^{-1} from V_R and change significantly between two epochs, we can consider the star as a candidate for being a close-binary member of the cluster, **"M, CB"**. When this happens, but error bars are too large, we tag the star as **"M, CB?"**. However, note that when the period is close to the difference in time between the epochs, we should not expect much change in RV.
    2. If the velocities are within 20 km s^{-1} from V_R and do not change by more than a few km s^{-1} between epochs (depending on the possible period, which is constrained by the difference with V_R), we possibly have a long-period member (period above 100 days): **"M, LP"**. When this is true, but error bars are too large, we tag a star as **"M, LP?"**.

- The membership status of the binaries (CB and LP) can only be secured once we have determined the full orbital solution, and thus derived the systemic velocity. If none of the above apply, we consider the star as a non-member, **"NM"**.

Table 4.3 Individual radial velocities measurements for blue and yellow stragglers in our sample. Binary classification according to their RV variability and rotational rates are reported in the last two columns.

ID[a]	*Gaia* DR2 Source Id.	RV_1 [km s^{-1}]	RV_2 [km s^{-1}]	RV_3 [km s^{-1}]	RV_4 [km s^{-1}]	Classification[a]	$< v \sin(i) >$ [km s^{-1}]
BS1	5856527386646253312	-29.61 ± 3.69	-17.00 ± 3.39	$+01.56 \pm 2.61$	-20.62 ± 4.61	M, CB	30
BS2	5856528348719355648	-26.09 ± 1.55	-26.21 ± 2.59	-24.39 ± 1.37	-25.46 ± 1.41	M	10
BS3	5856527524085202048	-24.23 ± 5.45	-17.25 ± 7.11	-00.02 ± 3.22	-02.55 ± 5.79	M, CB	30
BS4	5856528550550957184	-35.30 ± 8.45	-24.03 ± 11.07	-1.80 ± 6.59	-15.37 ± 6.72	M, CB	40
BS5	5856527661524172800	$+12.44 \pm 14.02$	-05.36 ± 8.46	-38.77 ± 19.04	$+19.70 \pm 11.51$	M, CB	60
BS6	5856527386646253440	-27.45 ± 5.14	-29.75 ± 3.30	-16.24 ± 3.31	-12.90 ± 3.35	M, LP	30
BS7	5856529242072194816	-24.08 ± 0.40	-24.30 ± 0.40	-24.02 ± 0.57	-23.91 ± 0.43	M	10
BS8	5856515601255190272	-35.96 ± 4.60	$+10.20 \pm 3.97$	-63.48 ± 5.40	-66.91 ± 4.47	M, CB	30
BS9	5856529001554008064	-24.14 ± 0.76	-25.11 ± 0.86	-23.84 ± 1.11	-22.82 ± 0.74	M	10
YS1	5856527622837778176	-24.51 ± 0.34	-24.65 ± 0.34	-24.56 ± 0.30	-24.03 ± 0.45	M	10

[a] This work.

4.4 Results

4.4.1 Photometric detections

As mentioned above we identified 53 possible blue stragglers in R21b, the very same BSS where analyse in the present Chapter. Of the 53 stragglers only six of them are in common with the BS population listed by AL07 for Collinder 261 and seven of our stars have already been noted as blue stragglers and binaries in previous studies (Mazur et al., 1995, Vats and van den Berg, 2017) —see Table B.1. In the following paragraphs we will explore the behavior of our BSS in comparison with those normal stars in Collinder 261.

4.4.1.1 Radial distribution

In order to investigate the cluster dynamical state of Collinder 261, we studied the blue straggler radial distribution and compared it to those not only of the red giant branch (RGB) — see § 2.7 for more details— but also to the red clump (RC), and MS stars, taken as representatives of the normal cluster population, and that therefore are expected to follow the cluster distribution.

Main sequence stars were selected from a region free of binary contamination. We considered as MS stars all those in the range $17 < G < 18$. This allowed us to obtain a populous sample of reference stars in the same range of G magnitude of BSS, i.e., in the same degree of completeness. Red clump stars were selected from the region between $G_{\rm TO} - 2.5 < G < 13$. As we already mentioned, the accurate astrometric solutions of *Gaia* let us identify the stellar population of Collinder 261 in a very reliable way.

Figure 4.5 shows, in different panels, the normalized cumulative distribution of the BS candidates (blue solid line), compared to those of MS stars (green dashed line), RGB stars (red dashed line) and RC stars (magenta dashed line). The BSS appear more centrally concentrated in the three cases. With levels of segregation almost identical when using RGB and MS (A_r^+=0.166 and 0.168 respectively) and with a slightly lower level of segregation (A_r^+=0.098) if RC stars are used as reference population. We suggest that the similarity of the radial profiles of BSS and RC stars is possibly due to the small-number statistics in our sample for both populations. It is worth mentioning that Carraro et al. (2014) found marginal evidence that the BSS of the old open cluster Melotte 66 are more concentrated than its clump stars, as in Collinder 261.

To quantify whether the radial distributions of BS, RGB, RC, and MS stars are extracted from the same parent distribution, thus indicating an absence of segregation, we used the k-sample A-D test. The test indicates a difference of 99.9% between the distributions of BS and MS stars, and a difference of 86.9% between the distributions of BS and RGB stars, which therefore favor the existence of a real mass segregation in Collinder 261. On the contrary, we do not find the population of BS stars to be centrally concentrated with respect to RC stars, as the A-D test gives a probability of 16.0% that both populations do not originate from the same distribution. The same observation was found by Carraro et al. (2014) in Melotte 66.

A cluster made up of stars of the same mass is dynamically relaxed on a timescale of

$$t_{\rm relax} \sim \frac{t_{\rm cross\,N}}{6\log(N)} \tag{4.2}$$

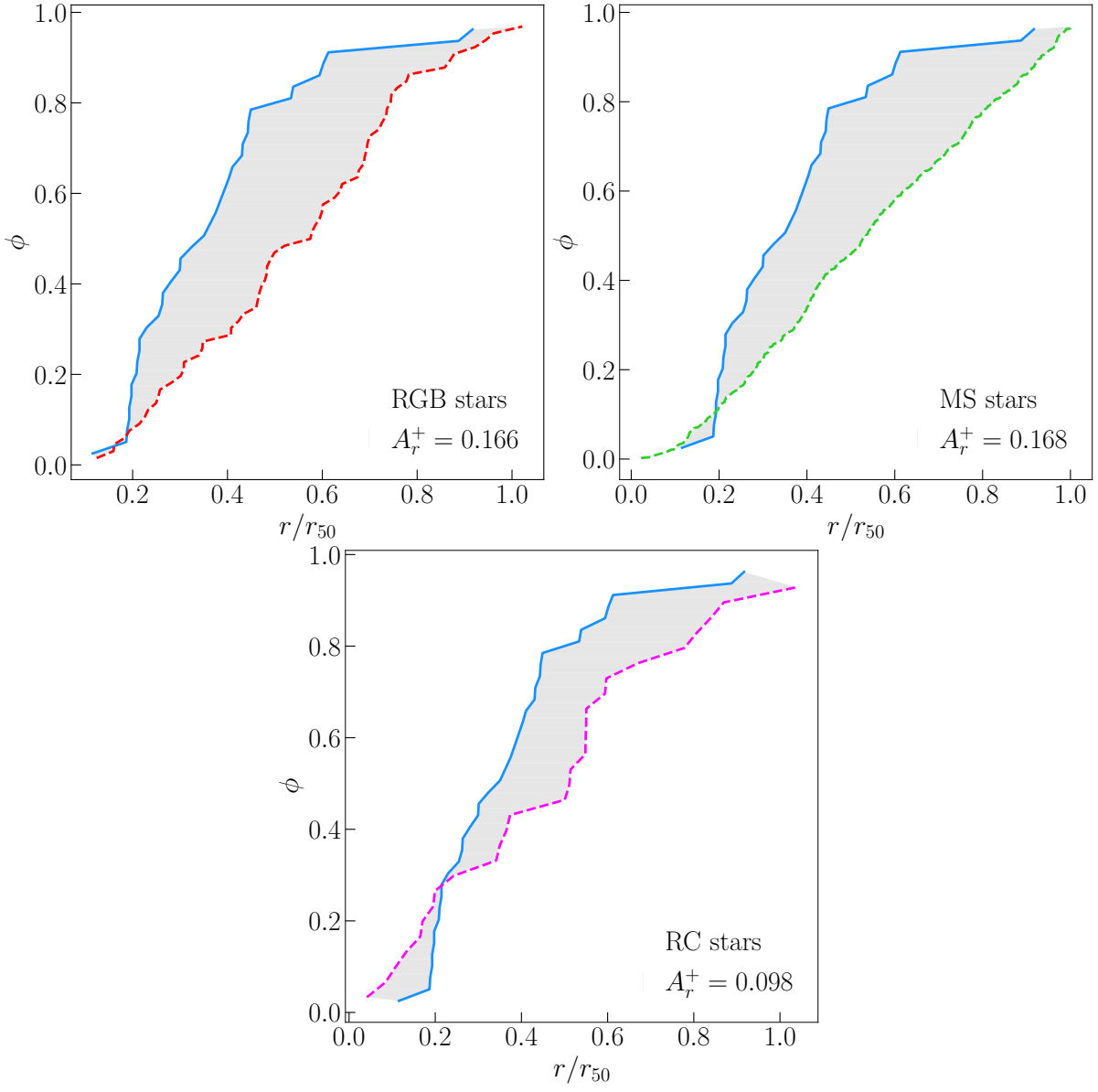

Figure 4.5 Cumulative spatial distribution of BSS (blue solid lined), main sequence stars (green dashed lined), red giant stars (red dashed line), and clump stars (magenta dashed line) in Collinder 261. All the populations are corrected by field contamination

where

$$t_{\rm cross} \sim \frac{D}{\sigma_v} \tag{4.3}$$

is the crossing time, N is the total number of stars, and σ_v is the velocity dispersion (Binney and Tremaine, 2008). The time $t_{\rm relax}$ is the characteristic scale in which the cluster reaches some level of kinetic energy equipartition with massive stars sinking to the core, and low-mass stars being transferred to the halo, so mass segregation in a star cluster scales with the relaxation time. Using the standard deviations of the projected proper motions ($\sigma_{\mu_\alpha} = 0.13$ mas yr^{-1} and $\sigma_{\mu_{\alpha*}} \simeq 0.14$ mas yr^{-1}), and the sizes of the cluster core and half-mass radius reported in Table 4.1, we obtain, for the cluster core, $t_{\rm relax,c} \sim 100$ Myr, and for the half-mass radius $t_{\rm relax,h} \sim 250$ Myr. These values are significantly smaller than the estimated age of Collinder 261 ($\sim$ 7–9 Gyr, Table 4.1). Consequently, this could explain the presence of mass segregation in this cluster, particularly in the core.

We made an attempt to link our findings for Collinder 261 with those of F12 for globular clusters by calculating the value of $\rm r_{min}$. We could not classify this cluster into any of the three families defined by F12, given the small number of BSs we have within $\rm r_{50} = 0.108$ deg — the value reported in CG18 for Collinder 261. The scenario is a bit different however, if we considered the whole extension of the cluster instead of only the stars within $\rm r_{50}$. To do so, we divided the field of view in 5 concentric annuli, each one containing approximately the same number of BSS (~ 11). Figure 4.6 plots the number of BS candidates with respect to that of reference stars in each annulus, as a function of the radial distance, and the colors are the same described above. When we compare the RC population and BSS stars, we note a maximum at $\rm r/r_{50} = 0.46$ or $r \sim 3'$ (see bottom panel of Figure 4.6); however, when we consider the errors (Poisson errors) this peak disappears and the distribution becomes flat. The same behavior was observed when comparing BSS with MS and RGB populations. Both ratios show a maximum value in the annuli closer to the center, followed by a minimum. The ratios within $\rm r/r_{50} = 1$ ($r \sim 6'$) display two minima at $\rm r/r_{50} = 0.3$ ($r \sim 2'$) and $\rm r/r_{50} = 0.8$ ($r \sim 5'$), and two maximum peaks at $\rm r/r_{50} = 0.15$ ($r \sim 1'$) and $\rm r/r_{50} = 0.46$. As in the previous case, these distributions become flat considering the errors. F12 discovered a tight anti-correlation between the core relaxation time and the shape of the radial distribution.

Clusters with a flat distribution—i.e., that show no signs of segregation of its BSS—should have a relaxation time of the order of the age of the Universe. Our findings do not match with their results, given that the small relaxation time we derive for the core of Collinder 261 is not compatible with a flat distribution. The last only points out what mentioned already in the introduction of this thesis; the A_r^+ (Fig. 4.5) parameter points to mass segregation occurring towards the center of Collinder 261, which at the same time is consistent with the short relaxation time derived above ($t_{relax,c} \sim 100$ Myr and $t_{relax,h} \sim 250$ Myr) while the radial distribution (Fig. 2.15) not —if the interpretation of F12 is assumed. So, we highly recommend on using A_r^+ (comparison between two cumulative distributions) instead of searching the position of a minimum in the radial distribution of OCs.

4.4.2 Spectroscopic detections

There are 10 stars in common between those observed with FLAMES and those in our catalog. Out of our 53 BS candidates, only nine were observed with FLAMES and one YS candidate, for which we decided to study its variability as well. Based on their RV variations, we attempted to roughly assess their binary nature, namely, to decide if they may be close or long-period binaries. Our results are plotted in Figure 4.7. All the probable binaries would need additional spectroscopic follow-up to be properly characterized, given the small number of observations. In total we found one long-period system, five close-binary systems, and three BS and one YS candidates without variations in their RV measurements.

4.4.2.1 Long-period binaries

Previous studies have revealed that the BS population in open clusters mostly contains long-period binaries (Geller et al., 2009). This kind of stars have periods ranging from a few days to decades, or even centuries, and it is very difficult to detect them spectroscopically and photometrically.

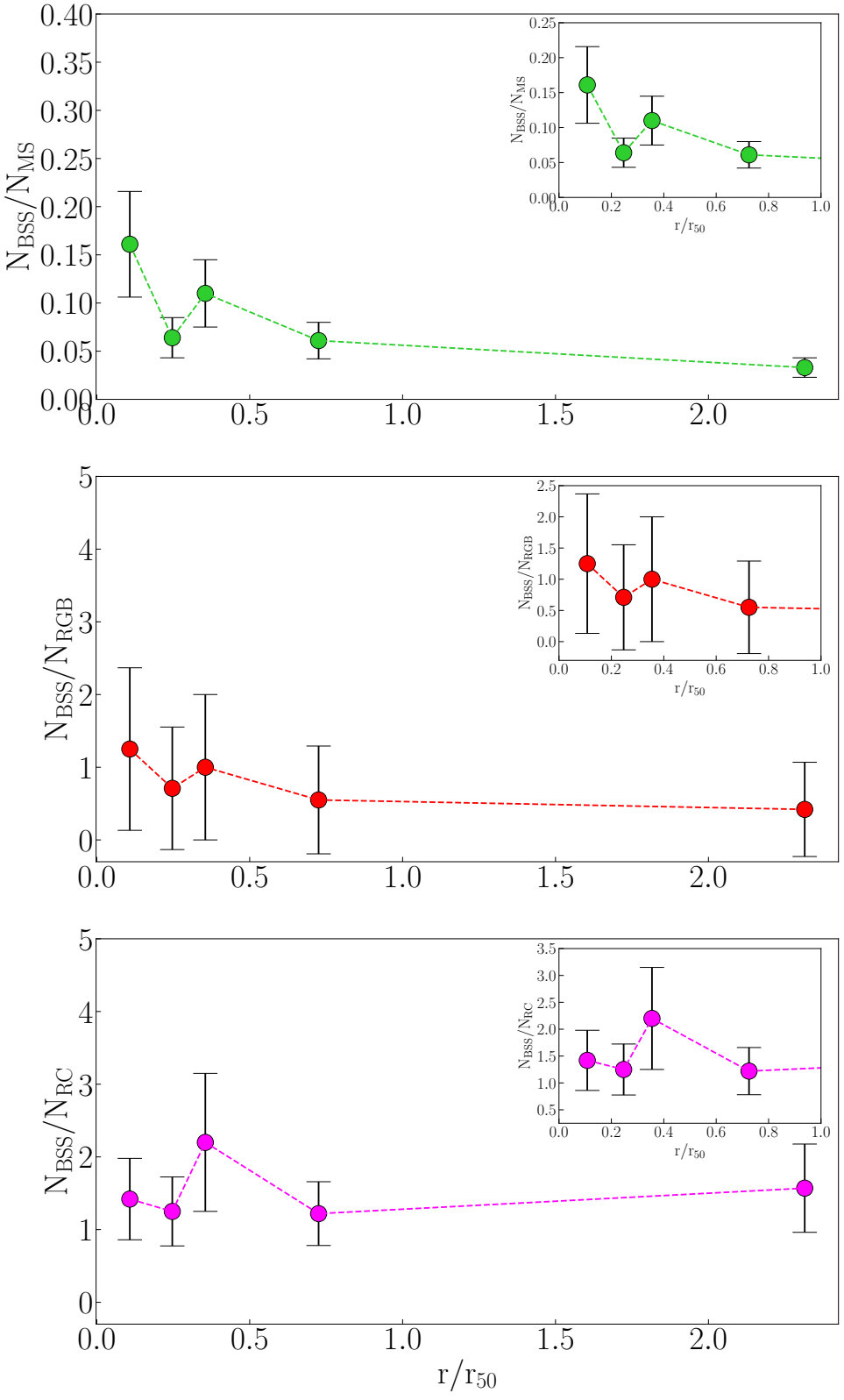

Figure 4.6 Number of BSS with respect to that of the reference stars: green for main sequence stars, red for red giant stars and magenta for clump stars, plotted as a function of the distance from the cluster center expressed in r/r_{50}. Errors are Poisson. All the populations are corrected by field contamination.

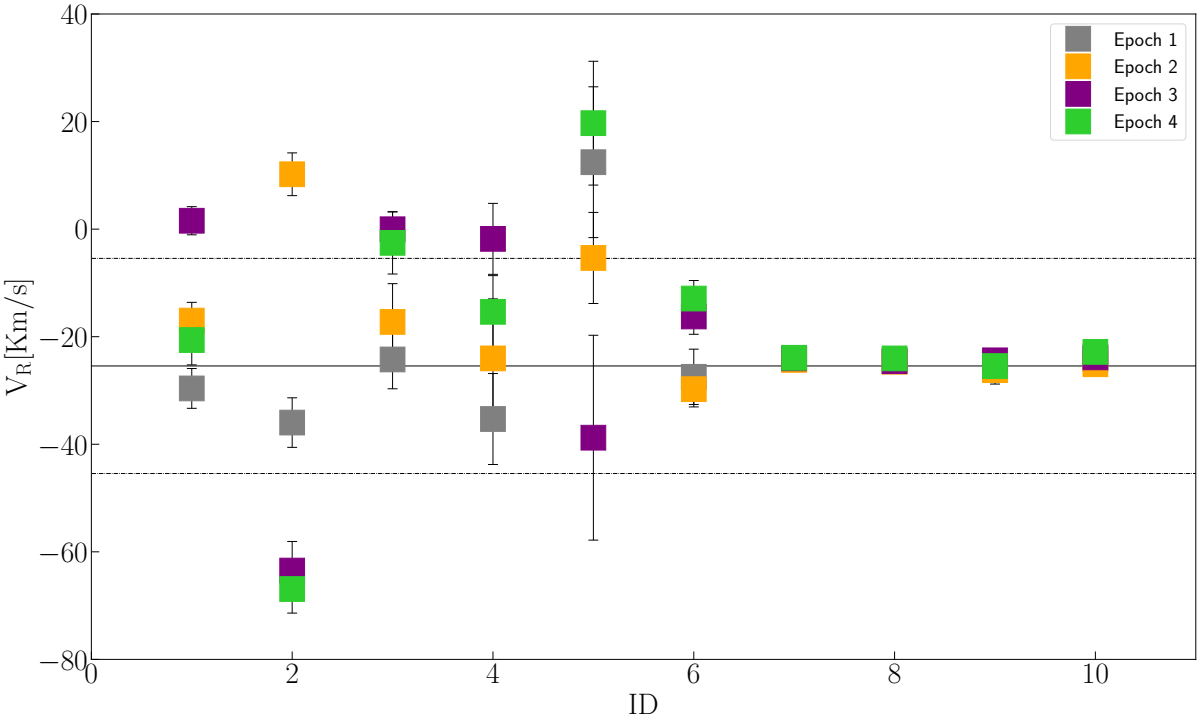

Figure 4.7 Radial velocity distribution of BS candidates in Collinder 261. Different colors indicate different epochs. The solid line represents the cluster mean radial velocity, while the two dashed lines indicate the ± 20 km s^{-1} band we discuss in the text. Errors plotted are the values given by `fxcor`.

Star BS6 (%100) is a member according to our astrometric criteria and, according with Figure 4.7, is a possible long-period binary stars (M, LP), is the only M, LP we found in our sample. This star is at 2.55′ from the cluster center.

4.4.2.2 Close binaries

Stars BS1, BS3, BS4, BS5 and BS8 are cluster members and are also classified as possible close-binary systems (M, CB). The presence of these stars within the BS populations is quite unknown; according with previous studies perform in OCs, they are less numerous than long-period binaries (e.g., NGC 188, Mathieu and Geller 2015; M67, Latham 2007), and their evolutionary histories involve dynamical encounters. According to Mazur et al. (1995), Collinder 261 is the star cluster that possesses the richest and most diversified population of short-period binaries found so far.

Stars BS1 and BS3 are at 2.50′, 2.58′ respectively from the cluster center.

Star BS4 has already been classified as an eclipsing binary of Algol type (i.e., detached, cf. Table B.1). The ASAS-SN Variable Stars Database[7] (Jayasinghe et al., 2019) gives an amplitude value of 1.87 mag. Mazur et al. (1995) give a period value of $P \sim 0.49135$ days. This star is at 0.53′ from the cluster center.

Star BS5 is a very well studied member of Collinder 261. It has already been classified as a semi-detached, eclipsing binary of β Lyrae type (Avvakumova et al., 2013). According to Samus' et al. (2017) and Jayasinghe et al. (2019), this binary has a period P of $\sim$ 0.8040604 days and a amplitude of 0.44 mag. This star lies at 1.70′ from the cluster center and, according to its upper limit of $v \sin(i)$, it is a fast rotator (see Table 4.3)

Star BS8 is a completely different case. In the literature it has been cataloged as a detached, eclipsing binary of Algol type (Avvakumova et al., 2013, Mazur et al., 1995, Samus' et al., 2017), and also as a genuine BSS according to AL07. Most Algol variables are quite close binaries, and therefore their periods are short, of typically a few days. Is also very well known that these stars are among the most active and X-ray luminous. Vats and van den Berg (2017) give an X-ray luminosity $L_{X,u} \sim 8.05$, and Mazur et al. (1995) a preliminary value of the period $P \sim 2.11$ days. This star lies at 3.29′ from the cluster center.

4.4.2.3 Non-radial velocity variables BSS

There are three blue stragglers in Collinder 261 that do not show significant radial-velocity variability: BS2 , BS7 and BS9. They lie at 1.43′, 0.49′ and 0.46′ respectively from the cluster center. The upper limit we obtained for their rotational velocities are reported in Table 4.3. It is possible that these non-velocity-variable blue stragglers are indeed long-period binaries, perhaps outside our detection limit. Star BS2 is the bluest BS in our sample and BS7 is the reddest.

[7] `https://asas-sn.osu.edu/variables`

4.4.2.4 Yellow Straggler

Star YS1 is considered to be a yellow straggler according to its position in the color-magnitude diagram, and because it lies beyond the red limit $(G_{\rm BP} - G_{\rm RP}) \approx 1.2$. This star is located at 1.67′ from the center and not significant rotation was found.

4.4.3 Mass estimations

We performed a mass estimation for BS4, BS5, and BS8. These stars are identified in the literature as eclipsing binaries, and are briefly described in § 4.2.1. To fit the orbits we used the RVs we obtained in § 4.3.1 and the periods reported in the literature (§ 4.4.2). For BS5 we divided the period by 2 (i.e., $P \approx 0.402$ days). For all stars we assumed that they are members, and that the mean velocity of the cluster is the systemic velocity γ of the binary. To obtain the mass of the secondary (M_2) stars, we first estimated the masses of the primaries (M_1) from the CMD. The masses we finally derived for BS4 are $M_1 \approx 1.5 M_\odot$ and $M_2 = 0.118 \pm 0.005 M_\odot$, for BS5 are $M_1 \approx 1.51 M_\odot$ and $M_2 = 0.21 \pm 0.01 M_\odot$, and for BS8 are $M_1 \approx 1.51 M_\odot$ and $M_2 = 0.42 \pm 0.02 M_\odot$. Figure 4.8 shows the RV curve for each star.

4.5 The case of Collinder 261 in TESS

Mazur et al. (1995) discovered 45 short-period eclipsing binaries in the Collinder 261 field, and estimated the frequency of the binary BSs among their sample within $\rm r/r_{50} \sim 1$ (6 arcmin) from the cluster center. They found a frequency of between 11% and 28%, supporting the hypothesis that a significant fraction of BSS formed as a result of mass transfer in close binary systems. As explained in § 2.8 we searched the 53 blue straggler candidates of Collinder 261 in TESS.

After a fast inspection we found that 45% (21 out of the 53) of the stragglers are short-period binaries —being post-CE systems or Algols— with orbital periods between 7 hours and two days. Nevertheless, after the inspection of the TPFs, we noticed three

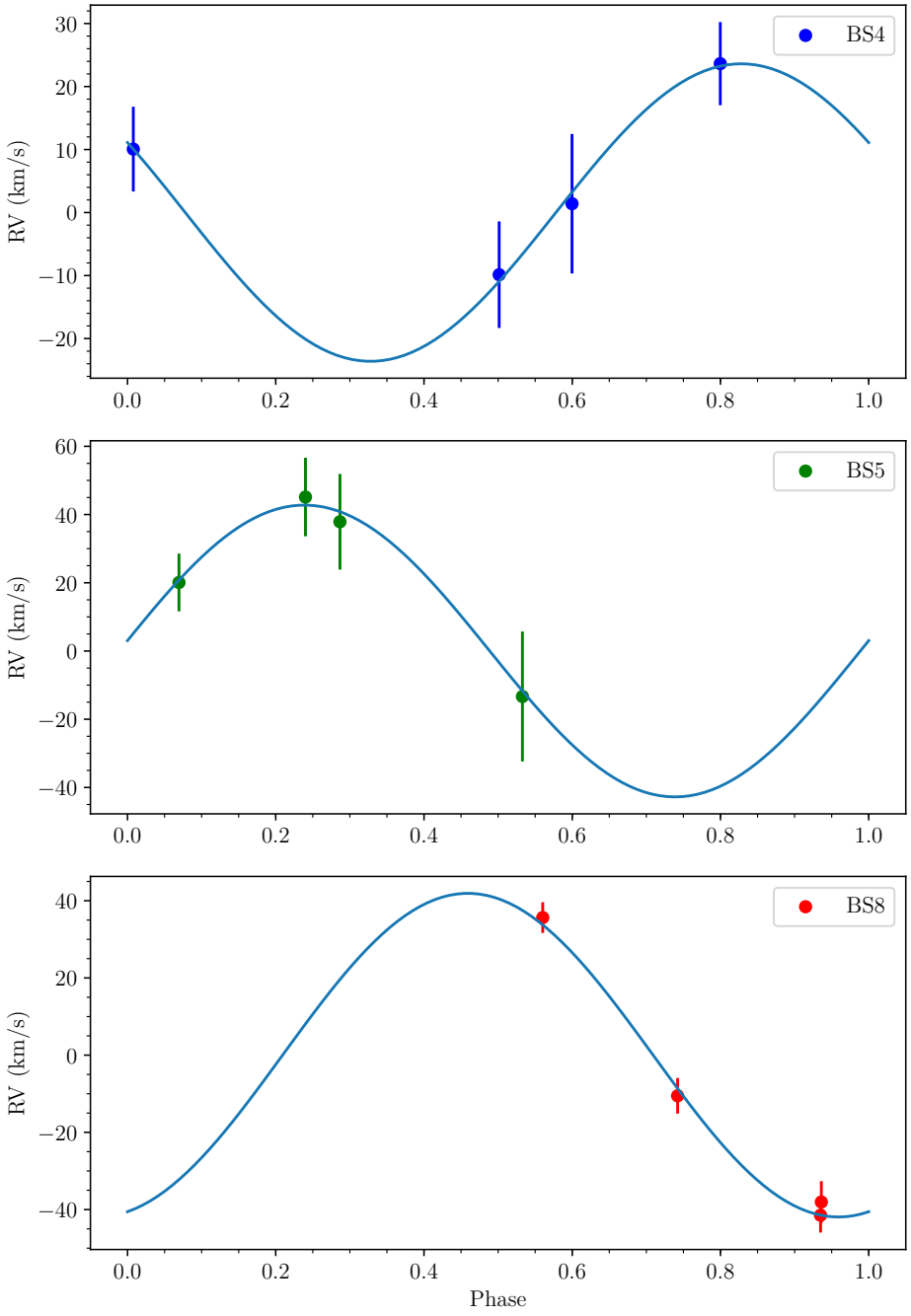

Figure 4.8 FLAMES radial velocity curves for three BSS short period binary BSS, on which we performed mass estimations of their companions M_2.

out of the 21 BSS have LC heavily contaminated by a near by and bright star, up to Δm=-1. This means the light extracted from that stars comes almost entirely from the bright star and not the BSS itself, reducing our percentge to 33%. We also noticed some of the BSS have very similar periods. In this context, it is quite probably one bright, relatively nearby EB have bleeded into the BSS-LCs. This behaviour, however, was expected since in general getting any light-curve for OCs from TESS is challenging given the large pixel size and crowded cluster fields. Figure 4.9 shows the light curve of the star *Gaia* DR2 5856515665648722688; the light curves of the remaining short-period binaries are in Appendix C, while the periods, *Gaia* IDs and Tess ID are reported in Table 4.4. The percentage we found strikingly disagrees with the fraction of short-period binaries found among BSS in NGC 188 and M67, where it is about 10%. In Figure 4.10 are shown all the short period binaries we found using TESS-PATHOS LCs; the Figure includes the stragglers with high and low rotational rates of § 4.3.1. We also added the stragglers with X-ray emission reported by Vats and van den Berg (2017), because the origin of the X-ray emission from bona fide cluster BSS is a sign of ongoing binary interaction, and thus provides an indication of the current system configuration. In Figure 4.10 all the short-period BSS are randomly distributed across the straggler region, and the same happens for the low- and fast-rotator stars—even though their number is not statistically significant. Our results however, do not indicate the remaining BSS (those with LCS, but on which no variability was found) are non-variable systems and/or single stars, they can be binaries with periods outside the detection of TESS baselines.

Unquestionably, more data either photometric or spectroscopic are needed in order to fully characterize the straggler population of Collinder 261. We hope our recently accepted proposal (PI: Rain; 109.22ZM.001) aimed to study the RV variability of the BSS can help us to better understand the straggler population of this cluster. Further for those with short periods we will be able to combine the RVs with TESS photometry and so fully characterize these systems and compute the orbital solution infer their properties and likely formation mechanism. If confirmed, the large fraction of very short period binaries among the stragglers represents a clear surprise and may tell us important facts about the relative importance of the various BSS formation mechanism as a function of the cluster age. Until today, this kind of studies is only available for few clusters, e.g NGC 188 and M67.

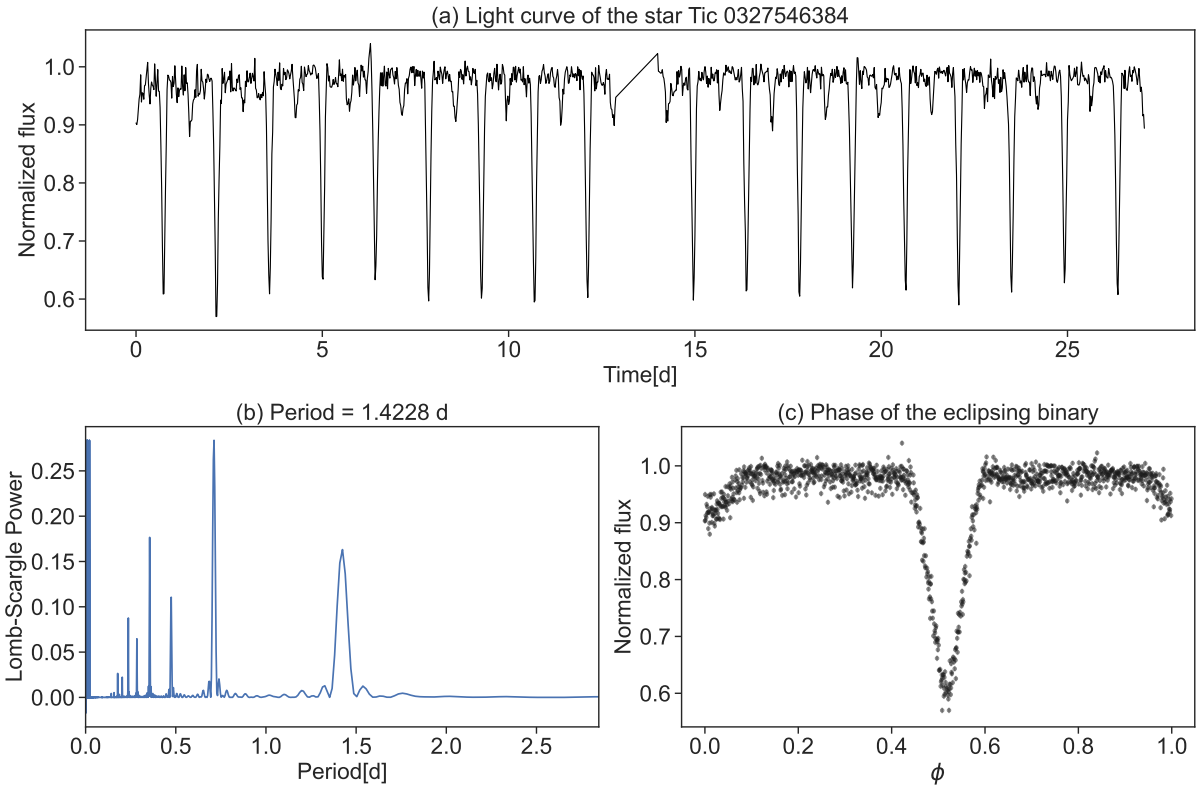

Figure 4.9 Panel (a) shows the normalized light curve of *Gaia* DR2 5856515665648722688 from sector 11. Panel (b) shows the Lomb-Scargle periodogram. Panel (c) is the phase transit of the eclipsing binary.

We also searched the YSS, we found two out of the three are in close-binary systems. The LCs are reported in Appendix B.

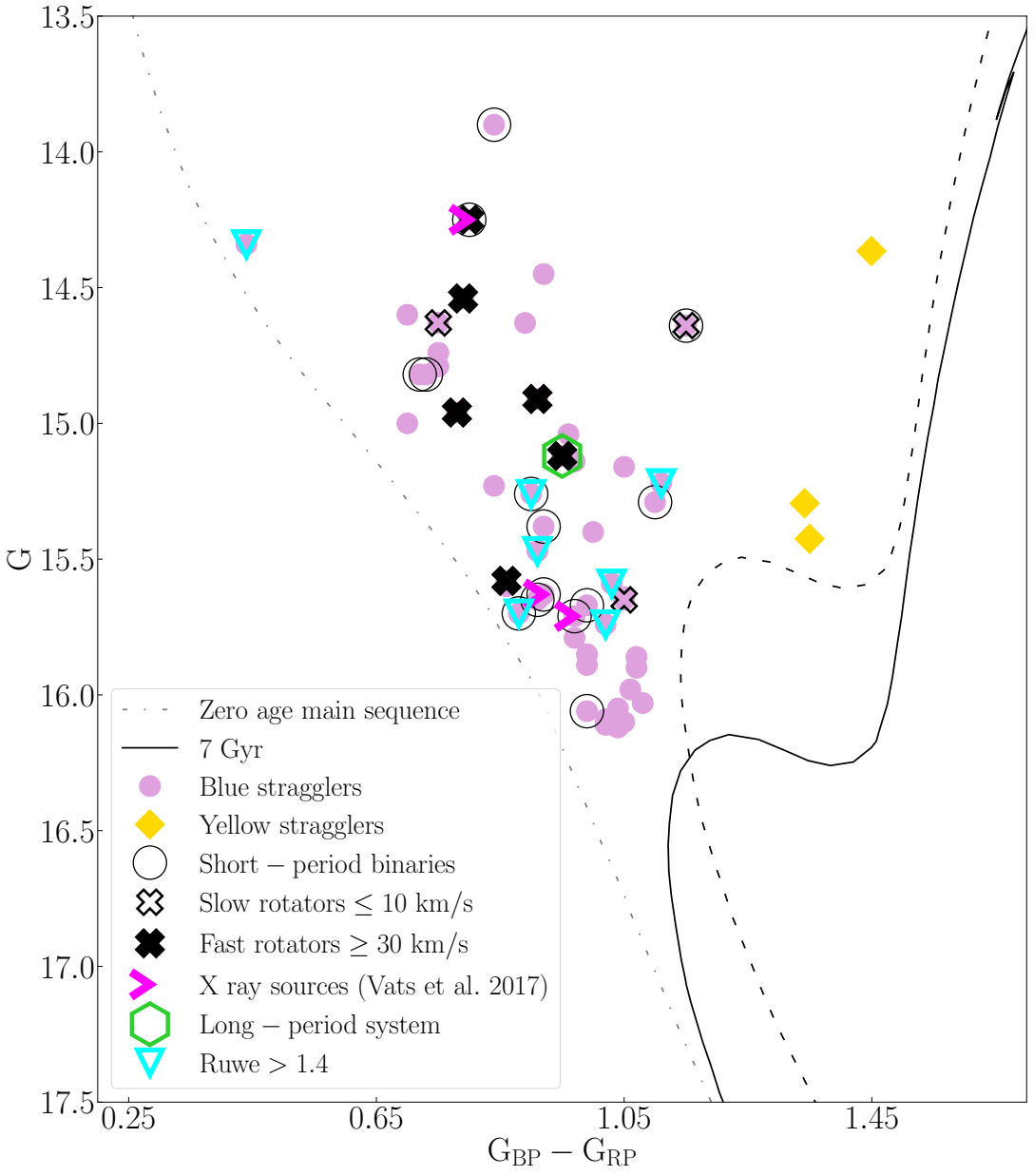

Figure 4.10 Color-magnitude diagram of Collinder 261. Purple filled circles and yellow filled diamonds are the blue and yellow straggler stars reported in Chapter 2. Open black circles are the short-period binaries we found in § 4.5, while filled and open black crosses are the fast and slow rotators of the binaries we identified in § 4.3.1. X-ray sources of Vats and van den Berg (2017) are in magenta symbols. We also added those stars that have a RUWE>1.4, indicative of a possible binarity.

Table 4.4 Periods of close-binary BSS systems in Collinder 261

Gaia DR2 ID	Tess Tic ID	Period [d]	Aperture
5856515188899621632	0327545566	0.518	PSF
5856529001554008064	0327766680	0.319	AP1
5856517010004497792	0327766459	1.049	PSF
5856515601255190272	0327546480	2.115	AP1
5856527524085206656	0327546308	0.332	PSF*
5856528623597294720	0327545871	0.461	AP1
5856515665648722688	0327546384	1.422	AP1*†
5856527558444963200	0327546164	0.804	AP1
5856517078723954944	0327766396	1.421	AP1
5856528962867671936	0327546031	0.400	AP1*
5856515669974676480	0327546409	1.422	AP1†
5856527455365743488	0327546246	0.428	AP1
5856527455365735680	0327546290	0.804	AP1†
5856527558444950656	0959852346	0.804	AP1†
5856528383078700288	0327546013	1.094	AP1*
5856432828647768960	0327153496	1.129	AP1
5856527455365740032	0327546276	0.428	AP1*
5856527730243676800	0327545961	1.092	AP1*

Notes:
[a] PSF is the point-spread function photometry and AP1 is the aperture photometry of 1-pixel radius used on PATHOS. They indicate where we found the eclipse in each straggler candidate.
* Fainter stars inside the 1-pixel radius.
† The star is on the same aperture pixel of another BSS wich also shows variability.

4.6 Summary and conclusions

In this chapter we have presented a detailed study of the blue and yellow straggler population of the old open cluster Collinder 261. Our main results are shown in Figure 4.1, Tables B.1, 4.3 and 4.4.

Following Bhattacharya et al. (2019), we used our BS candidates as test-particles to probe the dynamical state of Collinder 261. In particular, we found that BSs are more centrally concentrated than all the reference populations choose —RGB, RC MS stars (see Figure 4.5). To search for mass segregation, we normalized the BS population to several reference populations (RGB, MS, and RC stars); before each comparison, we performed an A-D test to check that the populations are not extracted from the same parent distribution, which should also indicate the presence of segregation. The test gives 99.9%, 86.9% and 16.0% of MS, RGB and RC, respectively, that are not drawn from the same distribution than the BSS. Considering the whole cluster extension ($2 \times \mathrm{r_{DAML02}}$) We found pronounced peaks and minima in the central regions of the cluster, similar to the ones found by Bhattacharya et al. (2019) in Berkeley 7. However, when taking into account the errors involved, these results were dismissed. We calculated the relaxation time of our cluster and found $t_{\mathrm{relax_c}} \sim 100$ Myr for the core, and $t_{\mathrm{relax_h}} \sim 250$ Myr for the half-light radius. Both values are quite small compared with the evolutionary age of our cluster (7–9 Gyr). Given these results, we were not able to place Collinder 261 in any of the families defined for globular clusters by F12.

In the second part of the chapter, we presented the first high-resolution spectroscopic study of the BS population of Collinder 261, adopting membership criteria more solid than the simple photometric one. So far, spectroscopic studies have been limited to a very small number of clusters. This is mostly because open clusters are believed to harbor many BS stars (Ahumada and Lapasset, 2007), and therefore studying them in detail represents a huge observational challenge. The reason, however, for which they host so many BS stars, has not been fully deciphered yet. For this study we obtained four epochs of RVs; based on their variations, we separated these stars into candidate members, probable close binaries, and long-period binaries. All the probable binaries would need additional spectroscopic follow-up to be properly characterized, given the

small number of epochs available. Unfortunately, the data that we have just presented cover only nine stars of the 53 possible BSs found in our analysis with *Gaia* and one star of the three YS candidates we identified in R21b. This is so because we originally used the photometric-based list of Ahumada and Lapasset (2007) to select the objects to be observed with FLAMES, a list that differs significantly from that defined in this work.

Collinder 261 is a cluster of intermediate richness (see Figure 4.1). Our spectroscopic results are shown in Figure 4.7. RVs for four epochs are available for 10 stars, among which we identified five as probable CB, and only one as LP binaries. Four stars did not show RV variations, among them one yellow straggler and three blue stragglers. We performed an estimation of the masses of BS4, BS5 and BS8. It is in our future plans to fit an orbit solution for the others BSS, since it will definitely help understand better the formation history and survival channels of blue straggler stars — Just in case the reader is wondering why we did not carry out this immediately, it is because when the work on Collinder 261 was published the TESS periods were not yet available. The TESS data analysis came during the latest stages of this thesis.

Finally, when cross-correlating our catalog with TESS, we found ∼33-45% of the stragglers are in close-binary systems. While the last gives some clues of the nature of the blue and yellow candidates, it is not enough to draw firm conclusions, regarding binarity among them. We hope that our recently accepted proposal will fill this gap of information. The LCs used in our analysis come from the PATHOS project. While tremendously useful, this work has not extracted the data of all the stragglers in Collinder 261, which opens the opportunity for carrying out a similar analysis not only in Collinder 261 but on the entire catalog, an ongoing process not included in the present Thesis.

Chapter 5

The Blue Straggler population of Trumpler 20, NGC 2477, and Trumpler 5

This chapter is mainly based on:

The blue straggler population of the open clusters Trumpler 5, Trumpler 20, and NGC 2477

Authors: M.J. Rain, G. Carraro, J.A. Ahumada, S. Villanova, H. M.J. Boffin, L. Monaco

The astronomical Journal, 2020, 161, 37R

it is also based in unpublished data and analysis

5.1 Introduction

Despite the presence of BSS in all stellar environments, after the *Gaia* releases there is a particular, increasing interest in studying these objects as members of open clusters (OCs). The general properties of this population have been extensively described in the previous chapters, so here we will specifically comment on three clusters. The old cluster Trumpler 5 (4 Gyr) has the largest $N_{\rm BSS}$ according with R21b. Old clusters are only ∼15% of the whole population of more than 2100 known OCs, and only ∼5% are older than 2 Gyr. However, old OCs are particularly important to constrain the formation and evolution, both dynamical and chemical, of the Milky Way disk. Given the age of Trumpler 5 it was quite natural for us to devote a paper to a detailed study of this object. In ESO programs 088.D-0045(A) and 0100.D-0054(A) the open clusters NCG 2477 (700 Myr) and Trumpler 20 (1 Gyr) were also included for the scope of the proposal, i.e., to study the blue straggler population as a function of the environment and the parent cluster properties. However, multiple drawbacks led to neither the paper or the data to see the light until now. As in the case of Collinder 261, none of the three clusters had previous spectroscopic and photometric studies dedicated to their straggler population, except just comments within a photometric analysis. At this point we consider important to remind the reader that straggler candidates used for the proposal came from the previous compilation of AL07. This chapter mimics the previous one, i.e., a similar methodology was used but on a different sample.

Cluster parameters are reported in Table 5.1. The data used on this study either photometric and spectroscopic, as well as the differential reddening corrections, cluster mean astrometric values, density profiles and field contamination analysis are described in § 5.2. The spectroscopic analysis, the radial velocities and rotational rates with their corresponding errors are describe in § 5.3. Finally, in § 5.4 we explore the radial distribution of the stragglers in Trumpler 5, and in § 5.5 we report the close-binary systems we found within the Transiting Exoplanet Survey TESS. We conclude and summarize in § 5.6.

Table 5.1 Main parameters of the open clusters under study.

Cluster	l [deg]	b [deg]	Distance [kpc]	$E(B-V)$ [mag]	R_a^1 [arcmin]	log(age) [yr]	[Fe/H] [dex]	V_R [km s^{-1}]
Trumpler 5	202.86	+1.05	3.19[b]	0.62[a]	15.4[a]	9.6[a]	-0.40 ± 0.00[a]	$+49.67 \pm 0.66$[c]
Trumpler 20	301.47	+2.22	3.56[b]	0.46[a]	16.0[a]	9.1[a]	$+0.17 \pm 0.03$[a]	-40.94 ± 1.20[e]
NGC 2477	253.56	−5.64	1.44[b]	0.31[a]	15.0[a]	8.8[a]	$+0.07 \pm 0.03$[a]	$+08.62 \pm 0.46$[d]

Notes:
[1]Apparent radius , [a]Dias et al. (2014) , [b]Cantat-Gaudin et al. (2018) [c]Monaco et al. (2014)
[d]Mishenina et al. (2015), [e]Carraro et al. (2014)

5.2 Datasets

5.2.1 Photometric data

The photometric data used for this analysis is the same one described in § 2.2 and 4.2.1, i.e., the Data Release 2 of the European Space Agency mission *Gaia*. In the present chapter, however, we used a slightly different procedure to select the straggler candidates; the procedure is described in the following sections. We started by quantifying the effect of differential reddening and field contamination in all three clusters: NGC 2477, Trumpler 5 and Trumpler 20. It is worth remarking that, at the moment our work was published, no authors had quantified both effects before with *Gaia* DR2.

5.2.1.1 Differential Reddening

The main effect of differential reddening (DR) in a CMD is a broadness (or dispersion) of the sequences of the cluster; this results from the differential presence of dust along the line of sight and across the field of view, causing different extinction values (Platais et al., 2008). For old open clusters ($\log(\mathrm{age}) \geq 1$ Gyr) the effects of DR are most noticeable in the TO and the RGB morphologies. In this context, the position of Trumpler 5 and Trumpler 20 in the Galactic disk and their high values of reddening (see Table 5.1) suggest that these two clusters are highly affected by DR. This is noticeable in the left panels of Figure 5.1, where the elongated red clump and the thick appearance of the main sequence and TO in Trumpler 5 are clear indicators of DR. In minor scale, the same effects are observed in the CMD of Trumpler 20. We will quantify, however,

Table 5.2 Details of the spectroscopic observations for Trumpler 20 (February 11–12 to March 3–4, 2012, and January 30–31 to March 28–29, 2018); Trumpler 5 (February 11–12 and 29 to March 28–29, 2018); and NGC 2477 (October 28–29, 2011 to March 8–9, 2012, and January 30–31 to March 3–4, 2018). All dates are Modified Julian Date (JD−2,400,000.5).

Trumpler 20			
Epoch	$\mathrm{MJD_{start}}$ [d]	$\mathrm{MJD_{end}}$ [d]	Exposure [s]
1	55969.306622551	55969.3344003785	2400.0043
2	55990.200693457	55990.2284712834	2400.0042
3	58149.292577118	58149.3203549282	2400.0028
4	58206.118721651	58206.1464994681	2400.0034
Trumpler 5			
Epoch	$\mathrm{MJD_{start}}$ [d]	$\mathrm{MJD_{end}}$ [d]	Exposure [s]
1	55969.166866965	55969.1923299766	2400.0042
2	55987.039632022	55987.0650950232	2200.0033
3	58177.077345320	58177.1028083142	2200.0027
4	58180.077972559	58180.1034357268	2200.0177
5	58206.000367976	58206.0258309702	2200.0027
NGC 2477			
Epoch	$\mathrm{MJD_{start}}$ [d]	$\mathrm{MJD_{end}}$ [d]	Exposure [s]
1	55863.327186374	55863.3445475059	1500.0018
2	55863.345536336	55863.3628974807	1500.0029
3	55995.200983276	55995.2183444288	1500.0036
4	58179.147028199	58179.1643893541	1500.0038
5	58181.169961441	58181.1873225822	1500.0026
6	58122.199733802	58122.2170949270	1500.0012
7	58135.279591133	58135.2969522545	1500.0009
8	58149.265756268	558149.2831174243	1500.0039

the effect of DR in the three clusters analyzed in this work. The DR correction was performed in two different ways. In the case of Trumpler 5, which is the cluster most affected by this problem, we missed most of its MS due to the cut in $G = 18$ (see CG18 for more details). On the other hand, its CMD shows a well defined RC dispersed along the reddening line. First of all we selected RC stars and determined the reddening law $R_G = A_G/E(G_{\rm BP} - G_{\rm RP})$ by a linear least square fit. We got $R_G = 1.79 \pm 0.05$. Then we selected an arbitrary point along the RC line as the zero-point for the reddening correction. This point has $G = 13.90$ and $(G_{\rm BP} - G_{\rm RP}) = 1.67$. Then, for each RC star we calculated the distance, both vertical and horizontal, with respect to the reference point. The vertical distance gives the differential A_G absorption at the position of the star, while the horizontal distance gives the differential $E(G_{\rm BP} - G_{\rm RP})$ reddening at

the position of the star. After this first step, for each star of the field (both cluster and non-cluster members) we selected the three nearest RC stars and calculated the mean differential A_G absorption and the mean differential reddening $E(G_{\rm BP} - G_{\rm RP})$, and finally subtracted this mean value from the star's $(G_{\rm BP} - G_{\rm RP})$ color and G magnitude.

For Trumpler 20 and NGC 2477, we used instead MS stars for the DR correction, since we have for them much longer and populated main sequences (see Fig. 5.1). We defined a line along the MS, and for each one of the selected MS stars, we calculated its distance from this line along the reddening law line. For this reddening law, the line was assumed the slope we found for Trumpler 5, i.e., $R_G = 1.79$. The vertical projection of this distance gives the differential A_G absorption at the position of the star, while the horizontal projection gives the differential reddening $E(G_{\rm BP} - G_{\rm RP})$ at the star's position. After this first step, for each star of the field (both cluster members and non-members) we selected the ten nearest MS stars and calculated the mean differential A_G absorption and the mean differential $E(G_{\rm BP} - G_{\rm RP})$, and finally subtracted this mean value to its $(G_{\rm BP} - G_{\rm RP})$ color and G magnitude.

We want to underline the fact that the number of reference stars used for the reddening correction (three for Trumpler 5 and ten for Trumpler 20 and NGC 2477), is a compromise between having a correction affected as little as possible by photometric random errors, and the highest possible spatial resolution. Figure 5.1 shows the uncorrected (left) and corrected (right) color-magnitude diagrams. Figure 5.2, finally, shows the reddening maps for each cluster.

5.2.2 Spectroscopic data

As described in § 4.2.2, the clusters were observed with the Fibre Large Array Multi Element Spectrograph (FLAMES)[1] attached to the Very Large Telescope (VLT) of the European Southern Observatory (ESO; Paranal Observatory, Chile), using the combination of the mid-resolution spectrograph GIRAFFE and the fiber link to UVES. NGC 2477 data were collected in two periods, October 2011 to March 2012, and January 2018 to March 2018. Data for clusters Trumpler 5 and Trumpler 20 were also obtained in two

[1] `http://www.eso.org/sci/facilities/paranal/instruments/flames.html`

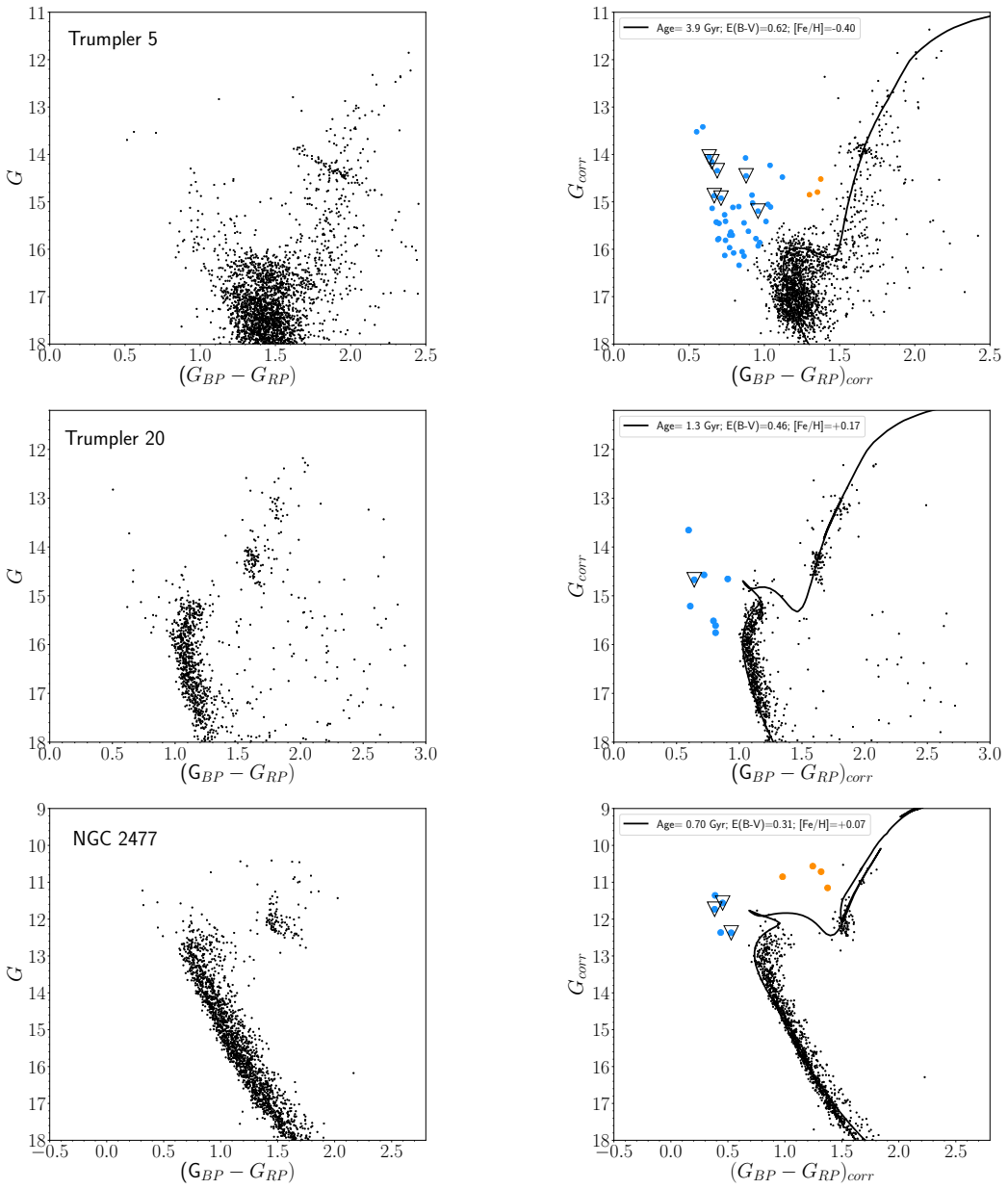

Figure 5.1 **Left panels:** Color-magnitude diagrams of Trumpler 5, Trumpler 20, and NGC 2477. Black dots are cluster members with $P_{\rm memb} \geq 50\%$, selected by Cantat-Gaudin et al. (2018). **Right panels:** Color-magnitude diagrams after the correction for DR, for stars with $P_{\rm memb} \geq 50\%$, and falling within their corresponding radius R (see § 5.2.6). Blue solid dots are our BSS candidates. Orange filled circles are yellow straggler stars. Black open triangles are the sources with spectroscopic data available in this work, cross-matched with BSS candidates of AL07 only for Trumpler 5 and NGC 2477, since Trumpler 20 was not included in the 2007 catalog. Isochrones are from Bressan et al. (2012).

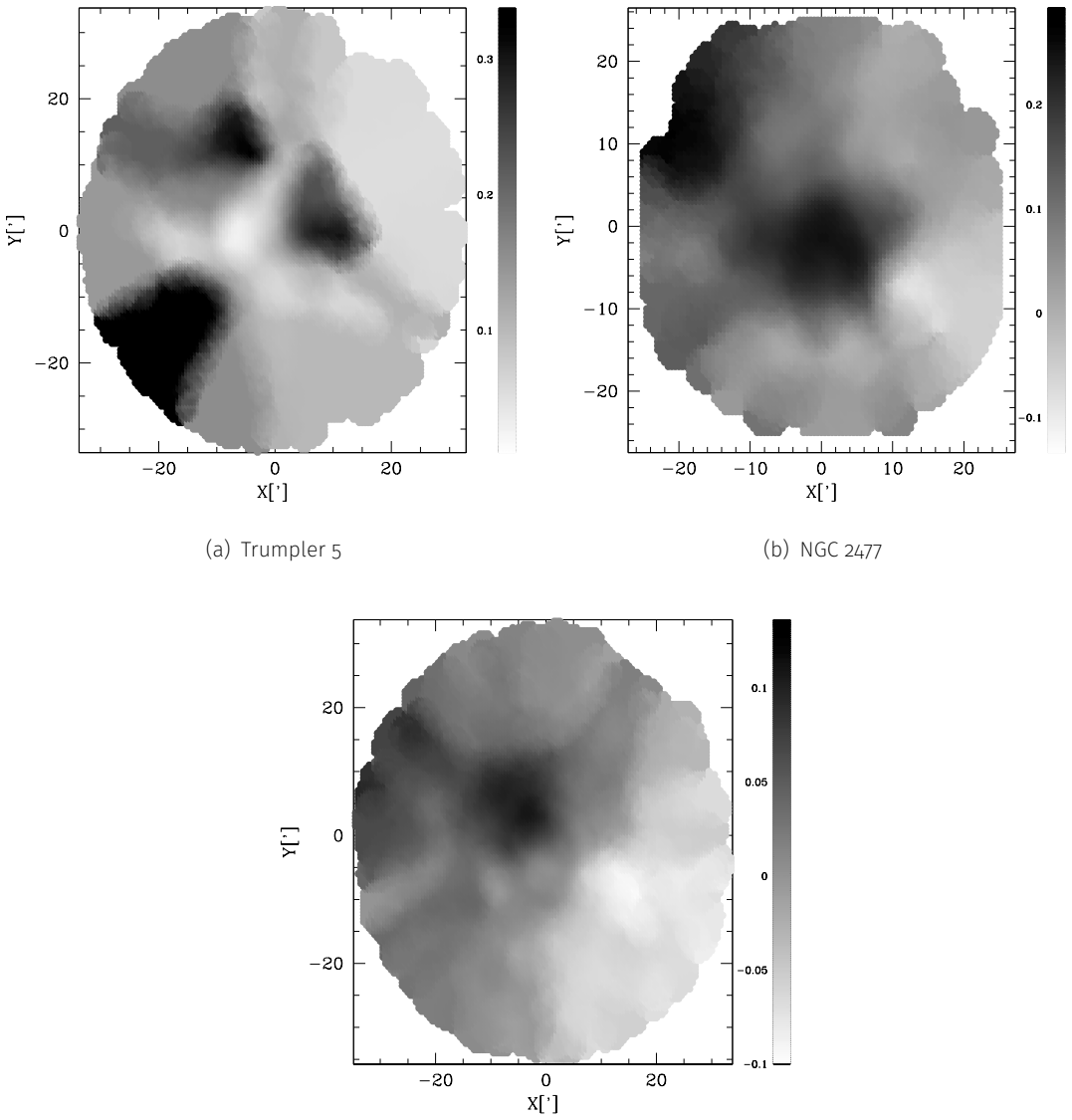

(a) Trumpler 5

(b) NGC 2477

(c) Trumpler 20

Figure 5.2 Reddening maps in RA (X) and Dec (Y) (expressed in arcmin) obtained for Trumpler 5, Trumpler 20, and NGC 2477 (from top to bottom). The intensity code indicates where differential reddening is stronger (darker) or weaker (lighter). The color bar corresponds to $\Delta \mathrm{E}(\mathrm{BP}-\mathrm{RP})$

periods, February 2012 to March 2012, and January 2018 to March 2018. These data were gathered under ESO programs 088.D-0045(A) and 0100.D-0052(A).

The UVES fibers were allocated to the cluster's clump stars. the reduction and analysis of the UVES data are described in Carraro et al. (2014), Mishenina et al. (2015), Monaco et al. (2014). GIRAFFE was used with the setup HR8 (491.7–516.3 nm). Integration time ranged between 1,500 sec and 2,400 sec depending on the cluster. In total, NGC 2477 was observed on eight epochs, Trumpler 5 on five epochs, and Trumpler 20 on four epochs. Some details of the observations are given in Table 5.2. As for the case of Collinder 261, we only performed the sky-subtraction and normalization using the IRAF packages `sarith` and `continuum`.

5.2.3 Cluster mean proper motions and parallaxes

For consistency, we carried out the same photometric analysis described in Chapter 3. To use the membership selection of CG18 with confidence, we calculated the mean proper motions and parallaxes values for the three clusters.

As mentioned elsewhere, in *Gaia* DR2 the radial velocity information is provided for targets with $G < 13$ mag. Here, we identify these objects in all three clusters. First, we selected giant stars with V_R measurements available and we calculated a first estimation of the mean V_R value and the corresponding rms for each cluster. Then, only stars within $V_R \pm \sigma$ were selected. The same procedure was performed on each cluster until reach considerable small values of the rms —of the order of the errors in *Gaia* radial velocities— and V_R values similar to those reported in Table 5.1. We ended up with 10, 38, and 79 stars for Trumpler 5, Trumpler 20, and NGC 2477, respectively.

Second, we searched *Gaia* counterparts of members previously identified in the literature with confirmed membership. For Trumpler 5 we used five red-clump stars identified as members by Monaco et al. (2014). In the case of Trumpler 20, we used a sample of five bona fide clump stars for which Carraro et al. (2014) determined the abundance of several elements and their ratios to confirm their membership. Finally, for NGC 2477 we used six giant stars analyzed and identified as members by Bragaglia

et al. (2008). We cross-correlated the position on the sky of these stars and the *Gaia* DR2 catalog, looking for the nearest neighbors within 1″. Finally, using both stars from the literature and the ones selected above we calculated the mean proper motions and parallaxes values. The values we found are reported in Table 5.4. Errors indicated are the standard deviations from the stars.

Our results are in remarkable agreement with the values in the literature (e.g., Cantat-Gaudin et al., 2018, Gao, 2018). However, all of them differ considerably from the values reported in DAML02. The most extreme case is that of Trumpler 20, with absolute differences (our work *minus* DAML02) of 4.87 mas yr^{-1} and 3.89 mas yr^{-1} for μ_δ and $\mu_\alpha \cos\delta$, respectively. These differences are unlikely to be caused by systematic errors in *Gaia* data, and probably arise from significant contamination by field stars and the lack of reliable cluster membership in the DAML02 catalog. For Trumpler 5 and NGC 2477 we found differences of 0.24 mas yr^{-1} and 0.42 mas yr^{-1}, and 1.84 mas yr^{-1} and 0.94 mas yr^{-1} for μ_δ and $\mu_\alpha \cos\delta$, respectively. The values we estimated were not used in the rest of this analysis, but we always employed those of CG18.

5.2.4 King profiles and structural parameters

For each cluster we determined the stellar density profiles and derived the structural parameters such as the core and tidal radius and concentration parameters (Table 5.3), using a King profile fitting approach (King, 1962). A possible link between cluster dynamical quantities and the BSS population is explored in § 5.4.

We constructed the radial density profile of the cluster following Salinas et al. (2012). We first divided all observed cluster members into concentric annuli; then, each annulus was in turn divided into eight sub-sectors defined by wedges of 45° centered on the cluster. The cluster center values here used are the ones reported by CG18, obtained using stars with $P_{\rm memb} \geq 50\%$. The density in each sub-sector was measured as the ratio between the number of stars within the sub-sector and the area of the sub-sector itself; this allowed us to obtain a mean stellar surface density and its uncertainty at the mid-point of each shell. The resulting profile was fitted with an isotropic single-mass

Table 5.3 Cluster structural parameters from the King profile fittings and derived quantities.

Cluster	N_* [arcmin]	r_c^a [arcmin]	r_t^b [arcmin]	R [arcmin]	c^c	$t_{\rm relax}$ [Myr]	$N_{\rm relax}$	age [Gyr]
Trumpler 5	1908	4.57 ± 1.07	48.97 ± 15.80	15	1.02 ± 0.02	124	31.45	3.9
Trumpler 20	850	4.07 ± 1.01	36.30 ± 9.27	13	0.95 ± 0.02	115	10.41	1.2
NGC 2477	1367	6.21 ± 1.59	16.90 ± 6.33	12	0.43 ± 0.10	130	5.38	0.7

Notes:
[a] Core radius
[b] Tidal radius
[c] Concentration parameter

King (1962) model:

$$n(r) = k \left(\frac{1}{\sqrt{1 + (r/r_c)^2}} - \frac{1}{\sqrt{1 + (r_t/r_c)^2}} \right)^2 + b, \tag{5.1}$$

were r_c is the core radius, r_t is the tidal radius, k is a scaling constant, and b is the background level. This last one was fixed by the non-linear least-squares method fitted to the total (cluster + background) density profile—i.e., we approximate the model by a linear one and the parameters were estimated by successive iterations—, the fitting gave us k, r_c, r_t, and b for each cluster. After obtaining the cluster parameters, another cluster center was found using the new value of r_t. With this new center, a new calculation of the radial profile was performed, resulting in a new r_t. The procedure was repeated until the position of the cluster center and the value of r_t stopped changing.

The final density profile for each cluster is shown in Figure 5.3. The open circles represent the observed density profile, while the black circles mark the background-subtracted profile, obtained as the difference between the observed profile and the background level. The structural parameters are given in Table 5.3, where $c = \log(r_t/r_c)$ is the concentration parameter. The derived parameters for Trumpler 20 and NGC 2477 are in good agreement with those measured by Donati et al. (2014) and Eigenbrod et al. (2004), respectively.

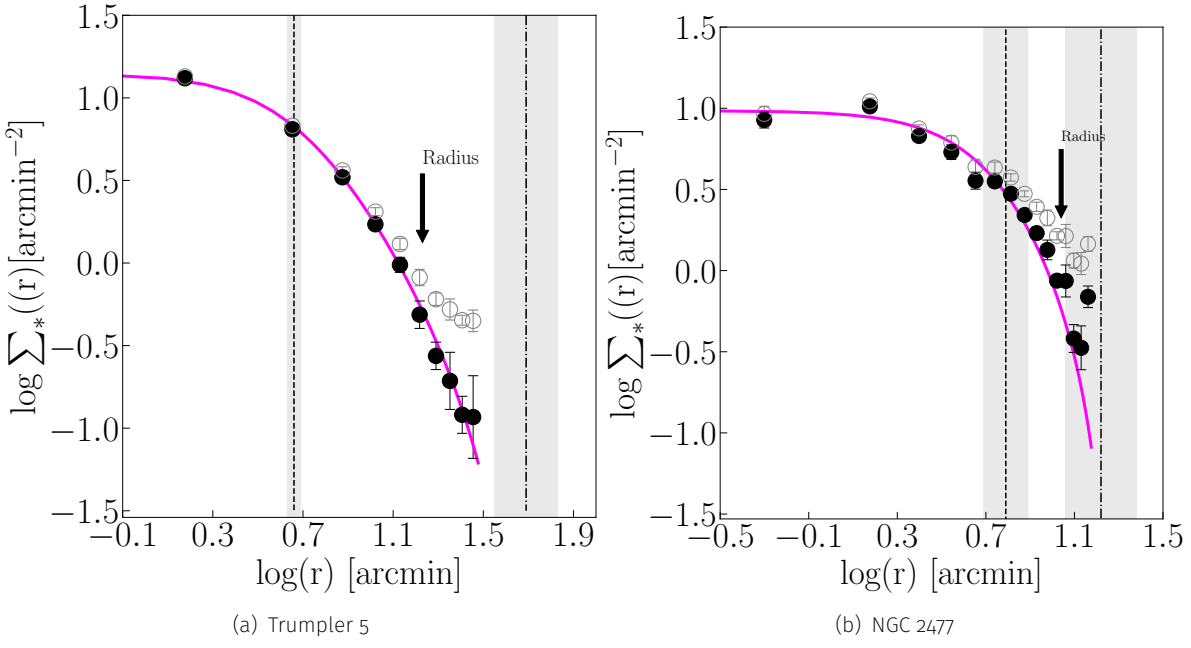

(a) Trumpler 5

(b) NGC 2477

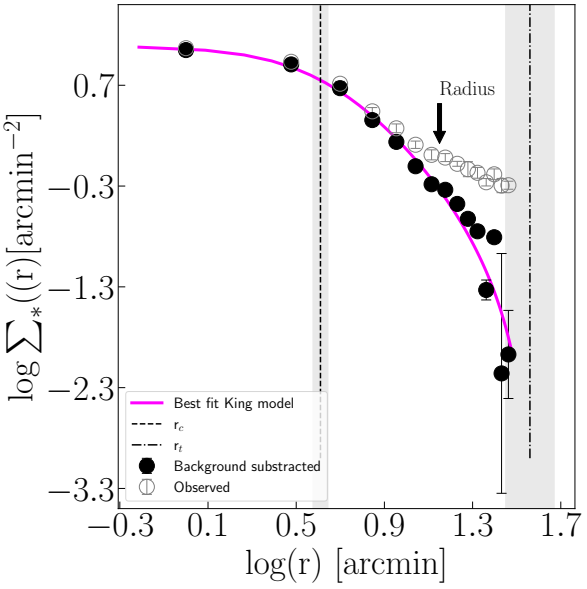

(c) Trumpler 20

Figure 5.3 Observed density profiles of NGC 2477, Trumpler 5, and Trumpler 20 (gray open circles). The background-subtracted profile (black filled circles) is the difference between the observed profile and the background level. The magenta line is the best fit King model. The dashed and dash-dotted vertical lines correspond to the values of the core and tidal radius, respectively, with their uncertainties plotted as grey shaded regions. The corresponding radius R is indicated for every cluster on each panel.

Table 5.4 Proper motions and parallaxes values.

Cluster	$\mu_\alpha \cos\delta^a$ [mas yr^{-1}]	μ_δ^a [mas yr^{-1}]	ϖ^a [mas]	$\mu_\alpha \cos\delta^b$ [mas yr^{-1}]	μ_δ^b [mas yr^{-1}]	ϖ^b [mas]
Trumpler 5	-0.59 ± 0.19	0.27 ± 0.18	0.28 ± 0.09	-0.53 ± 0.18	0.24 ± 0.09	0.30 ± 0.07
Trumpler 20	-7.08 ± 0.09	0.18 ± 0.08	0.25 ± 0.04	-7.09 ± 0.09	0.17 ± 0.04	0.24 ± 0.02
NGC 2477	-2.44 ± 0.16	0.87 ± 0.19	0.66 ± 0.03	-2.42 ± 0.17	0.88 ± 0.18	0.65 ± 0.03

Notes:
[a] Cantat-Gaudin et al. (2018)
[b] This work

5.2.5 Identification of the stragglers

We search the BSS in the same region describe in Chapter 2, § 2.3. We superimposed an isochrone for each cluster and a ZAMS of solar metallicity from Bressan et al. (2012) to the CMDs. The fitting parameters are indicated in each panel of Figure 5.1. A red limit in $(B-V)$ was defined in AL07 for Trumpler 5 only. Therefore, and as we did for Collinder 261 (R20 and § 4.2.1), to impose the same limit in the *Gaia* system we used the relation of Jordi et al. (2010):

$$C_1 = 0.0187 + 1.6814\,C_2 - 0.3357\,C_2^2 + 0.117\,C_2^3. \tag{5.2}$$

Adopting $C_2 \equiv (B-V) = 0.87$—the limit set in AL07—we found $C_1 \equiv G_{\rm BP} - G_{\rm RP} = 1.30$. We used the color of the TO to define the red limit for NGC 2477 and Trumpler 20, since AL07 did not give it for the first cluster, and did not include the second cluster in their catalog. Stars redder than this limit will be considered as possible yellow straggler stars (YSS).

As usual, the region was constrained with the equal-mass binary locus (not plotted) and with the upper limit of 2.5 magnitudes above the TO for the potential massive blue stragglers, for more information see § 2.3 and 2.3.1 respectively for more information.

5.2.6 Field contamination

In the color-magnitude diagrams of open clusters, the different evolutionary status of the stars and their corresponding sequences —i.e., main sequence, binary sequence,

turnoff point, sub-giant and giant branch and, in the case of the older clusters, the red clump— are usually well defined, and provide essential information on the physical properties of the stars which define them. These sequences are deformed by differential reddening (§ 5.2.1.1) and field contamination; these effects are particularly noticeable in clusters located towards the Galactic center. In this context, the decontamination of field stars is very important in the study of open clusters. Given the proximity to the Galactic plane of Trumpler 5 and Trumpler 20, and since we identified our BSS and YSS within a radius twice the apparent radius reported in DAML02, we expected field contamination from young stars that —as described in Carraro et al. (2008)— would occupy similar positions in the CMD as our straggler candidates. Our method for assessing membership using proper motions and parallaxes from *Gaia* DR2 decreases, but does not remove all the contamination by such field young stars. To do so, and following Vaidya et al. (2020), we limited each cluster's radius to distance from the center where there are more cluster stars than field stars. We estimated the cluster size as the radius *R* where the cluster density profile separates appreciably from that of the background (see Figure 5.3); the radii obtained this way are in Table 5.3. The rate of false positives was estimated by counting stars located inside an annular region—selected outside the tidal radius—with the same area as that of the cluster. All the selected sources are within $\mu_\alpha \cos\delta \pm \sigma$, $\mu_\delta \pm \sigma$, and $\varpi \pm \sigma$. We found 13 and 2 interlopers for Trumpler 5 and Trumpler 20, respectively. No contamination by field stars was observed in the case of NGC 2477. We refer the reader to § 2.4.2 for more information regarding field contamination in OC's when using *Gaia*.

5.2.7 Final detections

The straggler population of each cluster was selected as follows; First, the stragglers were identified over the entire extension of each cluster, as given by CG18. Then, each BS population was limited to the radius R estimated in § 5.2.6. Finally, for the three clusters we left out all stars with a membership probability ($P_{\rm memb}$) below 50%. This operative and conservative cut-off has been defined in the literature as the probability of containing the most likely members (Banks et al., 2020, Cantat-Gaudin et al., 2018, Carrera et al., 2019, Yontan et al., 2019). Using the above-mentioned restrictions we

Table 5.5 Blue and yellow straggler populations after each selection process.

Cluster	$N^a_{\rm BS}$	$N^b_{\rm BS}$	$N^c_{\rm BS}$	$N^a_{\rm YS}$	$N^b_{\rm YS}$	$N^c_{\rm YS}$
Trumpler 5	177	51	40	7	3	3
Trumpler 20	65	15	8	0	0	0
NGC 2477	5	5	5	4	4	4

Notes:
[a] Blue/Yellow stragglers over the entire extension of Cantat-Gaudin et al. (2018)
[b] Blue/Yellow stragglers within the cluster radius R calculated in § 5.2.6
[c] Blue/Yellow stragglers within the cluster radius R and with $P_{\rm memb} \geq 50\%$

thus defined *bona fide*, non-spurious BSS populations. Our results for each cluster are presented in Table 5.5.

Trumpler 5 is the cluster that hosts the largest population of BSS of our sample (see upper panels of Figure 5.1); two stars are located above the upper limit of 2.5 magnitudes defined for massive stragglers (§ 5.2.5). In the case of Trumpler 20, all stars visible in the CMD are within 1 mas yr^{-1}, and only one massive straggler candidate was identified. Finally, NGC 2477 does not harbor many BSS, and no massive stragglers are visible in its CMD.

Additionally, we compared our BSS candidates with those of AL07 in Trumpler 5 and NGC 2477 only, since Trumpler 20 was not included in AL07. To do so, we searched the *Gaia* counterparts of the AL07 candidates. For Trumpler 5, there are only seven BSS in common, and the rest are non-members. This is not surprising, given the position of this cluster at a low galactic latitude, and therefore expected to suffer from significant field contamination, which was not accounted for in AL07. In the case of NGC 2477, all BSS identified in AL07 are indeed members, but they are all concentrated around the cluster TO, as reported in § 2.4.1; among them, only three are in our list of BSS candidates.

5.3 Spectroscopic Analysis

This is also the first high-resolution spectroscopic analysis of the BSS population in the open clusters Trumpler 5, Trumpler 20, and NGC 2477. Unfortunately, as describe

Table 5.6 Individual radial velocity measurements for blue stragglers in Trumpler 5. Binary classification according to their radial velocity variability and rotational velocities is reported in the last two rows.

	Tr5-BS1	Tr5-BS2	Tr5-BS3	Tr5-BS4
RV_1	$+22.72 \pm 11.12$	$+46.03 \pm 3.65$	$+31.25 \pm 10.41$	$+31.71 \pm 13.75$
RV_2	$+24.87 \pm 6.68$	$+165.46 \pm 6.18$	$+67.26 \pm 13.90$	$+26.34 \pm 14.31$
RV_3	$+21.41 \pm 11.10$	-13.43 ± 3.16	$+25.84 \pm 12.41$	$+33.09 \pm 15.33$
RV_4	$+12.03 \pm 11.96$	-22.52 ± 3.69	$+57.84 \pm 18.19$	$+33.23 \pm 13.56$
RV_5	$+17.80 \pm 7.70$	-17.48 ± 3.10	-7.62 ± 16.13	$+24.28 \pm 15.29$
Class [a]	NM?	M, CB	M, CB	NM?
$v \sin i$ (km s^{-1})	150	30	270	170

	Tr5-BS5	Tr5-BS6	Tr5-BS7
RV_1	$+03.87 \pm 7.93$	$+26.92 \pm 12.25$	$+43.33 \pm 12.77$
RV_2	-09.56 ± 14.74	$+15.73 \pm 11.25$	$+49.34 \pm 8.01$
RV_3	-16.44 ± 6.35	$+13.40 \pm 12.77$	$+09.99 \pm 6.29$
RV_4	-13.80 ± 12.75	$+00.58 \pm 14.49$	$+23.49 \pm 5.44$
RV_5	-14.77 ± 12.95	$+10.75 \pm 14.70$	$+04.03 \pm 4.14$
Class [a]	NM, LP?	M, CB?	M, CB
$v \sin i$ (km s^{-1})	100	100	160

Notes:
NM: non-member
M: member
CB: close-binary system
LP: long-period binary.

Table 5.7 Same as in Table 5.6, for NGC 2477.

	NGC2477-BS1	NGC2477-BS2	NGC2477-BS3
RV_1	$+07.78 \pm 1.63$	$+11.83 \pm 2.64$	$+06.51 \pm 1.98$
RV_2	$+07.79 \pm 1.85$	$+11.80 \pm 2.80$	$+06.27 \pm 2.21$
RV_3	$+08.67 \pm 1.61$	$+13.01 \pm 2.30$	$+07.49 \pm 1.85$
RV_4	$+08.26 \pm 1.70$	$+11.68 \pm 2.00$	$+06.18 \pm 2.10$
RV_5	$+08.30 \pm 1.57$	$+11.32 \pm 2.14$	$+06.76 \pm 1.87$
RV_6	$+08.53 \pm 1.55$	$+10.92 \pm 1.98$	$+05.84 \pm 1.89$
RV_7	$+08.50 \pm 1.79$	$+11.63 \pm 1.87$	$+06.12 \pm 1.97$
RV_8	$+08.06 \pm 1.65$	$+10.16 \pm 2.27$	$+06.96 \pm 1.88$
Class[a]	M	M	M
$v \sin i$ (km s^{-1})	30	45	40

Notes:
M: member

Table 5.8 Same as in Table 5.6, for Trumpler 20.

	Tr20-BS1	Tr20-BS2	Tr20-BS3
RV_1	$+14.81 \pm 2.91$	-23.63 ± 1.16	-07.22 ± 4.73
RV_2	-56.68 ± 3.98	-26.36 ± 2.04	-07.97 ± 4.06
RV_3	$+22.40 \pm 2.57$	-00.27 ± 2.78	$+07.67 \pm 2.88$
RV_4	-57.29 ± 3.90	$+41.52 \pm 2.21$	-08.65 ± 1.95
Class[a]	M, CB	M, CB	NM, LP?
$v \sin i$ (km s^{-1})	40	50	90

Notes:
NM: non-member
M: member
CB: close-binary system
LP: long-period binary

previously in § 4.3 not all the candidates were observed with FLAMES, because when the observational time was allocated, we used a list of stars very different from that found in this work.

The spectroscopic analysis was carried out on seven out of the 40 blue stragglers in our list for Trumpler 5—plus one star with $P_{\rm memb} \leq 50\%$, on one out of our eight blue stragglers for Trumpler 20—and two stars not identified as BS in this study, given their low $P_{\rm memb}$, and in three out of the five blue stragglers in NGC 2477.

5.3.1 Radial and rotational velocities

The radial velocities were determined and the synthetic spectra calculated following § 4.3.1. Among the most interesting observational features of BSS is the projected rotational velocity ($v \sin i$). From the theoretical point of view, BSS driven from the proposed formation mechanisms (i.e mass transfer and collisions) are expected to rotate fast. In practice, however, from observations in stellar cluster BSS have been identified as low and fast-rotators (e.g Lovisi et al. 2010, 2013). In this sense braking mechanism has been suggested to occur and slow down the stars Sills et al. (2005). Given this complex scenario, we have introduce small changes with the aim of improve the precision in our measurements of $v \sin i$. The model atmospheres were calculated with parameters for F-type MS, or slightly evolved stars ($T_{\rm eff} = 7500$ K and $\log g = 4.0$ cm s^{-2}), adopting solar metallicity. The micro-turbulence was set as $\xi = 0.0$ km s^{-1}

for all templates. Then, the spectra were convolved with a Gaussian to model the instrumental resolution of the spectrograph, and rotational broadening was applied. Spectra were modeled assuming a $v \sin i$ value varying from 10 to 300 km s^{-1}, with a step of 10 km s^{-1}. For each target, synthetic spectra were then re-normalized to maintain the continuum level at 1 and to match the core-depth of the observed spectral lines. In this way, it was particularly easy to estimate the rotational velocity of the stars just comparing by eye the width of the observed and synthetic spectral lines. The error of this procedure depends critically on the S/N of the spectra. However, it was never above ± 10 km s^{-1}.

The radial velocities measurements for the blue population are reported in Table 5.6, 5.7 , and 5.8for Trumpler 5, NGC 2477 and Trumpler 20, respectively.

5.3.2 Errors

We followed the same procedure of R20; § 4.3.2 i.e., we built a distribution histogram based on the individual radial velocity errors given by `fxcor` and the differences between epochs, to which we fitted a simple Gaussian function. We considered the standard deviation σ of the Gaussian as the true radial velocity error. We plotted the histogram together with the Gaussian fit and the true error in Figure 5.4. We also calculated the mean `fxcor` error for each rotational rate. Stars rotating with velocities ranging between approximately 30 and 50 km s^{-1} have errors about 2–4 km s^{-1}, and stars rotating with velocities of 80–150 km s^{-1} have uncertainties of around 10 km s^{-1}; finally, the typical uncertainties for the fast rotator stars ($v \sin i > 150$ km s^{-1}) are about 15 km s^{-1}.

5.3.3 Spectroscopic detections

Several explanations have been proposed for the blue straggler phenomenon, although none is completely satisfactory. The binarity hypothesis is the most accepted one, mainly because it can in principle account for most of the observations. Mathieu

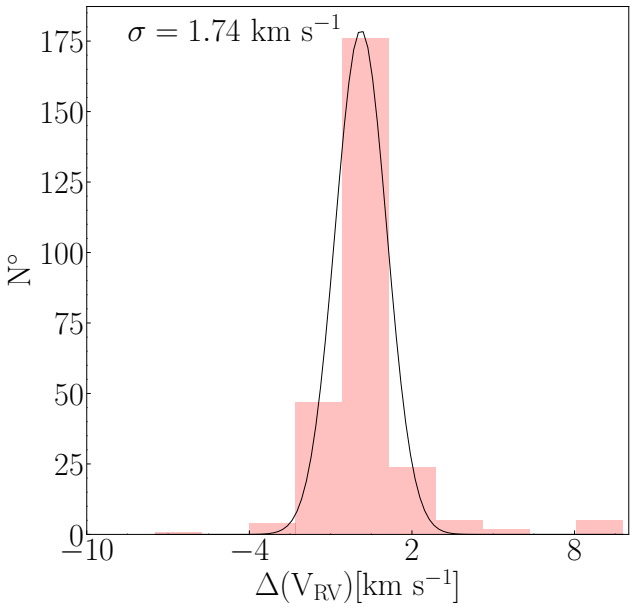

(a) Histogram

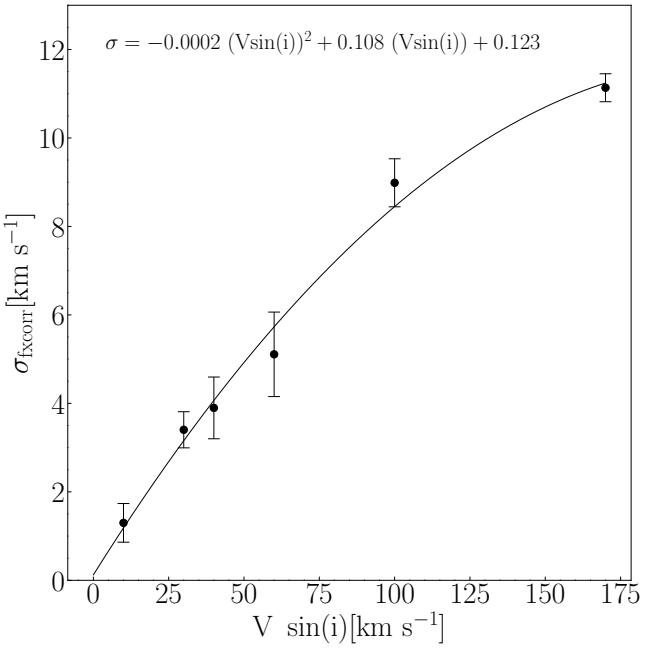

(b) fxcor mean errors

Figure 5.4 Panel (a) is the histogram of the differences—divided by the root square of 2—between pairs of radial velocities measurements for the same star. The best-fitting Gaussian to the distribution is plotted, and its standard deviation σ is indicated. Panel (b) instead correspond `fxcor` mean errors as a function of the upper rotational rates estimated for Trumpler 5, Trumpler 20 and NGC 2477.

and Geller (2009) have shown that the percentage of binaries among BSS is significantly larger than in the cluster main sequence (MS). Previous studies in OCs had revealed that the BSS population in open clusters mostly contains long-period binaries (Geller et al., 2009); these have periods ranging from a few years to decades or even centuries, and it is very difficult to detect them spectroscopically and photometrically. On the other hand, in R20 (§ 2) we found a significant amount of BSS in Collinder 261 being possible close binaries.

Following the description of § 4.3.3, and based on the radial velocity variations, we attempted to roughly assess the binary nature of the sample studied here, namely, to decide if they may be close, long-period binaries, or single stars without radial velocity variations. For each cluster, we have between four and eight radial velocities, obtained at epochs separated by days, months, and years (Table 5.2). All the probable binaries would need additional spectroscopic follow-up to be properly characterized, given the small number of observations.

5.3.3.1 Trumpler 5

This object contains a larger number of stars than many old open clusters in the Galaxy. Despite its distance relatively close to the sun (~ 3 kpc), given its location in a highly and differentially reddened region, not many photometric and spectroscopic studies have been carried out on their members, and none on its blue straggler population.

Out of our 40 BSS candidates, only seven were observed with FLAMES, for which five epochs of spectra were available. We classified stars Tr5-BS2 (80%), Tr5-BS3 (90%), Tr5-BS6 (100%), and Tr5-BS7 (100%) as members and possible close binaries (M, CB). On the other hand, we found three possible interlopers: Tr5-BS1 (80%), Tr5-BS4 (100%), and Tr5-BS5 (100%) which, according to our criteria and measured radial velocities, are not members. The high probability of membership ($P_{\rm memb}$) that this three receive from CG18 shows that a good astrometric solution —like that of *Gaia* DR2— is still not enough for a correct identification of a bona fide blue straggler, but that spectroscopic data are also needed. We found that almost all stars in Trumpler 5 observed with FLAMES are fast rotators (including the interlopers), except Tr5-BS2. The theoretical expectations for

rotation velocities of BSS are not well defined, but all current scenarios can plausibly spin up them. These stars are similar to those found by Mucciarelli et al. (2014), with the fastest rotating up to ~ 200 km s^{-1}.

5.3.3.2 Trumpler 20

Given its position in the inner disk (where not many old OCs reside), age, proximity, and mass, Trumpler 20 is particularly interesting. The blue straggler population of this cluster has been identified in a handful of photometric studies (AL95, AL07, Carraro et al. 2010), but not with spectroscopy. Unfortunately, only one star out of the eight BSS with $P_{\rm memb} \geq 50\%$ was observed with FLAMES. Star Tr20-BS1 (100%) is a possible close binary according to our criteria. Two stars with probabilities below 50% were also observed, namely Tr20-BS2 (10%) and Tr20-BS3 (30%), which were identified as one possible close binary (member) and a non-member (possible long-period binary), respectively. The particular case of Tr20-BS2 might caught the attention of the reader because of the low probability (is still a member though if the complete list of members given by CG18 is used and not the cut of $P_{\rm memb} \geq 50\%$) membership it has. However, missing genuine BSS is normal when having conservative criteria like ours. For this cluster, we measured radial velocities in four epochs for the three stars.

5.3.3.3 NGC 2477

This cluster is moderately old and slightly metal-poor. It is also known to be one of the clusters with the largest amount of member stars in the southern sky (Gao, 2018). For the five BSS we identified in the CMD (bottom panels of Figure 5.1), we obtained eight epochs of radial velocities for three stars: NGC2477-BS1 (100%), NGC2477-BS2 (90%), and NGC2477-BS3 (80%). Despite the high binary frequency ($\sim 36\%$) found by Eigenbrod et al. (2004), our radial velocity measurements indicate that these three stars are single non-variable members —although they could also be long-period binaries or binaries seen face-on. If we look into their projected rotational rates, BSS do not seem to rotate unusually fast, similarly to what Smith and Hesser (1983) found. In the work previously mentioned, NGC2477-BS2 (90%) or HART 7302 is classified as a G3IV-V dwarf and is

considered to be a probable interloper according to its position in the CMD, allegedly close to the cluster TO. However, in our CMD this object appears clearly separated from the TO and, given its proper motion, parallax, and radial velocities values, this star may be considered a member. Smith and Hesser (1983) give a rotational velocity of 50 km s^{-1} for this star, very close to the 45 km s^{-1} we found.

5.4 Cumulative Radial Distribution and Population Ratios

An analysis of the stellar radial distribution can only be carried out in Trumpler 5, given its significant number of blue stragglers. Unlike what we did in § 2.7, here we used the core radius calculated in § 5.2.4 instead of $\mathrm{r_{50}}$. We remind the reader that $\mathrm{r_c} < \mathrm{r_{50}}$.

The cumulative spatial distributions on the y-axis as a function of r/r_c is shown in the top panel of Figure 5.5. As mentioned elsewhere, the blue solid line indicates the normalized cumulative distribution of the BSS candidates in comparison with the sample of RGB stars (red dashed line).

BSS do not appear more centrally concentrated than the reference population on this cluster. Further, we found $\mathrm{A^{+}_{rc}} = -0.450$ when using stars within the core radius $\mathrm{r_c} = 4.57'$, this is slightly smaller than $\mathrm{A^{+}_{r50}} = -0.441$ we found in § 2.7 for stars within r_{50}, but still consistent. Our finding disagrees with what is observed in other clusters, whose BSS show high concentration in the cluster internal region relative to the evolved stars (Bhattacharya et al. 2019, Geller et al. 2008, Vaidya et al. 2020, R20).

For Trumpler 5, the A-D test indicates a difference of 99.9% between the distributions of BSS and RGB stars, i.e., both populations do not originate from the same distribution.

As in the case of Collinder 261, we divided the field of view in concentric annuli, such that each one has at least one BSS — in the case of Trumpler 5 we have a sufficiently high $\mathrm{N_{BSS}}$ to carry out this type of studied within r_c. The bottom panel of Figure 5.5 shows the number of BSS candidates with respect to that of RGB stars in each annulus, as a function of r/r_c . The ratio was corrected assuming that the field contamination

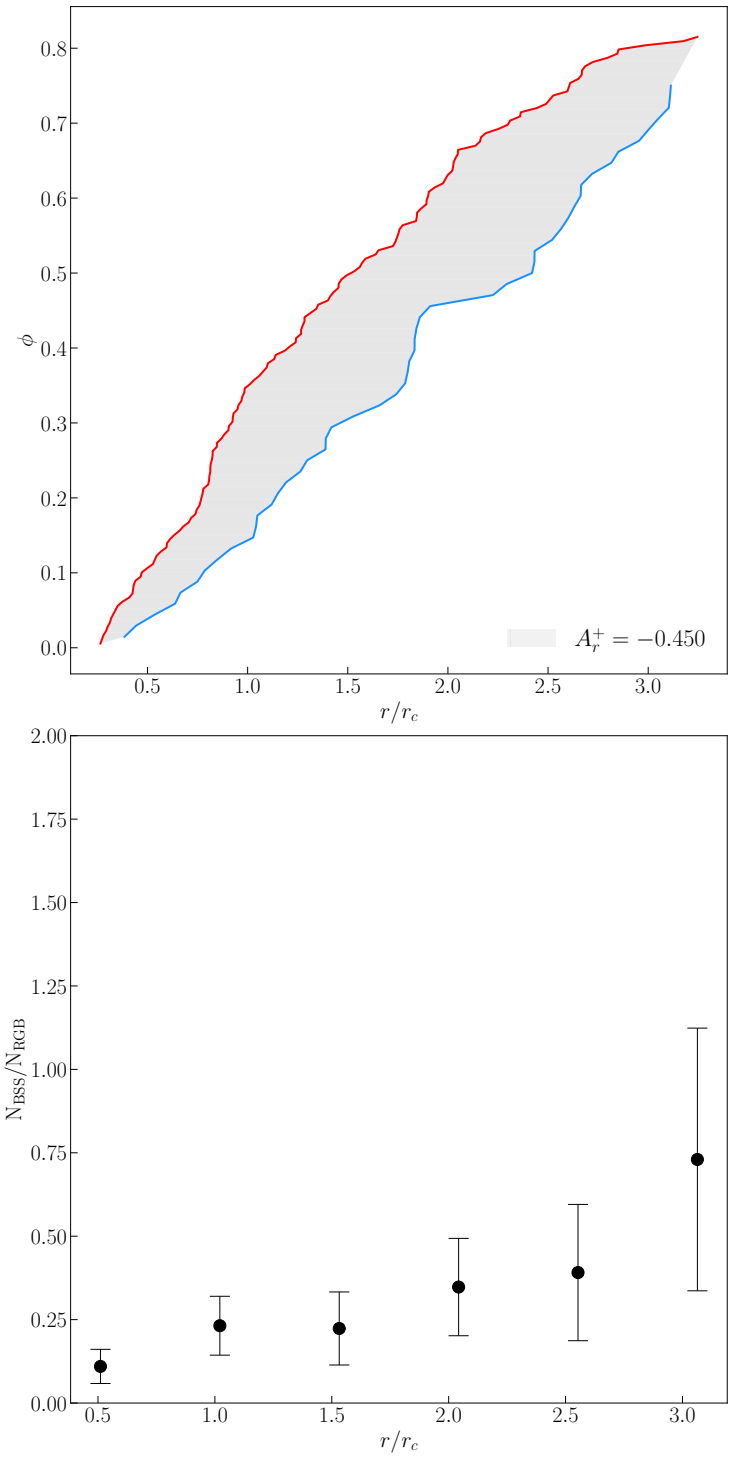

Figure 5.5 **Upper:** Cumulative spatial distribution of BSS (blue line) and RGB stars (red dashed line) in Trumpler 5. **Bottom:** Relative number of BSS to RGB stars, plotted as a function of the distance from the cluster center. Errors are Poisson distributed.

we found in § 5.2.6 is homogeneous. In the case of Trumpler 5 —and considering the errors— the distribution becomes flat, indicating that BS and RGB stars are more or less equally distributed both in the central part of the cluster and in its outskirts.

Comparing this distribution with those described by F12 for globular clusters, it appears to be somewhat similar to that of Family I clusters. In this family, the radial distribution of the stragglers is fully consistent with that of the reference population, and dynamical friction has not yet played a major role, even in the core.

For the sake of completeness, and following V20, we estimated the central relaxation time

$$t_{\rm relax,c} \sim \frac{t_{\rm cross}\, N_*}{6 \log N_*} \tag{5.3}$$

for the three clusters, where

$$t_{\rm cross} \sim D/\sigma_v \tag{5.4}$$

is the crossing time, N_* is the total number of stars (within the radius of each cluster and with $P_{\rm memb} \geq 50\%$), and σ_v is the velocity dispersion (Binney and Tremaine, 2008). In the calculations we employed the standard deviations of the projected proper motions of each cluster, as well as the core radius we derived from of King profiles (§ 5.2.4). Second, using the values of $t_{\rm relax,c}$ and the evolutionary age of each cluster, we estimated the parameter $N_{\rm relax}$ —define is § 2.7. These three parameters and the number of stars are reported in Table 5.3. Finally, using the value of $N_{\rm relax}$ we estimated $r_{\rm min}/r_c$ using equation (1) from V20, but only for Trumpler 5. The dynamical state of this cluster will be discussed in more detail in the Conclusions (§ 5.6).

5.5 Trumpler 5, NGC 2477, and Trumpler 20 in TESS

As in the case of Collinder 261, we searched the stragglers of Trumpler 5, NGC 2477, and Trumpler 20 in the TESS-PATHOS database. We followed the same procedure as § 4.5 for the normalization and "cleaning" of the LCs. What we found is that the picture of each cluster is quite different; while the LCs (in sectors 7 and 8) of all the straggler candidates of NGC 2477 were extracted, none of them turned out to be a close binary or

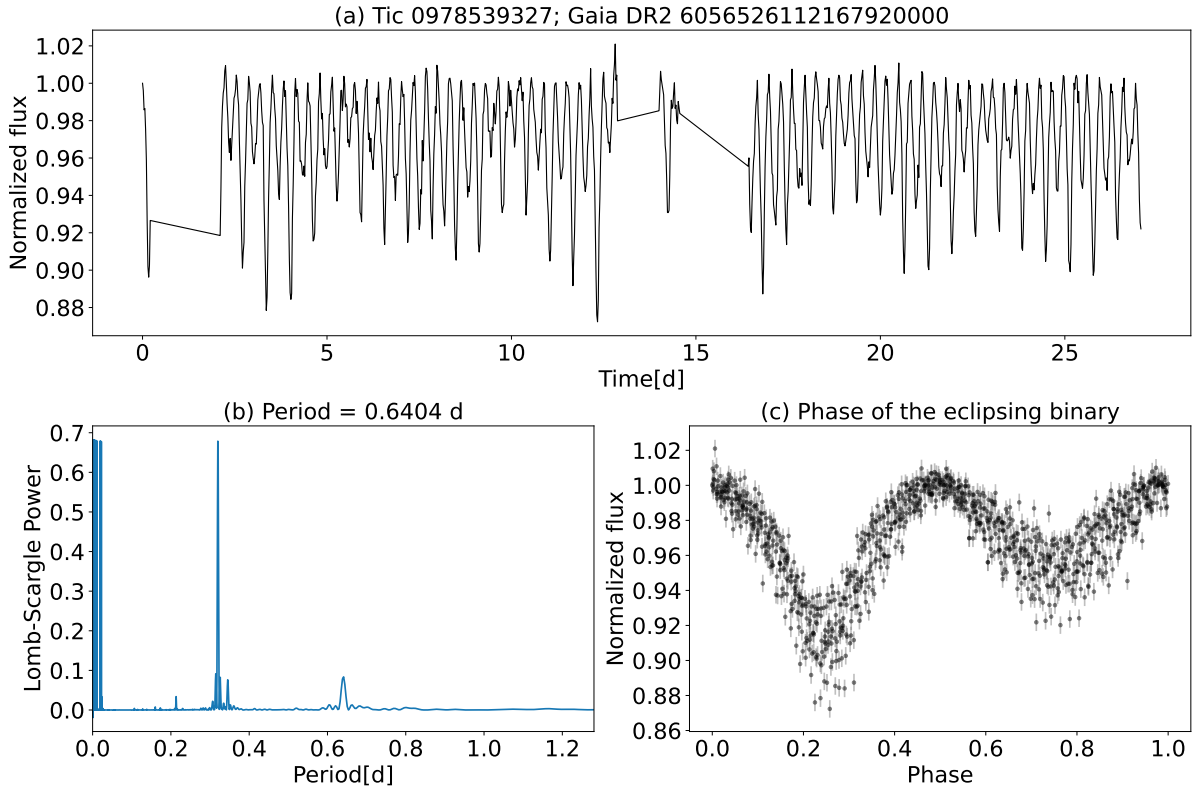

Figure 5.6 Panel (a) shows the normalized light curve of *Gaia* DR2 6056526112167920000 from sector 11. Panel (b) shows the Lomb-Scargle periodogram. Panel (c) is the phase transit of the eclipsing binary.

short period system. In Trumpler 20 instead, only three out of the eight stragglers were analyzed by the PATHOS team, and among these three stars only one is a close-binary —LC and period of star DR2 6056526112167920000 shown in Figure 5.6. If the case of the previous clusters was already demotivating on our search of close binaries, Trumpler 5 is just discouraging, because we only found 21 out of the 40 candidates, and from them only two showing clear eclipses— see Figure 5.7.

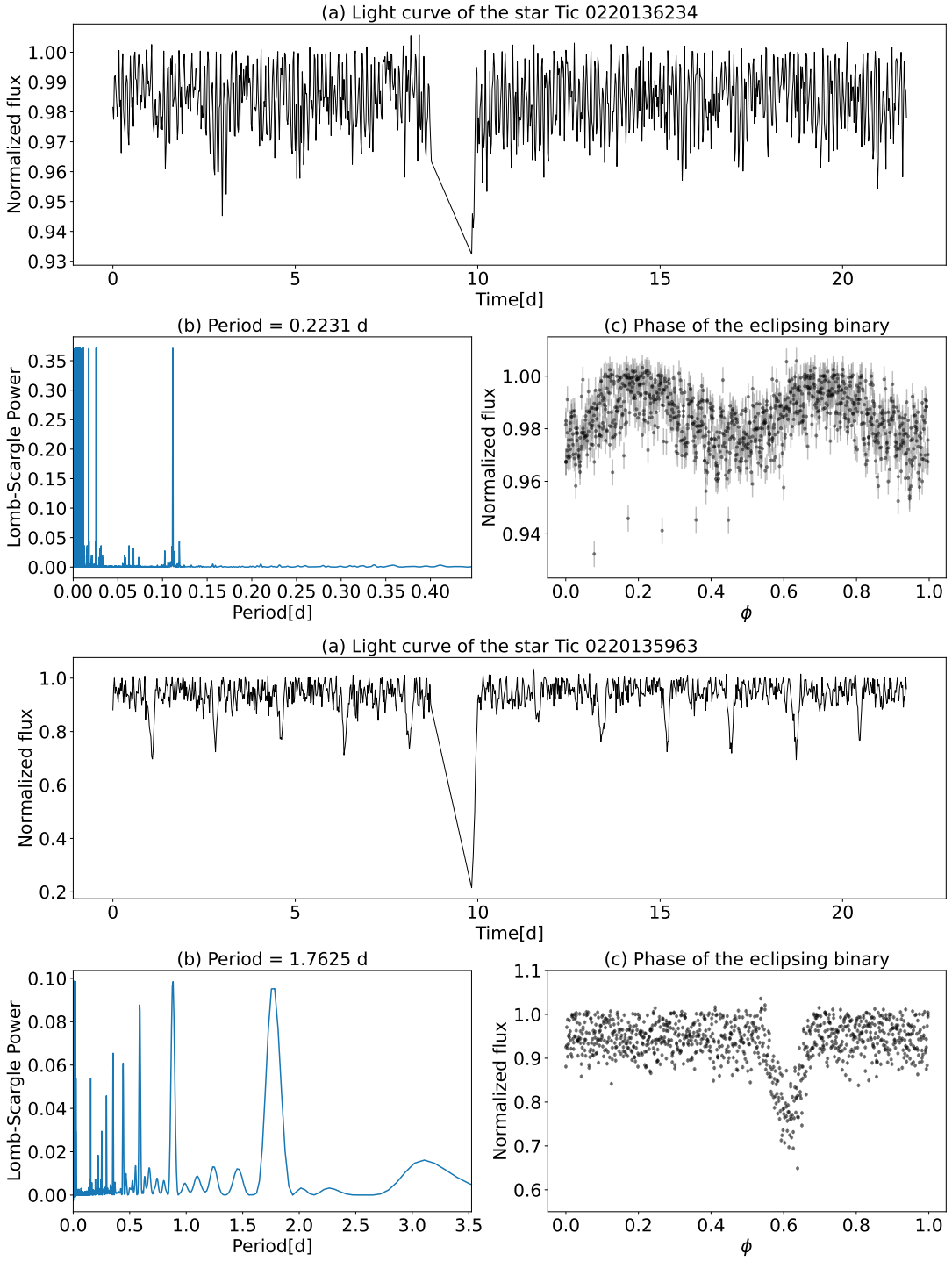

Figure 5.7 Panels (a) show the normalized Light-curves of stars *Gaia* DR2 3326784605519670000 and *Gaia* DR2 3326834598938940000. Panels (b) are the Lomb-Scargle periodogram and Panels (c) the transit phases of the eclipsing binaries.

5.6 Summary and Conclusions

In this chapter we have studied the blue and yellow straggler population of three open clusters, NGC 2477, Trumpler 5, and Trumpler 20, using the selection of cluster members published by CG18 and updated by CG20. Some methodological differences with respect to Chapter 4 were introduced, i.e., the selection —and the consequent change in numbers— of the straggler populations with the cluster radius R and the probability membership of each target $P_{\rm memb}$. In the case of Trumpler 5 and Trumpler 20 the numbers decrease considerably, while for NGC 2477 the straggler population barely changes. Using the most common and simple way to determine contamination coming from the field we found 13 and 2 interlopers in the blue straggler region of Trumpler 5 and Trumpler 20 respectively if the entire extension of the cluster is considered i.e., twice the apparent radius. The latter is, however, not unsurprising given their positions low onto the Galactic plane. No contamination was found in the yellow straggler region in all three clusters. A more accurate treatment of the field contamination must be done similarly to the one used in § 3.4, but also an agreement in the community needs to be settled on how select the candidates and open cluster members avoiding crowding and contamination problems as much as possible. A good example is using angular distances (or apertures) from the cluster center as performed in Leiner and Geller (2021), where the authors have a clear control of the contamination introduced in the sample. This method is however highly dependent on the cluster center.
When comparing with previous catalogs we found large inconsistencies in AL07 blue straggler candidates, especially in Trumpler 5, where only ∼6 % of the BSS listed in AL07 are members. In the case of NGC 2477, all AL07 BSS are members but they are all concentrated around the TO. Evidently, the quality of *Gaia* data contributes to improve the construction of better lists of blue straggler candidates.

Following Bhattacharya et al. (2019), R20, and V20, we used our candidates as test-particles to probe the dynamical state of Trumpler 5. Our goal was to explore the bimodal distribution of BSS in open clusters, which is poorly understood, unlike its GC counterpart. First, we compared BSS candidates with a reference population (RGB stars); exploring the normalized cumulative radial distributions, we found that BSS are not more centrally concentrated than RGB stars (top panel of Figure 5.5) in Trumpler 5.

Second, we plotted the ratio of BSS to RGB stars $N_{\rm BSS}/N_{\rm RGB}$ (see bottom panel of Figure 5.5); to do so, we split the field of view in concentric annuli, each one containing at least one BS. Based on his flat radial distribution, Trumpler 5 can be classified as a Family I-type cluster. Additionally, we calculated the predicted $r_{\rm min}$ using the correlation (Eq. 1) of V20 and the corresponding values of $N_{\rm relax}$ (Table 5.3), and obtained a value of $2.29\,r_c$. The distribution of Trumpler 5 is flat up to $3.28\,r_c$, with no clear signs of a minimum (if errors are considered) in the BSS radial distribution at the predicted $r_{\rm min}$. The case of Trumpler 5 is similar to both Berkeley 39 and NGC 6819 (see V20), whose estimated values of $N_{\rm relax}$ suggest that they are dynamically evolved, but that their radial distributions are flat.

This chapter presented the first high-resolution spectroscopic study of the BSS population of all three clusters and, as in Chapter 3, we complemented our photometric detections with spectroscopic data from FLAMES/GIRAFFE and using the very same rough classification based on radial velocity variability to assess their binary nature. In the case of Trumpler 5 only seven out of the 40 possible BSS were observed —reported in Table 5.6— among which we identified four as probable contact binaries, and three as non-members. All the stars are fast rotators, with the exception of star Tr5-BS2. We conclude that Trumpler 5 hosts 37 blue straggler candidates within $r \sim 3.28 r_c$. Our spectroscopic results for Trumpler 20 are reported in Table 5.8. Radial velocities for five epochs are available for three stars. Only one of these stars was safely classified as a BS candidate (within the radius R and with $P_{\rm memb} \geq 50\%$); this star is a possible close binary system. The remaining two stars with probabilities below 50% are Tr20-BS2 (10%) and Tr20-BS3 (30%), identified as one possible close binary (member) and a non-member, respectively. As mentioned elsewhere given our conservative criteria, it is is unavoidable that we would miss some genuine stragglers, and star Tr20-BS2 is an example. So we conclude Trumpler 20 hosts nine BSS. In the case of NGC 2477, our results are shown in Table 5.7. Radial velocities for eight epochs are available for three stars, and only one of them has probabilities high enough to be a BS candidate.

Although this work shows an improvement over the photometric selection of AL07, the contamination in both clusters is quite high and consistent with the results from our spectroscopic follow-up, where 3/7 stars observed were classified as non-members

in Trumpler 5. This shows, once again, that such a spectroscopic follow-up is rather essential to a proper understanding of these exotic populations in OCs.

Chapter 6

Summary and future plans

6.1 Conclusions and summary

In this thesis we have taken advantage of the unprecedented accuracy of *Gaia* data, plus high-quality photometric and spectroscopic observations, to get a more complete picture and a better understanding of the properties of blue straggler stars (BSS). This thesis presents the most comprehensive and homogeneous compilation of BSS in Galactic open clusters (OCs) so far, and it is also the first compilation of yellow straggler stars (YSS). The methodology we developed for this thesis, mostly described in Chapter 2, involves the use of broad-band photometry and BSS selection via astrometric criteria.

In Chapter 2 we presented our main results. We compiled two lists with nearly 900 blue straggler candidates and almost 80 yellow straggler stars, selected from a sample of ∼400 OCs. We have presented solid statistics and compared our findings with the two previous catalogs, confirming that most of the straggler there listed are not members. Following the same line, in § 2.6.2 we compared the relations between cluster age and their corresponding number of stragglers with that of the previous compilations. We conclude that no significant number of BSS are present in clusters with $\log(\mathrm{age}) < 7.3$ and no YSS in cluster with $\log(\mathrm{age}) < 8.2$. Also, in Chapter 2 we revisited the relation between the integrated magnitude and the stragglers reported to be presented in all

stellar systems: globular clusters, open clusters, dwarf spheroidal Galaxies. We showed that BSS in OCs do not follow the distribution reported before, compatible with dwarf spheroidal Galaxies, instead is more similar to the one of globular clusters. In § 2.7 we explored the radial segregation and the dynamical state in a few clusters, we reported BSS are more centrally concentrated in clusters with 1 Gyr, we have also provided the A_r^+ expanding the sample from 10 to ∼40 OCs on which this parameter has been reported. We also combined our detections with TESS photometry and we found a handful of clusters with a large fraction of short-period binaries which is in disagreement with that of the literature, these results are reported on § 2.8. Additionally, this discovery became the driver of some of the future plans described in § 6.2. In the particular case of BSS, these last finding will put more stringent observational constraints on the formation and evolution of these systems.

In chapter 3 we explored the impact of using *Gaia* EDR3 instead of *Gaia* DR2 for the construction of the catalog. We found that a systematic search of the stragglers using *Gaia* EDR3 leads to a decrease in the population of ∼3 blue stragglers per cluster. But also, taking advantage of the improvement in precision and accuracy of *Gaia* EDR3, we investigated the less explored dependencies of the $N_{\rm BSS}$ with the binary fraction, mass and number of binaries in each cluster. We found dependencies with all three parameters, with the highest one of the order of $\rm N_{BSS} \propto N_{bin}^{0.6}$.

In Chapter 4 we focused on the specific sample of BSS in the open cluster Collinder 261. First, we used the stragglers as test particles to probe the dynamical state of the cluster. We showed that the BSS are more centrally concentrated than MS, RGB and RC stars. We derived the central relaxation time and we found it to be considerable small in comparison with the evolutionary age of the cluster. In our search of the parameter r_{min} we could not classify this cluster with any of the families defined for GCs. The combination of our photometric detections together with high-resolution spectra allowed us to identify a handful of binaries. We assessed their membership and binary nature by using the radial velocity variability technique. We reported five close binaries, one long-period binaries and four non-variable stars —the last can be the outcomes of a merger or very-long-period binaries outside our detection limit. In this chapter, we also cross-matched our photometric detections with TESS photometry and found that Collinder 261 has the largest (so far known) percentage of short-period binaries among

the stragglers. We reported the period of nearly 20 binaries in the range between 0.5 to 2 days. We also showed that they do not occupy any special place in the CMDs, and that they are distributed randomly.

Finally in Chapter 5 we mimic the procedure of Chapter 4 in three different OCs but introducing some methodological changes. As a summary, we classified Trumpler 5 as family I as well — with a flat stragglers' distribution. We showed, however, the $\mathrm{N_{relax}}$ points toward a completely different scenario in which Trumpler 5 should be a dynamically evolved cluster. The radial velocities we derived allowed us to recognized six close-binaries and one long-period binary; we confirmed the membership of nine candidates but we also ruled out the membership of three straggler candidates in Trumpler 5 and two on Trumpler 20.

To summarize, the work presented in this thesis allowed us to look at the straggler population in open clusters from different perspectives. This thesis however, did not focus on the binary characterization of the stragglers and their companions because of the scarce amount of data available, so no firm conclusions in term of formation mechanism could be drawn from this thesis. While not solving the problem of BSS formation, this thesis, however, has shed lights on the environments in which blue straggler stars feel more comfortable. Finally, we have provided interesting individual cases than can be further studied.

6.2 Future plans

As discussed in Chapter 2, this new compilation is just the first step and will hopefully boost new studies of blue and yellow straggler stars. Two are the approaches that we aimed to take as future avenues. First, we will continue the search of interesting individual cases such as those we found in Chapter 2, § 2.8 and using TESS. By the moment this thesis will be published, it is highly probable that the third *Gaia* data release (*Gaia* DR3) will be out. This new release will be a real festival of variability results, with ≈25 different types of variability detected. *Gaia* DR3 will be the first in which binary models will be considered in the processing of the positions, velocities, and fluxes.

This will likely change the values available —based on the single star assumption— but will provide some additional parameters directly related to the binary nature of the source. *Gaia* DR3 will contain around 1.5×10^5 binaries with orbits, but also mean RVs for about 33 million stars with $G_{RVS} < 14$ mag and RVs spectra for approximately 1 million of stars with $G_{RVS} < 12$ with effective temperature T_{eff} even beyond 7000 K. In the new catalog, half of the stragglers (blue and yellow include) candidates fulfilled these conditions, which means that for 50% of them, we should be able to explore their binary nature just using *Gaia* DR3. As mentioned elsewhere, the majority of the BSS are either close binaries with orbital periods of a few days or less, or long period binaries with orbital periods around 1,000 days and a white dwarf companion. The relative proportion of these two types of binaries seems to depend on the cluster, so we will try to understand what parameters of the OCs is responsible for this. With its identification of many binaries, release of orbits and of light curves of many eclipsing binaries, *Gaia* DR3 should bring a completely new light on this and allows us to answer this fundamental question. The release will also provide much additional information on other binaries in the clusters —whether on the main sequence or among the cluster's white dwarfs— that will also be interesting to study.

Second, we aimed to perform a systematic intermediate-to high-resolution spectroscopic survey among the straggler candidates. By combining southern spectrograph like UVES, FLAMES/GIRAFFE, and FORS together with northern ones like HERMES we should be able to cover the majority of the BSS candidates we reported. This ongoing project —already started with my favorite open cluster Collinder 261[1]— aims to recover the orbital periods of the shortest systems and be able to discover the binaries with periods up to several years. It will allow us to characterize the BSS binary population of > 30 open clusters, and put constraints on its binary fraction but also on the occurrence of binary-BSS (either long or short periods) and those stars without variability —which can be the outcome of merger or collision. Figure 6.1 gathers both, the percentage of binaries among the exotic stars and the age of five OCs. Without considering NGC 6791 —since only its bright BSS were observed and it is probable that the binary fraction value will change by including the faintest ones— there seems to be a mild correlation with age, with young clusters having the lowest binary fractions values and

[1]ESO spectrograph FLAMES/GIRAFFE+UVES

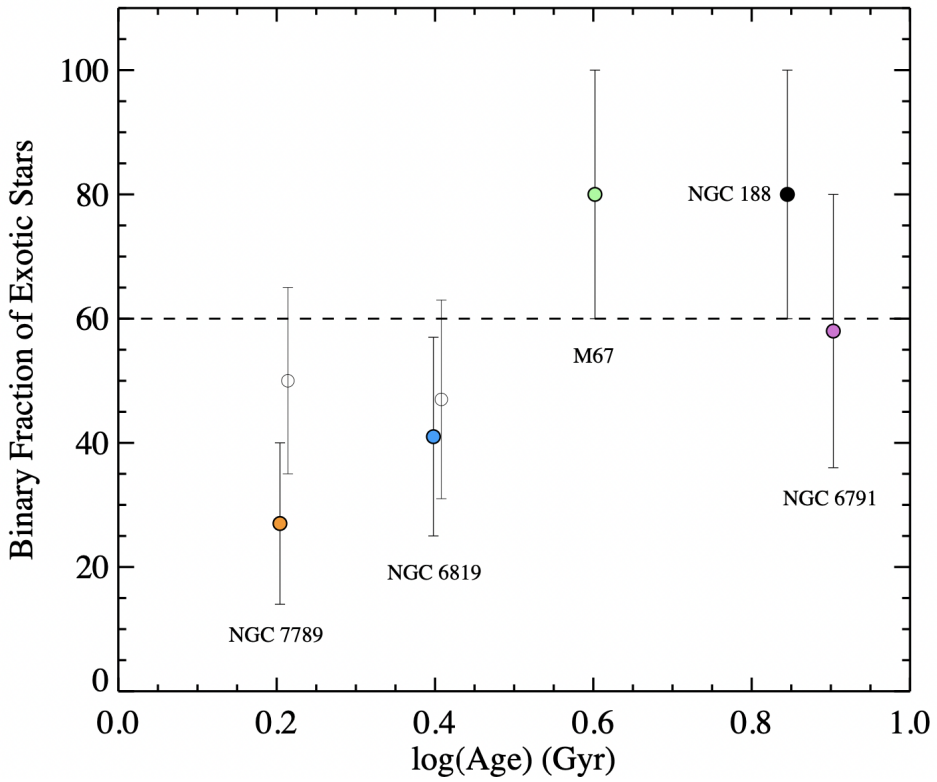

Figure 6.1 The detected binary fraction among exotic stars (BS, yellow giants, and SSGs) in open clusters versus cluster age are plotted as solid points from Katelyn Milliman's Thesis. The dashed line marks the overall average binary fraction of 60% ± 8% for all clusters. The open circles for NGC 7789 and NGC 6819 (plotted at an arbitrary age offset) represent the binary fraction after the authors incorporated very rapid rotators under a set of broad assumptions.

vice-versa. This may suggest a change in the dominant blue straggler formation scenario for different cluster ages. We hope to be able to clear the picture by adding more data to this diagram.

With our data, we should be able to assess whether there is a correlation between the orbital period (and thus the mass transfer mechanism) and the position in the CMD (which is related to the amount of accreted mass). We will also be able to combine our radial velocities with TESS photometry to fully characterize the short-period systems and infer their properties and likely formation mechanism. For all BSS, we will determine the mass from the location in the CMD, using stellar isochrones, and the temperature and gravity from the spectra.

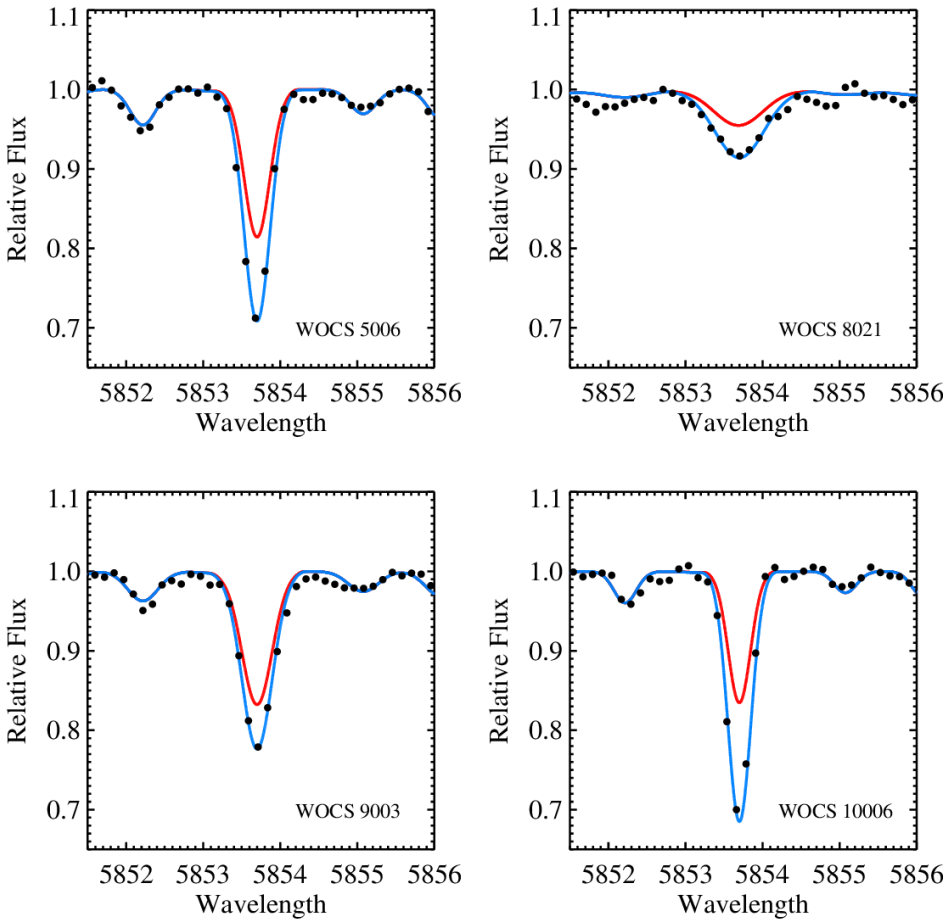

Figure 6.2 The spectra for the blue stragglers with significant barium excess are shown (black dots). Overplotted are the computed profiles with [Ba/Fe] = 0.0 (red line) and the fitted barium abundance (blue line). Image from Milliman et al. (2014)

Then, using our spectra, we can determine the abundance of elements in the BSS (e.g., CNO, Ba, Ca, Fe), and by comparison with the cluster's composition, we will infer if the mass transfer polluted the star. Within this framework, stars that we will identify having periods around 1,000 days and showing Barium enhancement can be assumed to be BSS formed by case C-MT— as demonstrated in Milliman et al. (2014) —see Figure 6.2. The same stars can be further studied in the ultraviolet to confirm that they possess a white dwarf companion, similar to those in NGC 188 (Gosnell et al., 2014, 2015). But also, to test relations between BSS and chemically peculiar stars such us Ba stars, carbon dwarfs, subgiant CH, CEMP-s, etc.

We can conclude that, even though the results presented in this thesis have advanced

our understanding of blue straggler stars, many of the open questions about BSS remain unanswered, and also, new ones have raised. The observational investigation of BSS and related families is far from being finished. New high-quality observations, as well as a detailed theoretical investigation of the physical mechanisms specially involved in binary interactions, are still crucial to address important questions about the straggler evolution but also of low- and intermediate-mass binary systems, the progenitors of BSS.

Appendix A

A.1 Light-curves complementary data

A.1.1 Light-curves of the open cluster Berkeley 32

According with § 2.4.2 this cluster has a contamination rate of 0.14 and is classified in Group III, i.e., among those clusters with the highest contamination rates. The very similar periods and phase transits of the stragglers (LCs below) make us suspect there is a nearby EB whose light has bled with that of (at least) three stragglers. Even though their Target Pixel Files (TPFs) do not show closed by stars within 1-pixel of radius and -2 (for brightest stars) $<\Delta m <$ 2 (for fainter stars). The stars "contaminated" are TIC 0758962138, 0235542907 and 0235541152. The percentage of short-period-BSS for this cluster is of 22% wich reduces to 11% by taking out the above mentioned stars.

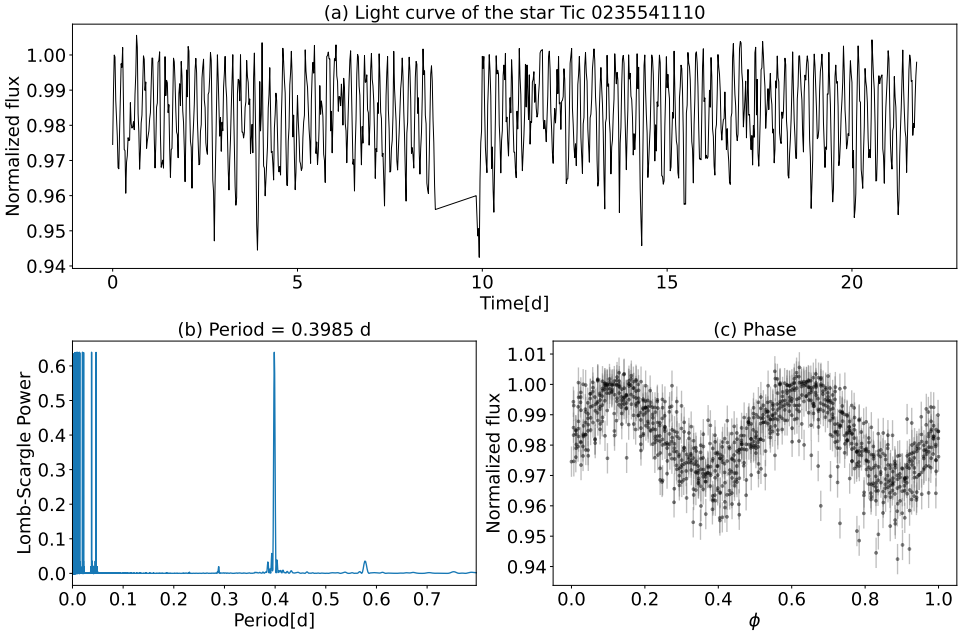

Figure A.1 Panel (a) shows the normalized light curve of Tic 0235541110 of cluster Berkeley 32 from sector 6. Panel (b) shows the Lomb-Scargle periodogram. Panel (c) is the phase transit of the eclipsing binary.

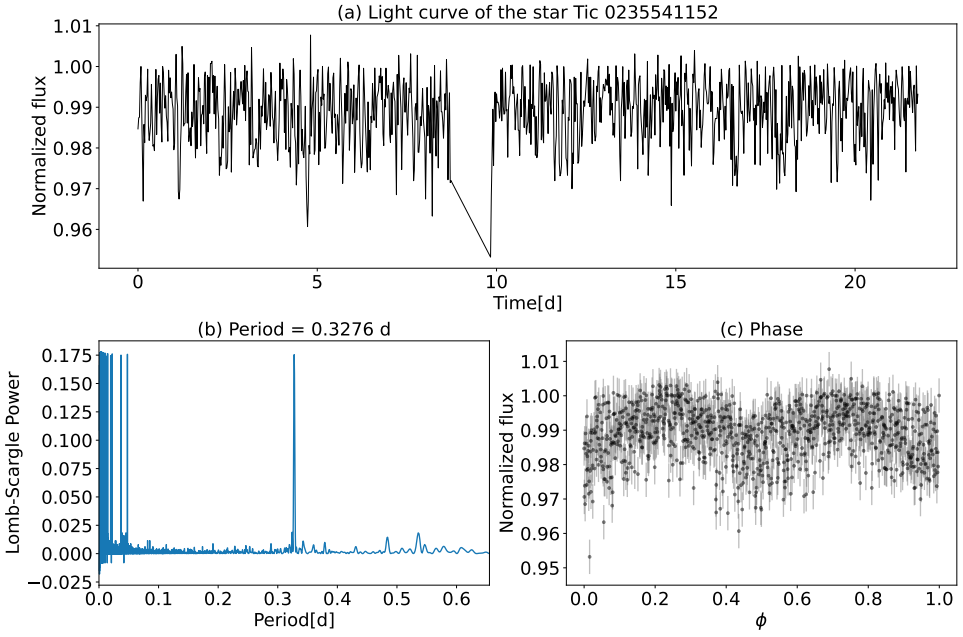

Figure A.2 same as Figure A.1 but for Tic 0235541152

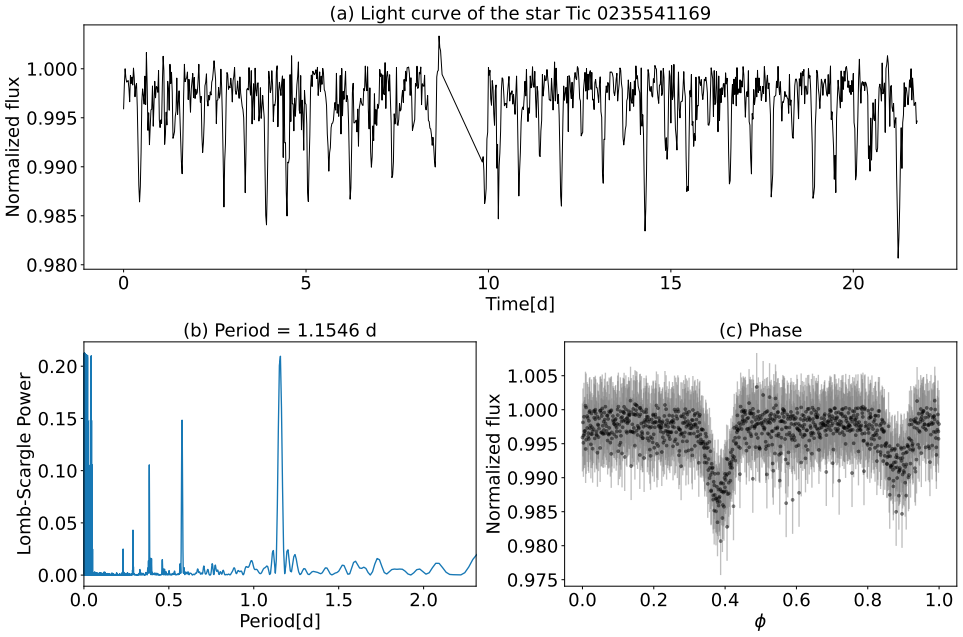

Figure A.3 same as Figure A.1 but for Tic 0235541169

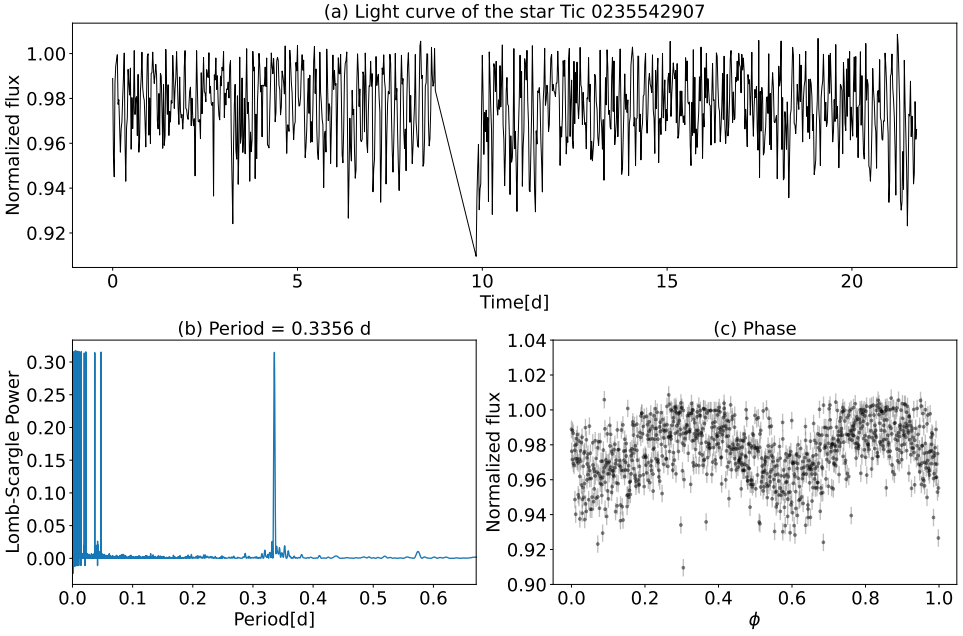

Figure A.4 same as Figure A.1 but for Tic 0235542907

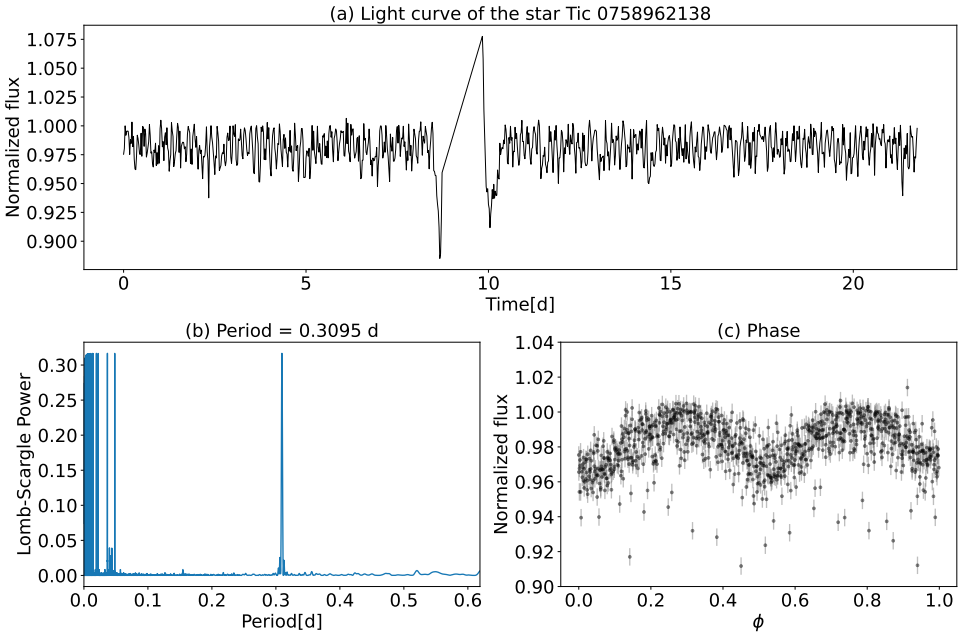

Figure A.5 same as Figure A.1 but for Tic 0758962138

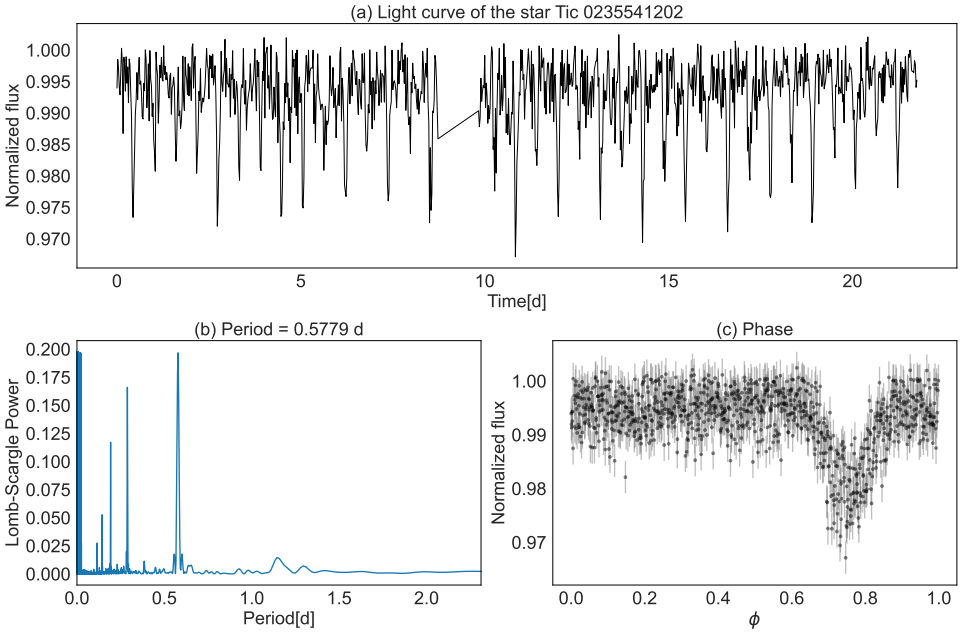

Figure A.6 same as Figure A.1 but for Tic 0235541202, this star is a YSS!

A.1.2 Light-curves of the open cluster NGC 1193

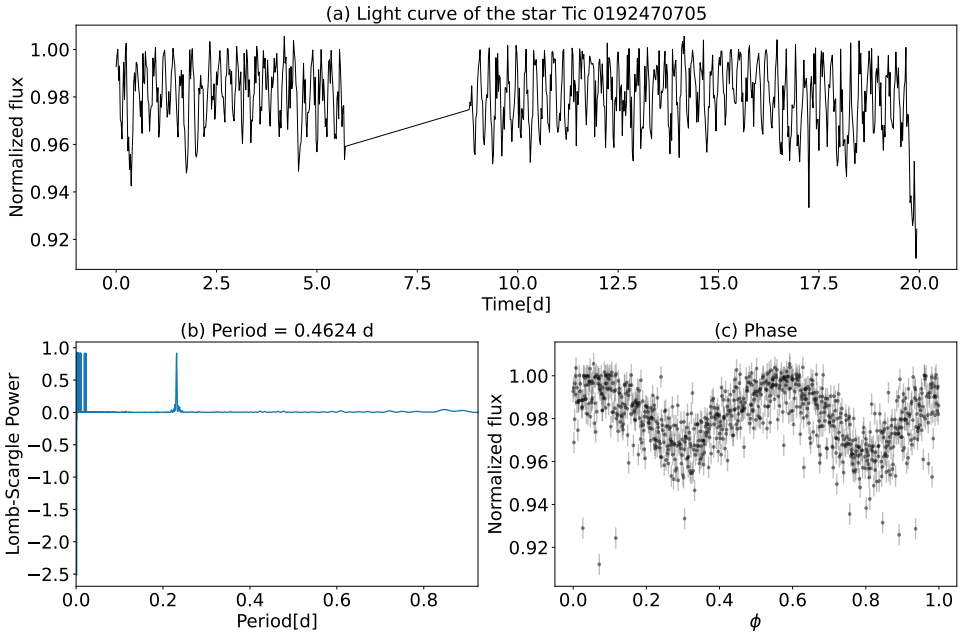

Figure A.7 Panel (a) shows the normalized light curve of Tic 0192470705 of cluster NGC 1193 from sector 6. Panel (b) shows the Lomb-Scargle periodogram. Panel (c) is the phase transit of the eclipsing binary.

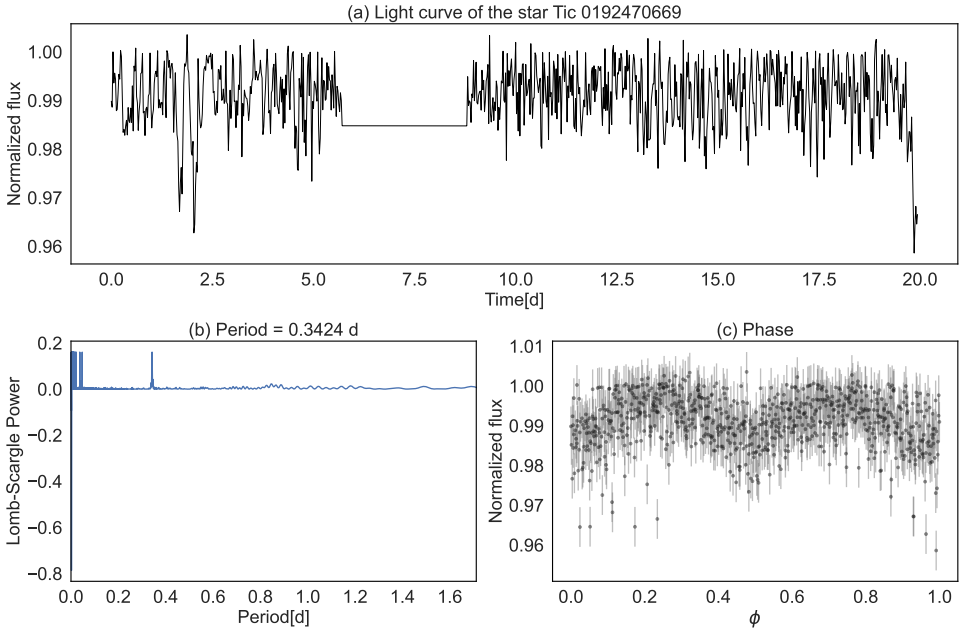

Figure A.8 same as Figure A.7 but for Tic 0192470669

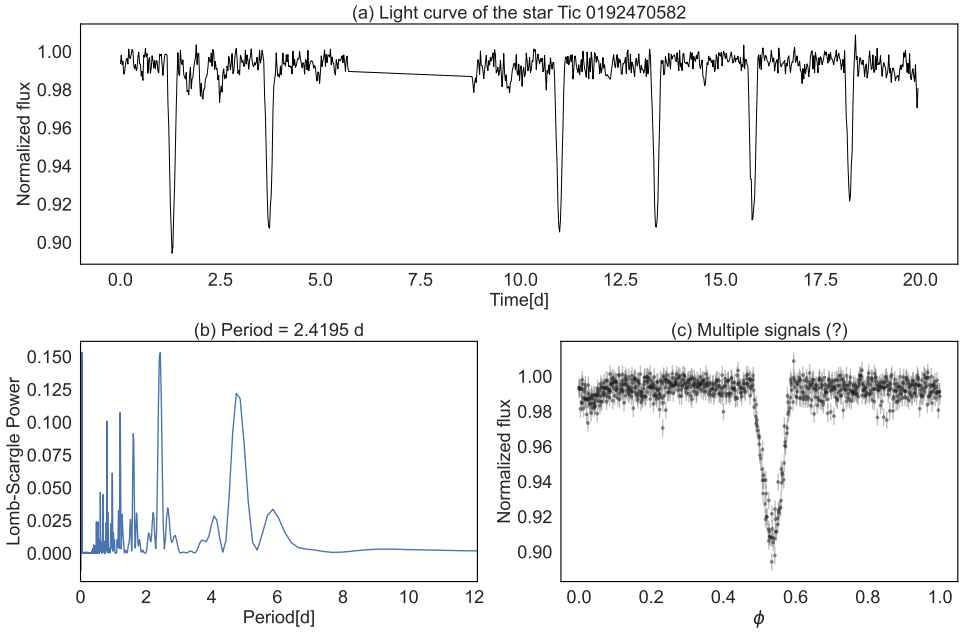

Figure A.9 same as Figure A.7 but for Tic 0192470582

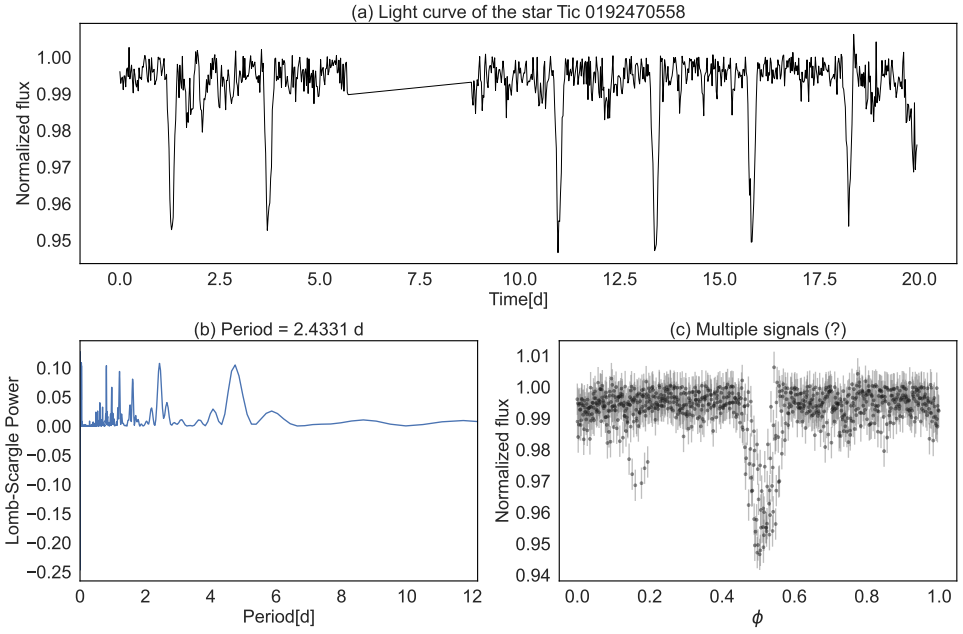

Figure A.10 same as Figure A.7 but for Tic 0192470558

A.1.3 Light-curves of the open cluster Melotte 66

We classified Melotte 66 in Group I, i.e, within those with less than 5% of "field contamination" on their BSS population. Despite the low contamination, we found two stars with the same period, phase transit and LC. The stars are TIC 0060193648 and 0060193692, when inspecting their TPFs we found they are at a distance of 11.32 pixels (238 arcsec), so we can safely assumed they are not the same star, but instead both are contaminated by other sources. In the case of TIC 0060193692 the LC seems to be contaminated by several fainter stars and the same happens with TIC 0060193648, whose LC seems to be contaminated by two brighter stars. By leaving out from our statistics this two stars, the percentage of short-period BSS in Melotte 66 decreases from 29% to 14%.

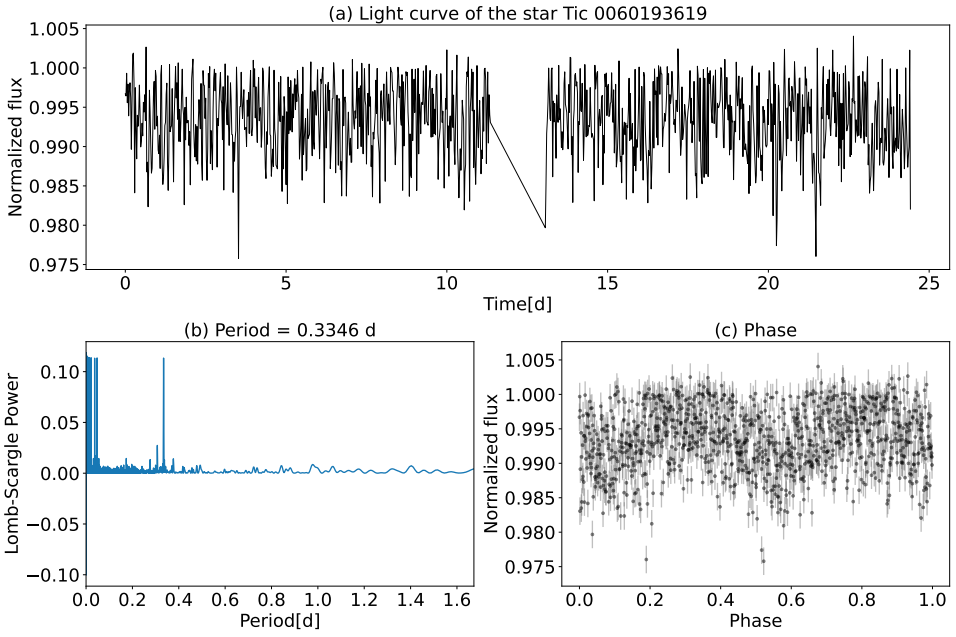

Figure A.11 Panel (a) shows the normalized light curve of Tic 0060193619 of cluster Melotte 66 from sector 7. Panel (b) shows the Lomb-Scargle periodogram. Panel (c) is the phase transit of the eclipsing binary.

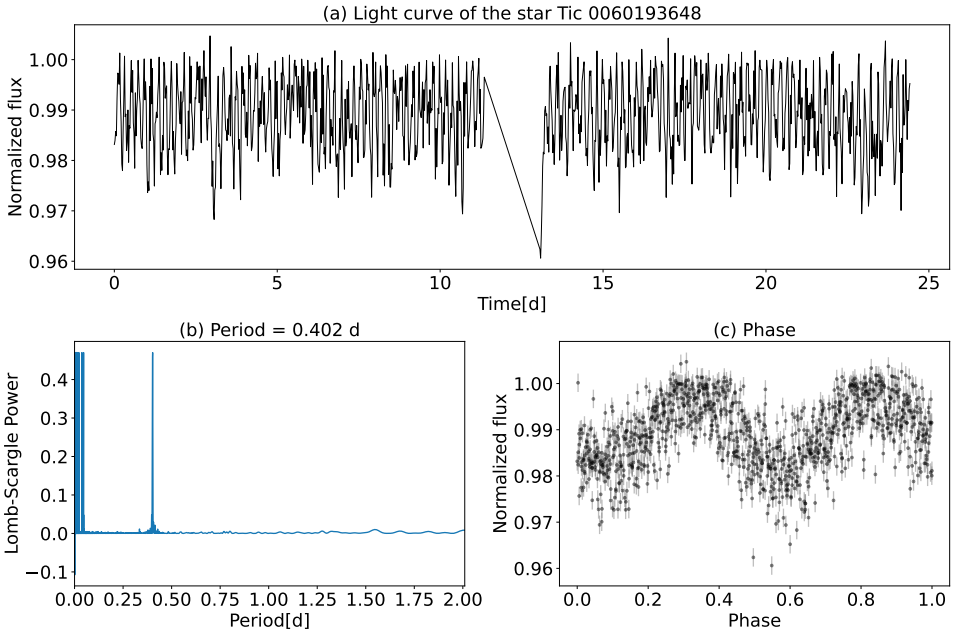

Figure A.12 Same than Figure A.11 but for Tic 006019364

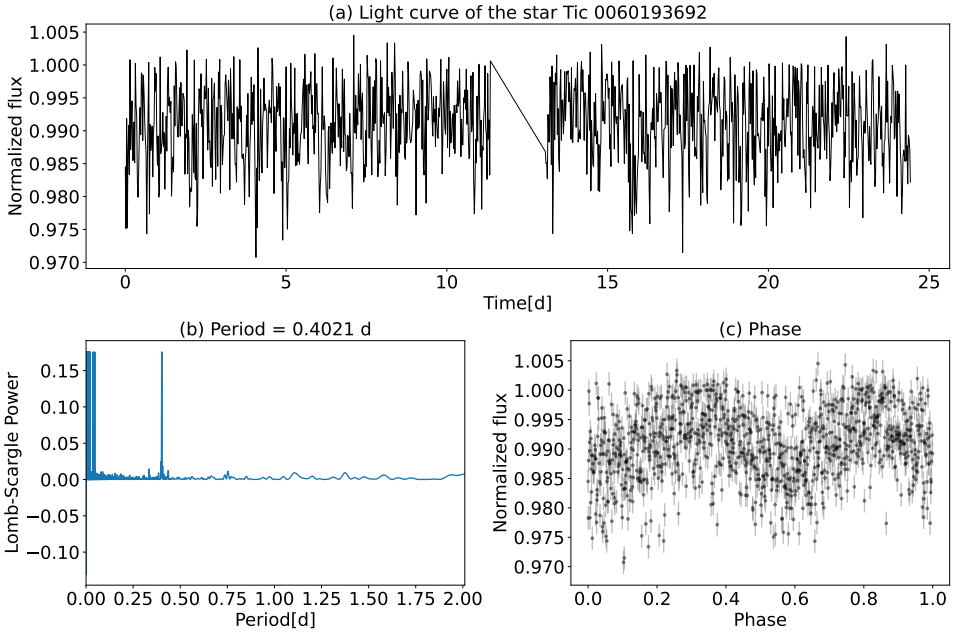

Figure A.13 Same than Figure A.11 but for Tic 0060193692

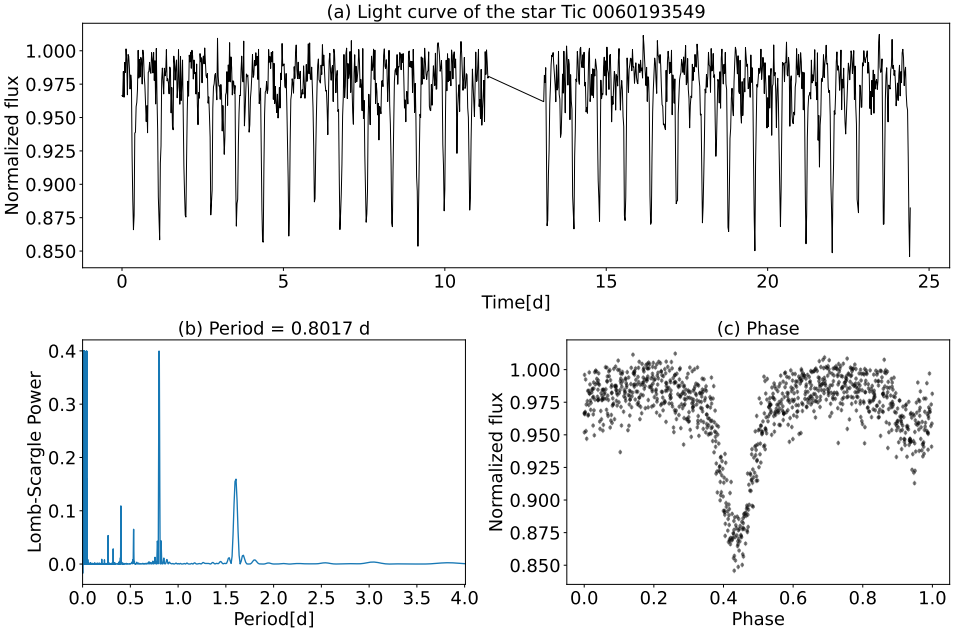

Figure A.14 Same than Figure A.11 but for Tic 0060193549

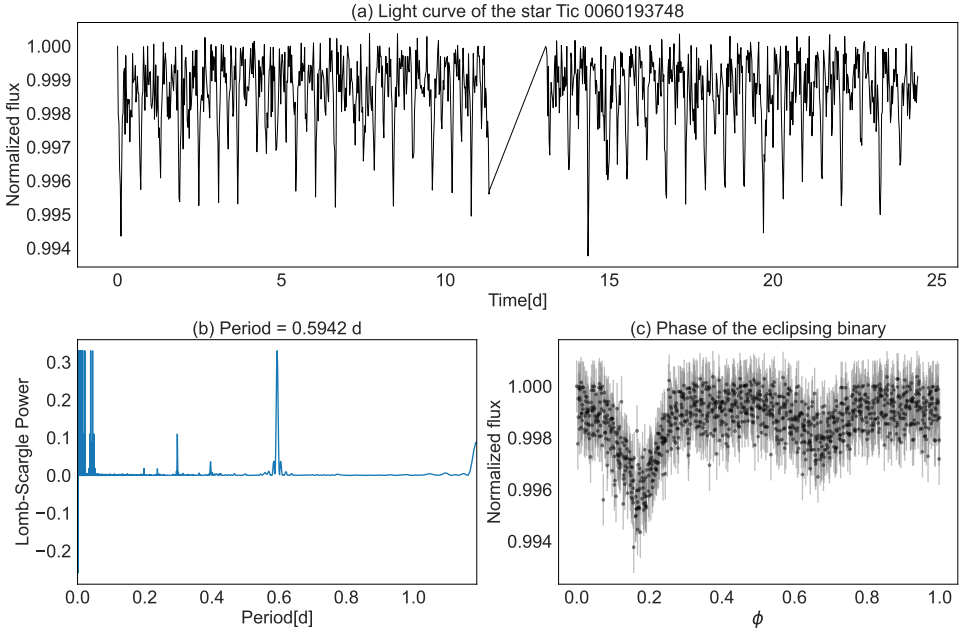

Figure A.15 Same than Figure A.11 but for Tic 0060193748. This star is a YSS!

A.1.4 Light-curves of the open cluster King 2

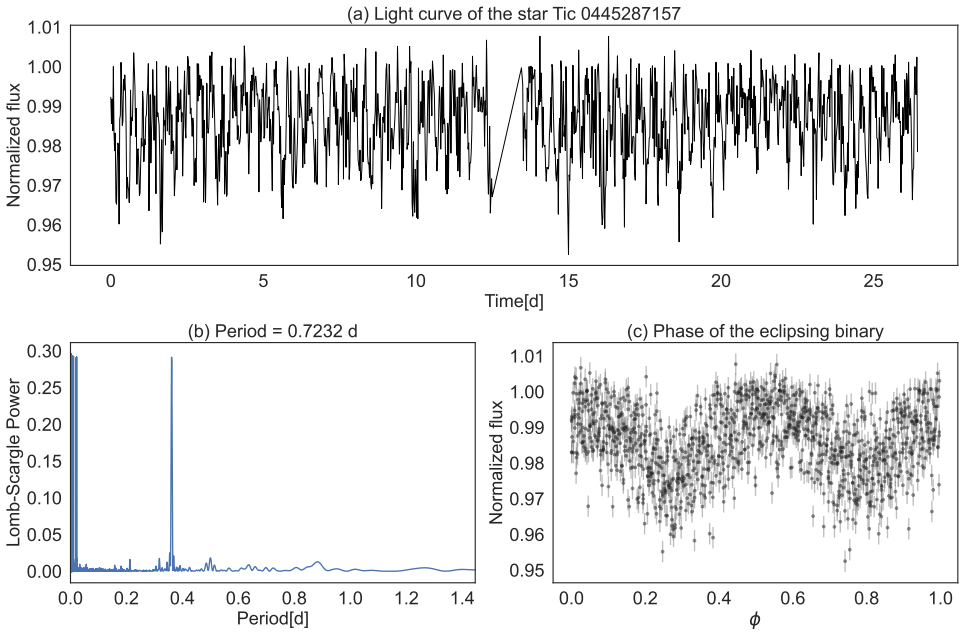

Figure A.16 Panel (a) shows the normalized light curve of Tic 0445287157 of cluster King 2 from sector 24 . Panel (b) shows the Lomb-Scargle periodogram. Panel (c) is the phase transit of the eclipsing binary. This star is a YSS!

A.1.5 Light-curves of the open cluster NGC 7142

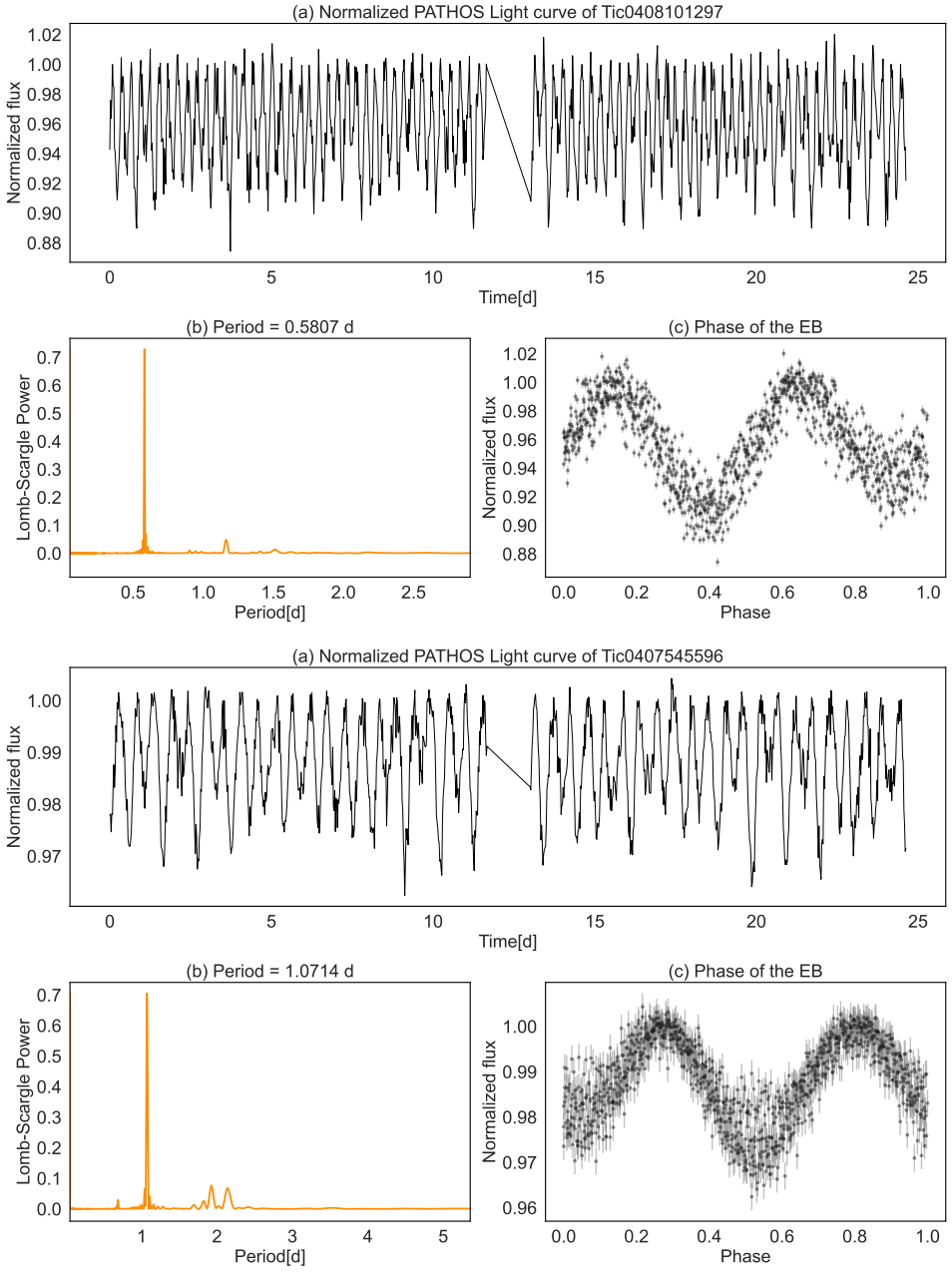

Figure A.17 Panel (a) shows the normalized light curve of Tic 0408101297 and Tic 0407545596 of cluster NGC 7142 from sector 24 . Panel (b) shows the Lomb-Scargle periodogram. Panel (c) is the phase transit of the eclipsing binaries.

A.1.6 Light-curves of the open cluster NGC 2243

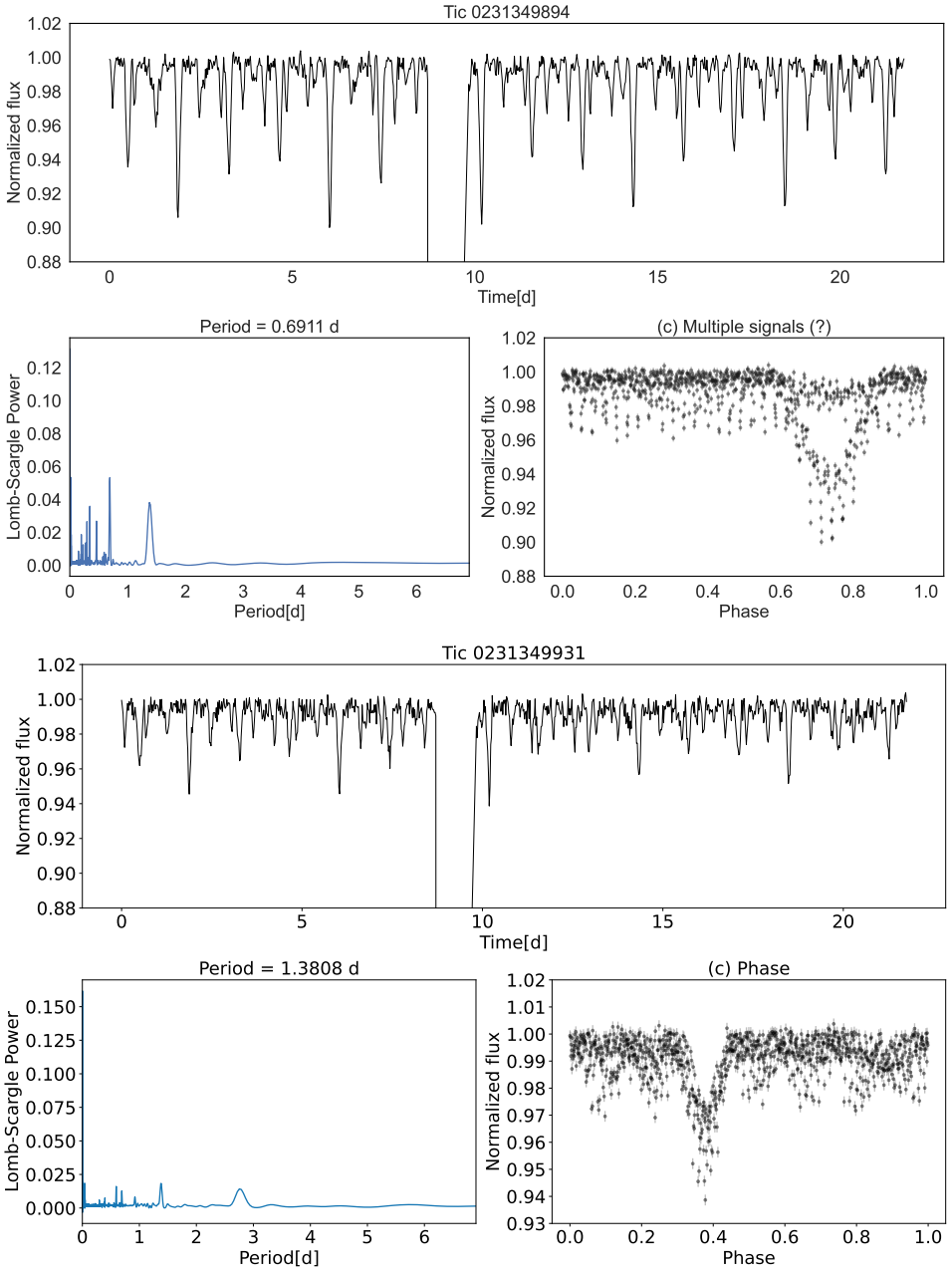

Figure A.18 Panel (a) shows the normalized LC's of the stars Tic 0231349894 and Tic 0231349931 of the cluster NGC 2243 from sector 6. Panel (b) shows the Lomb-Scargle periodograms. Panel (c) the phases of the "binaries".

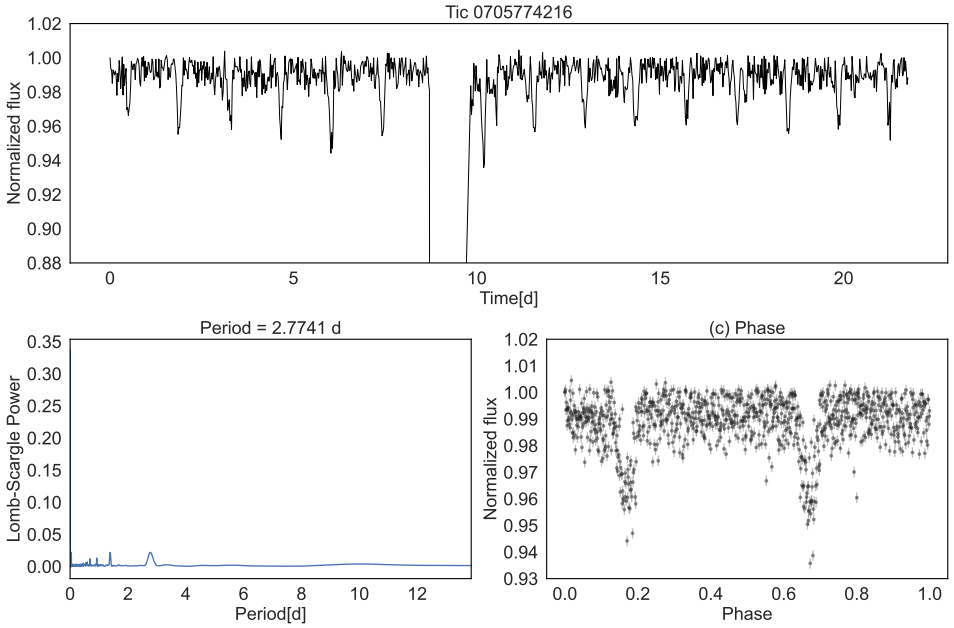

Figure A.19 Same than Figure A.17 but for Tic 0705774216

A.1.7 Light-curves of the open cluster NGC 2141

NGC 2141 is a group II cluster. We did not fond however, neither similar periods and/or nearby contaminants on the LC's of the short-period-BSS.

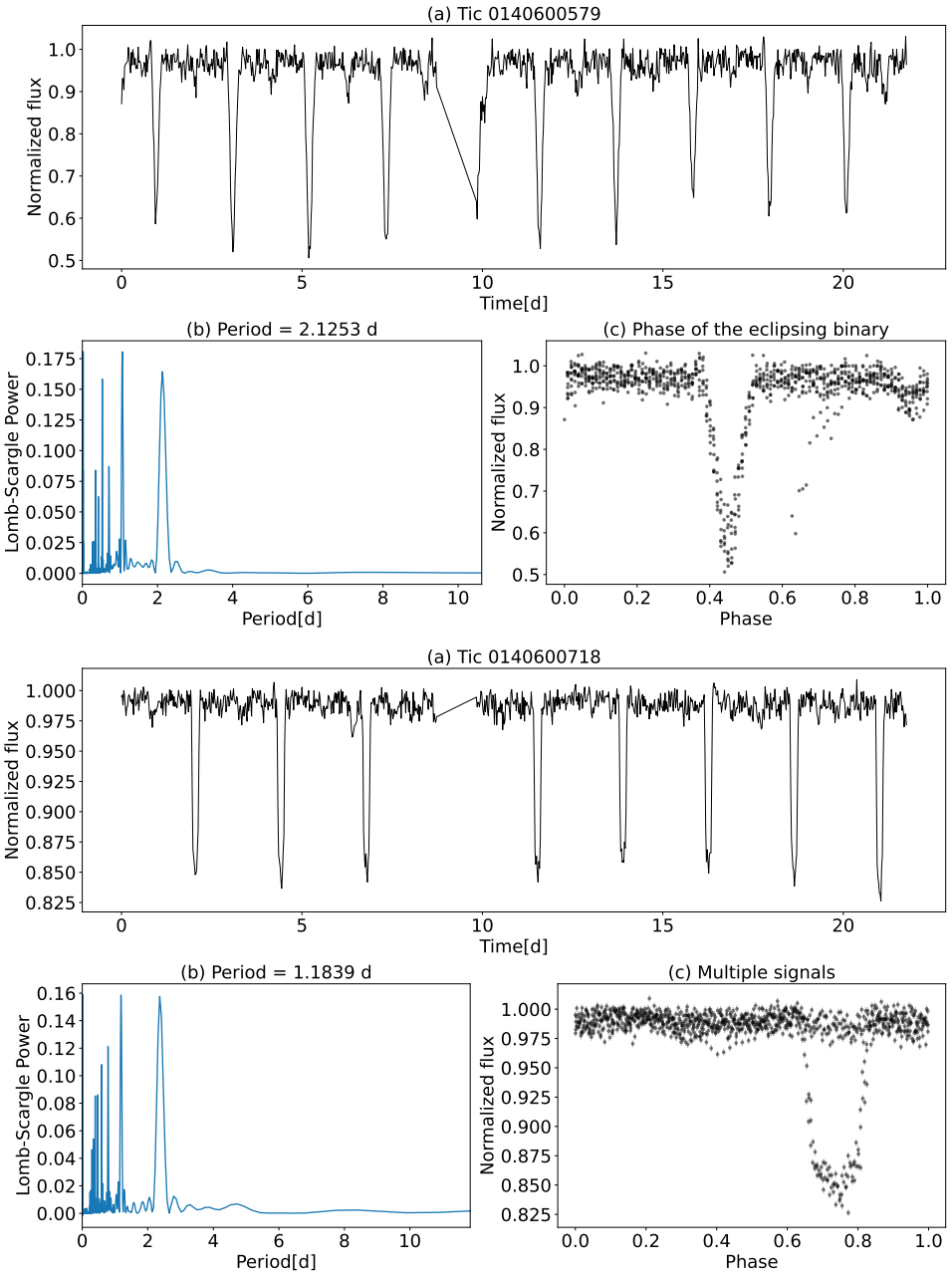

Figure A.20 Panel (a) shows the normalized light curve of the stars Tic 0140600579 and Tic 0140600718 of cluster NGC 2141 from sector 6. Panel (b) shows the Lomb-Scargle periodogram. Panel (c) the phases transit of the "binaries".

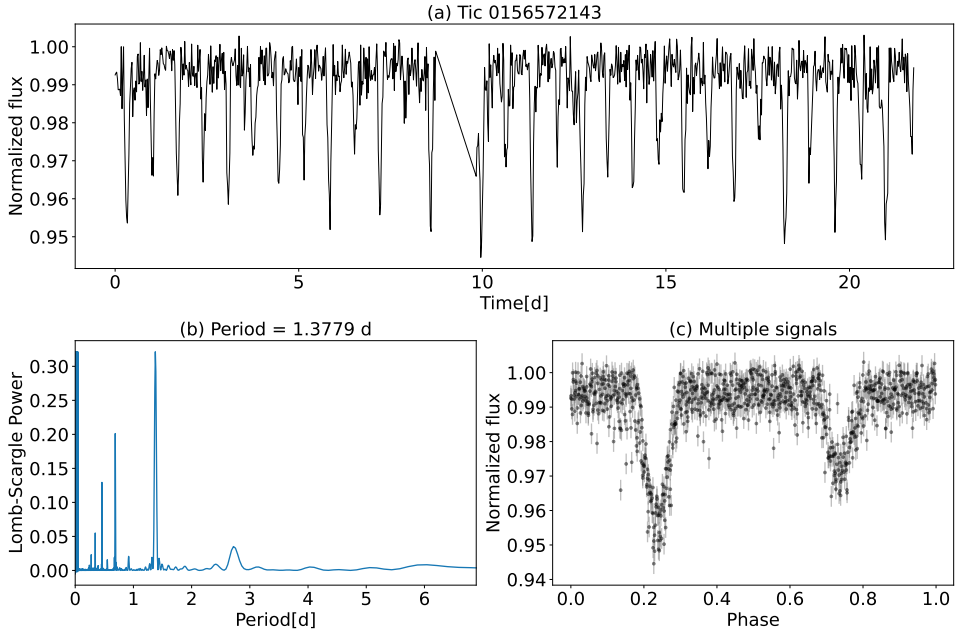

Figure A.21 Same than Figure A.20 but for Tic 0156572143

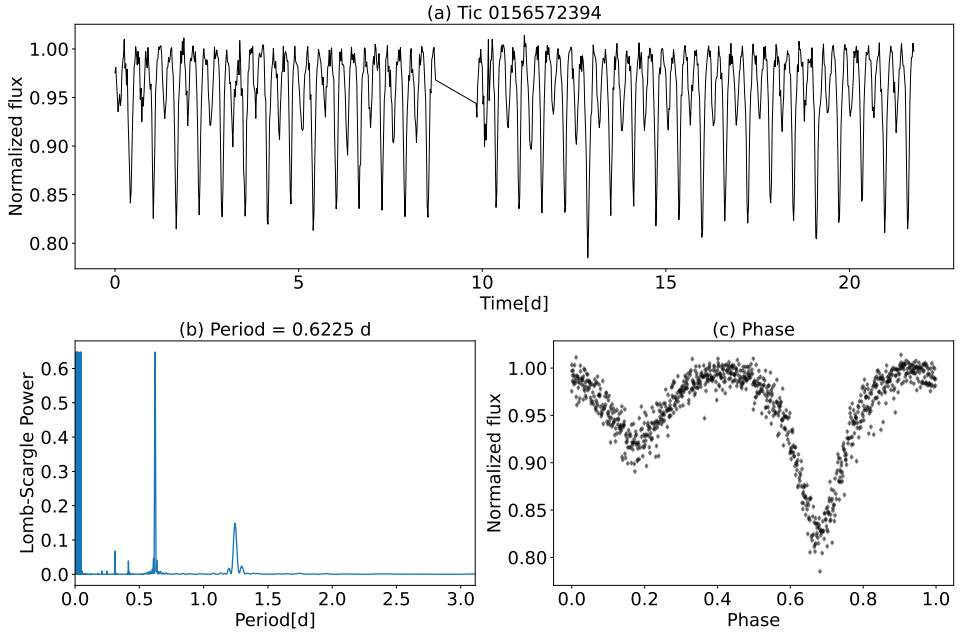

Figure A.22 Same than Figure A.20 but for Tic 0156572394

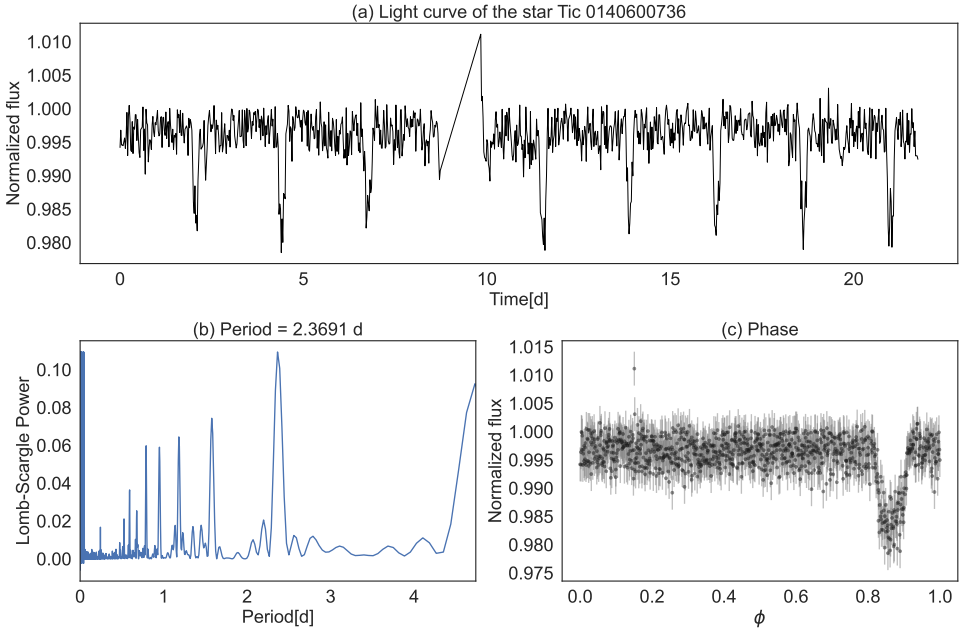

Figure A.23 Same than Figure A.20 but for Tic 0140600736. This star is a YSS!

A.1.8 Light-curves of the open cluster Berkeley 20

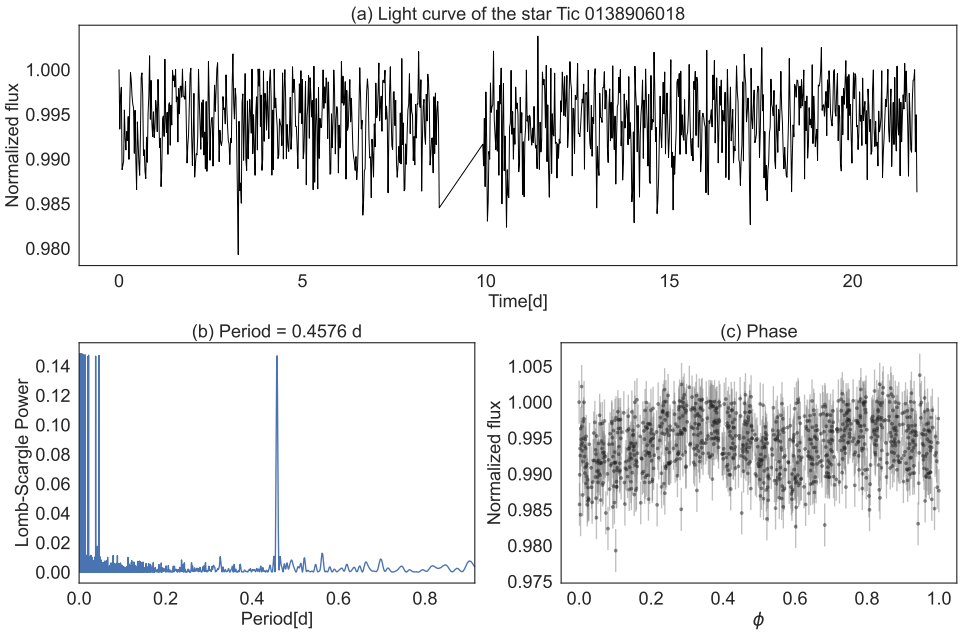

Figure A.24 Panel (a) shows the normalized light curve of Tic 0138906018 (from sector 6) a yellow straggler in the cluster Berkeley 20. Panel (b) shows the Lomb-Scargle periodogram. Panel (c) is the phase transit of the eclipsing binary.

A.1.9 Blue straggler specific frequencies

In the following lines we describe some of the most common BSS specific frequencies used in the literature by many authors.

1) Double normalized ratio:

$$R_{\rm BSS} = \frac{(N_{\rm BSS}/N_{\rm BSS}^{\rm tot})}{(L^{\rm sampled}/L_{\rm tot}^{\rm sampled})} \tag{A.1}$$

where $N_{\rm BSS}$ and $N_{\rm BSS}^{\rm tot}$ are the number of blue stragglers in a given region and the total number of such stars, respectively. The quotient $L^{\rm sampled}/L_{\rm tot}^{\rm sampled}$ is the fraction of light sample in the same region, with respect to the total measured luminosity. This ratio is equal to unity for any population (e.g., red giants or horizontal-branch stars) whose radial distribution follows that of the cluster's integrated luminosity.

2) Specific frequency in terms of the luminosity:

$$S4_{\rm BSS} = \frac{N_{\rm BSS}}{L_s} \tag{A.2}$$

where $N_{\rm BSS}$ is the number of blue straggler stars L_s is the sampled integrated bolometric luminosity in units of $10^4\ L_\odot$. In general it is important to take caution when normalizing with integrated properties, since some cluster parameters such as concentration and central density are correlated with the integrated luminosity, and so introduce false correlations with the blue straggler population (Djorgovski, 1993, Ferraro et al., 1995).

3) Specific frequency from Bolte et al. (1993):

$$F_{\rm BSS} = \frac{N_{\rm BSS}}{N_{\rm bright}} \tag{A.3}$$

where $N_{\rm bright}$ is the number of all stars brighter than two magnitudes below the HB level. While useful, this method is limited to the quality of the photometric survey.

Such bright stars are often saturated due to the long exposure needed to reach the TO region. In fact, the bright end ($G \leq 13$) in *Gaia* is limited by photometric calibration errors, is here where saturation and flux loss becomes important. Furthermore, even though most of the clusters of our sample do not have stars in that magnitude regime it is a risk if some of these very bright stars are missing, because this will affect directly the normalization. This method is not feasible in our sample.

4) Specific frequency from Ferraro et al. (2003):

$$F_{\rm pop}^{\rm BSS} = \frac{N_{\rm BSS}}{N_{\rm pop}} \tag{A.4}$$

here $N_{\rm pop}$ is the number of stars belonging to a cluster normal population adopted as reference (generally the HB population[1], or a segment of the RGB or MS). This normalized ratio is a purely observational quantity and can be easily computed, which is a great advantage over the other normalizations described above. In general the observed number of HB stars ($N_{\rm HB}$) is the ideal indicator of the cluster light distribution. This feature, however, is not visible in the CMD of young clusters. In open clusters, the clump region (red component of the HB) is much less clearly defined and much less populated than the entire HB in globular clusters.

Given that more blue stragglers should be expected in larger clusters, we can scale the number of blue stragglers observed in the cluster by the number of MS, TO and RGB stars in the cluster. We defined the specific frequency used in § 3.5 as follows

$$F_{\rm ref}^{\rm BSS} = \log\left(\frac{N_{\rm BSS}}{N_{\rm ref}}\right) \tag{A.5}$$

Where ref = MS, TO and RGB. So, $N_{\rm MS}$ is the number of cluster main sequence stars up to 1 magnitude below the TO, adopted as a proxy of the cluster richness. $N_{\rm TO}$ is the number of sources above the main sequence turnoff stars but fainter and redder than the straggler population, and bluer than the sub-giant branch (SGB) stars. In both

[1]Here HB is for the entire HB population, i.e. the blue, the variable and the red components of the HB

cases we avoided the binary region. Finally, N_{RGB} is the number of RGB stars selected as the stars brighter and redder than the base of the RGB on our isochrone.

Appendix B

B.1 Collinder 261 complementary data

B.1.1 Table of BSS in Collinder 261

TABLE B.1: Blue and yellow straggler candidates from *Gaia* DR2 data. [a]Classification of the stars according to their binary nature, as reported in the astronomical database SIMBAD (Wenger et al., 2000): • EB β Lyrae, $\star$ EB Algol, † EB W UMa.

Gaia DR2 Source Id.	G [mag]	$G_{\rm BP}$ [mag]	$G_{\rm RP}$ [mag]	μ_{α^*} [mas yr^{-1}]	μ_α [mas yr^{-1}]	$\bar{\omega}$ [mas]	$P_{\rm memb}$ [%]	Class[a]
5856432828647768960	15.00	15.28	14.57	-6.48 ± 0.03	-2.63 ± 0.04	0.30 ± 0.02	100	BS
5856437089255328384	15.23	15.57	14.73	-6.30 ± 0.05	-2.80 ± 0.04	0.37 ± 0.02	100	BS
5856511271928032256	14.74	15.03	14.28	-6.39 ± 0.03	-2.79 ± 0.04	0.31 ± 0.02	100	BS
5856530272864404224	15.40	15.80	14.80	-6.29 ± 0.05	-2.98 ± 0.05	0.30 ± 0.03	100	BS
5856527455365735680	15.26	15.61	14.71	-6.27 ± 0.05	-2.82 ± 0.05	0.29 ± 0.03	100	BS
5856516597687652352	15.89	16.31	15.31	-6.48 ± 0.05	-2.86 ± 0.06	0.29 ± 0.04	90	BS
5856527455365740032	15.16	15.59	14.54	-6.46 ± 0.04	-2.63 ± 0.04	0.33 ± 0.02	90	BS
5856527386646253312	14.54	14.85	14.05	-6.38 ± 0.03	-2.94 ± 0.03	0.29 ± 0.02	90	BS
5856527386646253440	15.12	15.45	14.50	-6.42 ± 0.04	-2.58 ± 0.05	0.33 ± 0.03	100	BS
5856527524085206656	13.90	14.24	13.39	-6.31 ± 0.03	-2.81 ± 0.03	0.29 ± 0.02	100	BS
5856517010004497792	15.65	16.03	15.11	-6.64 ± 0.05	-2.85 ± 0.06	0.34 ± 0.03	90	BS•
5856528348719355648	14.63	14.92	14.16	-6.38 ± 0.03	-2.88 ± 0.03	0.35 ± 0.02	100	BS
5856528623597294720	14.82	15.08	14.34	-6.76 ± 0.04	-2.75 ± 0.04	0.33 ± 0.02	70	BS
5856517078723954944	15.29	15.68	14.57	-6.48 ± 0.04	-2.81 ± 0.04	0.32 ± 0.03	100	BS
5856527558444960128	14.60	14.86	14.16	-6.11 ± 0.03	-2.69 ± 0.04	0.37 ± 0.02	100	BS
5856527455365743488	14.82	15.09	14.37	-6.42 ± 0.04	-2.49 ± 0.05	0.27 ± 0.03	100	BS
5856527661524172800	14.91	15.28	14.36	-6.34 ± 0.04	-2.56 ± 0.04	0.28 ± 0.02	100	BS•

5856527730243676800	15.60	15.94	15.07	−6.33 ± 0.05	−2.60 ± 0.05	0.33 ± 0.03	100	BS
5856528383078700288	15.71	16.11	15.14	−6.38 ± 0.05	−2.67 ± 0.06	0.28 ± 0.03	100	BS⋆
5856528726676132096	15.85	16.23	15.24	−6.28 ± 0.06	−2.70 ± 0.06	0.34 ± 0.04	100	BS
5856528520517692032	15.64	16.06	15.00	−6.54 ± 0.05	−2.79 ± 0.05	0.32 ± 0.03	100	BS
5856528589237173120	15.22	15.65	14.53	−6.22 ± 0.04	−2.45 ± 0.04	0.37 ± 0.03	100	BS
5856529242072194816	15.65	16.09	15.04	−6.40 ± 0.06	−2.82 ± 0.06	0.31 ± 0.04	100	BS
5856517284882496128	14.63	15.00	14.10	−6.41 ± 0.03	−2.81 ± 0.03	0.26 ± 0.02	100	BS
5856528348719366528	15.47	15.83	14.91	−5.98 ± 0.05	−2.58 ± 0.05	0.34 ± 0.03	90	BS
5856515601255190272	14.25	14.57	13.76	−6.29 ± 0.03	−2.67 ± 0.03	0.31 ± 0.02	100	BS⋆
5856514879700797696	14.34	14.49	14.05	−6.41 ± 0.03	−2.72 ± 0.03	0.32 ± 0.02	100	BS
5856528550550957184	14.96	15.25	14.47	−6.27 ± 0.04	−2.88 ± 0.04	0.28 ± 0.03	90	BS⋆
5856529379511194240	14.79	15.07	14.32	−6.12 ± 0.03	−2.65 ± 0.03	0.29 ± 0.02	100	BS
5856527524085202048	15.58	15.90	15.04	−6.57 ± 0.05	−2.78 ± 0.05	0.30 ± 0.03	100	BS
5856432656849042688	16.03	16.50	15.41	−6.52 ± 0.06	−2.69 ± 0.06	0.29 ± 0.03	100	BS
5856420729693697408	16.12	16.57	15.52	−6.47 ± 0.06	−2.63 ± 0.06	0.33 ± 0.04	100	BS
5856419531427900672	15.90	16.36	15.28	−6.46 ± 0.05	−2.68 ± 0.05	0.30 ± 0.04	80	BS
5856437742090215680	15.79	16.20	15.22	−6.72 ± 0.06	−2.51 ± 0.05	0.24 ± 0.03	80	BS
5856436298981175168	16.09	16.52	15.49	−6.50 ± 0.06	−2.45 ± 0.05	0.34 ± 0.03	100	BS
5856436367700747392	15.98	16.43	15.37	−6.24 ± 0.07	−2.54 ± 0.06	0.43 ± 0.03	80	BS
5856483303104274560	15.12	15.54	14.57	−5.75 ± 0.04	−2.48 ± 0.04	0.40 ± 0.02	50	BS
5856512680677308160	16.10	16.55	15.49	−6.34 ± 0.06	−2.77 ± 0.27	0.27 ± 0.05	100	BS
5856528962867671936	16.06	16.46	15.46	−6.50 ± 0.07	−2.79 ± 0.06	0.20 ± 0.04	100	BS
5856528486157936384	16.05	16.47	15.42	−6.13 ± 0.07	−2.61 ± 0.06	0.41 ± 0.04	100	BS
5856528486157941376	16.11	16.52	15.50	−6.24 ± 0.07	−2.86 ± 0.06	0.32 ± 0.04	100	BS
5856527764603421184	15.86	16.31	15.23	−6.15 ± 0.07	−2.77 ± 0.06	0.27 ± 0.04	100	BS
5856529001554008064	14.64	15.12	13.97	−6.28 ± 0.03	−2.84 ± 0.04	0.30 ± 0.02	100	BS
5856528761035882496	15.38	15.74	14.82	−6.20 ± 0.05	−2.80 ± 0.05	0.22 ± 0.03	100	BS†
5856529276431965696	16.37	16.76	15.81	−6.19 ± 0.07	−2.97 ± 0.07	0.30 ± 0.05	100	BS
5856517211839051392	15.59	16.00	14.96	−6.72 ± 0.06	−1.91 ± 0.06	0.48 ± 0.04	70	BS
5856527558444963200	15.67	16.06	15.07	−6.23 ± 0.05	−2.84 ± 0.06	0.23 ± 0.03	100	BS
5856529276431950080	15.04	15.43	14.47	−6.46 ± 0.04	−2.84 ± 0.04	0.25 ± 0.03	100	BS
5856527558444950656	15.74	16.10	15.08	−6.05 ± 0.09	−2.67 ± 0.09	0.17 ± 0.06	100	BS
5856533326555127168	16.11	16.52	15.48	−6.33 ± 0.07	−3.09 ± 0.06	0.25 ± 0.04	100	BS
5856515665648722688	15.63	15.99	15.07	−6.18 ± 0.05	−2.86 ± 0.05	0.21 ± 0.03	100	BS⋆
5856515669974676480	15.70	16.01	15.13	−5.92 ± 0.08	−2.75 ± 0.07	0.44 ± 0.05	90	BS
5856519037229366144	14.45	14.83	13.90	−5.57 ± 0.03	−2.43 ± 0.03	0.53 ± 0.02	80	BS
5856435130750056576	14.36	15.02	13.57	−6.00 ± 0.03	−3.01 ± 0.02	0.14 ± 0.01	60	YS
5856527622837778176	15.29	15.89	14.55	−6.30 ± 0.05	−2.76 ± 0.04	0.30 ± 0.03	100	YS
5856515601255187712	15.42	16.02	14.67	−6.30 ± 0.04	−2.54 ± 0.04	0.27 ± 0.03	100	YS

B.1.2 Light-curves of short-period binaries in Collinder 261

The following figures correspond to the remaining 20 short-period BSS found among the blue straggler population of Collinder 261.

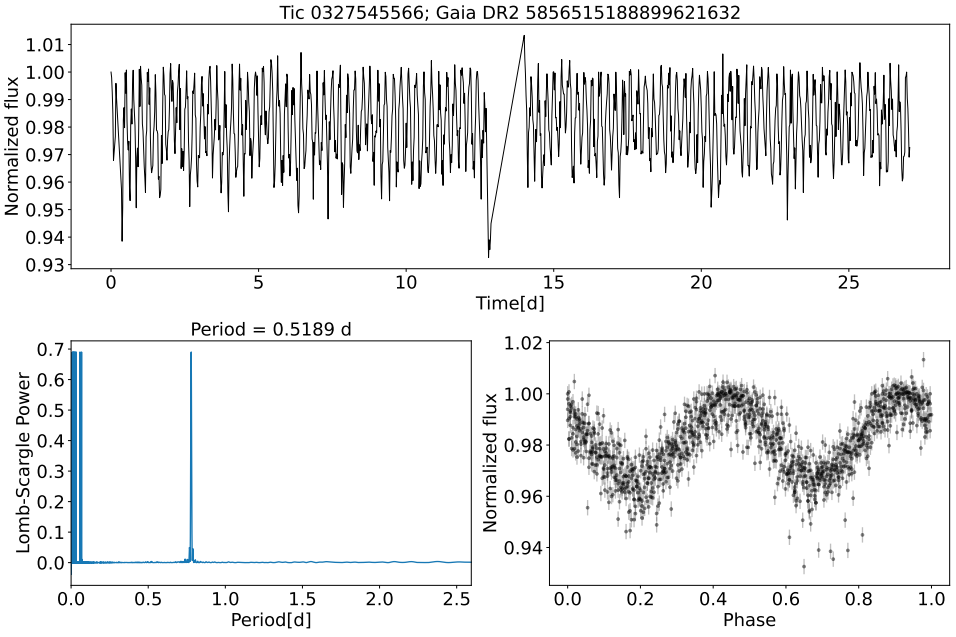

Figure B.1 Panel (a) shows the normalized light curve of *Gaia* DR2 5856515188899621632 from sector 11. Panel (b) shows the Lomb-Scargle periodogram. Panel (c) is the phase transit of the eclipsing binary.

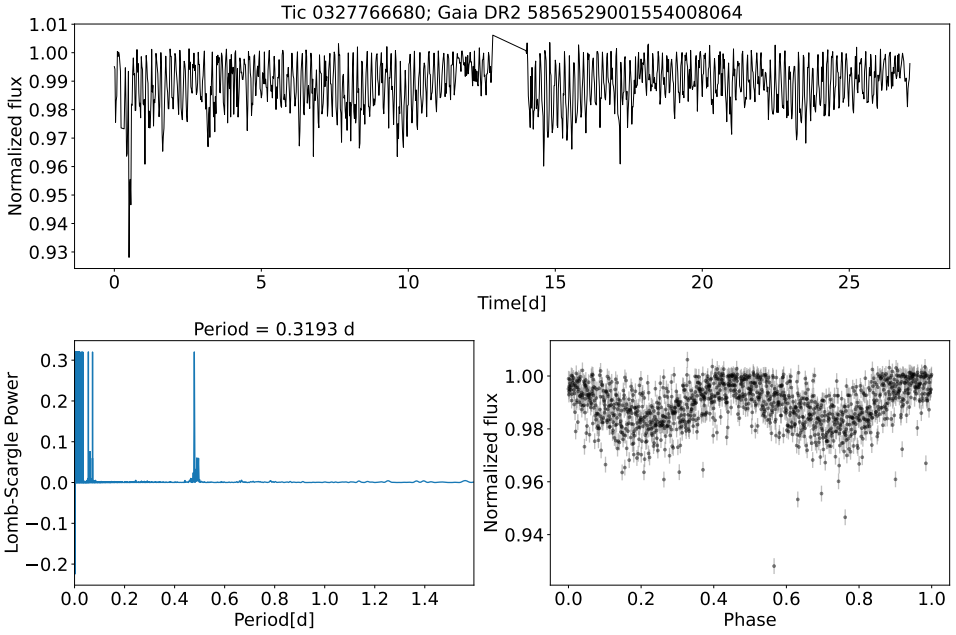

Figure B.2 Same as Figure B.1 but for *Gaia* DR2 5856529001554008064

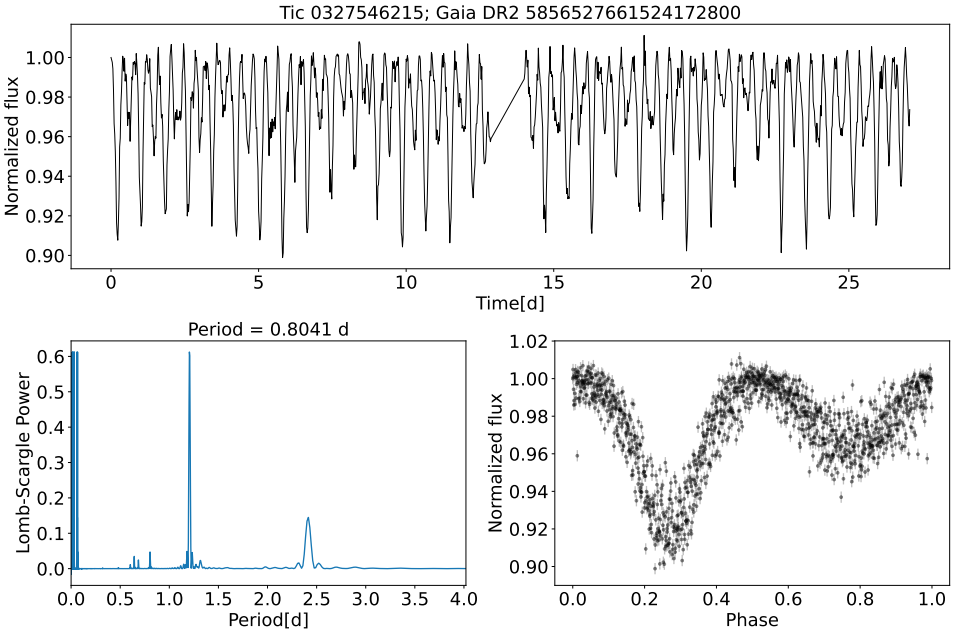

Figure B.3 Same as Figure B.1 but for *Gaia* DR2 5856527661524172800

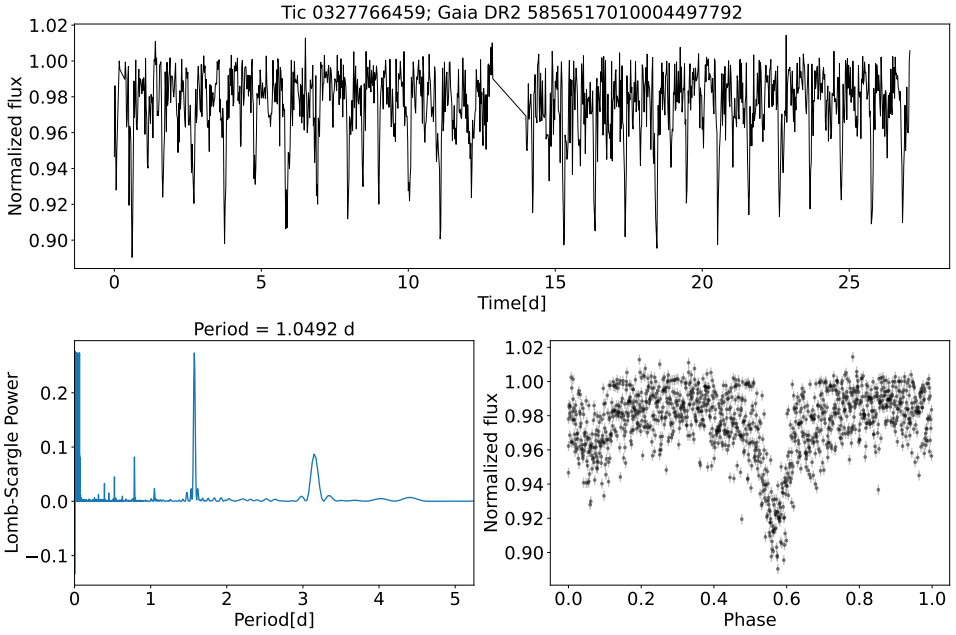

Figure B.4 Same as Figure B.1 but for *Gaia* DR2 5856517010004497792

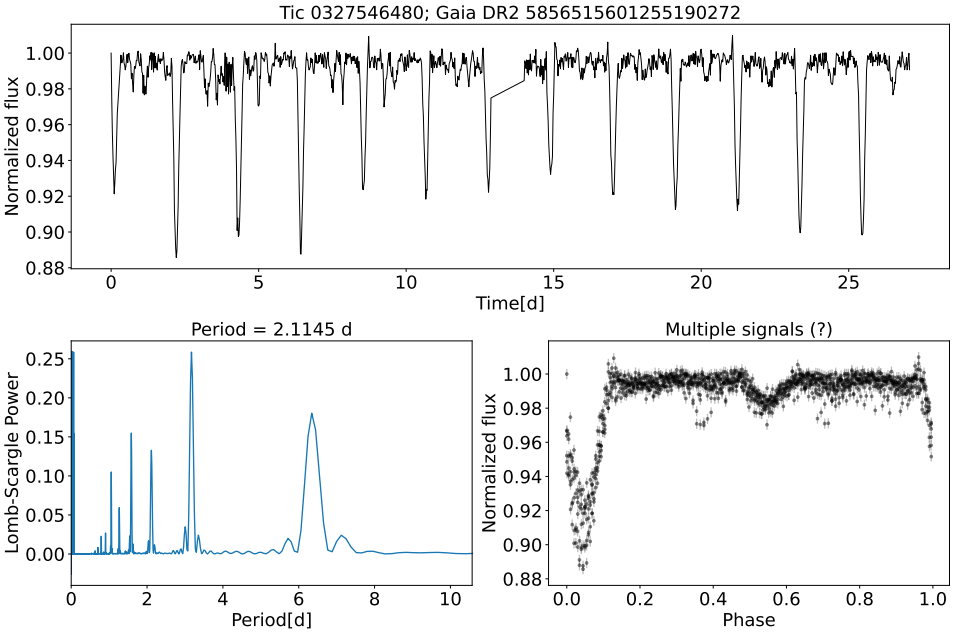

Figure B.5 Same as Figure B.1 but for *Gaia* DR2 5856515601255190272

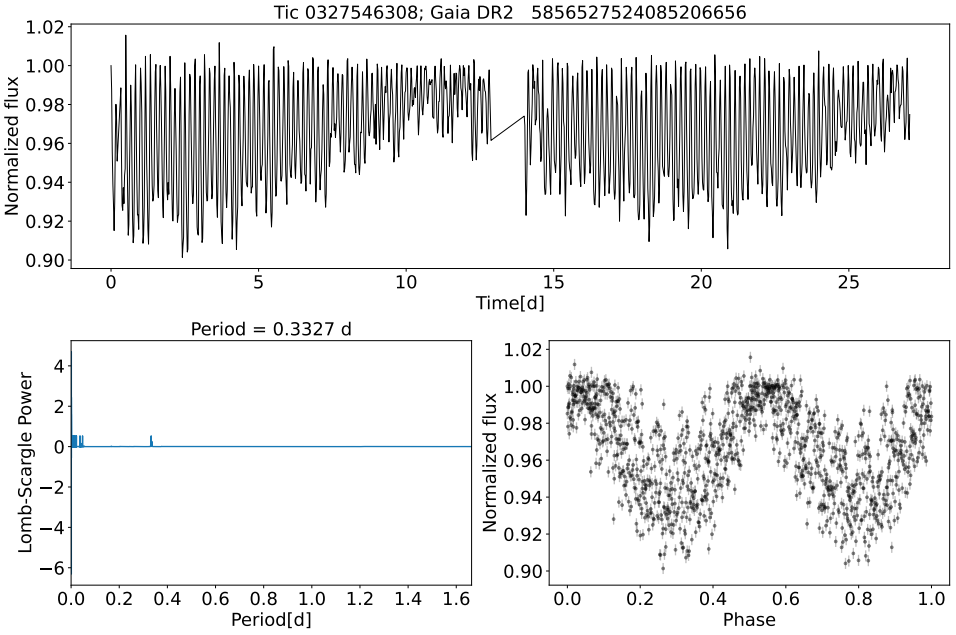

Figure B.6 Same as Figure B.1 but for *Gaia* DR2 5856527524085206656

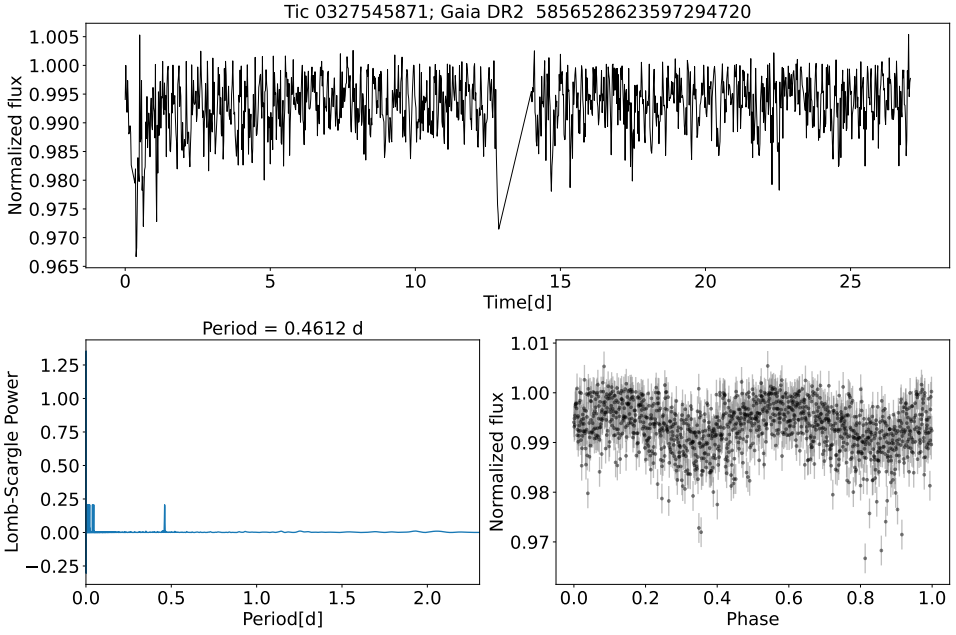

Figure B.7 Same as Figure B.1 but for *Gaia* DR2 5856528623597294720

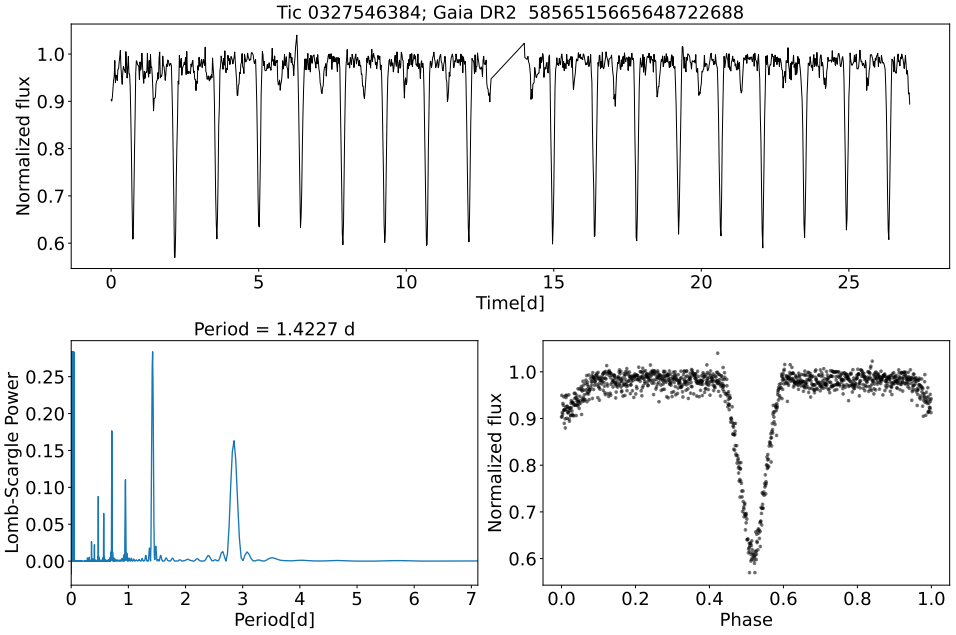

Figure B.8 Same as Figure B.1 but for *Gaia* DR2 5856515665648722688

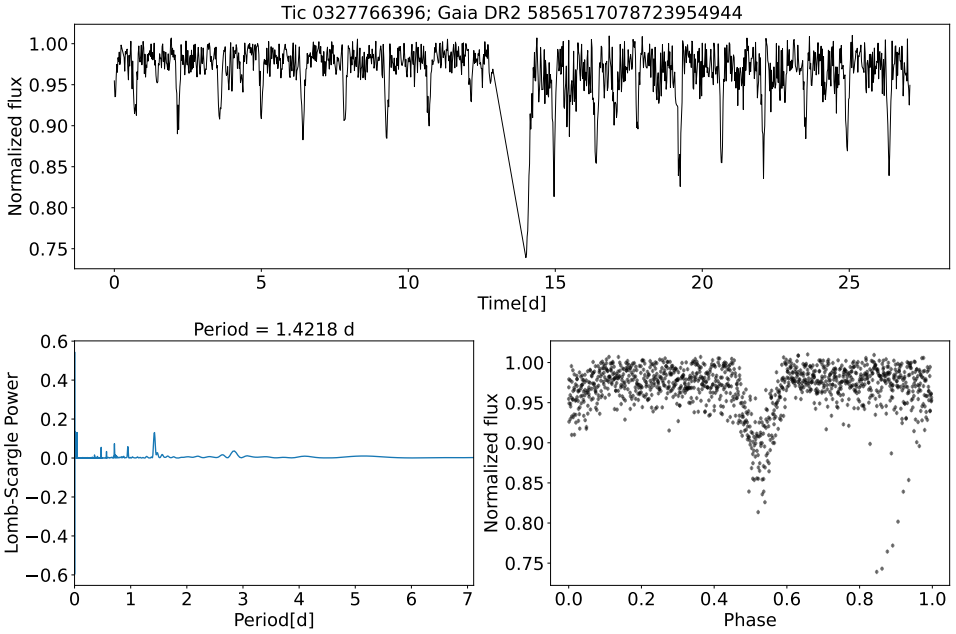

Figure B.9 Same as Figure B.1 but for *Gaia* DR2 5856517078723954944

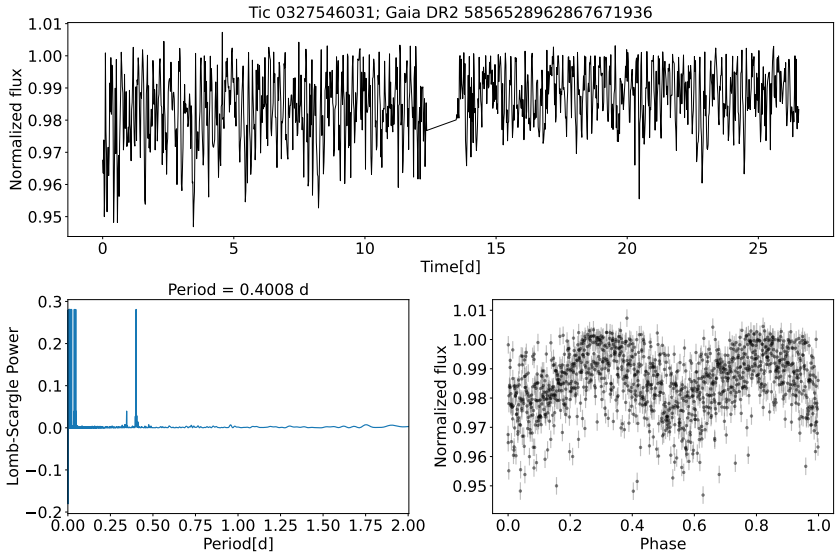

Figure B.10 Same as Figure B.1 but for *Gaia* DR2 5856528962867671936

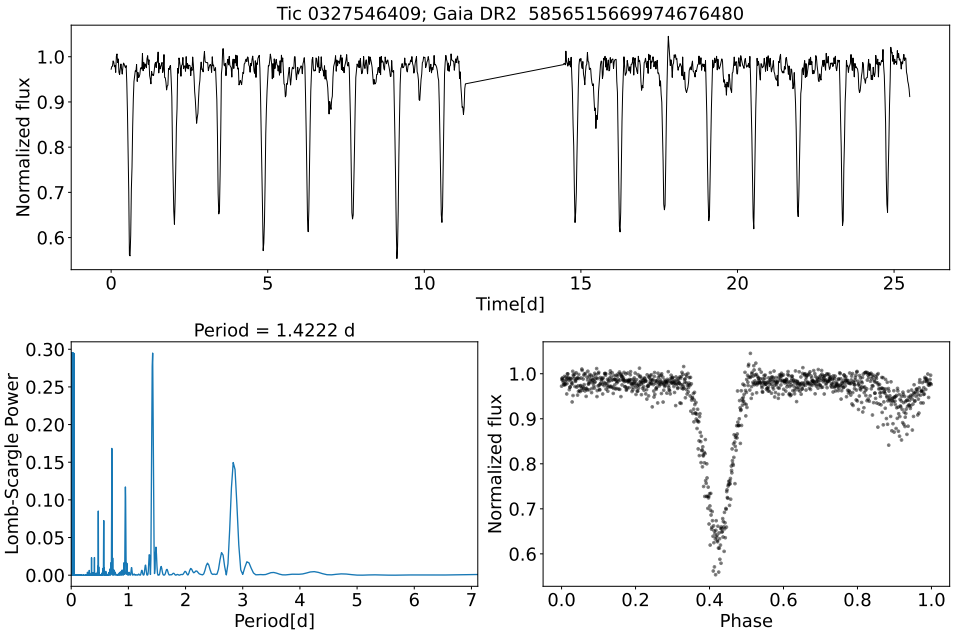

Figure B.11 Same as Figure B.1 but for *Gaia* DR2 5856515669974676480

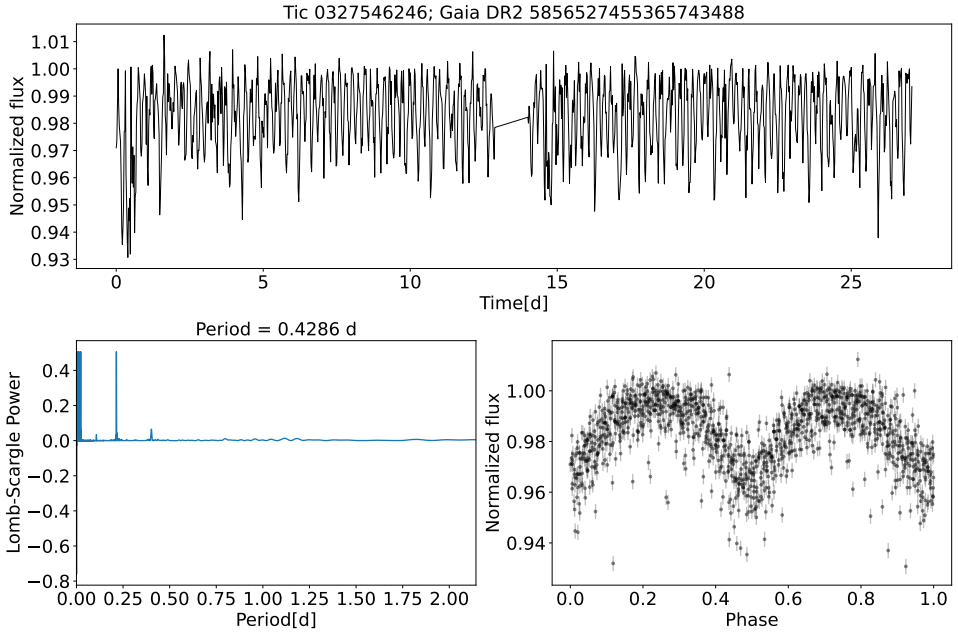

Figure B.12 Same as Figure B.1 but for *Gaia* DR2 5856527455365743488

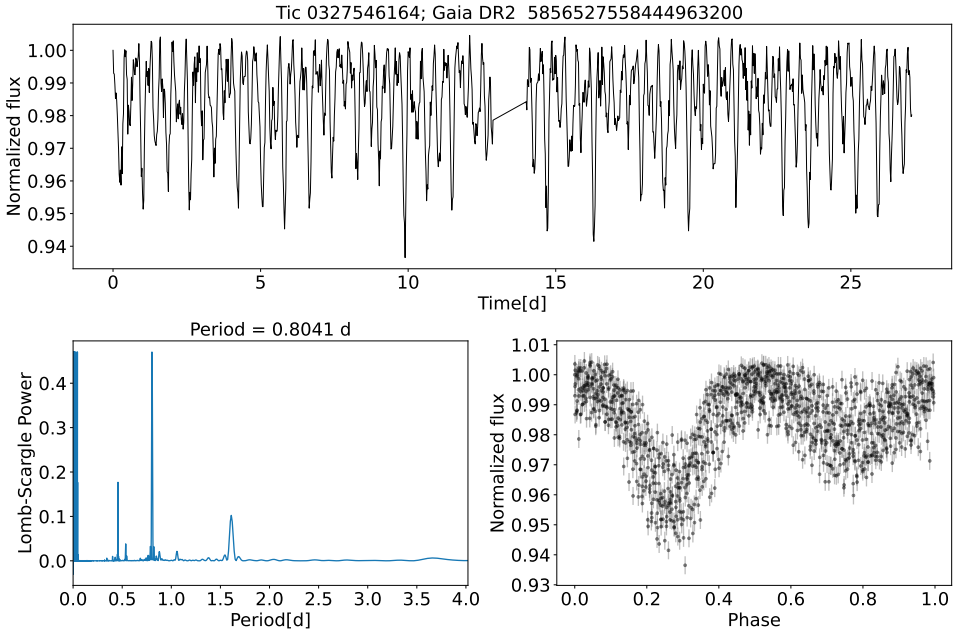

Figure B.13 Same as Figure B.1 but for *Gaia* DR2 5856527558444963200

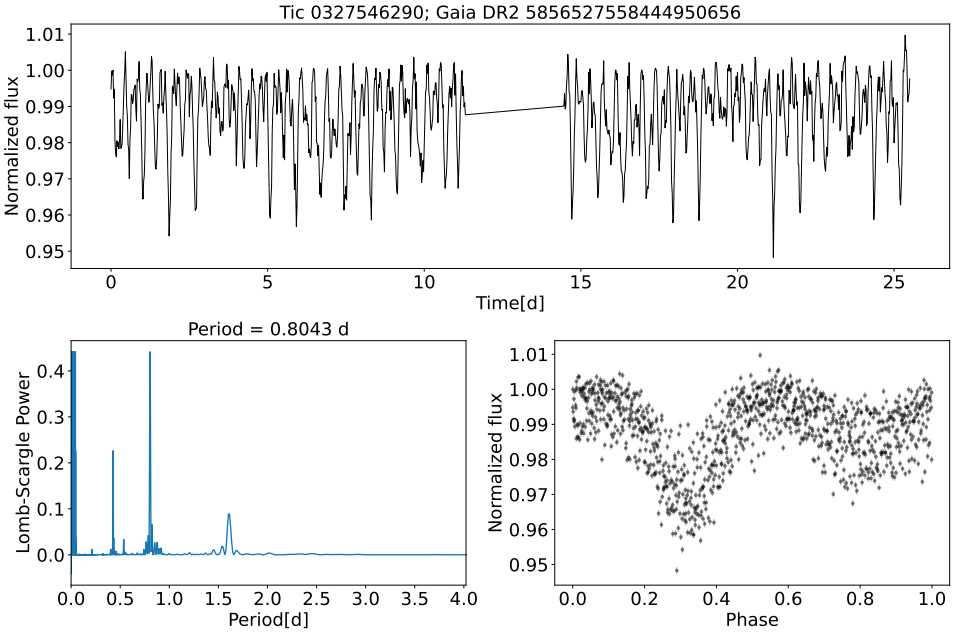

Figure B.14 Same as Figure B.1 but for *Gaia* DR2 5856527455365735680

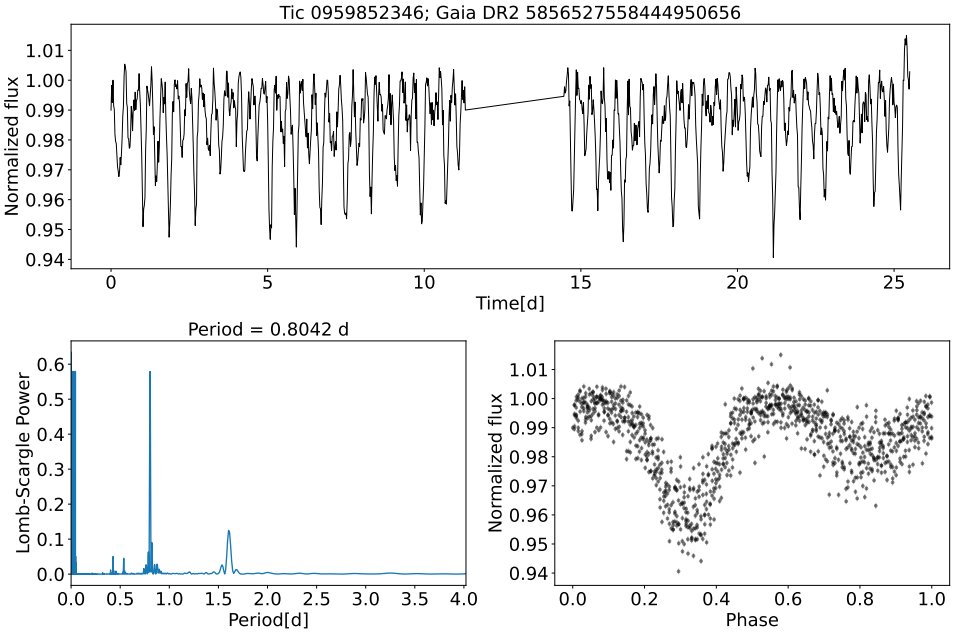

Figure B.15 Same as Figure B.1 but for *Gaia* DR2 5856527558444950656

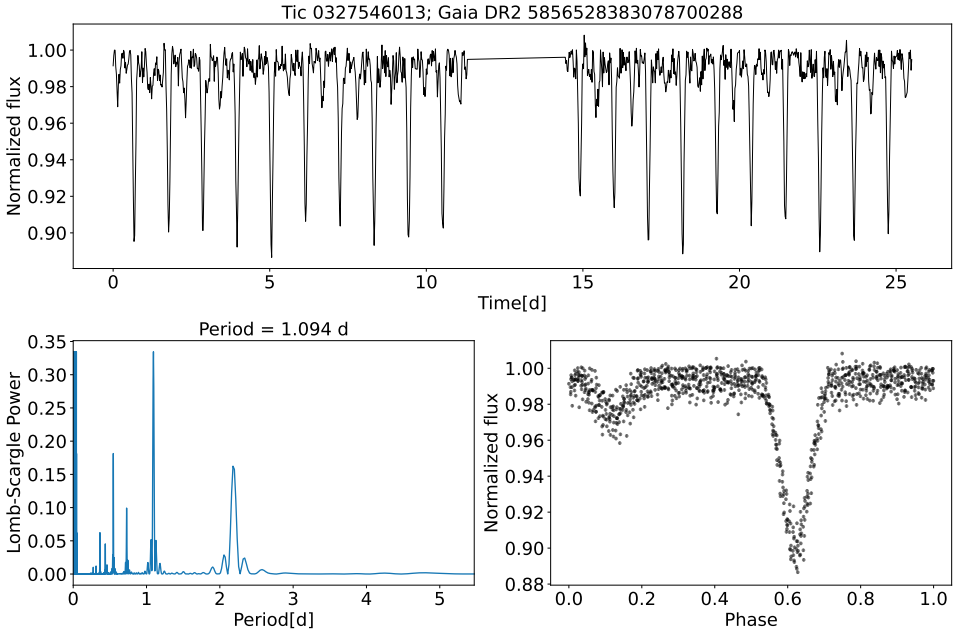

Figure B.16 Same as Figure B.1 but for *Gaia* DR2 5856528383078700288

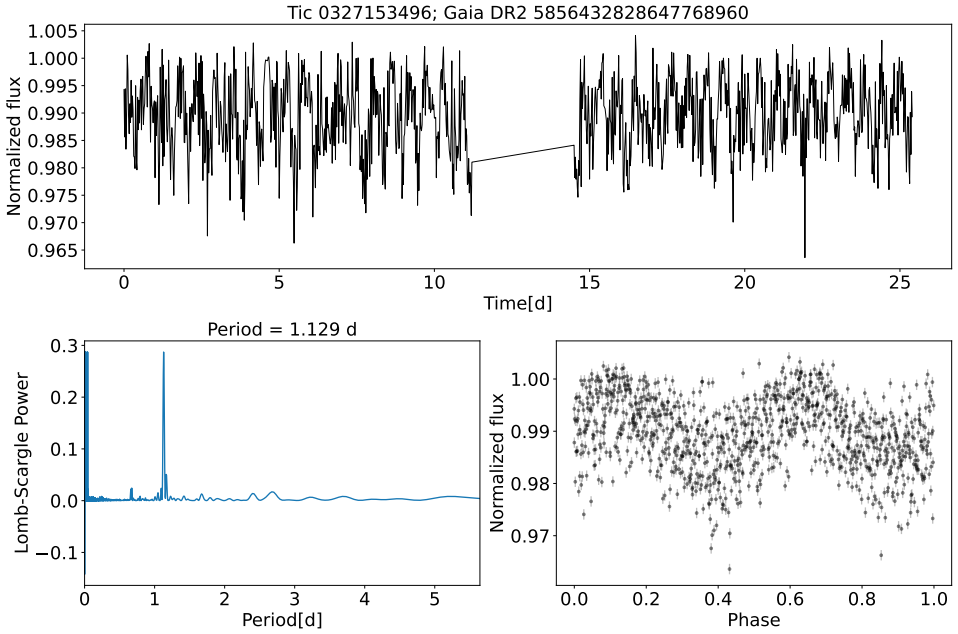

Figure B.17 Same as Figure B.1 but for *Gaia* DR2 5856432828647768960

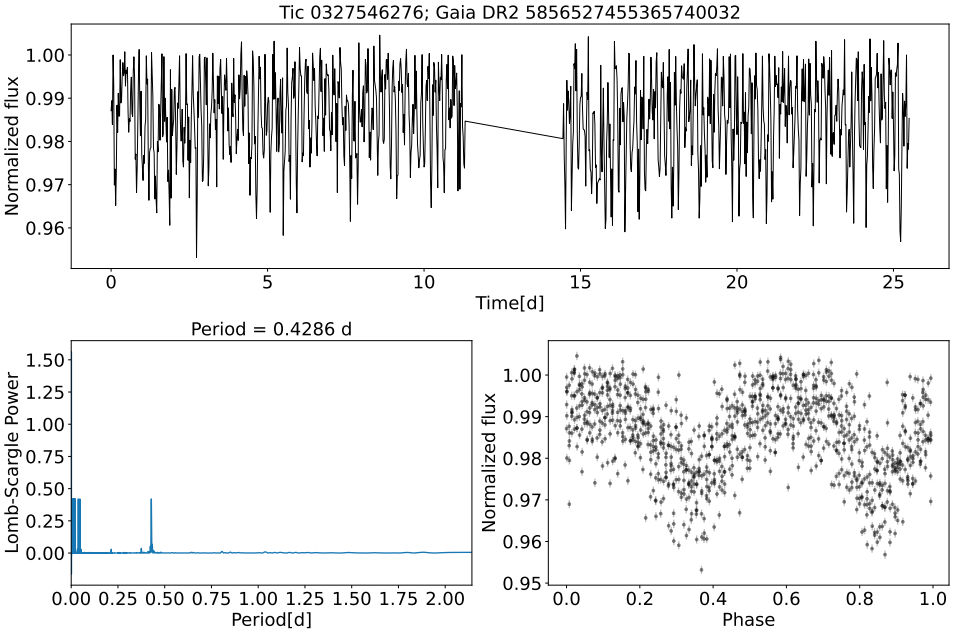

Figure B.18 Same as Figure B.1 but for *Gaia* DR2 5585652745536574003 2

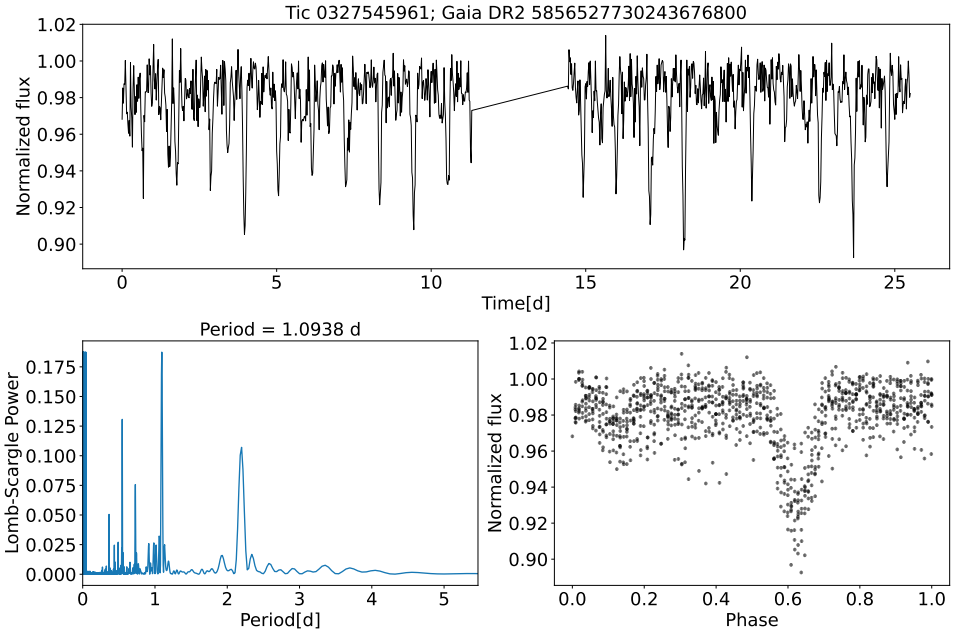

Figure B.19 Same as Figure B.1 but for *Gaia* DR2 5856527730243676800

B.1.3 Yellow stragglers of Collinder 261

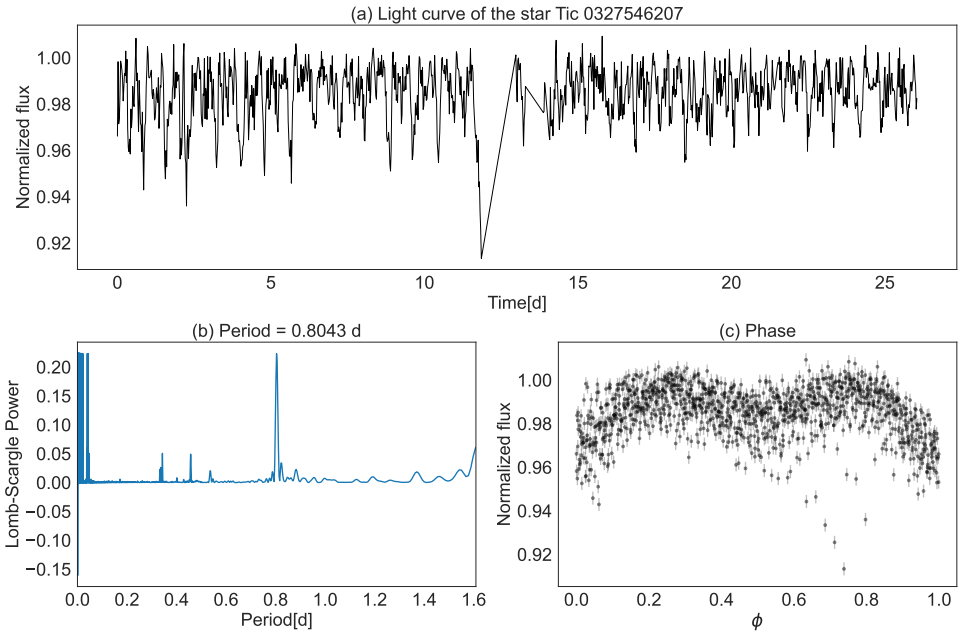

Figure B.20 Same as Figure B.1 but for Tic 0327546207. This star is a YSS!

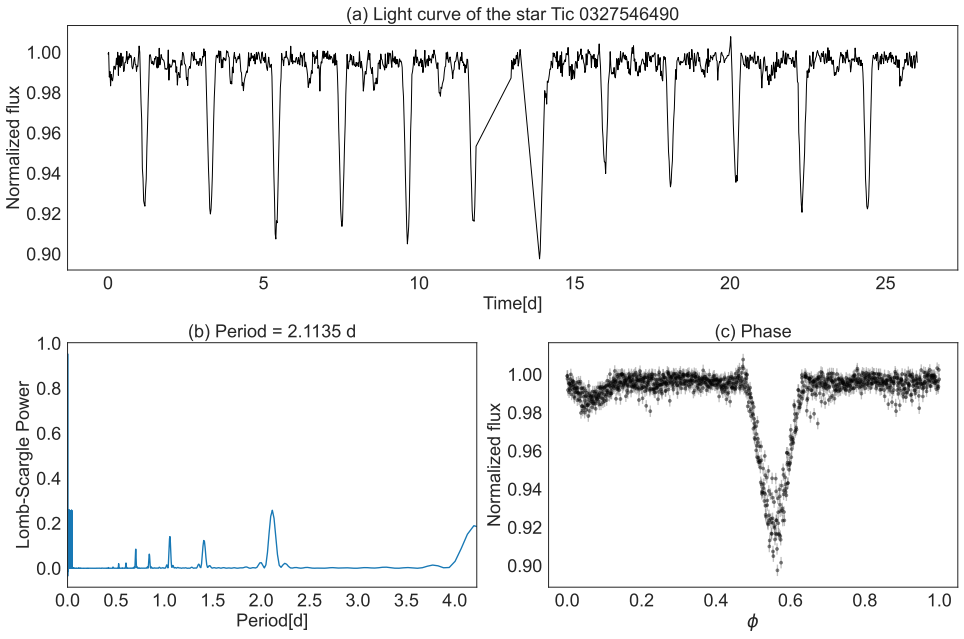

Figure B.21 Same as Figure B.1 but for Tic 0327546490. This star is a YSS!

Appendix C

C.1 Specific frequency vs. cluster parameters

Here we compare the specific frequency of BSS with the cluster age, binary fraction, mass, and number of binaries. The specific frequency was calculated as

$$F_{\mathrm{MS}}^{\mathrm{BSS}} = \log(N_{\mathrm{BSS}}/N_{\mathrm{MS}})$$

where N_{MS} is the number of MS stars selected on a range of 0.5 magnitude at 1 magnitude down the cluster MSTO.

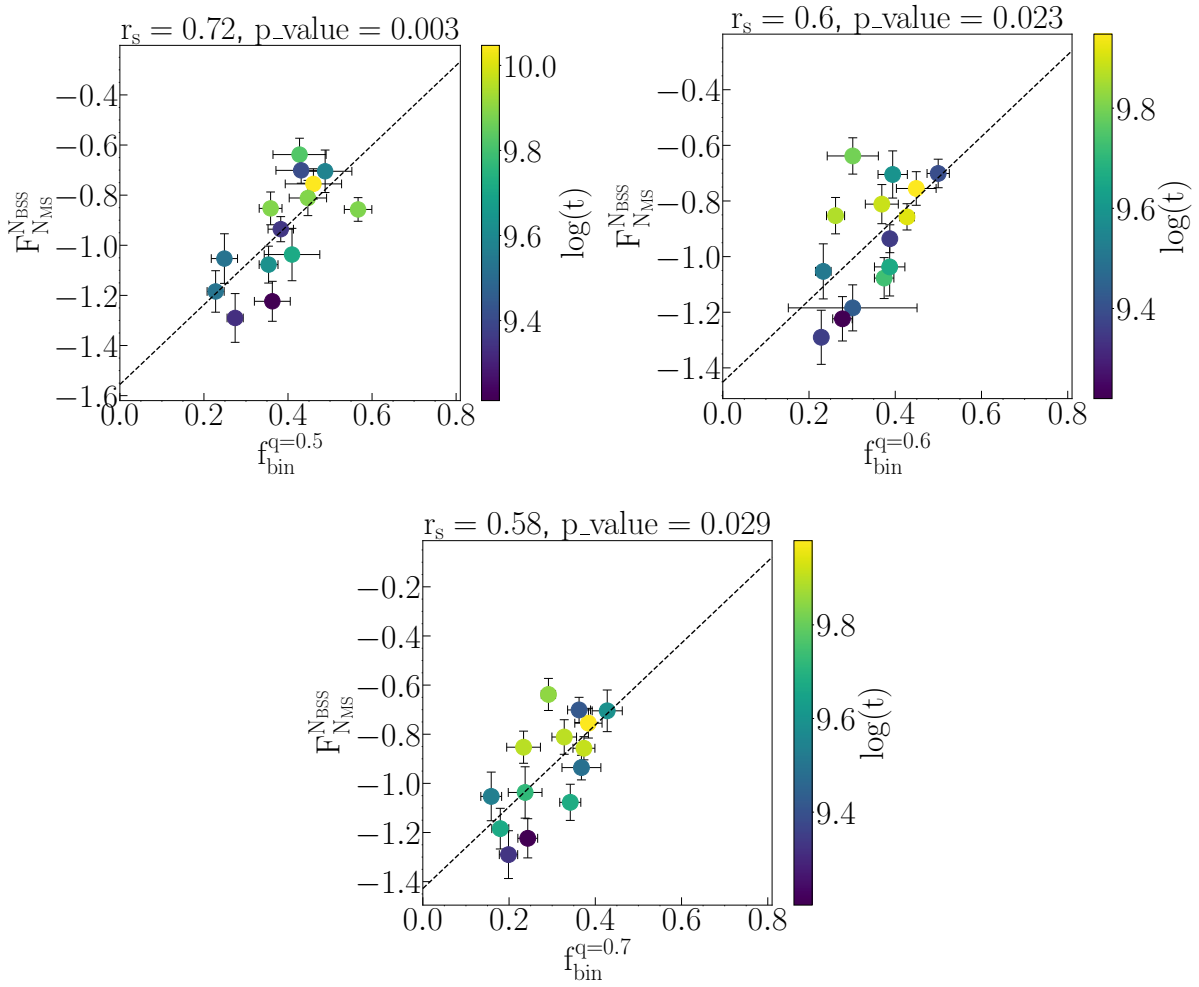

Figure C.1 Specific frequency of BSS as a function of binary fraction. The black filled circles are the fourteen clusters of our sample. Errors are Poissonian. Each plot corresponds to the different values of mass ratio (q) we used in `ASteCA` i.e., $q_{\rm min}$ = 0.5, 0.6 and 0.7.

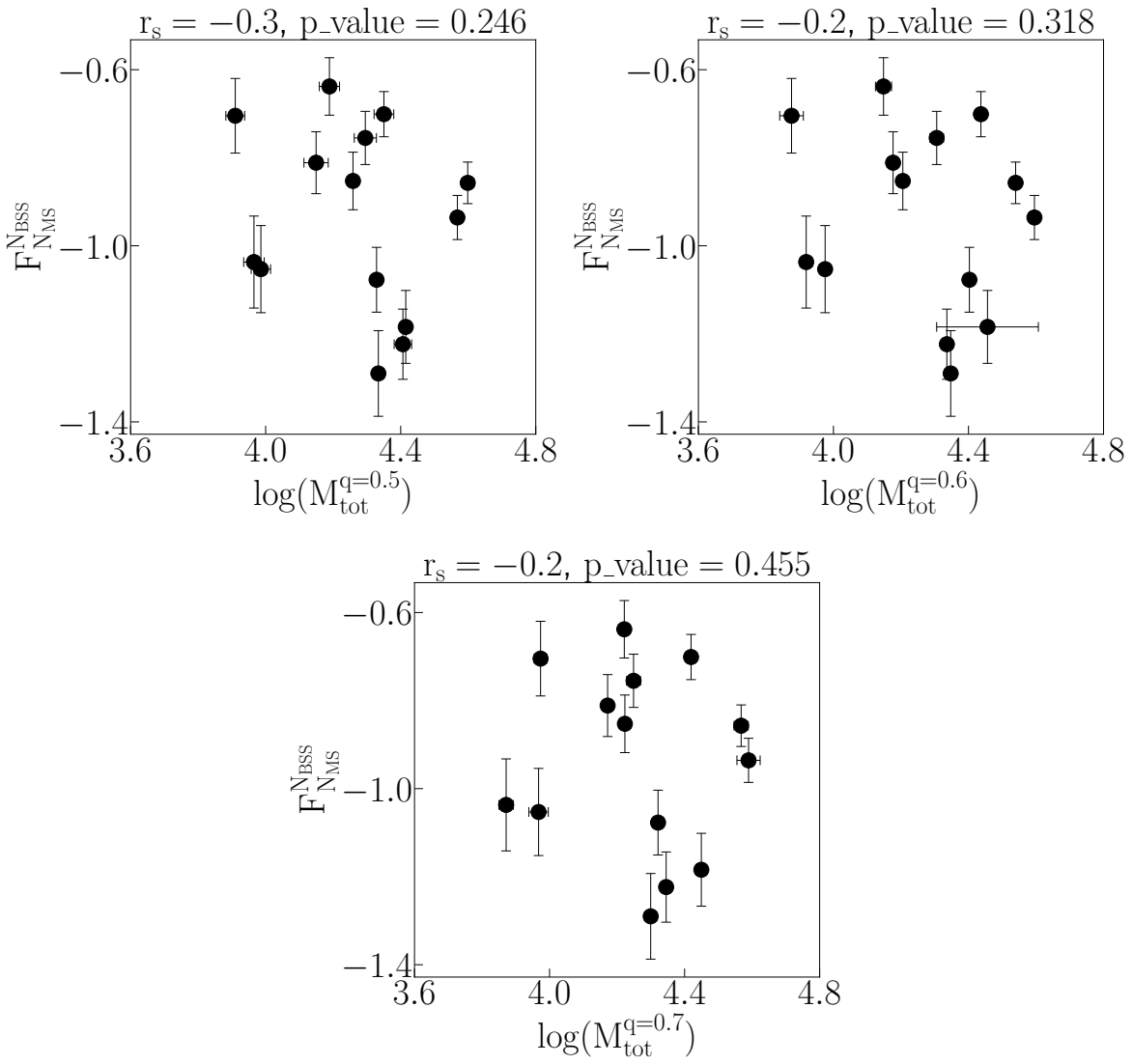

Figure C.2 Specific frequency of BSS as a function of the cluster total mass. Each plot corresponds to the different values of mass ratio (emphq) we used in `ASteCA`, i.e., $q_{\rm min} =$ 0.5, 0.6, and 0.7.

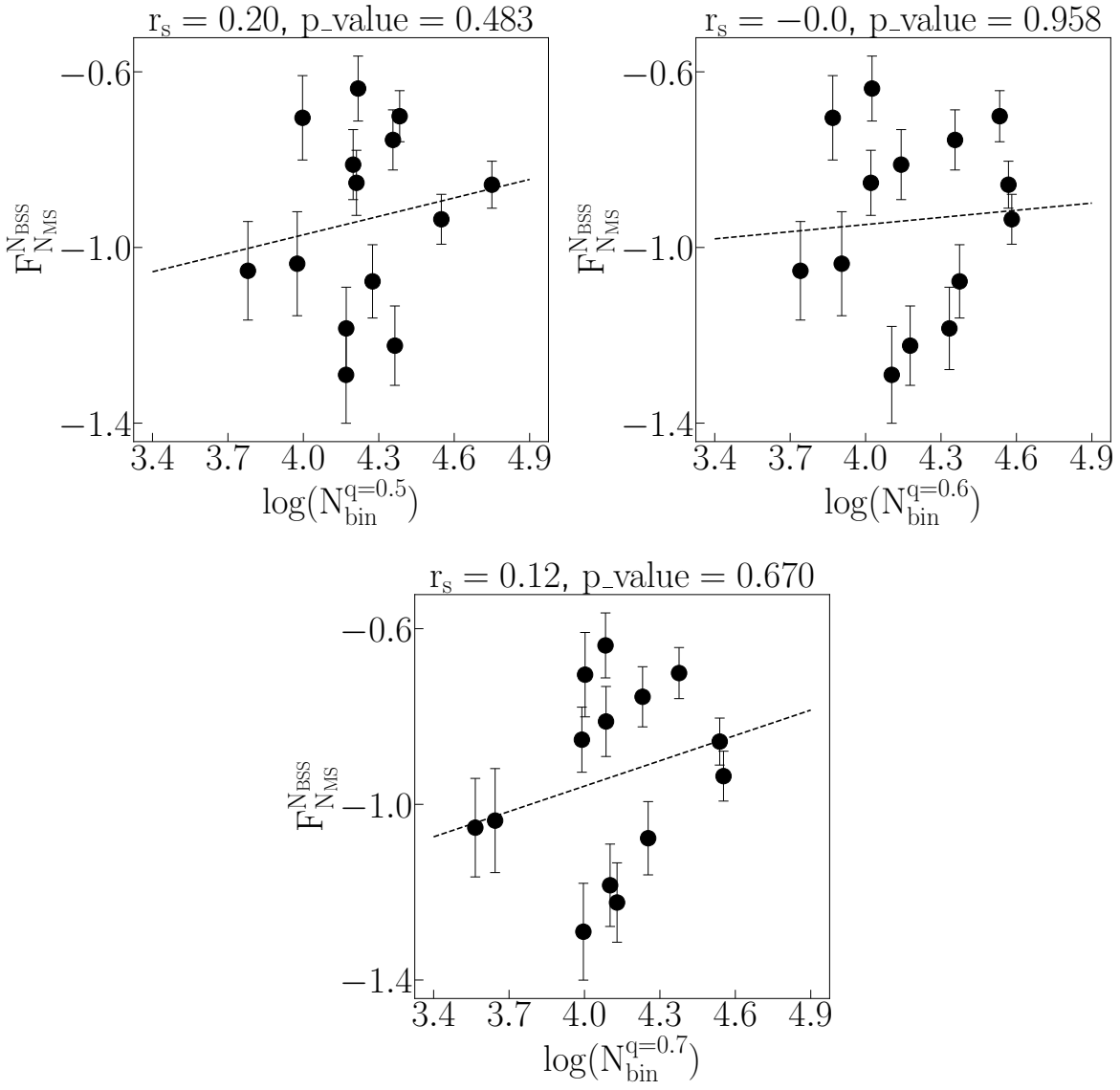

Figure C.3 Specific frequency of BSS as a function of the number of binaries on each cluster. The dashed black line indicates the best fit to the data. Each plot corresponds to the different values of mass ratio (q) we used in *ASteCA*, i.e., $q_{\rm min} = 0.5$, 0.6, and 0.7.

C.2 Color magnitude diagrams

Here we reported the remaining color magnitude-diagram of Chapter 3. The data comes from *Gaia* EDR3 and the members were selected using pyUPMASK as described in § 3.2. Both blue and yellow stragglers are shown within their corresponding regions.

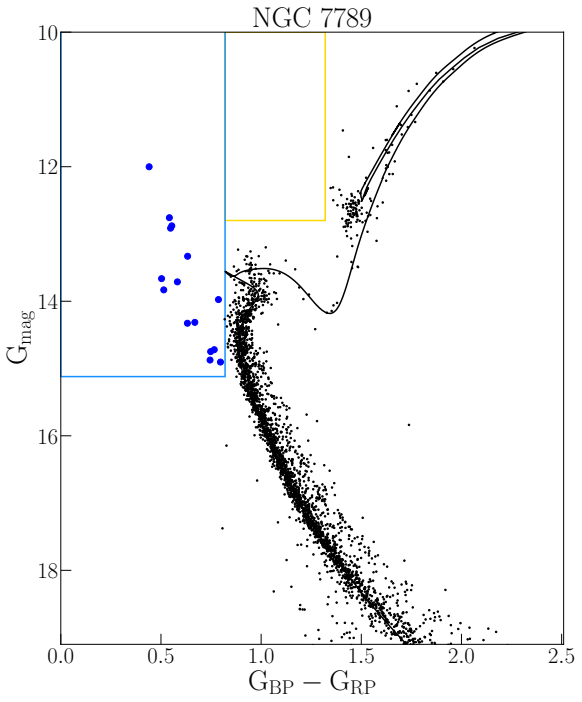

Figure C.4 Color-magnitude diagrams of the open cluster NGC 7789. The black filled circles are the *Gaia* members selected as described in § 3.2. Blue and Yellow filled circles are the Blue and Yellow straggler stars selected as described in § 2.3. Black line is the corresponding isochrone (Dotter, 2016) with the age, A_V and [Fe/H] value of the cluster.

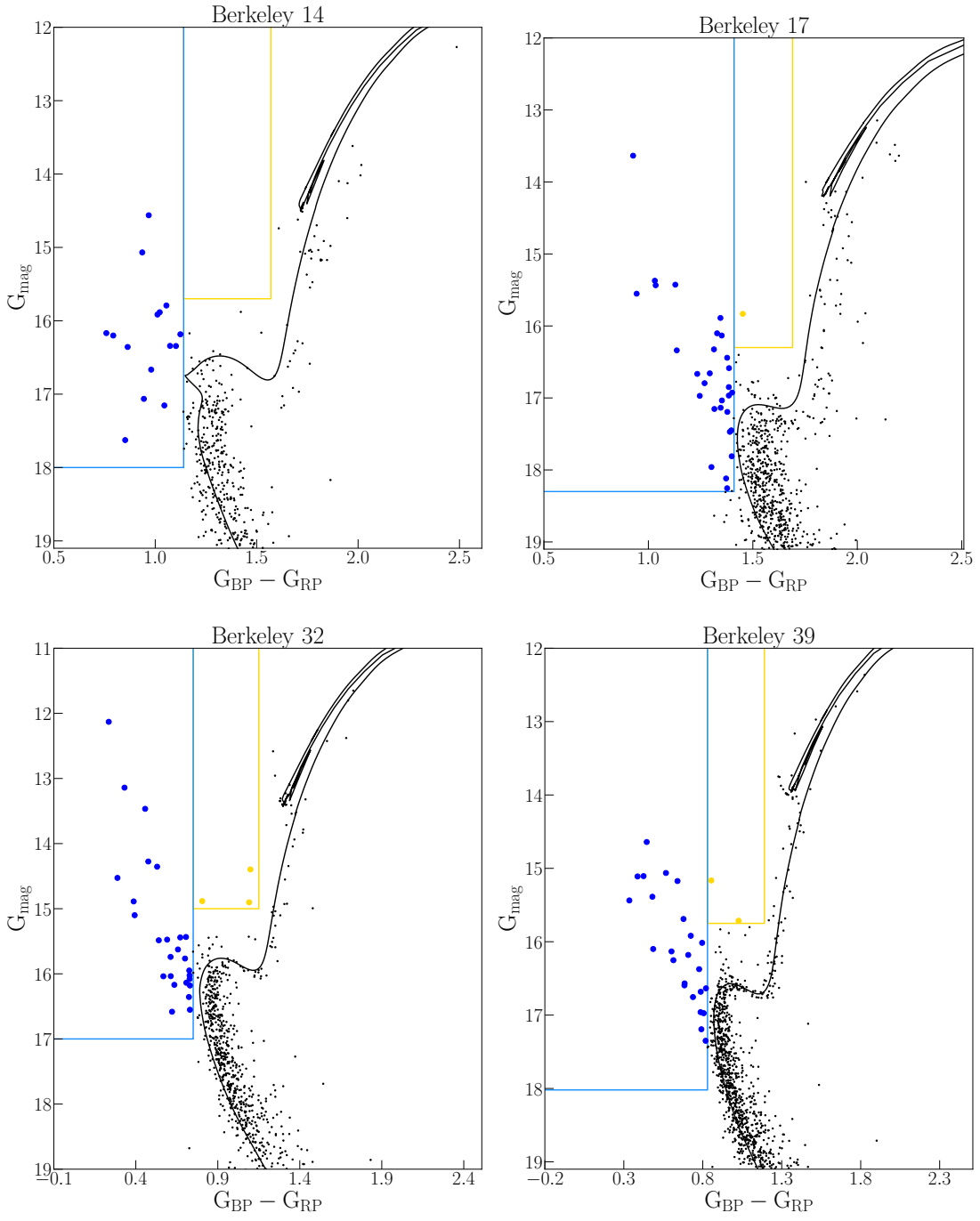

Figure C.5 same as Fig. C.4.

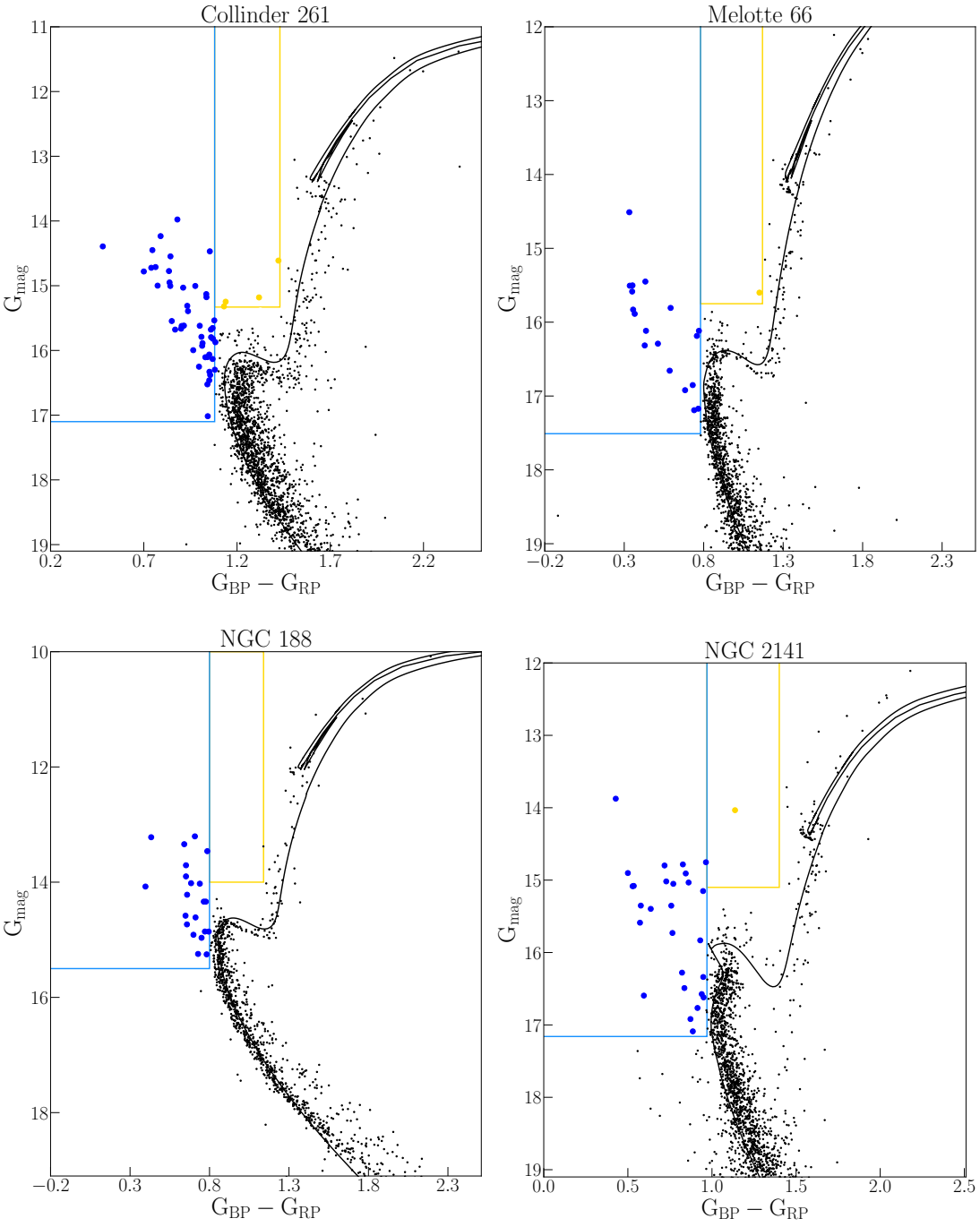

Figure C.6 same as Fig. C.4.

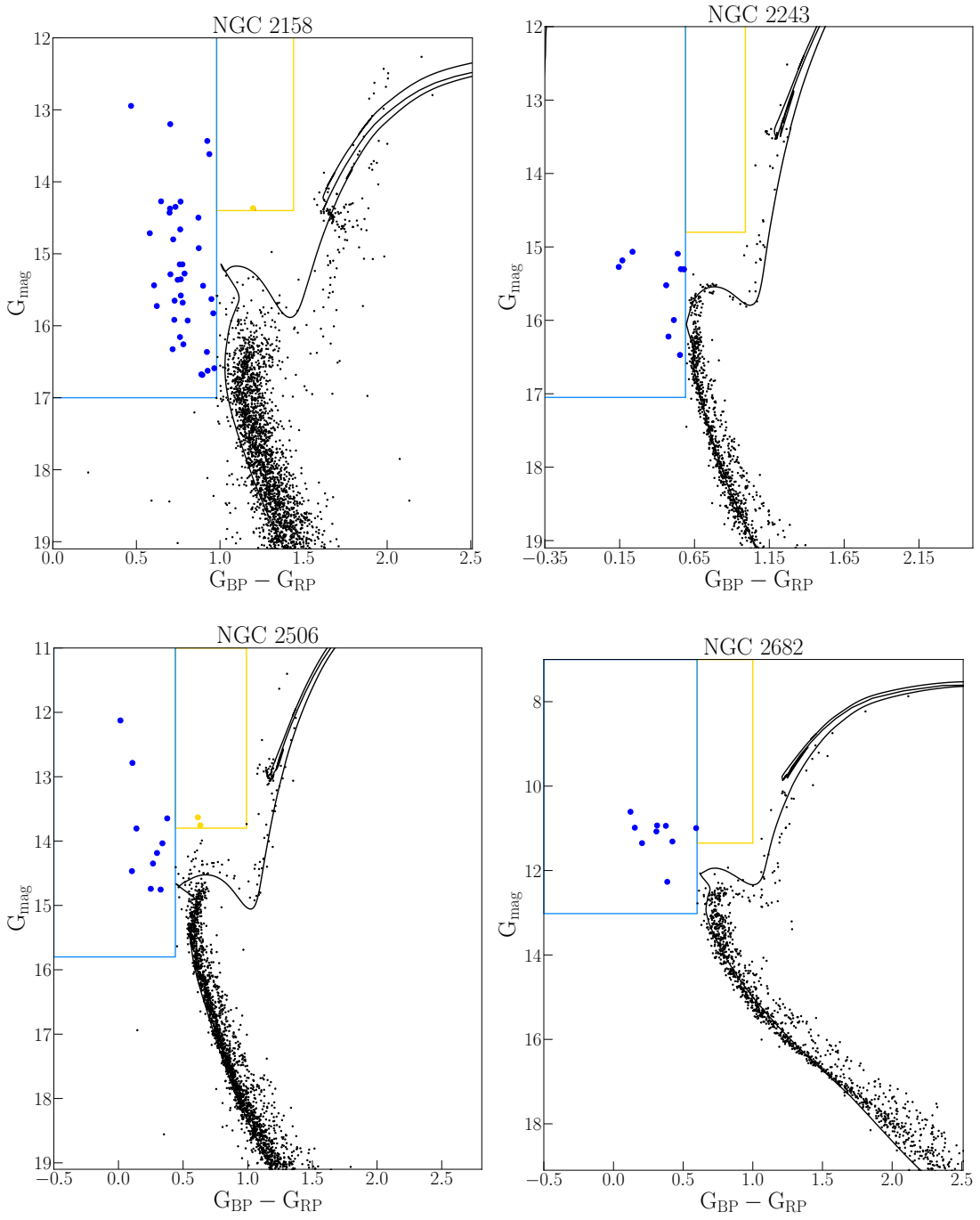

Figure C.7 same as Fig. C.4.

Appendix D

D.1 Radial distributions

The following figures are the cumulative radial distributions —that compare the Cumulative radial distributions of BSS and RGB — of the remaining clusters. For more information we refer the reader to S 2.7.

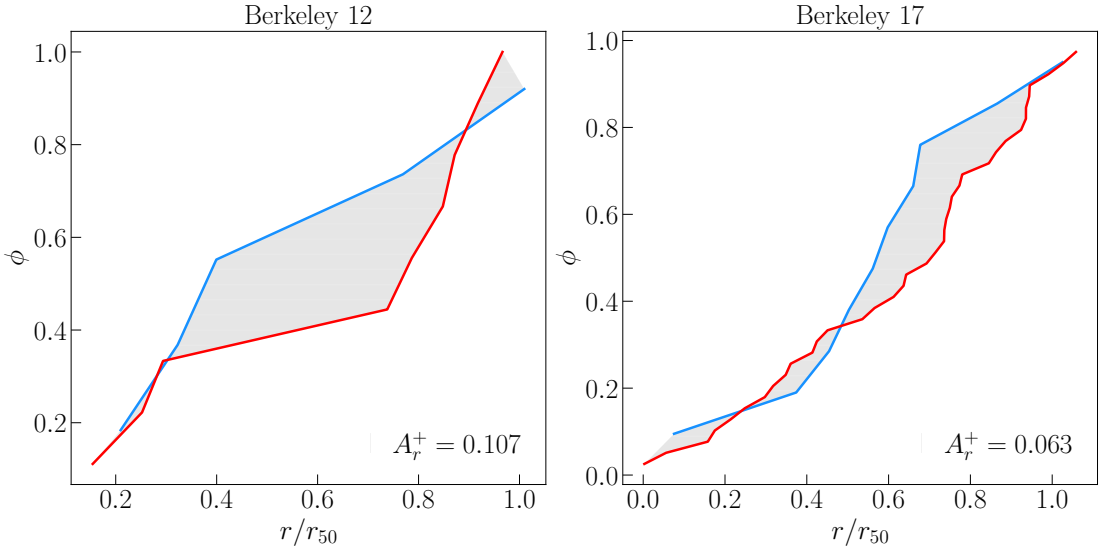

Figure D.1 Cumulative radial distribution of BSS (blue line) and RGB (red line) observed within one r_{50}. The size of the area between the two curves (shaded in gray) corresponds to the labeled valued of A_r^+.

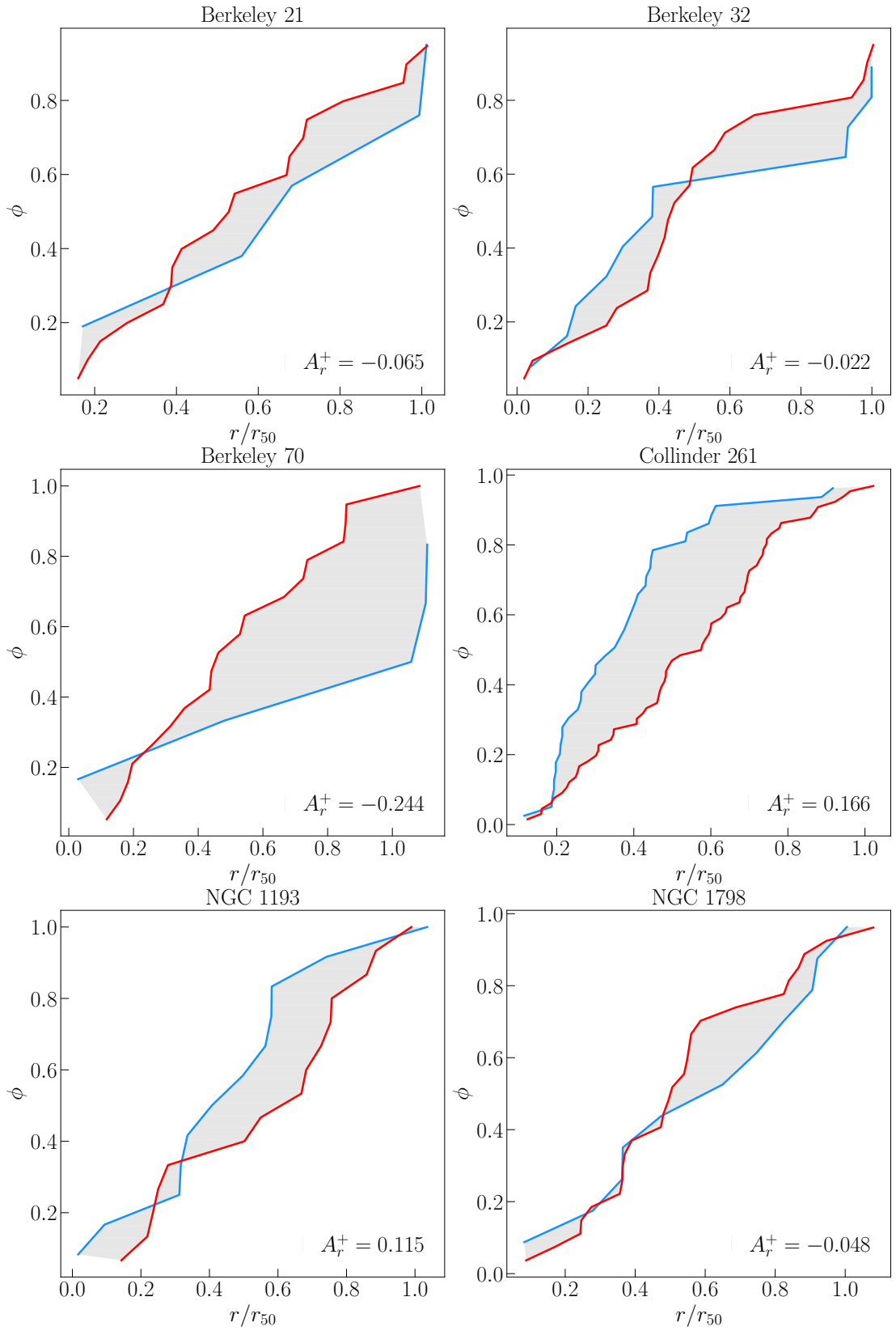

Figure D.2 same as Fig. D.1

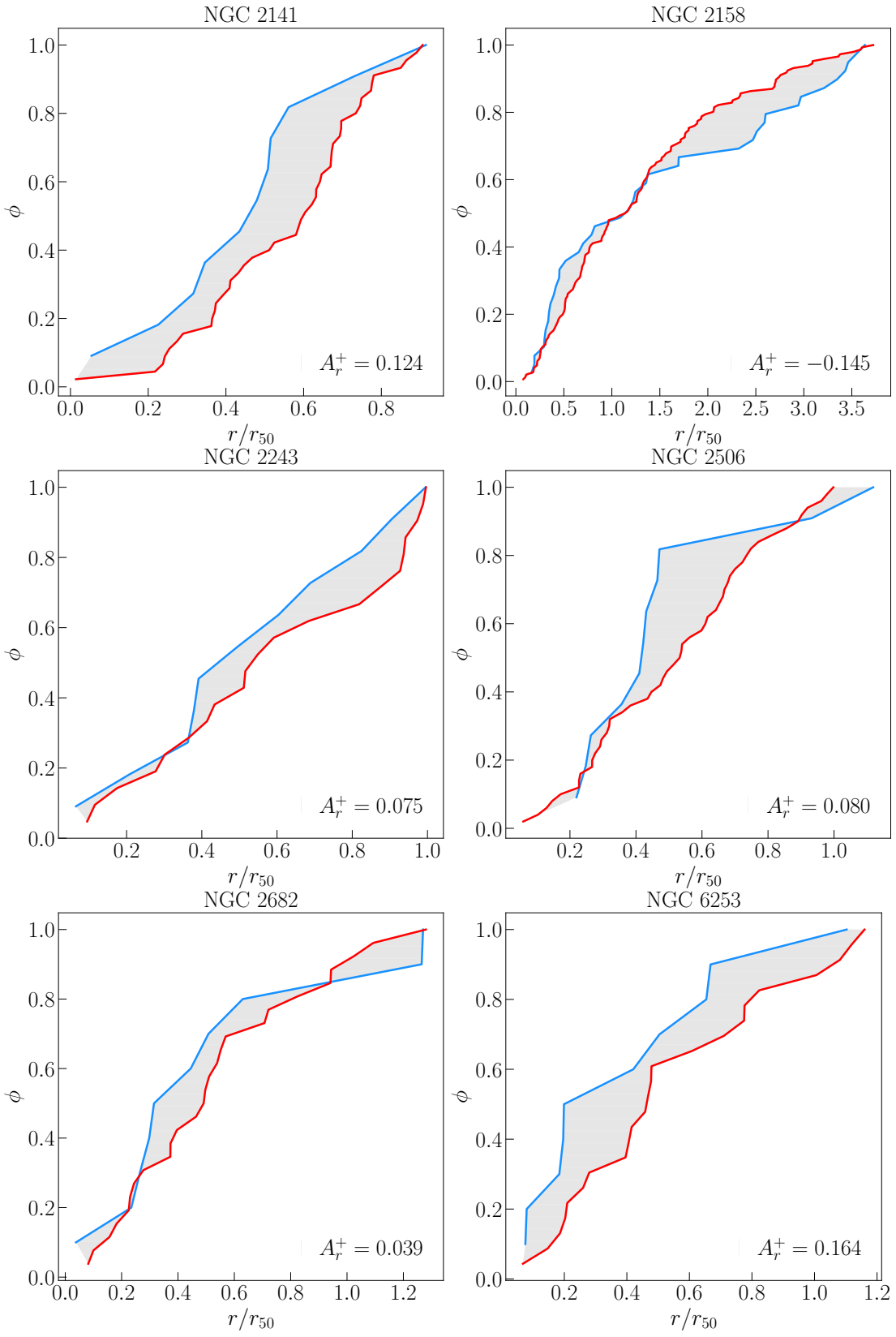

Figure D.3 same as Fig. D.1

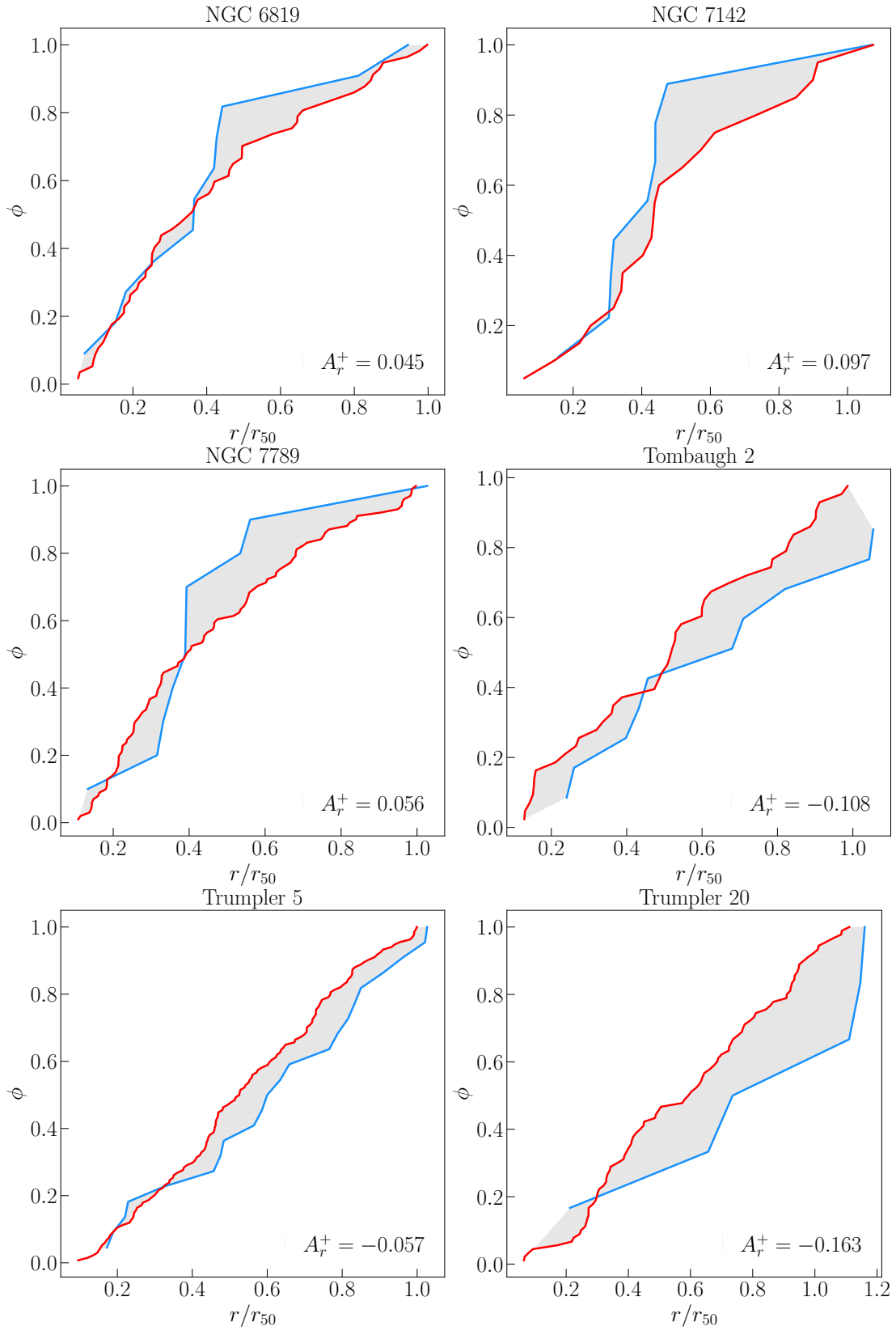

Figure D.4 same as Fig. D.1

Bibliography

Abate, C., O. R. Pols, R. G. Izzard, S. S. Mohamed, and S. E. de Mink (2013, April). Wind Roche-lobe overflow: Application to carbon-enhanced metal-poor stars. *A&A 552*, A26.

Ahumada, J. and E. Lapasset (1995, Feb). Catalogue of blue stragglers in open clusters. *A&AS 109*, 375–382.

Ahumada, J. A. and E. Lapasset (2007, February). New catalogue of blue stragglers in open clusters. *A&A 463*, 789–797.

Albrow, M. D., R. L. Gilliland, T. M. Brown, P. D. Edmonds, P. Guhathakurta, and A. Sarajedini (2001, October). The Frequency of Binary Stars in the Core of 47 Tucanae. *ApJ 559*(2), 1060–1081.

Alessandrini, E. and Cosmic-Lab Team (2016, January). N-body simulations with BSSs: defining mass segregation indicators. *MEMSAI 87*, 513.

Aller, A., J. Lillo-Box, D. Jones, L. F. Miranda, and S. Barceló Forteza (2020, March). Planetary nebulae seen with TESS: Discovery of new binary central star candidates from Cycle 1. *A&A 635*, A128.

Andrievsky, S. M., D. Schönberner, and J. S. Drilling (2000, April). Blue stragglers in open clusters. Part II. *A&A 356*, 517–528.

Antonini, F., S. Chatterjee, C. L. Rodriguez, M. Morscher, B. Pattabiraman, V. Kalogera, and F. A. Rasio (2016, January). Black Hole Mergers and Blue Stragglers from Hierarchical Triples Formed in Globular Clusters. *ApJ 816*(2), 65.

Arenou, F., X. Luri, C. Babusiaux, C. Fabricius, A. Helmi, T. Muraveva, A. C. Robin, F. Spoto, A. Vallenari, T. Antoja, T. Cantat-Gaudin, C. Jordi, N. Leclerc, C. Reylé, M. Romero-Gómez, and et al. (2018, Aug). Gaia Data Release 2. Catalogue validation. *A&A 616*, A17.

Arimoto, N. and M. Simoda (1981, May). On the Number Ratio of Horizontal Branch Stars to Red Giant Stars in Globular Clusters. *Ap&SS 76*(1), 73–81.

Avvakumova, E. A., O. Y. Malkov, and A. Y. Kniazev (2013, October). Eclipsing variables: Catalogue and classification. *Astronomische Nachrichten 334*, 860.

Bai, L., J. Zhong, L. Chen, J. Li, and J. Hou (2022, May). Discovery of Extended Structure Around Open Cluster COIN-Gaia 13 Based on Gaia EDR3. *Research in Astronomy and Astrophysics 22*(5), 055022.

Bailer-Jones, C. A. L., J. Rybizki, M. Fouesneau, G. Mantelet, and R. Andrae (2018, August). Estimating Distance from Parallaxes. IV. Distances to 1.33 Billion Stars in Gaia Data Release 2. *AJ 156*(2), 58.

Banks, T., T. Yontan, S. Bilir, and R. Canbay (2020, March). Vilnius photometry and Gaia astrometry of Melotte 105. *Journal of Astrophysics and Astronomy 41*(1), 6.

Beccari, G., E. Dalessandro, B. Lanzoni, F. R. Ferraro, A. Sollima, M. Bellazzini, and P. Miocchi (2013, Oct). Deep Multi-telescope Photometry of NGC 5466. I. Blue Stragglers and Binary Systems. *ApJ 776*(1), 60.

Beccari, G., A. Sollima, F. R. Ferraro, B. Lanzoni, M. Bellazzini, G. De Marchi, D. Valls-Gabaud, and R. T. Rood (2011, August). The Non-segregated Population of Blue Straggler Stars in the Remote Globular Cluster Palomar 14. *ApJL 737*(1), L3.

Benz, W. and J. G. Hills (1987, December). Three-dimensional Hydrodynamical Simulations of Stellar Collisions. I. Equal-Mass Main-Sequence Stars. *ApJ 323*, 614.

Benz, W. and J. G. Hills (1992, April). Three-dimensional Hydrodynamical Simulations of Colliding Stars. III. Collisions and Tidal Captures of Unequal-Mass Main-Sequence Stars. *ApJ 389*, 546.

Bertelli Motta, C., A. Pasquali, E. Caffau, and E. K. Grebel (2018, November). A chemical study of M67 candidate blue stragglers and evolved blue stragglers observed with APOGEE DR14. *MNRAS 480*(4), 4314–4326.

Bhattacharya, S., K. Vaidya, W. P. Chen, and G. Beccari (2019, April). The blue straggler population of the old open cluster Berkeley 17. *A&A 624*, A26.

Binney, J. and S. Tremaine (2008). *Galactic Dynamics: Second Edition*. Princeton University Press.

Boffin, H. M. J., G. Carraro, and G. Beccari (2014, Jun). Ecology of Blue Straggler Stars. *arXiv e-prints 413*, arXiv:1406.3909.

Bolte, M., J. E. Hesser, and P. B. Stetson (1993, May). Canada-France-Hawaii Telescope Observations of Globular Cluster Cores: Blue Straggler Stars in M3 (NGC 5272, GC 1339+286). *ApJL 408*, L89.

Bossini, D., A. Vallenari, A. Bragaglia, T. Cantat-Gaudin, R. Sordo, L. Balaguer-Núñez, C. Jordi, A. Moitinho, C. Soubiran, L. Casamiquela, R. Carrera, and U. Heiter (2019, March). Age determination for 269 Gaia DR2 open clusters. *A&A 623*, A108.

Bragaglia, A., P. Sestito, S. Villanova, E. Carretta, S. Randich, and M. Tosi (2008, Mar). Old open clusters as key tracers of Galactic chemical evolution. II. Iron and elemental abundances in NGC 2324, NGC 2477 NGC 2660, NGC 3960, and Berkeley 32. *A&A 480*(1), 79–90.

Bragaglia, A. and M. Tosi (2006, Mar). The Bologna Open Cluster Chemical Evolution Project: Midterm Results from the Photometric Sample. *AJ 131*(3), 1544–1558.

Breger, M. and J. C. Wheeler (1980, August). Photometry and polarimetry of the extreme blue straggler K 1211 in NGC 7789. *PASP 92*, 514–517.

Bressan, A., P. Marigo, L. Girardi, B. Salasnich, C. Dal Cero, S. Rubele, and A. Nanni (2012, November). PARSEC: stellar tracks and isochrones with the PAdova and TRieste Stellar Evolution Code. *MNRAS 427*, 127–145.

Cantat-Gaudin, T. and F. Anders (2020, January). Clusters and mirages: cataloguing stellar aggregates in the Milky Way. *A&A 633*, A99.

Cantat-Gaudin, T., C. Jordi, A. Vallenari, A. Bragaglia, L. Balaguer-Núñez, C. Soubiran, D. Bossini, A. Moitinho, A. Castro-Ginard, A. Krone-Martins, L. Casamiquela, R. Sordo, and R. Carrera (2018, Oct). A Gaia DR2 view of the open cluster population in the Milky Way. *A&A 618*, A93.

Carraro, G., E. Costa, and J. A. Ahumada (2010, October). Photometric Characterization of the Galactic Star Cluster Trumpler 20. *AJ 140*(4), 954–961.

Carraro, G., G. de Silva, L. Monaco, A. P. Milone, and R. Mateluna (2014, June). Updated properties of the old open cluster Melotte 66: Searching for multiple stellar populations. *A&A 566*, A39.

Carraro, G., R. A. Vázquez, and A. Moitinho (2008, May). Blue straggler stars in Galactic open clusters and the effect of field star contamination. *A&A 482*, 777–781.

Carraro, G., S. Villanova, L. Monaco, G. Beccari, J. A. Ahumada, and H. M. J. Boffin (2014, February). Chemical abundance analysis of the old, rich open cluster Trumpler 20. *A&A 562*, A39.

Carrera, R., A. Bragaglia, T. Cantat-Gaudin, A. Vallenari, L. Balaguer-Núñez, D. Bossini, L. Casamiquela, C. Jordi, R. Sordo, and C. Soubiran (2019, March). Open clusters in APOGEE and GALAH. Combining Gaia and ground-based spectroscopic surveys. *A&A 623*, A80.

Carretta, E., A. Bragaglia, R. G. Gratton, and M. Tosi (2005, October). High-resolution spectroscopy of the old open cluster Collinder 261: abundances of iron and other elements. *A&A 441*(1), 131–140.

Castelli, F. and R. L. Kurucz (2003, Jan). New Grids of ATLAS9 Model Atmospheres. In N. Piskunov, W. W. Weiss, and D. F. Gray (Eds.), *Modelling of Stellar Atmospheres*, Volume 210 of *IAU Symposium*, pp. A20.

Chatterjee, S., F. A. Rasio, A. Sills, and E. Glebbeek (2013, November). Stellar Collisions and Blue Straggler Stars in Dense Globular Clusters. *ApJ 777*(2), 106.

Chen, X. and Z. Han (2008, March). Binary coalescence from case A evolution: mergers and blue stragglers. *MNRAS 384*(4), 1263–1276.

Chen, X. and Z. Han (2009, June). Primordial binary evolution and blue stragglers. *MNRAS 395*(4), 1822–1836.

Clark, L. L., E. L. Sandquist, and M. Bolte (2004, December). The Blue Straggler and Main-Sequence Binary Population of the Low-Mass Globular Cluster Palomar 13. *AJ 128*(6), 3019–3033.

da Silveira, M. D., C. B. Pereira, and N. A. Drake (2018, June). Red giants and yellow stragglers in the young open cluster NGC 2447. *MNRAS 476*(4), 4907–4931.

Dalessandro, E., F. R. Ferraro, D. Massari, B. Lanzoni, P. Miocchi, G. Beccari, A. Bellini, A. Sills, S. Sigurdsson, A. Mucciarelli, and L. Lovisi (2013, December). Double Blue Straggler Sequences in Globular Clusters: The Case of NGC 362. *ApJ 778*(2), 135.

Dalessandro, E., B. Lanzoni, F. R. Ferraro, F. Vespe, M. Bellazzini, and R. T. Rood (2008, July). Another Nonsegregated Blue Straggler Population in a Globular Cluster: the Case of NGC 2419. *ApJ 681*(1), 311–319.

Davies, M. B., G. Piotto, and F. de Angeli (2004, March). Blue straggler production in globular clusters. *MNRAS 349*(1), 129–134.

de Marchi, F., F. de Angeli, G. Piotto, G. Carraro, and M. B. Davies (2006, November). Search and analysis of blue straggler stars in open clusters. *A&A 459*, 489–497.

De Silva, G. M., K. C. Freeman, M. Asplund, J. Bland-Hawthorn, M. S. Bessell, and R. Collet (2007, March). Chemical Homogeneity in Collinder 261 and Implications for Chemical Tagging. *AJ 133*, 1161–1175.

Dias, W. S., B. S. Alessi, A. Moitinho, and J. R. D. Lépine (2002, July). New catalogue of optically visible open clusters and candidates. *A&A 389*, 871–873.

Dias, W. S., H. Monteiro, T. C. Caetano, J. R. D. Lépine, M. Assafin, and A. F. Oliveira (2014, April). Proper motions of the optically visible open clusters based on the UCAC4 catalog. *A&A 564*, A79.

Dias, W. S., H. Monteiro, A. Moitinho, J. R. D. Lépine, G. Carraro, E. Paunzen, B. Alessi, and L. Villela (2021, June). Updated parameters of 1743 open clusters based on Gaia DR2. *MNRAS 504*(1), 356–371.

Diedenhofen, B. and J. Musch (2015, 04). cocor: A comprehensive solution for the statistical comparison of correlations. *PLOS ONE 10*(4), 1–12.

Djorgovski, S. (1993, January). Physical Parameters of Galactic Globular Clusters. In S. G. Djorgovski and G. Meylan (Eds.), *Structure and Dynamics of Globular Clusters*, Volume 50 of *Astronomical Society of the Pacific Conference Series*, pp. 373.

Donati, P., T. Cantat Gaudin, A. Bragaglia, E. Friel, L. Magrini, R. Smiljanic, A. Vallenari, M. Tosi, R. Sordo, G. Tautvaišienė, S. Blanco-Cuaresma, and et al. (2014, January). The Gaia-ESO Survey: Reevaluation of the parameters of the open cluster Trumpler 20 using photometry and spectroscopy. *A&A 561*, A94.

Dotter, A. (2016, January). MESA Isochrones and Stellar Tracks (MIST) 0: Methods for the Construction of Stellar Isochrones. *ApJS 222*(1), 8.

Eggen, O. J. (1983, March). Pseudocepheids. I. R Puppis, HR 4441, HR 4511, and AI CMi. *AJ 88*, 386–403.

Eggen, O. J. and J. Iben, I. (1988, January). Stellar Evolution: Theory and the Real World II. Blue Stragglers, Star Bursts, and Binary Stars. In V. M. Blanco and M. M. Phillips (Eds.), *Progress and Opportunities in Southern Hemisphere Optical Astronomy. The CTIO 25th Anniversary Symposium*, Volume 1 of *Astronomical Society of the Pacific Conference Series*, pp. 239.

Eigenbrod, A., J. C. Mermilliod, J. J. Clariá, J. Andersen, and M. Mayor (2004, August). Red giants in open clusters. XI. Membership, duplicity, and structure of NGC 2477. *A&A 423*, 189–197.

Evans, D. W., M. Riello, F. De Angeli, J. M. Carrasco, P. Montegriffo, C. Fabricius, C. Jordi, L. Palaversa, C. Diener, G. Busso, C. Cacciari, F. van Leeuwen, P. W. Burgess, and et al. (2018, Aug). Gaia Data Release 2. Photometric content and validation. *A&A 616*, A4.

Feinstein, A. D., B. T. Montet, D. Foreman-Mackey, M. E. Bedell, N. Saunders, J. L. Bean, J. L. Christiansen, C. Hedges, R. Luger, D. Scolnic, and J. V. d. M. Cardoso (2019, September). eleanor: An Open-source Tool for Extracting Light Curves from the TESS Full-frame Images. *PASP 131*(1003), 094502.

Ferraro, F. R., G. Beccari, E. Dalessandro, B. Lanzoni, A. Sills, R. T. Rood, F. F. Pecci, A. I. Karakas, P. Miocchi, and S. Bovinelli (2009, December). Two distinct sequences of blue straggler stars in the globular cluster M 30. *Nature 462*(7276), 1028–1031.

Ferraro, F. R., F. Fusi Pecci, and M. Bellazzini (1995, February). Blue stragglers in Galactic globular clusters: playing with specific quantities. *A&A 294*, 80–88.

Ferraro, F. R., B. Lanzoni, E. Dalessandro, G. Beccari, M. Pasquato, P. Miocchi, R. T. Rood, S. Sigurdsson, A. Sills, E. Vesperini, M. Mapelli, R. Contreras, N. Sanna, and A. Mucciarelli (2012, Dec). Dynamical age differences among coeval star clusters as revealed by blue stragglers. *Nature 492*(7429), 393–395.

Ferraro, F. R., B. Lanzoni, S. Raso, D. Nardiello, E. Dalessandro, E. Vesperini, G. Piotto, C. Pallanca, G. Beccari, A. Bellini, M. Libralato, J. Anderson, A. Aparicio, L. R. Bedin, S. Cassisi, A. P. Milone, S. Ortolani, A. Renzini, M. Salaris, and R. P. van der Marel (2018, June). The Hubble Space Telescope UV Legacy Survey of Galactic Globular Clusters. XV. The Dynamical Clock: Reading Cluster Dynamical Evolution from the Segregation Level of Blue Straggler Stars. *ApJ 860*(1), 36.

Ferraro, F. R., B. Paltrinieri, F. Fusi Pecci, C. Cacciari, B. Dorman, R. T. Rood, R. Buonanno, C. E. Corsi, D. Burgarella, and M. Laget (1997, August). HST observations of blue Straggler stars in the core of the globular cluster M 3. *A&A 324*, 915–928.

Ferraro, F. R., F. F. Pecci, C. Cacciari, C. Corsi, R. Buonanno, G. G. Fahlman, and H. B. Richer (1993, December). Blue Stragglers in the Galactic Globular Cluster M3: Evidence for two Populations. *AJ 106*, 2324.

Ferraro, F. R., E. Sabbi, R. Gratton, G. Piotto, B. Lanzoni, E. Carretta, R. T. Rood, A. Sills, F. Fusi Pecci, S. Moehler, G. Beccari, S. Lucatello, and N. Compagni (2006, August). Discovery of Carbon/Oxygen-depleted Blue Straggler Stars in 47 Tucanae: The Chemical Signature of a Mass Transfer Formation Process. *ApJL 647*(1), L53–L56.

Ferraro, F. R., A. Sills, R. T. Rood, B. Paltrinieri, and R. Buonanno (2003, May). Blue Straggler Stars: A Direct Comparison of Star Counts and Population Ratios in Six Galactic Globular Clusters. *ApJ 588*(1), 464–477.

Fisher, J., K.-P. Schröder, and R. C. Smith (2005, August). What a local sample of spectroscopic binaries can tell us about the field binary population. *MNRAS 361*(2), 495–503.

Gaia Collaboration, A. G. A. Brown, A. Vallenari, T. Prusti, J. H. J. de Bruijne, C. Babusiaux, C. A. L. Bailer-Jones, M. Biermann, D. W. Evans, L. Eyer, and et al. (2018, August). Gaia Data Release 2. Summary of the contents and survey properties. *A&A 616*, A1.

Gaia Collaboration, A. G. A. Brown, A. Vallenari, T. Prusti, J. H. J. de Bruijne, C. Babusiaux, M. Biermann, O. L. Creevey, D. W. Evans, and L. Eyer et al (2021, May). Gaia Early Data Release 3. Summary of the contents and survey properties. *A&A 649*, A1.

Gaia Collaboration, T. Prusti, J. H. J. de Bruijne, A. G. A. Brown, A. Vallenari, C. Babusiaux, C. A. L. Bailer-Jones, U. Bastian, M. Biermann, D. W. Evans, and j. . A&A. k. . s. y. . . m. . n. v. . . e. . A. p. . A. d. . . a. . a. e. . . p. . a. a. . h. a. . P. et al., title = "The Gaia mission".

Gao, X.-h. (2018, December). Memberships, Distances, and Proper Motions of the Open Clusters NGC 2112, NGC 2477, NGC 7789, and Collinder 261 from Gaia-DR2. *PASP 130*(12), 124101.

Gao, Y., S. Toonen, and N. Leigh (2022, March). Stellar Triples as a Source for Ba Stars. *arXiv e-prints*, arXiv:2203.05357.

Gebran, M., M. Vick, R. Monier, and L. Fossati (2010, November). Chemical composition of A and F dwarfs members of the Hyades open cluster. *A&A 523*, A71.

Geller, A. M. (2010, Jan). *Binary stars and blue stragglers in the old open cluster NGC 188*. Ph. D. thesis, The University of Wisconsin - Madison.

Geller, A. M., J. R. Hurley, and R. D. Mathieu (2013, Jan). Direct N-body Modeling of the Old Open Cluster NGC 188: A Detailed Comparison of Theoretical and Observed Binary Star and Blue Straggler Populations. *AJ 145*(1), 8.

Geller, A. M., D. W. Latham, and R. D. Mathieu (2015, September). Stellar Radial Velocities in the Old Open Cluster M67 (NGC 2682). I. Memberships, Binaries, and Kinematics. *AJ 150*(3), 97.

Geller, A. M. and R. D. Mathieu (2011, Oct). A mass transfer origin for blue stragglers in NGC 188 as revealed by half-solar-mass companions. *Nature 478*(7369), 356–359.

Geller, A. M., R. D. Mathieu, H. C. Harris, and R. D. McClure (2008, June). WIYN Open Cluster Study. XXXII. Stellar Radial Velocities in the Old Open Cluster NGC 188. *AJ 135*, 2264–2278.

Geller, A. M., R. D. Mathieu, H. C. Harris, and R. D. McClure (2009, Apr). WIYN Open Cluster Study. XXXVI. Spectroscopic Binary Orbits in NGC 188. *AJ 137*(4), 3743–3760.

Gosnell, N. (2015, January). Blue Straggler Stars: A Window Into Alternative Pathway Stellar Products. In *Frank N. Bash Symposium 2015 (BASH2015)*, pp. 5.

Gosnell, N. M., E. M. Leiner, R. D. Mathieu, A. M. Geller, C. Knigge, A. Sills, and N. W. C. Leigh (2019, November). Constraining Mass-transfer Histories of Blue Straggler Stars with COS Spectroscopy of White Dwarf Companions. *ApJ 885*(1), 45.

Gosnell, N. M., R. D. Mathieu, A. M. Geller, A. Sills, N. Leigh, and C. Knigge (2014, Mar). Detection of White Dwarf Companions to Blue Stragglers in the Open Cluster NGC 188: Direct Evidence for Recent Mass Transfer. *ApJL 783*(1), L8.

Gosnell, N. M., R. D. Mathieu, A. M. Geller, A. Sills, N. Leigh, and C. Knigge (2015, Dec). Implications for the Formation of Blue Straggler Stars from HST Ultraviolet Observations of NGC 188. *ApJ 814*(2), 163.

Gozzoli, E., M. Tosi, G. Marconi, and A. Bragaglia (1996, November). CCD photometry of the old open cluster Collinder 261. *MNRAS 283*, 66–76.

Gray, R. O. and C. J. Corbally (1994, February). The calibration of MK spectral classes using spectral synthesis. 1: The effective temperature calibration of dwarf stars. *AJ 107*, 742–746.

Grevesse, N. and A. J. Sauval (1998, May). Standard Solar Composition. *ssr 85*, 161–174.

Hills, J. G. and C. A. Day (1976, Feb). Stellar Collisions in Globular Clusters. *17*, 87.

Hole, K. T., A. M. Geller, R. D. Mathieu, I. Platais, S. Meibom, and D. W. Latham (2009, July). WIYN Open Cluster Study. XXIV. Stellar Radial-Velocity Measurements in NGC 6819. *AJ 138*(1), 159–168.

Huang, C. X., J. Burt, A. Vanderburg, M. N. Günther, Shporer, and et al. (2018, December). TESS Discovery of a Transiting Super-Earth in the pi Mensae System. *ApJL 868*(2), L39.

Hurley, J. R., O. R. Pols, S. J. Aarseth, and C. A. Tout (2005, October). A complete N-body model of the old open cluster M67. *MNRAS 363*(1), 293–314.

Iben, Icko, J. (1986, January). On the binary star origin of blue stragglers. *MEMSAI 57*, 453–464.

Jadhav, V. V., S. Pandey, A. Subramaniam, and R. Sagar (2021, October). UOCS. IV. Discovery of diverse hot companions to blue stragglers in the old open cluster King 2. *Journal of Astrophysics and Astronomy 42*(2), 89.

Jadhav, V. V., N. Sindhu, and A. Subramaniam (2019, November). UVIT Open Cluster Study. II. Detection of Extremely Low Mass White Dwarfs and Post-Mass Transfer Binaries in M67. *ApJ 886*(1), 13.

Jadhav, V. V. and A. Subramaniam (2021, October). Blue straggler stars in open clusters using Gaia: dependence on cluster parameters and possible formation pathways. *MNRAS 507*(2), 1699–1709.

Janson, M., F. Hormuth, C. Bergfors, W. Brandner, S. Hippler, S. Daemgen, N. Kudryavtseva, E. Schmalzl, C. Schnupp, and T. Henning (2012, July). The AstraLux Large M-dwarf Multiplicity Survey. *ApJ 754*(1), 44.

Jayasinghe, T., K. Z. Stanek, C. S. Kochanek, B. J. Shappee, T. W.-S. Holoien, T. A. Thompson, J. L. Prieto, S. Dong, M. Pawlak, O. Pejcha, J. V. Shields, G. Pojmanski, S. Otero, C. A. Britt, and D. Will (2019, June). The ASAS-SN catalogue of variable stars - II. Uniform classification of 412 000 known variables. *MNRAS 486*, 1907–1943.

Jenkins, J. M., D. A. Caldwell, H. Chandrasekaran, J. D. Twicken, S. T. Bryson, E. V. Quintana, and et al. (2010, April). Overview of the Kepler Science Processing Pipeline. *ApJL 713*(2), L87–L91.

Jiang, D., X. Chen, L. Li, and Z. Han (2017, November). Contribution of Primordial Binary Evolution to the Two Blue-straggler Sequences in Globular Cluster M30. *ApJ 849*(2), 100.

Jordi, C., M. Gebran, J. M. Carrasco, J. de Bruijne, H. Voss, C. Fabricius, J. Knude, A. Vallenari, R. Kohley, and A. Mora (2010, November). Gaia broad band photometry. *A&A 523*, A48.

Kaluzny, J. (1994, Jul). Photometric Study of the Extremely Old Open Cluster Berkeley 17. *Acta Astronomica 44*, 247–256.

Kaluzny, J., I. B. Thompson, S. M. Rucinski, W. Pych, G. Stachowski, W. Krzeminski, and G. S. Burley (2007, August). The Clusters Ages Experiment (CASE). II. The Eclipsing Blue Straggler OGLEGC 228 in the Globular Cluster 47 Tuc. *AJ 134*(2), 541–546.

Katz, D., P. Sartoretti, M. Cropper, P. Panuzzo, G. M. Seabroke, Y. Viala, K. Benson, R. Blomme, G. Jasniewicz, A. Jean-Antoine, H. Huckle, M. Smith, S. Baker, F. Crifo, Y. Damerdji, M. David, C. Dolding, Y. Frémat, and et al. (2019, Feb). Gaia Data Release 2. Properties and validation of the radial velocities. *A&A 622*, A205.

King, I. (1962, October). The structure of star clusters. I. an empirical density law. *AJ 67*, 471.

Knigge, C., N. Leigh, and A. Sills (2009, January). A binary origin for 'blue stragglers' in globular clusters. *Nature 457*(7227), 288–290.

Landsman, W. and T. Simon (1998, December). Helium White Dwarf Companions of Field Late-Type Stars. In *American Astronomical Society Meeting Abstracts*, Volume 193 of *American Astronomical Society Meeting Abstracts*, pp. 37.03.

Landsman, W. and T. P. Stecher (1997, May). Ultraviolet imagery of the old open clusters M67, NGC 188, and NGC 6791. In W. H. Waller (Ed.), *American Institute of Physics Conference Series*, Volume 408 of *American Institute of Physics Conference Series*, pp. 390–394.

Lanzoni, B., E. Dalessandro, S. Perina, F. R. Ferraro, R. T. Rood, and A. Sollima (2007, December). The Surprising External Upturn of the Blue Straggler Radial Distribution in M55. *ApJ 670*(2), 1065–1073.

Lanzoni, B., F. R. Ferraro, E. Alessandrini, E. Dalessand ro, E. Vesperini, and S. Raso (2016, December). Refining the Dynamical Clock for Star Clusters. *ApJL 833*(2), L29.

Lapasset, E. and J. Ahumada (1996, October). Discovery of an eclipsing blue straggler in NGC 2354. *A&A 314*, 448–452.

Latham, D. W. (2007, Aug). Spectroscopic binaries in M 67. *Highlights of Astronomy 14*, 444–445.

Leigh, N., C. Knigge, A. Sills, H. B. Perets, A. Sarajedini, and E. Glebbeek (2013, January). The origins of blue stragglers and binarity in globular clusters. *MNRAS 428*(1), 897–905.

Leigh, N., A. Sills, and C. Knigge (2009, 10). Stellar populations in globular cluster cores: evidence for a peculiar trend among red giant branch stars. *Monthly Notices of the Royal Astronomical Society: Letters 399*(1), L179–L183.

Leigh, N., A. Sills, and C. Knigge (2011, September). An analytic model for blue straggler formation in globular clusters. *MNRAS 416*(2), 1410–1418.

Leiner, E., R. D. Mathieu, D. Stello, A. Vand erburg, and E. Sandquist (2016, November). The K2 M67 Study: An Evolved Blue Straggler in M67 from K2 Mission Asteroseismology. *ApJL 832*(1), L13.

Leiner, E., R. D. Mathieu, A. Vanderburg, N. M. Gosnell, and J. C. Smith (2019, August). Blue Lurkers: Hidden Blue Stragglers on the M67 Main Sequence Identified from Their Kepler/K2 Rotation Periods. *ApJ 881*(1), 47.

Leiner, E. M. and A. Geller (2021, February). A Census of Blue Stragglers in Gaia DR2 Open Clusters as a Test of Population Synthesis and Mass Transfer Physics. *ApJ 908*(2), 229.

Leonard, P. J. T. (1996, Oct). The Implications of the Binary Properties of the M67 Blue Stragglers. *ApJ 470*, 521.

Lindegren, L., J. Hernández, A. Bombrun, S. Klioner, U. Bastian, M. Ramos-Lerate, A. de Torres, H. Steidelmüller, C. Stephenson, D. Hobbs, U. Lammers, and et al. (2018, Aug). Gaia Data Release 2. The astrometric solution. *A&A 616*, A2.

Lomb, N. R. (1976, February). Least-Squares Frequency Analysis of Unequally Spaced Data. *Ap&SS 39*(2), 447–462.

Lombardi, J., F. A. Rasio, and S. L. Shapiro (1995, June). On Blue Straggler Formation by Direct Collisions of Main-Sequence Stars. *ApJL 445*, L117.

Lovisi, L., A. Mucciarelli, F. R. Ferraro, S. Lucatello, B. Lanzoni, E. Dalessandro, G. Beccari, R. T. Rood, A. Sills, F. Fusi Pecci, R. Gratton, and G. Piotto (2010, August). Fast Rotating Blue Stragglers in the Globular Cluster M4. *ApJL 719*(2), L121–L125.

Lovisi, L., A. Mucciarelli, B. Lanzoni, F. R. Ferraro, and E. Dalessandro (2013, January). Blue straggler stars in globular clusters: chemical and kinematical properties. *MEMSAI 84*, 232.

Lucatello, S. and R. G. Gratton (2003, August). Rotation in Globular Cluster stars. Turn-off and subgiant stars in NGC 104, NGC 6397 and NGC 6752. *A&A 406*, 691–702.

Lund, M. N., R. Handberg, D. L. Buzasi, L. Carboneau, O. J. Hall, F. Pereira, D. Huber, D. Hey, T. Van Reeth, and T'DA Collaboration (2021, December). TESS Data for Asteroseismology: Light-curve Systematics Correction. *ApJS 257*(2), 53.

Lund, M. N., R. Handberg, G. R. Davies, W. J. Chaplin, and C. D. Jones (2015, June). K2P^2—A Photometry Pipeline for the K2 Mission. *ApJ 806*(1), 30.

Mapelli, M., S. Sigurdsson, M. Colpi, F. R. Ferraro, A. Possenti, R. T. Rood, A. Sills, and G. Beccari (2004, April). The Contribution of Primordial Binaries to the Blue Straggler Population in 47 Tucanae. *ApJL 605*(1), L29–L32.

Mapelli, M., S. Sigurdsson, F. R. Ferraro, M. Colpi, A. Possenti, and B. Lanzoni (2006, Nov). The radial distribution of blue straggler stars and the nature of their progenitors. *MNRAS 373*(1), 361–368.

Martinez, C. F., N. Holanda, C. B. Pereira, and N. A. Drake (2020, March). High-resolution spectroscopy of red giants and 'yellow stragglers' in the southern open cluster NGC 2539. *MNRAS 494*(1), 1470–1489.

Mateo, M., H. C. Harris, J. Nemec, and E. W. Olszewski (1990, August). Blue Stragglers as Remnants of Stellar Mergers: The Discovery of Short-Period Eclipsing Binaries in the Globular Cluster NGC 5466. *AJ 100*, 469.

Mathieu, R. D. (2000, January). The WIYN Open Cluster Study. In R. Pallavicini, G. Micela, and S. Sciortino (Eds.), *Stellar Clusters and Associations: Convection, Rotation, and Dynamos*, Volume 198 of *Astronomical Society of the Pacific Conference Series*, pp. 517.

Mathieu, R. D. and A. M. Geller (2009, Dec). A binary star fraction of 76 per cent and unusual orbit parameters for the blue stragglers of NGC 188. *Nature 462*(7276), 1032–1035.

Mathieu, R. D. and A. M. Geller (2015, Jan). The Blue Stragglers of the Old Open Cluster NGC 188. In *Ecology of Blue Straggler Stars*, Volume 413, pp. 29.

Mathieu, R. D., D. W. Latham, and R. F. Griffin (1990, December). Orbits of 22 Spectroscopic Binaries in the Open Cluster M67. *AJ 100*, 1859.

Mazur, B., W. Krzeminski, and J. Kaluzny (1995, Mar). Discovery of 45 short-period eclipsing binaries in the field of the old open cluster Collinder 261. *MNRAS 273*(1), 59–71.

McCrea, W. H. (1964, Jan). Extended main-sequence of some stellar clusters. *MNRAS 128*, 147.

Mermilliod, J. C., J. Andersen, D. W. Latham, and M. Mayor (2007, October). Red giants in open clusters. XIII. Orbital elements of 156 spectroscopic binaries. *A&A 473*(3), 829–845.

Milliman, K., R. D. Mathieu, and S. C. Schuler (2013, June). Surface Abundances of NGC 188 Blue Stragglers as a Clue to Formation History. In *American Astronomical Society Meeting Abstracts*, Volume 222 of *American Astronomical Society Meeting Abstracts*, pp. 214.05.

Milliman, K. E., R. D. Mathieu, A. M. Geller, N. M. Gosnell, S. Meibom, and I. Platais (2014, August). WIYN Open Cluster Study. LX. Spectroscopic Binary Orbits in NGC 6819. *AJ 148*(2), 38.

Milone, A. P., G. Piotto, L. R. Bedin, A. Aparicio, J. Anderson, A. Sarajedini, A. F. Marino, A. Moretti, M. B. Davies, B. Chaboyer, A. Dotter, M. Hempel, A. Marín-Franch, S. Majewski, N. E. Q. Paust, I. N. Reid, A. Rosenberg, and M. Siegel (2012, April). The ACS survey of Galactic globular clusters. XII. Photometric binaries along the main sequence. *A&A 540*, A16.

Mishenina, T., T. Gorbaneva, M. Pignatari, F.-K. Thielemann, and S. A. Korotin (2015, December). Mn abundances in the stars of the Galactic disc with metallicities -1.0 [Fe/H] 0.3. *MNRAS 454*, 1585–1594.

Momany, Y., E. V. Held, I. Saviane, S. Zaggia, L. Rizzi, and M. Gullieuszik (2007, June). The blue plume population in dwarf spheroidal galaxies. Genuine blue stragglers or young stellar population? *A&A 468*(3), 973–978.

Monaco, L., H. M. J. Boffin, P. Bonifacio, S. Villanova, G. Carraro, E. Caffau, M. Steffen, J. A. Ahumada, Y. Beletsky, and G. Beccari (2014, Apr). A super lithium-rich red-clump star in the open cluster Trumpler 5. *A&A 564*, L6.

Monteiro, H. and W. S. Dias (2019, August). Distances and ages from isochrone fits of 150 open clusters using Gaia DR2 data. *MNRAS 487*(2), 2385–2406.

Mucciarelli, A., L. Lovisi, F. R. Ferraro, E. Dalessand ro, B. Lanzoni, and L. Monaco (2014, Dec). Spinning Like a Blue Straggler: The Population of Fast Rotating Blue Straggler Stars in ω Centauri. *ApJ 797*(1), 43.

Nardiello, D., M. Deleuil, G. Mantovan, L. Malavolta, G. Lacedelli, M. Libralato, L. R. Bedin, L. Borsato, V. Granata, and G. Piotto (2021, August). A PSF-based Approach to TESS High quality data Of Stellar clusters (PATHOS) - IV. Candidate exoplanets around stars in open clusters: frequency and age-planetary radius distribution. *MNRAS 505*(3), 3767–3784.

Nardiello, D., G. Piotto, M. Deleuil, L. Malavolta, M. Montalto, L. R. Bedin, L. Borsato, V. Granata, M. Libralato, and E. E. Manthopoulou (2020, July). A PSF-based Approach to TESS High quality data Of Stellar clusters (PATHOS) - II. Search for exoplanets in open clusters of the Southern ecliptic hemisphere and their frequency. *MNRAS 495*(4), 4924–4942.

Nazé, Y. and G. Rauw (2008, November). High-resolution X-ray spectroscopy of θ Carinae. *A&A 490*(2), 801–806.

Oelkers, R. J. and K. G. Stassun (2018, September). Precision Light Curves from TESS Full-frame Images: A Different Imaging Approach. *AJ 156*(3), 132.

Pandey, S., A. Subramaniam, and V. V. Jadhav (2021, October). UOCS - VI. UVIT/AstroSat detection of low-mass white dwarf companions to four more blue stragglers in M67. *MNRAS 507*(2), 2373–2382.

Penoyre, Z., V. Belokurov, N. Wyn Evans, A. Everall, and S. E. Koposov (2020, May). Binary deviations from single object astrometry. *MNRAS 495*(1), 321–337.

Pera, M. S., G. I. Perren, A. Moitinho, H. D. Navone, and R. A. Vazquez (2021, June). pyUPMASK: an improved unsupervised clustering algorithm. *A&A 650*, A109.

Perets, H. B. and D. C. Fabrycky (2009, June). On the Triple Origin of Blue Stragglers. *ApJ 697*(2), 1048–1056.

Perren, G. I., E. E. Giorgi, A. Moitinho, G. Carraro, M. S. Pera, and R. A. Vázquez (2020, May). Sixteen overlooked open clusters in the fourth Galactic quadrant. A combined analysis of UBVI photometry and Gaia DR2 with ASteCA. *A&A 637*, A95.

Perren, G. I., A. E. Piatti, and R. A. Vázquez (2017). Astrophysical properties of star clusters in the magellanic clouds homogeneously estimated by asteca. *A&A 602*, A89.

Perren, G. I., R. A. Vázquez, and A. E. Piatti (2015, April). ASteCA: Automated Stellar Cluster Analysis. *A&A 576*, A6.

Peterson, R. C., R. T. Rood, and D. A. Crocker (1995, November). Rotation and Oxygen Line Strengths in Blue Horizontal-Branch Stars. *ApJ 453*, 214.

Piotto, G., F. De Angeli, I. R. King, S. G. Djorgovski, G. Bono, S. Cassisi, G. Meylan, A. Recio-Blanco, R. M. Rich, and M. B. Davies (2004, April). Relative Frequencies of Blue Stragglers in Galactic Globular Clusters: Constraints for the Formation Mechanisms. *ApJL 604*(2), L109–L112.

Platais, I., C. Melo, J. P. Fulbright, V. Kozhurina-Platais, P. Figueira, S. A. Barnes, and R. A. Méndez (2008, December). Trumpler 20 - an old and rich open cluster†‡. *MNRAS 391*(3), 1482–1488.

Press, W. H. and G. B. Rybicki (1989, March). Fast Algorithm for Spectral Analysis of Unevenly Sampled Data. *ApJ 338*, 277.

Preston, G. W. and C. Sneden (2000, August). What Are These Blue Metal-Poor Stars? *AJ 120*(2), 1014–1055.

Prš a, A., A. Kochoska, K. E. Conroy, N. Eisner, D. R. Hey, and et al. (2022, jan). TESS eclipsing binary stars. i. short-cadence observations of 4584 eclipsing binaries in sectors 1–26. *The Astrophysical Journal Supplement Series 258*(1), 16.

Raghavan, D., H. A. McAlister, T. J. Henry, D. W. Latham, G. W. Marcy, B. D. Mason, D. R. Gies, R. J. White, and T. A. ten Brummelaar (2010, September). A Survey of Stellar Families: Multiplicity of Solar-type Stars. *ApJS 190*(1), 1–42.

Rain, M. J., J. A. Ahumada, and G. Carraro (2021, June). A new, Gaia-based, catalogue of blue straggler stars in open clusters. *A&A 650*, A67.

Rain, M. J., G. Carraro, J. A. Ahumada, S. Villanova, H. Boffin, and L. Monaco (2021, January). The Blue Straggler Population of the Open Clusters Trumpler 5, Trumpler 20, and NGC 2477. *AJ 161*(1), 37.

Rain, M. J., G. Carraro, J. A. Ahumada, S. Villanova, H. Boffin, L. Monaco, and G. Beccari (2020, Feb). A Study of the Blue Straggler Population of the Old Open Cluster Collinder 261. *AJ 159*(2), 59.

Rao, K. K., K. Vaidya, M. Agarwal, and S. Bhattacharya (2021, December). Determination of dynamical ages of open clusters through the A^+ parameter - I. *MNRAS 508*(4), 4919–4937.

Recio-Blanco, A., G. Piotto, A. Aparicio, and A. Renzini (2002, June). Rotation of Hot Horizontal-Branch Stars in the Globular Clusters NGC 1904, NGC 2808, NGC 6093, and NGC 7078. *ApJL 572*(1), L71–L74.

Recio-Blanco, A., G. Piotto, A. Aparicio, and A. Renzini (2004, April). Rotation velocities of hot horizontal branch stars in the globular clusters NGC 1904, NGC 2808, NGC 6093, and NGC 7078: The database. *A&A 417*, 597–604.

Ricker, G. R., J. N. Winn, R. Vanderspek, D. W. Latham, G. Á. Bakos, J. L. Bean, Z. K. Berta-Thompson, T. M. Brown, L. Buchhave, and N. R. Butler (2015, January). Transiting Exoplanet Survey Satellite (TESS). *Journal of Astronomical Telescopes, Instruments, and Systems 1*, 014003.

Rucinski, S. M. (2000, July). W UMA-Type Binary Stars in Globular Clusters. *AJ 120*(1), 319–332.

Sahu, S., A. Subramaniam, M. Simunovic, J. Postma, P. Côté, N. Kameswera Rao, A. M. Geller, N. Leigh, M. Shara, T. H. Puzia, and P. B. Stetson (2019, May). Detection of a White Dwarf Companion to a Blue Straggler Star in the Outskirts of Globular Cluster NGC 5466 with the Ultraviolet Imaging Telescope (UVIT). *ApJ 876*(1), 34.

Sales Silva, J. V., V. J. Peña Suárez, O. J. Katime Santrich, C. B. Pereira, N. A. Drake, and F. Roig (2014, November). High-resolution Spectroscopic Observations of Binary Stars and Yellow Stragglers in Three Open Clusters : NGC 2360, NGC 3680, and NGC 5822. *AJ 148*(5), 83.

Salinas, R., L. Jílková, G. Carraro, M. Catelan, and P. Amigo (2012, April). Structural parameters and blue stragglers in Sagittarius dwarf spheroidal galaxy globular clusters. *MNRAS 421*(2), 960–970.

Samus', N. N., E. V. Kazarovets, O. V. Durlevich, N. N. Kireeva, and E. N. Pastukhova (2017, Jan). General catalogue of variable stars: Version GCVS 5.1. *Astronomy Reports 61*(1), 80–88.

Sandage, A. R. (1953, Jan). The color-magnitude diagram for the globular cluster M 3. *AJ 58*, 61–75.

Sandquist, E. L., M. Bolte, and L. Hernquist (1997, March). Composition Mixing during Blue Straggler Formation and Evolution. *ApJ 477*(1), 335–345.

Sandquist, E. L., D. W. Latham, M. D. Shetrone, and A. A. E. Milone (2003, February). The Blue Straggler RS Canum Venaticorum Star S1082 in M67: A Detailed Light Curve and the Possibility of a Triple. *AJ 125*(2), 810–824.

Santucci, R. M., V. M. Placco, S. Rossi, T. C. Beers, H. M. Reggiani, Y. S. Lee, X.-X. Xue, and D. Carollo (2015, March). The Frequency of Field Blue-Straggler Stars in the Thick Disk and Halo System of the Galaxy. *ApJ 801*(2), 116.

Sarna, M. J. and J. P. De Greve (1996, March). Chemical Evolution of Algols. *37*, 11.

Scargle, J. D. (1982, December). Studies in astronomical time series analysis. II. Statistical aspects of spectral analysis of unevenly spaced data. *ApJ 263*, 835–853.

Scholz, F. W. and M. A. Stephens (1987). K-sample anderson–darling tests. *Journal of the American Statistical Association 82*(399), 918–924.

Sigurdsson, S., M. B. Davies, and M. Bolte (1994, August). Modeling the Radial Distribution of Blue Stragglers in M3. *ApJL 431*, L115.

Sills, A., T. Adams, and M. B. Davies (2005, April). Blue stragglers as stellar collision products: the angular momentum question. *MNRAS 358*(3), 716–725.

Sills, A., J. A. Faber, J. Lombardi, James C., F. A. Rasio, and A. R. Warren (2001, February). Evolution of Stellar Collision Products in Globular Clusters. II. Off-Axis Collisions. *ApJ 548*(1), 323–334.

Sills, A., A. Karakas, and J. Lattanzio (2009, February). Blue Stragglers After the Main Sequence. *ApJ 692*(2), 1411–1420.

Sills, A., J. Lombardi, James C., C. D. Bailyn, P. Demarque, F. A. Rasio, and S. L. Shapiro (1997, September). Evolution of Stellar Collision Products in Globular Clusters. I. Head-on Collisions. *ApJ 487*(1), 290–303.

Simunovic, M., T. H. Puzia, and A. Sills (2014, November). The Blue Straggler Star Population in NGC 1261: Evidence for a Post-core-collapse Bounce State. *ApJL 795*(1), L10.

Singh, G., S. Sahu, A. Subramaniam, and R. K. S. Yadav (2020, December). Peculiarities in the Horizontal Branch Stars of Globular Cluster NGC 1851: Discovery of a Blue Straggler Companion to an EHB Star. *ApJ 905*(1), 44.

Smith, H. A. and J. E. Hesser (1983, September). Spectroscopy of upper-main-sequence and blue straggler stars in the intermediate-age cluster NGC 2477. *PASP 95*, 277–283.

Sollima, A., B. Lanzoni, G. Beccari, F. R. Ferraro, and F. Fusi Pecci (2008, April). The correlation between blue straggler and binary fractions in the core of Galactic globular clusters. *A&A 481*(3), 701–704.

Sterken, C. (2005, July). The O-C Diagram: Basic Procedures. In C. Sterken (Ed.), *The Light-Time Effect in Astrophysics: Causes and cures of the O-C diagram*, Volume 335 of *Astronomical Society of the Pacific Conference Series*, pp. 3.

Sun, M., R. D. Mathieu, E. M. Leiner, and R. H. D. Townsend (2021, February). WOCS 5379: Detailed Analysis of the Evolution of a Post-mass-transfer Blue Straggler. *ApJ 908*(1), 7.

Tian, B., L. Deng, Z. Han, and X. B. Zhang (2006, August). The blue stragglers formed via mass transfer in old open clusters. *A&A 455*(1), 247–254.

Tonry, J. and M. Davis (1979, Oct). A survey of galaxy redshifts. I. Data reduction techniques. *AJ 84*, 1511–1525.

Tosi, M., A. Bragaglia, and M. Cignoni (2007, June). The old open clusters Berkeley 32 and King 11. *MNRAS 378*(2), 730–740.

Tylenda, R., M. Hajduk, T. Kamiński, A. Udalski, I. Soszyński, M. K. Szymański, M. Kubiak, G. Pietrzyński, R. Poleski, Ł. Wyrzykowski, and K. Ulaczyk (2011, April). V1309 Scorpii: merger of a contact binary. *A&A 528*, A114.

Vaidya, K., A. Panthi, M. Agarwal, S. Pandey, K. K. Rao, V. Jadhav, and A. Subramaniam (2022, April). UOCS - VII. Blue straggler populations of open cluster NGC 7789 with UVIT/AstroSat. *MNRAS 511*(2), 2274–2284.

Vaidya, K., K. K. Rao, M. Agarwal, and S. Bhattacharya (2020, June). Blue straggler populations of seven open clusters with Gaia DR2. *MNRAS 496*(2), 2402–2421.

van den Berg, M., J. Orosz, F. Verbunt, and K. Stassun (2001, August). The blue straggler S 1082: A triple system in the old open cluster M 67. *A&A 375*, 375–386.

Vanderplas, J. (2015, February). Gatspy: General Tools For Astronomical Time Series In Python.

VanderPlas, J. T. and Ž. Ivezić (2015, October). Periodograms for Multiband Astronomical Time Series. *ApJ 812*(1), 18.

Vats, S. and M. van den Berg (2017, March). A Chandra X-Ray Census of the Interacting Binaries in Old Open ClustersCollinder 261. *ApJ 837*, 130.

Walborn, N. R. (1979, August). A radial velocity study of the chemically peculiar B star Theta Carinae. *PASP 91*, 442–445.

Wenger, M., F. Ochsenbein, D. Egret, P. Dubois, F. Bonnarel, S. Borde, F. Genova, G. Jasniewicz, S. Laloë, S. Lesteven, and R. Monier (2000, April). The SIMBAD astronomical database. The CDS reference database for astronomical objects. *A&AS 143*, 9–22.

Yontan, T., S. Bilir, Z. F. Bostancı, T. Ak, S. Ak, T. Güver, E. Paunzen, H. Ürgüp, M. Çelebi, B. A. Akti, and S. Gökmen (2019, September). CCD UBV photometric and Gaia astrometric study of eight open clusters—ASCC 115, Collinder 421, NGC 6793, NGC 7031, NGC 7039, NGC 7086, Roslund 1 and Stock 21. *Ap&SS 364*(9), 152.